TUTKIMUSRAPORTTI
REPORT OF INVESTIGATION 95

Electrical prospecting for ore deposits in the Baltic Shield

Part 2: Electromagnetic methods

Edited by S.-E. Hjelt and A. Fokin

GEOLOGIAN TUTKIMUSKESKUS
GEOLOGICAL SURVEY OF FINLAND

Espoo 1990

GEOLOGIAN TUTKIMUSKESKUS
Tutkimusraportti 95

GEOLOGICAL SURVEY OF FINLAND
Report of Investigation 95

Editors
S.-E. Hjelt and A. Fokin

ELECTRICAL PROSPECTING FOR ORE DEPOSITS IN THE BALTIC SHIELD

Part 2: Electromagnetic methods

Espoo 1990

ISBN 951-690-390-8
ISSN 0781-4240

Helsinki 1990. Valtion painatuskeskus

ELECTRICAL PROSPECTING FOR ORE DEPOSITS IN THE BALTIC SHIELD

Part 2: Electromagnetic methods
Editors: S.-E. Hjelt and A. Fokin

ПРИМЕНЕНИЕ ЭЛЕКТРОРАЗВЕДКИ НА РУДНЫХ МЕСТОРОЖДЕНИЯХ БАЛТИСКОГО ЩИТА

Вып. 2. Электроразведка переменном током

Редактор с финской стороны - С.-З. Ельт
Редактор с советской стороны - А. Фокин

Теоретические вопросы и моделирование

Методика и аппаратуры

Пезультать электромагнитых измерений

PREFACE

Cooperation in the use of geophysical methods within the framework of the agreement on Scientific and Technical Cooperation in Geology between Finland and the Soviet Union began in 1975. The exchange visits paid by Finnish and Soviet scientists in the first couple of years provided an overall view of the geophysical exploration methods in use in the Baltic Shield areas of each country. In 1977-80 the cooperation was focused on magnetic bore hole measurements; the results were published in Finland in 1981 as a collection of articles in English entitled "Interpretation of bore hole magnetic data and some special problems of magnetometry" in a series of reports from the University of Oulu.

As a result of the growing popularity and increasing scope of electrical methods in prospecting the theme selected for 1981-85 was "Electrical prospecting methods on the Baltic Shield". The work was divided into two phases: 1981-82 - galvanic methods and 1983-84 - inductive methods; only ground and drill hole methods were included. Each phase consisted of introductory reports, field and laboratory visits, quantitative interpretation with various methods of theoretical and practical survey data, examination of case histories, and comparison of results. The cooperation has made it possible to follow recent developments in equipment and methods of interpretation in exploration geophysics in both countries. In the Soviet Union the project was undertaken by the Production Geological Amalgamation "Sevzap-geologia" (SZPGO), and in Finland by the Geological Survey of Finland, the Department of Geophysics of the University of Oulu, Outokumpu Oy and Rautaruukki Oy.

The results of the cooperation have been published as two reports in a series of Report of Investigation from the Geological Survey of Finland. Report 73 deals with galvanic methods and Report 95 with inductive methods. The undersigned express their gratitude to the Geological Survey of Finland, which made it possible to publish the results of the cooperation, and to the Finnish-Soviet Commission for Scientific and Technical cooperation for their financial support.

M. Ketola *N. Khrustalev*

Key words: geophysical methods, electromagnetic methods, electromagnetic induction, mineral exploration, crust, Precambrian, Baltic Shield, Finland, USSR

Theory and modelling

THE INFLUENCE OF THE ELECTRICAL CONDUCTIVITY OF THE SURROUNDING MEDIUM ON THE ANOMALY IN INDUCTIVE METHODS OF ELECTRICAL PROSPECTING (FROM CALCULATION AND MODELLING)

by

A. Savin and G. Vargin

Savin, A. & Vargin, G., 1990. The influence of the electrical conductivity of the surrounding medium on the anomaly in inductive methods of electrical prospecting (from calculation and modelling). *Geologian tutkimuskeskus, Tutkimusraportti 95.* 8-19, 7 figs.

Presented are the results of comparing the calculated values for the anomalous effect above spherical models of conductors placed in conductive whole space and half-space. When evaluating the anomalous effect in ground electrical induction prospecting, it seems sufficient to confine oneself to the calculations for a case of a conductive sphere in a conductive whole space.

The variation of a medium-to-object conductivity ratio from 1/10000 to 1/100 does not, in fact, affect the maximum value of the anomalies or, correspondingly, on the depth of penetration of prospecting, while the optimal frequency of the EM field depends basically on the conductivity of the surrounding medium.

The influence of the conductivity of the medium on the anomalous effect in both dipole profiling and TEM measurements is illustrated by model cases.

Key words: electromagnetic methods, electromagnetic induction, numerical models, transient methods, electrical conductivity, anomalies, mineral exploration, geophysical surveys

Савин, А.И., Варгин, Г.И., 1990. Влияние электропроводности вмещающей среды на аномальный эффект в индукционных методах электроразведки по результатам расчетов и моделирования. Геологический центр финляндии, Рапорт исследования 95. 8-19, Идд. 7.

Приводятся результаты сопоставления расчетов аномального эффекта над моделью проводника в форме шара, помещенного в проводящее простпанство и подупространство. Для оценки аномального эффекта при проведении работ индукционными методами электроразведки на дневкой поверхности можно ограничиться расчетами для случая проводящего шара в проводящем пространстве.

Показано, что изменение отношения удельных проводимостей среды и объекта в пределах от 1/10000 до 1/100 практически не отражается на максимальном значении аномалий и, соответственно, на глубинности поисков, а оптимальная частота электромагнитного поля в основном зависит от удельной проводимости среды.

Влияние электропроводности среды на аномальный эффект в методах дипольного профилирования и переходных процессов иллюстрируется примерами моделирования.

Analysis of spherical conductors

One of the most important and intricate points in analyzing the behaviour of electrical induction prospecting methods is the influence of the surrounding medium on the anomalies caused by highly conductive orebodies.

The most common procedure in studying the anomalous effects involves the computation of the field above a sphere that imitates an isometric orebody. This particular body geometry in modelling provides the advantage of obtaining such analytical solutions as enable the anomalous effect to be calculated and thoroughly analyzed. In some cases, a sphere approximates a certain type of ore model; in particular, the Nud-II copper-nickel deposit in the Kola peninsula corresponds to this type (Vargin et al., 1985). The results of calculations above the sphere model can also be applied to objects of other geometries. The considerations given to the behaviour of anomalies above a sphere when analyzing the efficiency of electrical induction methods can hardly cause an overestimation of the depth penetration since a sphere displays the most attenuation of an anomaly with depth.

In the dipole induction profiling method using a transmitting coil with a vertical axis, we need to calculate the components of the magnetic field intensity produced by a vertical harmonic magnetic dipole located on the horizontal surface of the conductive half-space containing a spherical inhomogeneity (Fig. 1a). The conductivity of the upper half-space, lower half-space and the sphere proper is marked as σ_1, σ_2 and σ_3, respectively; the magnetic permeability is consequently μ_1, μ_2, and μ_3, with μ_1 and μ_2 assumed as equal to μ_0, the magnetic permeability of vacuum. To simplify the problem, the dipole is located so as to coincide with the vertical axis running through the centre of the sphere.

Since the solution to this problem is far from being easy, several versions of approximate solutions have been proposed. They include substitution of the half-space by the whole space (March, 1953), cf., Fig. 1b, or by a concentric sphere (Negi, 1962; Negi et al., 1973; Raval, 1973; Sochelnikov, 1974; Savin, 1975) - Fig.1c. Such approximations simplified the problem solution, yet failed to clear up the point of whether these assumptions are possible. On the other hand, the mutual discrepancy in results of simulating a sphere in the surrounding medium and concentric spheres (Savin, 1975) indicated that at least one of these models is inappropriate for quantitative estimation.

There exist early solutions to the problem (Dyakonov, 1959; Ogunade et al., 1974) corresponding to the model shown in Fig. 1a. Because of some inaccuracies in these solutions, however, the results cannot be used. Therefore, the authors of the present article, together with Simovski-Veitkov, have found a solution (Vargin et al., 1983; Savin et al., 1985) that enabled comparing the results of the calculations for each of three model cases. Shown in Fig. 2 is an example of a comparison of the characteristics of real and imaginary components of the anomalous portion of the normalized vertical magnetic field

$$h_z = H_z/m\ 4\ \pi r^3,$$

as a function of parameter

$$\alpha_3 = \omega\mu_3\ \sigma_3 \cdot a^2,$$

where

m – magnetic dipole molent,
H_z – anomalous vertical component of the magnetic field intensity,
ω – cyclic frequency,
"r" and "a" – as in Fig. 1.

The anomaly

$$H_z = H_{z\Sigma} - H_{zo}$$

means a difference between the intensity values of a total field $H_{z\Sigma}$ and "normal field" H_{zo}.

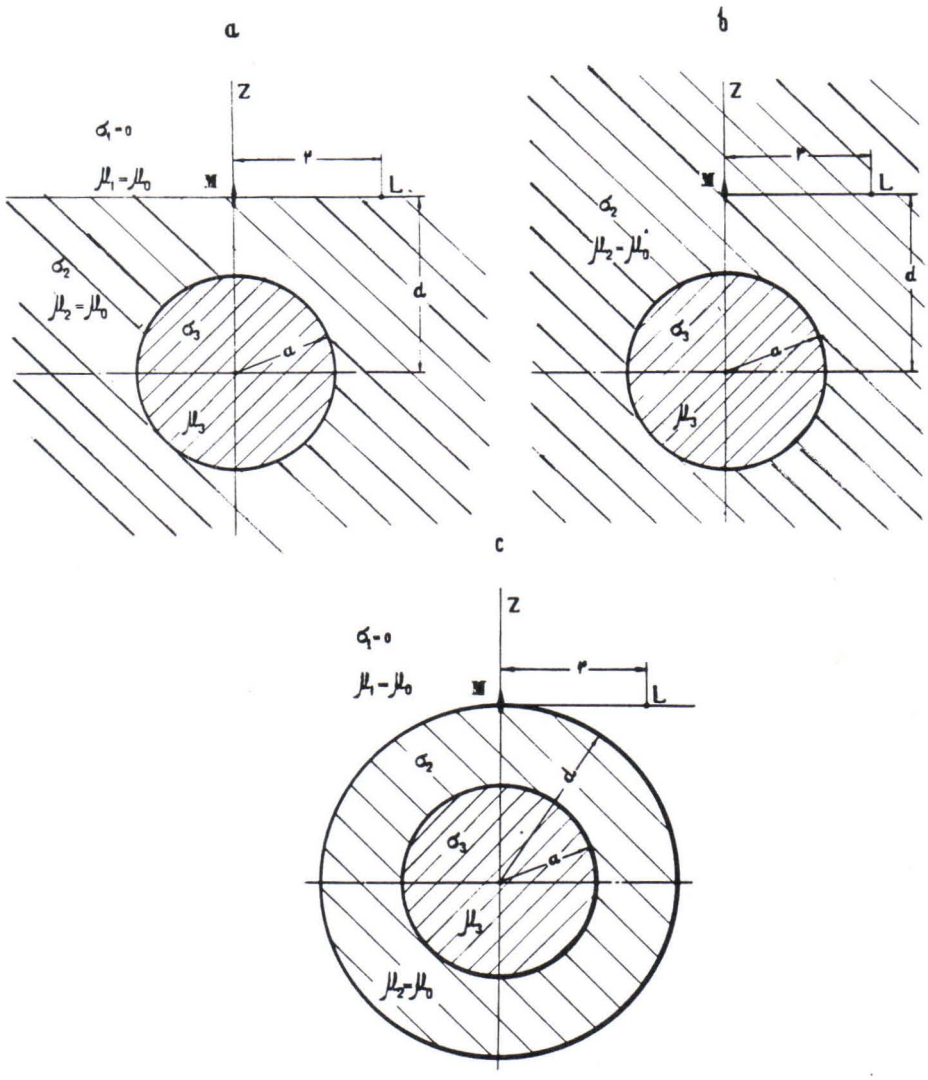

Fig. 1. Types of models applied for studing the influence of the surrounding medium. M – magnetic dipole, L – measurement point.

Fig. 2 shows that the occupation of the whole space by the conductive material (curve 3) leads to the "attenuation" of Re h_z and Im h_z at low α_3 values. Using the concentric sphere model (curve 5), where a half-space is generally not filled completely with conductive material, makes Re h_z and Im h_z subject to distortion in precisely the opposite sense.

Yet the results of calculations over the object in the whole space do not differ much from those obtained over the object in the half-space (cf., additional samples of comparison in Fig. 3). This enables one to employ, and with an accuracy high enough to meet practical requirements, the solution for the model presented in Fig. 1b. A further advantage of this particular model is the possibility of making calculations even when the system geometry is not axially symmetric.

All these things considered, we made use of the solution of March (1953) for calculating the anomalies in the dipole induction profiling method. The results presented here refer to the

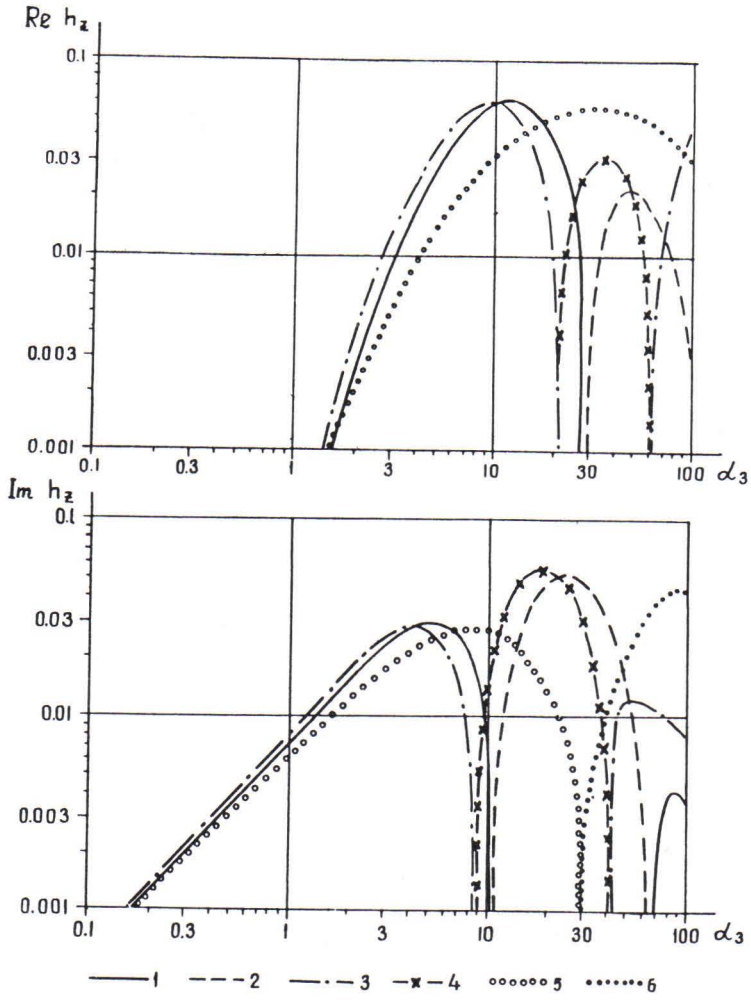

Fig. 2. Re h_z and Im h_z characteristics with a/d = 0.5, r/d = 4, $\mu_2/\mu_3 = 1$, $\sigma_2\sigma_3 = 1/64$.
1, 2 - for a sphere in the conductive half-space; 3, 4 - same in the conductive whole space; 5, 6 - same inside a conductive sphere with large dimensions; 1, 3, 5 - negative values; 2, 4, 6 - positive values.

most common modification of dipole induction profiling: measuring the vertical magnetic component in a field of the vertical magnetic dipole (the ZZ-array). Sample curves for different r/d ratios are shown in Fig. 3. The surrounding medium affects the anomaly profiles as differences in "h_z" and in the form for two values of ratio σ_2/σ_3. The anomalous values for $\sigma_2/\sigma_3 = 1/100$ are much higher than those for $\sigma_2/\sigma_3 = 1/10000$ under otherwise equivalent conditions. This peculiarity is a well-known fact, which in the geophysical literature is called the "negative screening effect" (Gaur, 1963; Negi, 1967).

Nomograms for spherical conductors

Now, it is a common practice in dipole induction profiling to measure in the field a modulus of the total field $|h_z|$ as compared with that of a normal field $|h_{z0}|$. In this case, attention

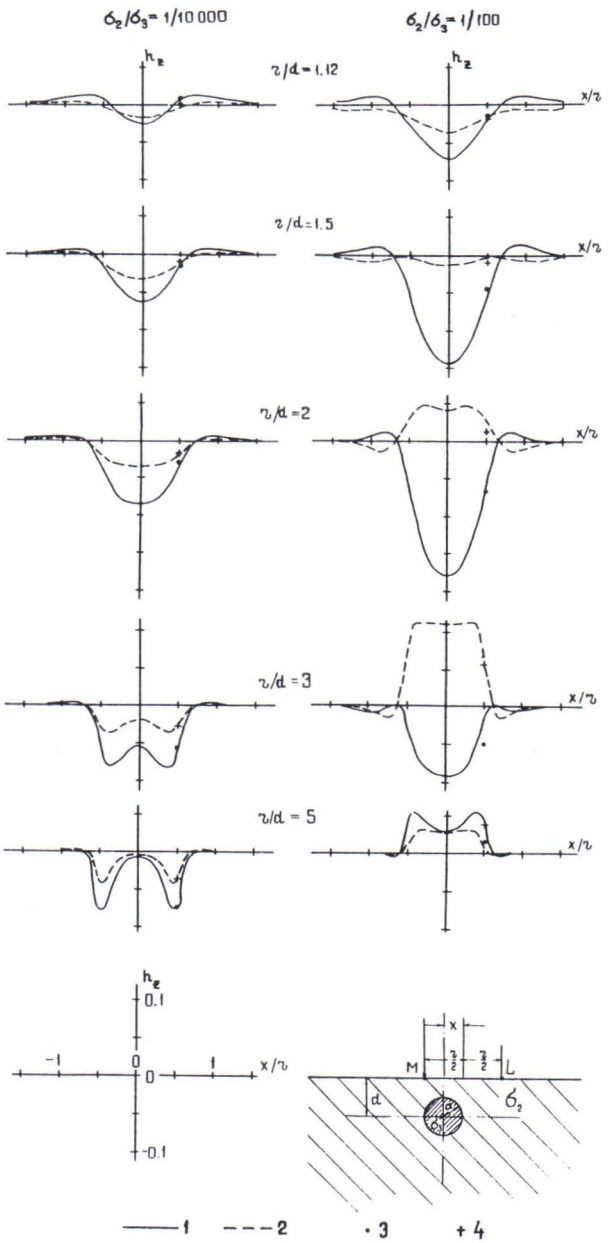

Fig.3. Graphs of h_z above a sphere in conductive medium, with a/d = 0.5; $\alpha_3 = 40$; σ_2/σ_3 = 1/10000 and 1/100. 1, 2 - according to the results of calculation above the sphere in conductive whole space; 3, 4 - same above the sphere in conductive half-space; 1, 3 - Re h_z; 2, 4 - Im h_z.

is drawn to the anomaly of the total field modulus expressed through a relation

$$h_{za} = \frac{\sqrt{(\mathrm{Re}\, h_{z0} + \mathrm{Re}\, h_z)^2 + (\mathrm{Im}\, h_{z0} + \mathrm{Im}\, h_z)^2}}{|h_{z0}|} - 1.$$

As long as the anomalies differ considerably in their form under different conditions, the efficiency of dipole induction profiling can be described by the so-called "span" of anomaly A_z,

$A_Z = (h_{za})_{max} - (h_{za})_{min}$. For ratios σ_2/σ_3 = 1/10000 and 1/100 respectively at $\mu_3/\mu_2 = 1$, the results of calculations are represented as nomograms (Fig. 4) connecting the r/d and a/d ratios with the optimal "α_3" values, which make the A_Z - span reach its maximum.

The nomograms in Fig.4 give us an idea of the size of the anomaly in particular for two values of the object-to-surroundings resistivity ratio. The nomograms also enable methodic problems to be solved, viz., to determine the optimal values of array spacing "r" (from r/d), the EM-field frequencies (from "α_3") and the lowermost depth of detecting an isometric object (from a/d). Provided we have field data enough to distinguish a maximum value in the frequency characteristic, nomograms can be of use in interpretation.

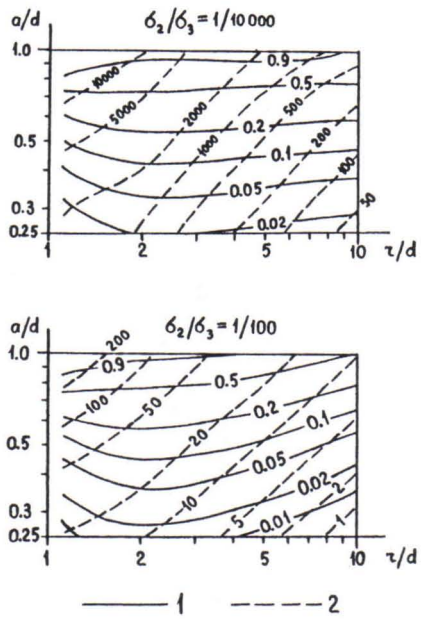

Fig.4. Nomograms connecting ratios a/d and r/d with values of anomalies A_Z(1) and corresponding optimal α_3 (2) values above a sphere in a conductive half-space, with σ_2/σ_3 = 1/10000 and 1/100.

Based on the analysis of nomograms and on initial data required for their drawing, the following conclusions can be made concerning the technique used and its effectiveness in dipole induction profiling:

1. When a sphere lies deep enough (a/d < 0.6) the optimal r/d ratio does not depend on the resistivity ratio; it is on the average 2 to 2.3. An unmotivated increase of array spacing "r" to more than (2 + 2.3)d causes a decrease of the anomaly.

2. Increasing the conductivity of the surrounding medium (at least up to $\sigma_2 = \sigma_3/100$) does not, in fact, decrease the anomalous effect, while only decreasing the optimal α_3 value.

3. Optimal "α_3" values correspond (by this we mean $\xi_2 = \sqrt{\alpha_3 \cdot \sigma_2/\sigma_3} \cdot \tau/\alpha$) to the reduced distances $\xi_2 = |k_2|\, r - 2.81 \cdot 10^{-3} \sqrt{f \cdot \sigma_2} \cdot r$ (where k_2 - wave number of a medium) covering relatively small limits, from 1.8 to 3.6. Knowing this fact, we can easily determine an optimal frequency "f", which depends upon the conductivity σ_2 of a medium and bears actually no relation whatsoever to the properties, size and depth of the object in question.

Platelike (flat) conductors

Unlike isometric objects, which are fairly rare, orebodies possessing a bedlike form are quite common in the Baltic Shield (Eloranta, 1981; Vargin et al., 1985). Modelling is basically used when studying the influence of the conductivity of the surrounding medium upon the anomalies produced by bedlike bodies. For dipole induction profiling, most of the modelling with the surrounding medium simulated by water solutions was carried out in India (Gupta, Mary, 1971; Gaur et al., 1972, 1973; Verma, Gaur, 1975). Water solutions ensure a high resistivity contrast between the medium and the object. For low-contrast materials like metal (Zakharov, 1975), graphite, coal, etc., are most frequently used. Shown in Fig.5 is an example of modelling over a thin vertical plate made of lead (Savin, 1978); the latter, when in a molten state, was poured as a filler into a slot in a solid-state graphite as a background medium. The thickness of the lead plate was t = 0.5 cm, the vertical distance from the coils to the top edge of the plate is d = 1.2 cm and that to the graphite model, c = 0.8 cm; the array spacing "r" is 6.65 cm. The resistivity values of lead and graphite were $\rho_3 = 1/\sigma_3 = 3.7 \cdot 10^{-7}\Omega m$ and $\rho_2 = 1/\sigma_2 = 1.2 \cdot 10^{-5}\Omega m$, respectively. Fig. 5 shows the real and imaginary components ($h_{z\Sigma}$) corresponding to the measurements on frequencies 80, 315,1250, 5000 and 20000 Hz. To ascertain the influence of the medium the same measurements were carried out in the air ($\rho_2 = \infty$).

The results correspond to the ratio $\alpha_3/\alpha_2 = 0.4$, where $\alpha_3 = \mu_0\sigma_3\omega tr$ is the plate induction parameter and $\alpha_2 = \mu_0\delta_2\omega r^2$ the induction parameter of the medium ($\alpha_2 = 0$ in the air). On low frequencies, when $\alpha_3 = 0.57$, the anomalies Re h_z and Im h_z over a plate in the medium practically do not differ from those in the air. With increasing α_3, the discrepancy between them becomes more and more evident and distortions of the anomaly form also takes place. The anomalous effect in the medium is sometimes higher than in the air, which just confirms a so-called "negative screening effect".

The present state of knowledge in modelling above plates in a conductive medium appears to be insufficient for drawing the nomograms of similar bodies as shown in Fig.4. Yet the most common regularities in the influence of the conductive surrounding medium on the plate anomalies are not likely to differ from those of anomalies above a sphere. It seems that it is precisely from this standpoint that one should decide on the technique of dipole induction profiling when prospecting for ore-layer (platelike) targets occurring among rocks with relatively low resistivity.

Time domain measurements

As far as TEM is concerned, the approach to a study of the influence of the surrounding medium was the same as in the dipole induction profiling. In calculating the anomalous effect, use was made of a sphere in the whole space (Singh, 1973; Makagonov, 1977b), a model of concentric spheres (Hjelt, 1971; Nabighian, 1971; Rao, 1972; Raval, 1973; Makagonov, 1977a; Kamenetski, Timofeev, 1979; Nagendra et al., 1980) and a sphere in a halfspace (a model that corresponds best of all to the problem and which is given a somewhat more scrupulous solution) (Kamenetski et al., 1975; Lee, 1975).

For the study of the anomalous effect in TEM, we decided to use the model of a vertical magnetic dipole field above a sphere in a homogeneous half-space (Fig. 1a) (Savin et al., 1984) and to present the results using generalized dimensionless characteristics. In this case, the computations involve the calculated anomalous part of the azimuthal normalized electric field $e_\varphi = (E_\varphi/j\omega\mu_0 m) \cdot 4\pi r^2$, where E_φ - anomaly of the azimuthal component of the electric field intensity, j - imaginary unit. According to the reciprocity principle, the results of measuring E_φ in the field of a vertical magnetic dipole are identical to the results of measuring H_z in the field of an azimuthal electric dipole. Integration of the electric dipole moment along the circular contour

helps to associate the magnetic intensity with the circular current along the contour in the plane that divides both half-spaces and has its axis running through the centre of the sphere. The

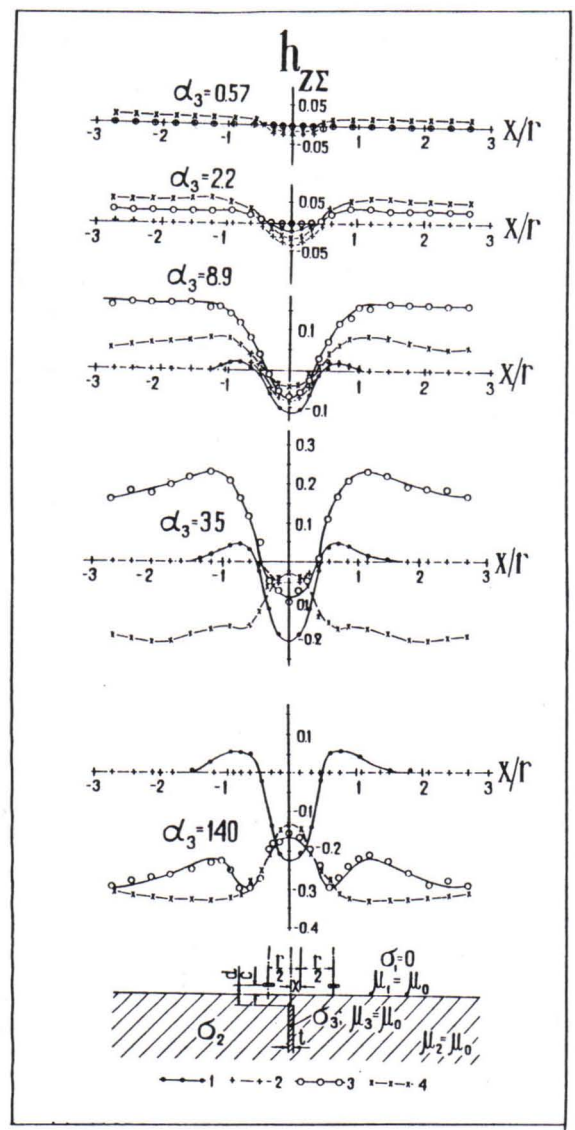

Fig. 5. Results of modelling dipole induction profiling above a thin vertical layer (plate). 1 - (Re $H_{z\Sigma}$ - 1) over a plate in a nonconducting medium (in the air); 2 - Im $H_{z\Sigma}$ over a plate in a nonconducting medium (in the air); 3 - (Re $H_{z\Sigma}$ - 1) over a plate in a conductive medium; 4 - Im $H_{z\Sigma}$ over a plate in a conducting medium.

transition from the harmonic to the transient mode is effected by the Fourier-Laplace transformation.

The results of the calculations are presented in terms of a function ψ, its argument being a parameter $t/\mu_3\sigma_3a^2$, where "t" denotes time when the transient process is measured. The emf "U" in the receiving coil placed in the centre of the circular loop with I and with radius r is

derived from the formula:

$$U = \frac{\mu_0 I S}{2\pi} \cdot \frac{(a/d)^3}{(1 + d^2/r^2)^{3/2}} \cdot \frac{6}{25} \psi ,$$

where S - effective area of a receiving coil.

When $t/(\mu_3\sigma_3 a^2)$ is high enough, the results of the ψ - calculations can be used to analyze the data obtained by a single- or incorporated-loop array modification of TEM. In this case, the emf (U) across the receiving loop is expressed by the formula:

$$U = \frac{\pi \mu_0 I r}{2t} \cdot \frac{(a/d)^3 (r/d)^3}{(1 + r^2/d^2)^3} \cdot \frac{6}{25} \psi .$$

The characteristics of function ψ for various ratios σ_2/σ_3 with dimensions are shown in Fig. 6. It is obvious that by increasing the ratio σ_2/σ_3, we shift the extreme ψ values towards greater time periods. In the area of remarkably long time periods, the anomaly might become larger with an increasing ratio σ_2/σ_3 (under otherwise equivalent conditions), which corresponds to the already mentioned "negative screening effect".

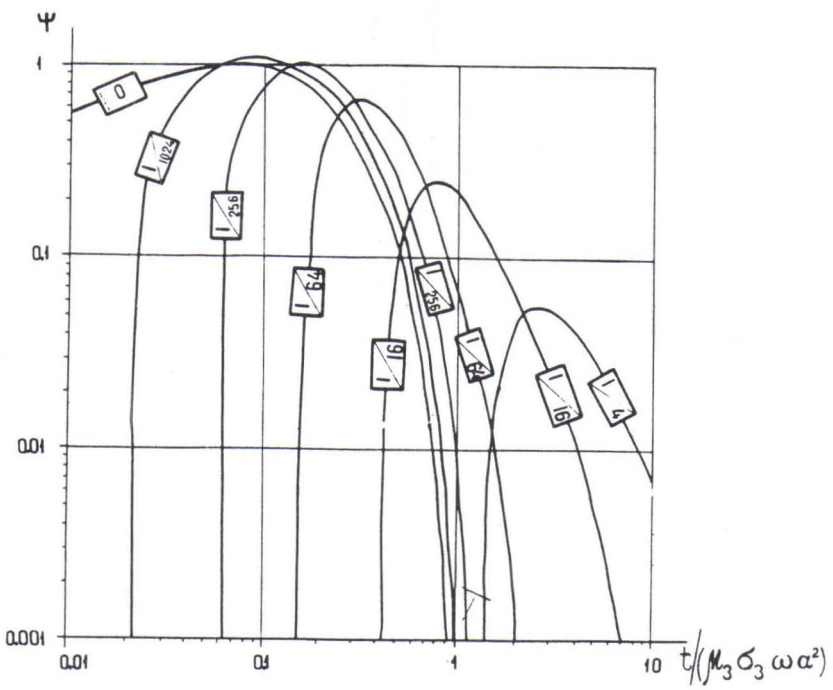

Fig. 6. Characteristics of function ψ ($t/\mu_3\sigma_3 a^2$) with $\mu_2/\mu_3 = 1$, a/d = 0.5, r/d = 4. The curve codes correspond to σ_2/σ_3 values.

Practical examples

A study of the anomalous effect of composite geoelectric sections requires the use of modelling. Modelling results imitating the ore target of the Windy Belt zone (Vargin et al., 1985) are represented in Fig. 7. The surrounding medium was simulated by a solution of potassium chloride ($\rho_{2\text{-}3} = 7.1 \cdot 10^{-2}$ Ωm) but the ore object by graphite ($\rho_5 = 1.1 \cdot 10^{-5}$Ωm) and the layer of Quaternary sediments, together with a bed imitating the layer of apo-olivinite serpentinites, by a special compound with resistivities of $\rho_1 = 1.15 \cdot 10^{-2}$ Ωm and $\rho_4 = 7.0 \cdot 10^{-3}$ Ωm, respectively. A square-loop array with a side length of 2 l = 8 cm was used. Measurements were carried out in the frequency range 1.25 to 80 kHz. Conversion of the harmonic field characteristics into transient field characteristics was made with the Fourier-Laplace transformation. The transition from modelling conditions to the actual in-field ones is based on the well-known similarity parameter. In this particular case, the relations were as follows: $L_n = 2.5 \cdot 10^3 L_m$, $\rho_n = 2.8 \cdot 10^4 \rho_m$, $t_n = 2.2 \cdot 10^2 t_m$, where L is any linear dimension while the indexes "n" and "m" stand for field (natural) and modelling conditions. The values plotted in Fig.7 correspond to the actual field (natural) conditions.

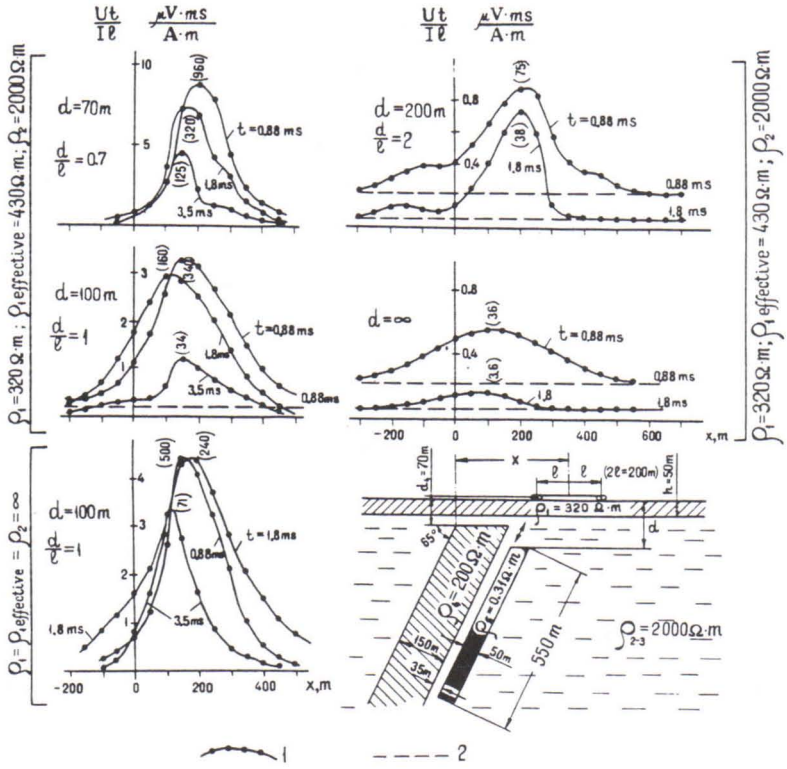

Fig. 7. Results of TEM modelling above a model of the Windy Belt ore.
1 - graphs of Ut (II); 2 - level of the normal field. In the brackets - extreme values of U/I in μV/A. The dimensions of layers ρ_4 and ρ_5 in the field along the strike are 1250 and 1000 m respectively.

The modelling procedure involved variations in the immersion depth of an ore object (the latter being immersed down the dip of the layer). Now, being high enough for detection at d = 70 and 100 m respectively, the U/I anomaly at d = 200 m is comparable with the interfering

anomaly (exceeding it 2 to 2.5 times only) associated with the apo-olivinite serpentinite zone (cf., graphs at d = 200 m and d = ∞). Comparing with the same model, yet without the background medium and top horizontal layer ($\rho_1 = \rho_{2-3} = \infty$) gives us an idea of the extent of the screening effect produced by the host rocks and the Quaternary sediments.

The measurements performed provided the basis for evaluating the capabilities of TEM prospecting under certain field conditions.

Conclusions

Based on analysis of the available data as to the influence of the surrounding conductive medium upon the anomalies in the electrical induction methods, the following conclusions can be drawn:

1. When determining the anomalous effect in the ground electrical induction methods, a whole conductive space can be used instead of a conductive half-space. Such substitution does not cause any noticeable distortions in the calculation results; on the other hand, it essentially simplifies the calculations made for solving the normal and inverse geophysical problems.

2. A change in the medium-to-object conductivity ratio in the range of 1/10000 to 1/100, which is typical of most of the ore deposits in the Baltic Shield, does not, in fact, affect the maximum value of the anomalies and, consequently, the depth of penetration. The optimal frequency of the EM-field corresponding to this value, however, turns out to be a function of the conductivity ratio.

References

Dyakonov, 1959. EM wave diffraction for the case of a sphere in a half-space (Дифракция электромагнитных волн на шапе, расположенном в полупростпанстве). Bull. USSR Acad. Sci., Geophysics 11, 1579-1590.

Eloranta, E., 1981. Features of morphology of Finnish ore deposits (Piirteitä Suomen malmiesiintymien malmioiden morfologiasta). Geologi 33, No. 8, 121-123.

Gaur, V.K.,1963. EM model experiments simulating an airborne method of prospecting. Bulletin of National Geophysical Research Institute, Hyderabad 1, 167-174.

Gaur, V.K., Verma, O.P. & Gupta, C.P., 1972. Enhancement of electromagnetic anomalies by a conducting overburden. Geophysical Prospecting 20: 580-604.

Gaur, V.K. & Verma, O.P., 1973. Enhancement of electromagnetic anomalies by a conducting overburden (II). Geophysical Prospecting 21, 159-184.

Gupta, D.S. & Mary, V.M., 1971. A study of some effects of a conducting host rock with a new modelling apparatus. Geophysics 36,166-183.

Hjelt, S.E., 1971. The transient electromagnetic field of a two-layer sphere. Geoexploration 9, 213-230.

Kamenetski, F. & Timofeev, V., 1978. On the negative screening effect (ОБ "отрицательном экранировании"). Bull. USSR Acad. Sci. Solid-Earth Geophysics 3, 96-101.

Kamenetski, F. (ed.), 1976. A manual to the application of the transient method in the exploratory geophysics (Руководство по применению метода переходных процессов в рудной геофизике). Leningrad, Nedra, 128 p.

Kamenetski, F., Makagonov, P. & Mukhina, N., 1975. The transient signal in incorporated loops on the surface of a two-layer medium containing a spherical inhomogeneity in its second layer. (Неустановившийся сигнал в совмещенных петлях на поверхности двухслойной среды со сферической неодиородностью во втором слое). (Bull. VUZ). Geology and Exploration 8,122-129.

Lee, T., 1975. Transient electromagnetic response of a sphere in a layered medium. Geophysical Prospecting 23, 492-512.

Makagonov, P., 1977a. Normal and inverse problems taken from the inductive electroprospecting theory for the envelope system. (Прямая и обратная задача теории индуктивной электроразведки для системы оболчек). (Bull. VUZ) Geology and Exploration 10, 134-142.

Makagonov, P.A., 1977b. A system of algorithms for interpreting the electrical induction prospecting data. (Система алгоритмов интерпретации данных индуктивой электроразведки). Deposited in VINITI, August 8 No. 3182-77, Dep., 35 p.

March, H.W., 1953. The field of magnetic dipole in presence of conducting sphere. Geophysics 18, 671-684.

Nabighian, M.N., 1971. Quasi-static transient response of a conducting permeable two-layer sphere in a dipole field. Geophysics 36, 25-37.

Nagendra, R., Ramprasada, R.I.B. & Bhimasankaram, V.I.S., 1980. Influence of a conducting shield in the one-loop version of the transient pulse induction method. Geophysical Prospecting 28, 269-282.

Negi, J.C., 1967. EM screening due to a disseminated spherical zone over a conducting sphere. Geophysics 32, 69-87.

Negi, J.G., Gupta, C.P. & Raval, U., 1973. Electromagnetic response of a permeable inhomogeneous conducting sphere. Geoexploration 2, 1-20.

Ogunade S.O., Ramaswamy, V. & Dosso, H.W., 1974. Electromagnetic response of a conducting sphere buried in a conducting earth. Journal of Geomagnetism and Geoelectricity 26, 417-427.

Rao, K.N.N., Gupta, C.P. & Raval, U., 1973. Electromagneticresolution in time- domain for a covered spherical conductor. Geophysical Research Bulletin 10, 189-205.

Raval, U., 1973. Ambiguity in the electromagnetic interpretation due to a conducting halo surrounding the target. Pure and Appl. Geophys. 104, 574-581.

Savin A., Simovski-Veitkov, I. & Vargin, G.V.,1985. Dipole inductive profiling above a sphere buried in a homogeneous half-space. (Дипольное индуктивное профилирование над шаром, погруженным в однородное полупространство). Bull. USSR Acad. Sci., J. Physics of the Earth 4, 55-66.

Savin, A., 1975. Influence of the background medium on the anomalies in dipole induction profiling. (Влияние вмещающей срелы на аномалии индуктивного дипольного профилирования). Express-information of OCNTI, VIEMS, series IX - Regional, exploratory and petroleum geophysics, Moscow, Iss. I: 1-21.

Singh, S.K., 1973. Electromagnetic transient response of a conducting sphere in a conducting medium. Geophysics 38, 864-893.

Sotchelnikov, V., 1974. Coaxially-layered conducting sphere in the alternating field of magnetic and electric depoles. (Проводящий концентрически-слоистый шар в переменном поле магнитного и злектрического диполей). Marine geology and geophysics. Riga, Zinatne, Iss. 4, 32-37.

Vargin, G.V., Savin, A. & Simovski-Veitkov, I., 1983. Improving the technique of examining the influence of the background medium on the dipole induction profiling anomalies of the ore objects in Karelia. (Усовершенствование методики учета влияния вмещающей среды на аномалии ДНИ от рудных объектов Карелии). Pp. 54-62 in: Results of geophysical investigations in the Precambrian formations of Karelia. Geol. Inst. of Karelian Branch of USSR Acad. Sci., Petrozavodsk.

Vargin, G.V., Borovko, N. & Savin, A., 1986. Construction of geoelectrical models for copper-nickel deposits of the Kola-Karelian region. (Построение геозлектрических моделей медноникелевых местопождений Карело-Кольского региона). This issue (Part I).

Verma, O.P. & Gaur, V.K., 1975. Transformation of electromagnetic anomalies brought about a conducting host rock. Geophysics 40, 473-489.

Zakharov, V., 1975. Electrical prospecting using a dipole induction profiling technique (Злектроразведка методом дипольного индуктивного профилирования). Leningrad, Nedra, 224 p.

THE TRANSMISSION SURFACE ANALOGY IN CALCULATING FIELDS OF 2D MODELS

by

H. Soininen, P. Saksa and I. Suppala

Soininen, H., Saksa, P. & Suppala, I., 1990. The transmission surface analogy in calculating fields of 2D models. *Geologian tutkimuskeskus, Tutkimusraportti 95.* 20-27, 5 figs, one table.

The transmission surface algorithm is based on the similarity between Maxwell's equations and transmission line equations. A program package for modelling two-dimensional structures is presented. The primary source can be either a plane wave or an infinite line current source. It is also possible to use the program package as part of an iterative model-fitting scheme because the partial derivatives of the fields can readily be calculated with respect to the model resistivities at the same time as the forward problem is solved.

Some modelling results for the audiomagnetotelluric (AMT) method are presented as an application of a program package. For deep-seated elongated bodies, E-parallel polarization gives more information on the electrical structure than does H-parallel polarization. Nomograms for interpretation of vertical conductance and depth of a thin two-dimensional conductive body are given.

Key words: electromagnetic methods, electromagnetic induction, numerical models, two-dimensional models, transient methods, audiomagnetotelluric methods, electrical conductivity

Сойнинен, Х., Сакса, П., Суппала, И., 1990. Аналогия поверхности передачи в вычислении полей при двумерном моделировании. Геологический центр финляндии, Рапорт исследования 95. 20-27, Идд. 5.

Алгоритм поверхности передачи основан на подобии уравнений максвелла и уравнений линии передачи. В работе представлен пакет программ для моделирования двумерных структур. Первичным источником может быть или плоская болна или бесконечный линейный источник тока. Пакет программ может также использоваться как часть итеративной схемы лодбора модели, так как частичные произбодные полей по отношению к модельным солротивлениям легко вычисляются одновременно с решением прямой задачи.

В качестве примепа применения пакета программ показаны некоторые пезультаты моделирования для звукочастотного магнитотеллурического метода (Змт). В случае глубоко залегающих удлиненных тел поляризация, параллельная Е, несет больше информации о электрической структуре объекта чем поляризация по Н. Даны номограммы для интерпретации вертикальной электропроводности и глубины залегания маломощного двумерного проводящего тела.

Introduction

The transmission surface algorithm, or network solution technique, is based on the similarity between Maxwell a equations and transmission line equations. This technique was first applied to geophysical problems by Madden and Thompson (1965). It has since been used for two-dimensional problems by Swift (1967,1971), Madden and Vozoff (1971), Madden (1972), Smith (1975), and others. Brewitt-Taylor and Johns (1980) have presented an algorithm for three-dimensional problems.

In this paper we shall present a program package for numerical calculation of two-dimensional structures for plane wave incidence and for an infinite line current source. It is also possible to calculate efficiently the partial derivatives of the fields with respect to the model parameters at the same time as the forward problem. Thus the program package can be used as part of an iterative model-fitting program (Soininen, 1980).

Formulation of the problem

Let us consider a two-dimensional structural model (Fig. 1), assuming $e^{-i\omega t}$ time dependence. Maxwell's equations

$$\nabla x\ E = i\omega\mu\ H, \qquad \nabla x\ H = (\sigma - i\omega\varepsilon)E \tag{1}$$

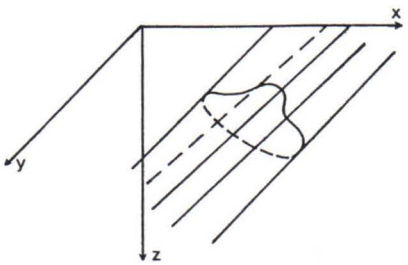

Fig. 1. Two-dimensional model and coordinate system.

now separate for the two polarizations (1) H parallel to the strike with $H(0, H_y, 0)$ and $E(E_x, 0, E_z)$, and (2) E parallel to the strike with $H(H_x, 0, H_z)$ and $E(0, E_y, 0)$. The resulting equations are:

H-parallel

$$\partial H_y/\partial x = (\sigma - i\omega\varepsilon)\ E_z,$$
$$\partial H_y/\partial z = -(\sigma - i\omega\varepsilon)\ E_x, \tag{2}$$
$$\partial E_x/\partial z - \partial E_z/\partial x = i\omega\mu H_y,$$

and E-parallel

$$\partial E_y/\partial x = + i\omega\mu\ H_z,$$
$$\partial E_y/\partial z = - i\omega\mu\ H_x, \tag{3}$$

$$\partial H_x/\partial z - \partial H_z/\partial x = (\sigma - i\omega\varepsilon) E_y.$$

In the network solution, equations (2) and (3) are solved numerically for an arbitrary cross-section using discrete approximation over a finite grid. The technique is based on the analogy between transmission line equations and equations (2) and (3). The transmission line equations are (Harrington, 1961)

$$\begin{aligned} \nabla V &= -Z I, \\ \nabla \cdot I &= -YV, \end{aligned} \tag{4}$$

where V is the voltage, I is the current along the line, Z is the distributed impedance and Y is the distributed admittance per unit length. The one dimensional transmission line equations (4) can be extended to two-dimensional transmission surface equations:

$$\begin{aligned} \partial V/\partial x &= -Z I_x, \\ \partial V/\partial z &= -Z I_z, \\ \partial I_x/\partial x &+ \partial I_z/\partial z = -Y V. \end{aligned} \tag{5}$$

Comparing equations (5) with equations (2) and (3), we can derive the following analogies (Table 1).

Table 1. Analogies between Maxwell's equations and transmission surface equations.

E-parallel	Transmission surface eq.	H-parallel
E_y	V	H_y
H_z	I_x	$-E_z$
$-H_x$	I_z	E_x
$-i\omega\mu$	Z	$\sigma - i\omega\varepsilon$
$\sigma - i\omega\varepsilon$	Y	$-i\omega\mu$

Forming of network

To form an electrical network that simulates a two-dimensional structure, the earth model must be sectioned into a grid of rectangles or elements, and the lumped circuit parameters Z_d (d = v, h) and Y_c determined for each element. The nodes of our circuit are placed at the corners of each element. The lumped parameters are defined as

$$\begin{aligned} Z_v &= Z\Delta z/\Delta x, \\ Z_h &= Z\Delta x/\Delta z, \\ Y_c &= Y\Delta z \cdot \Delta x, \end{aligned} \tag{6}$$

where Z_v is the vertical impedance, Z_h is the horizontal impedance and Y_c is the admittance. Δx and Δz are the element size in the x and z direction.

Boundary and source conditions

To terminate the grid the lumped terminal impedances are calculated at the bottom of the grid from the characteristic impedance

$$Z_C = \sqrt{Z/Y}/\Delta x. \tag{7}$$

The bottom layer is thus assumed to extend into infinity.

A one-dimensional transmission line problem is solved along the sides of the grid assuming that lateral inhomogeneities are far enough away from the sides of the grid.

For plane wave incidence, a constant source is applied at the top of the grid. To ensure that the secondary fields are zero at the source, it must be placed far from the earth-air boundary. We must introduce sufficiently thick air layers above the ground and then put a constant source at the top of the layers.

The horizontal magnetic field is independent of the conductivity of a layered earth. Thus for the E-parallel polarization constant vertical current I_Z is put at the top of the air layers, whereas for the H-parallel polarization constant voltage V is put at the top of the grid. For the modelling of possible topographic effects, we have included air layers for both polarizations (Smith, 1975).

Forming the linear set of equations

After the mesh parameters and boundary conditions are satisfied the equation of electrical current continuity can be written at each node ij.

$$\frac{V_{neighbour} - V_{ij}}{Z_{connecting}} + Y_{ij} V_{ij} = S_{ij}, \tag{8}$$

where V_{ij} is the voltage of the ijth node, $V_{neighbour}$ is the voltage at one of the four nearest neighbour nodes of V_{ij}, Y_{ij} is the admittance of the ijth node, $Z_{connecting}$ is the lumped impedance to the adjacent node and S_{ij} is a current source term. Applying conservation of the current at each node point, we obtain the linear set of equations

$$AV = S, \tag{9}$$

where A is a (m x n) x (m x n) system matrix, which is a banded, sparse, diagonally dominant matrix. V and S are vectors of (m x n) length. It should be mentioned that system matrix A is essentially the same as that which would be obtained by the finite difference method. As a solution of equation (9), we get the nodal voltages in our mesh and by using the analogies shown in Table 1 we can now calculate the required electric and magnetic field components.

Infinite line current source

The algorithm presented can be used for calculating two-dimensional anomalies for an infinite line current source. Thus it is possible to model Turam responses over two-dimensional inhomogeneities aligned parallel to the long axis of the transmitting loop. The transmitting loop is approximated by one (or two) infinite line current sources. This problem is solved like the E-parallel case. Swift (1971) has represented the current source by replacing the plane-wave

source by a finite S_{ij} just above the surface of the Earth. In the present work, we calculate the secondary voltages V^s instead of the total voltages V, because the secondary field structure is simpler and smoother in the regions with sharp spatial variations of the primary field (near the current source) (Varentsov, 1983). Now the source term S_{ij} in equation (8) (conductivity and dielectric inhomogeneities) is $-(Y_{ij}- Y^\circ_{ij})V^\circ_{ij}$, where Y°_{ij} is the normal admittance of the base structure and V°_{ij} is the primary voltage (primary E°_y). Boundary conditions are approximated by characteristic impedances (7) at the top and sides of the model.

Calculation of partial derivatives for inversion

Generalized linear inverse and iterative model-fitting has proved to be an effective tool in the interpretation of electromagnetic sounding measurements in plane-layered regions (Glenn et al., 1973; Ward et al., 1973). The inversion of more complex conductivity structures has been difficult because of the long computing time needed. In the inversion, both the forward problem and the partial derivatives of the fields with respect to the model parameters must be calculated. Oristaglio and Worthington (1980) have developed a two-dimensional inversion for EM data using a finite element method. Their algorithm permitted the resistivities of the elements or blocks in a two-dimensional model of predetermined geometry to be optimized. A similar technique can be used in a network solution. Let us differentiate equation (9) with respect to model resistivity ρ_i. The result is (the source being independent of model parameters):

$$A\,(\partial V/\partial \rho_i) = -\,(\partial A/\partial \rho_i)V. \qquad (10)$$

Equation (10) is the same equation as (9) but with a different right-hand side. The new source term is the product of the derivative of the system matrix with respect to parameter ρ and the column vector of voltages V. Equation (10) is solved through a process of forward-reduction and back-substitution with the new right-hand sides. The partial derivatives are calculated as accurately as the fields themselves and the accuracy is independent of conductivity values. The computation is also fast in terms of computer time, since it takes only about 3 % extra time per conductivity value to calculate partial derivatives. The final derivatives of the desired field components are calculated by using the analogies presented in Table 1.

Applications

One of the applications of the present program package has been the analysis of two-dimensional responses for the audiomagnetotelluric (AMT) method (Saksa, 1983). The model discussed in this paper is presented in Fig. 2 with the notation used.

The anomaly profiles of E-parallel and H-parallel polarizations for two-dimensional models are quite different from each other in the AMT-frequency range. The H-parallel anomaly is caused mainly by variation in surface charge density at the boundaries of the body. With outcropping structures, the abrupt change in the normal component of the electric field and its effect on apparent resistivity values will outline boundaries of electrical structures clearly (Strangway et al., 1973). The behaviour of the E-parallel anomaly is in contrast smooth and continuous.

The situation will change, however, when the depth of the two-dimensional model increases. In this case, the difference between the E-parallel and H-parallel anomalies is striking as shown by the calculated model curves in Fig. 3. The upper surface of the model is at a depth of 200 m. The H-parallel anomaly has practically disappeared but the E-parallel anomaly is

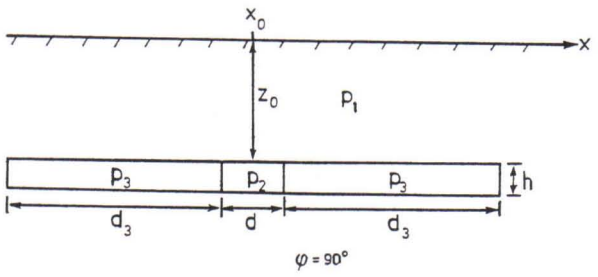

Fig. 2. Two-dimensional plate model.

strong over a wide frequency range. We can conclude that for the exploration of deep-seated elongated bodies, the E-parallel polarization contains more information on the electrical structure than does the H-parallel polarization.

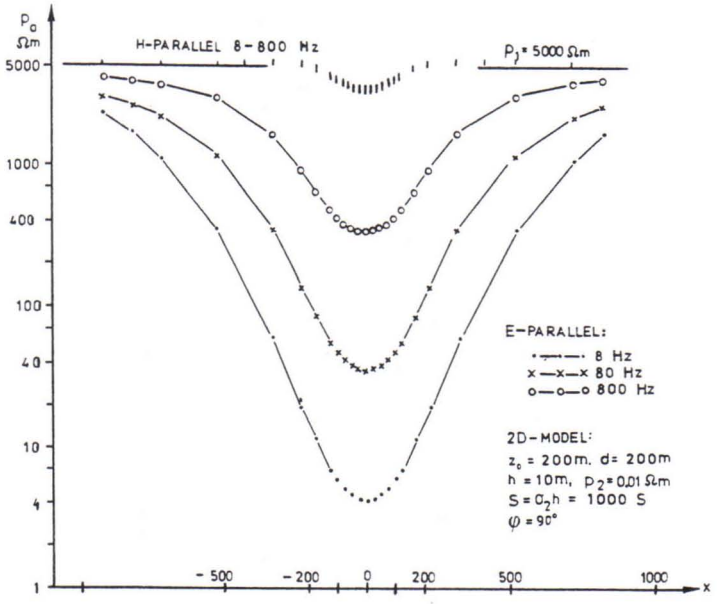

Fig. 3. Apparent resistivity anomalies for E-parallel and H-parallel cases.

Next, we shall analyze methods for resolving the resistivity and thickness of a thin two-dimensional model. According to the model calculations, the vertical conductance $S_2 = \sigma_2 h$ of the model can be interpreted from AMT measurements within the depth range z_0 = 50-1000 m and at a width of d = 50-200 m. Fig. 4 shows the relation between the frequency f_{min} that gives the lowest apparent resistivity value along the profile across the conductive body and vertical conductance S_2 of the two-dimensional model.

Fig. 5 is an example of nomograms compiled for the direct interpretation of the depth of conductive models. The model parameters are again the same as in Fig. 3. The minimum values of apparent resistivity are picked from the calculated AMT profiles (above the center of the

body). The nomogram is designed for a frequency of 8 Hz and for a model with a width of 100 m.

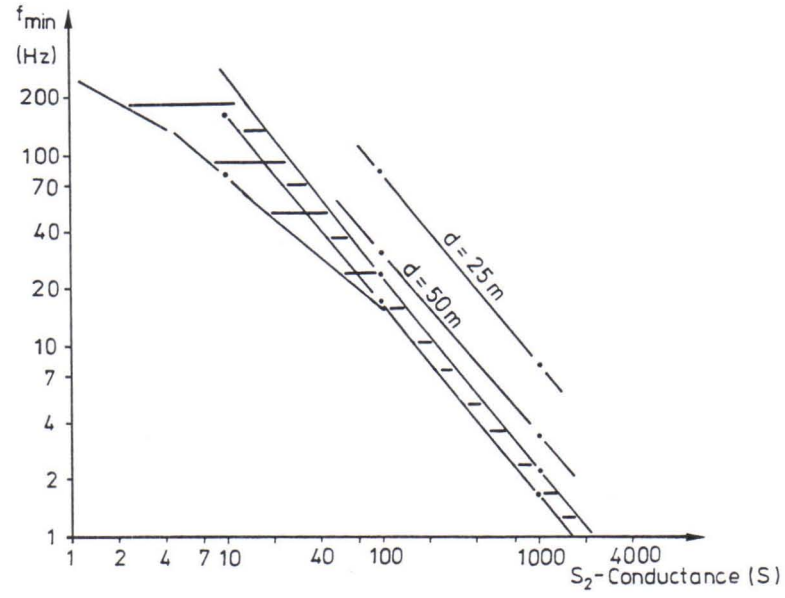

Fig. 4. Nomogram for the interpretation of the vertical conductance of a two-dimensional model.

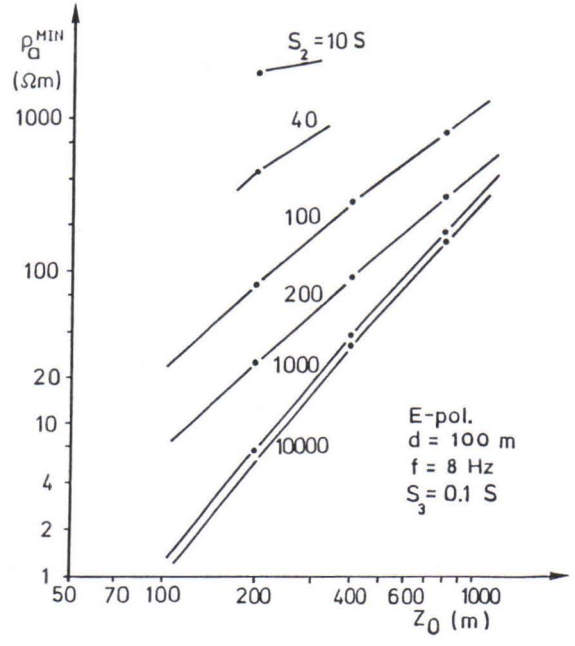

Fig. 5. Nomogram for the interpretation of depth to the upper surface of a two-dimensional model.

Conductance values S_2 (and S_3) can be determined using, for example, the nomogram in Fig. 4. The nomogram in Fig. 5 also indicates the behaviour of the profile curves when the depth to the two-dimensional model and the vertical conductance is varied.

Summary

The present work describes a program package intended for two-dimensional numerical EM computation. The transmission surface analogy used is one of many possible procedures for solving EM boundary value problems. It has proved to be easy to use, flexible for modelling complex conductivity structures and cheap in terms of computational time.

The ability to calculate the partial derivatives of field components with respect to model resistivities at the same time as the forward problem means that the program can be used in inversion. Hence interpretation is more effective and information can be obtained about the sensitivity of the solution to possible errors in the data and the degree of nonuniqueness associated with the model.

References

Brewitt-Taylor, C.R. & Johns, P.B., 1980. On the construction and numerical solution of transmission-line and lumped network models of Maxwell's equations. Int. J. num. Math. Engng.15,13-30.

Glenn, W.E., Ryu, J., Ward, S.H., Peeples, W.J. & Phillips, J.R., 1973. The inversion of vertical magnetic dipole sounding data. Geophysics 38, 1109-1129.

Harrington, R.F., 1961. Time-harmonic electromagnetic fields. McGraw-Hill, New York.

Madden, T., 1972. Transmission systems and network analogies in geophysical forward and inverse problems. Earth and Planetary Sci. Dept., MIT, RPT, 72-3.

Madden, T. & Thompson W., 1965. Low frequency electromagnetic oscillations of the earht-ionosphere cavity. Rev. Geophys. Space Phys.3, 211-254.

Madden, T.R. & Vozoff, K., 1971. VLF model suite, explanatory booklet. Lexington, Massachusetts.

Oristaglio, M.L. & Worthington, M.H., 1980. Inversion of surface and borehole electromagnetic data for two-dimensional electromagnetic conductivity models. Geophys. Prosp. 28, 633-657.

Saksa, P., 1983. Sähkömagneettisista lähdekentistä ja niiden soveltamisesta audio-magnetotelluuriseen menetelmään. Unpublished M. Eng. thesis (in Finnish), Helsinki Univ. of Technol.

Smith, B.D., 1975. Interpretation of electromagnetic field measurements: Ph.D. Thesis, University of Utah.

Soininen, H.T., 1980. Sähkömagneettisten menetelmien kaksidimensionaalinen inversio toteutettuna vastusverkkoanalogialla. Unpublished M. Eng. Thesis (in Finnish) Helsinki Univ. Technol.

Strangway, D.W., Swift, C.M., Jr. & Holmer, R.C., 1973. The application of audio-frequency magnetotellurics (AMT) to mineral exploration: Geophysics 28,1159-1175.

Swift, C.M., Jr., 1967. A magnetotelluric investigation of an electrical conductivity anomaly in the southwestern United States. Ph.D. Thesis, Geophys. Lab., MIT.

Varentsov, Iv.M., 1983. Modern trends in the soulution of forward and inverse 3D electromagnetic induction problems: Geophys. Surv. 6, 55-78.

Ward, S.H., Peeples, W.J. & Ryu, J., 1973. Analysis of geoelectromagnetic data: in Methods in Computational Physics 13: Geophysics 163-236.

TYPE CURVES FOR MAGNETIC DIPOLES AND THEIR USE IN COMPUTER INTERPRETATION

by

T. Valkeila and M. Rossi

Valkeila, T., & Rossi, M., 1990. Type curves for magnetic dipoles and their use in computer interpretation. *Geologian tutkimuskeskus, Tutkimusraportti 95.* 28-37, 4 figs, one table.

Many electromagnetic methods have a magnetic dipole as a source. Their mathematical interpretation is difficult and has resulted in the importance of scale models and type curves. In the first part of this paper, we describe the scale model measurements made in Finland.

The second part deals with the utilization of calculated and measured type curves. First, we present an algorithm based on the interpolation of Slingram anomalies. Then, we describe an interpretation program based on this algorithm.

Key words: electromagnetic methods, electromagnetic induction, numerical models, physical models, inverse problem, data processing, Slingram

Валкейла, Т., Росси, М., 1990. Типовые кривые для магнитных диполей и их применение в автоматизированной интериретации. Геологический центр финляндии, Рапорт исследования 95. 28-37. Идд. 4.

Во многих злектромагнитных методах в качестве источника полагаются магнитные диполи. Их математическая интерпретация затруднительна, что обусловливает важность масштабных моделей и типовых кривых. В первом разделе данной статьи описываются измерения на масштабных моделях в финляйндии.

Во втором разделе статьи рассматривается применение расчитанных и замеренных типовых кривых. Сперва приводится алгоритм, основанный на интерполяции аномалий при методе горизонтальной петли (Slingram). Затем описывается интерпретационная программа, основанния на зром алгоритме.

Introduction

An important class of electromagnetic methods consists of those with the magnetic dipole as a source. These can be divided into two parts, depending on the nature of the signal. The harmonic continuous wave is used with the frequency domain methods and a pulse wave with the time domain methods. In Finland, frequency-domain measurements are used almost as widely as the magnetic survey. This hold for both the Slingram method and airborne electromagnetic methods.

It would be very practical if the theoretical solution could be formulated in a short mathematical expression. For the magnetic dipole, however, this has succeeded only with rather simple models. Geologically, more representative models have to be calculated numerically with a computer.

Scale model measurements are another way of solving the theoretical fields. This paper reviews briefly the history of Finnish research work in this field with the help of a table.

Algorithm based on the interpolation of model curves

The use of a computer in the interpretation requires an algorithm for the theoretical result of the model. If we are aiming at an interactive graphic program, the algorithm must be fast; a numerical solution with integral equations is far too slow.

In 1978, Valkeila presented a solution based on of Pelton's original idea (1977). In this solution, stored in the memory of a computer, there are previously calculated and measured model curves from which the final result is obtained by interpolation. The digitized model curves, each of which contains 15-40 points, can also be called a data bank.

The interpolation is carried out in two phases. A single model curve is constructed by fitting a parabola with three successive digitized points. The spaces between the model curves are then solved with the linear interpolation. The interpolation is shown in Fig. 1.

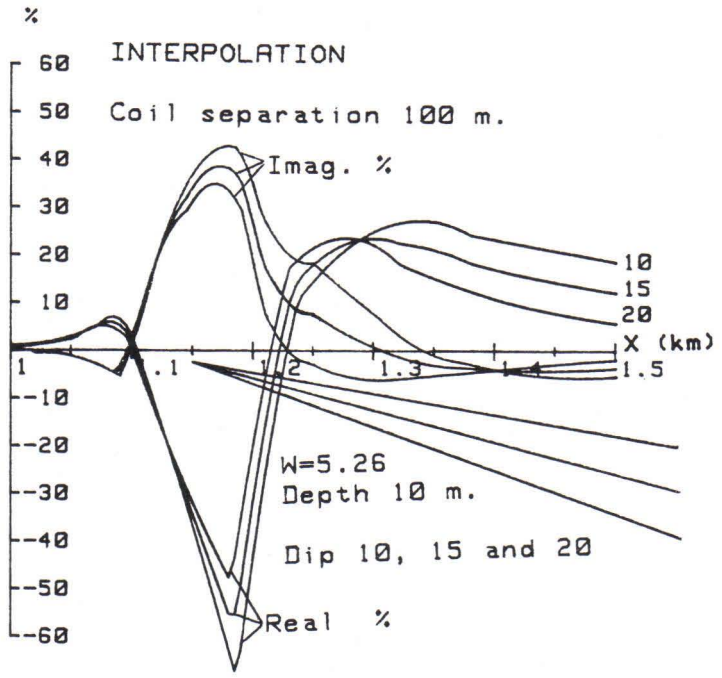

Fig. 1. A model curve with a dip of 15 degrees interpolated between model curves of 10 and 20 degrees.

Table 1. Type curves for magnetic dipoles documented in Finland in 1967-1985.

coil config.	type of scatterer	surround-ings	response parameter	value of r.p.	α	h/a	x/a	p/a	e/a	h_1/a	b/a	remarks	ref.
ZZ/3/	thin plate	free space	W=μδwad	1.75... ∞ (6)	30°... 90°(5)	0.10... 0.60(5)	-2... +2...						/4/
ZZ	thin plate	free space	W=μδwad	0.20... 60 (21)	0°	0.10... 0.40(4)	0						/4/
ZZ	2 thin plates	free space	W=μδwad	∞	45°, 90°(3)	0.10... 0.60(5)	-1.5.. +4		0.5... 2 (4)				/4/
ZZ	thick plate	free space	W=μδwap	∞	30°... 90°(5)	0.10... 0.60(5)	-2... +2	0.5, 1.0				horizontal and dipping upper edges	/4/
ZZ	half space	free space	W=$\sqrt{\mu\delta w}$, χ	1-14(10) .001-10		0 0-.6(6)	0 0					conductive susceptive	/4/
XX	1 or 2 thin plates	free space	W=μδwdh	0.5... 80 (11)	90°, 0°..90°	0.33... ∞ (3)						coincident loops	/1/
YY	thin plate	free space	W=μδwdh	0.5... 80 (11)	90, 0°..90°							coincident loops	/1/
ZZ	1 or 2 thin plates	free space	W=μδwdh	0.5... 80 (11)	90°	0.33... ∞ (4)						coincident loops	/1/
XZ	1 or 2 thin plates	free space	W=μδwdh	0.5... 80 (11)	90°, 0°..90°	0.33... ∞ (4)						coincident loops	/1/
ZZ	thin plate	free space	W=μδwad	∞	90°	0.10... 0.60(5)	0				0.4... ∞		/5/
ZZ	2 thin plates	free space	W=μδwad	1.75... 150 (4)	45°... 135°(3)	0.1, 0.3	-2... +3		0.5... 2 (4)				/5/

coil config.	type of scatterer	surround-ings	response parameter	value of r.p.	α	h/a	x/a	p/a	e/a	h_1/a	b/a	remarks	ref.
ZZ	thick plate	free space	W=μδwap χ	∞ 0.325	90° 0°,90°	0.10... 0.80(6)	-1.5.. +7	2,4 0.25,0.5			3.0, 6.0	conductive susceptive	/5/
ZZ	syncline, anticline	free space	W=μδwad	150	45°... 135°(3)	0.10... 0.60(5)	range 8a					r/a=3.2, contour maps	/5/
ZZ	complex shapes											extensive case histories	/5/
ZZ	thin plate	horizontal plate	W=μδwad $W_1=\mu_1\delta_1$wad	5.3... 69.3(5), 0...1.28(5)	45°, 90°	0.20	-1.5.. +1.5			0.10		positive screening	/7/
ZZ	thin plate	with and without a plate	W=μδwad W_1=μ,δ, wad	0.9... 44(12), .25... 15(17)	30°... 90° (5),0°	.05... 0.60(6)	-2... +2			0.05.. 0.20(3)		follow-up work of /4/ and /7/	/10/
ZZ	thin or thick plate	free space	W=μδwad W=μδwap	.9..44(17) 7.1... 40 (4)	5°.. 30°(4) 90°	0.10... 0.60(5)	-1... +6, -2.5.. +2.5	1.0,2.0			5.0	small dip angles	/6/
ZZ	1 or 2 thin plates	free space	W=τ/μδad δd=30	0.07... 0.2, 4 channels	30°... 110°(5)	0.10... 0.60(4)	range 4a		0.5, 1.5			crone PEM transient response	/16/
ZZ	thin plate	free space	δd (a=0.1m)	1260... 1710 (3)	0°	0.2... 1.2 (3)						PEM transient and step response	/15/
ZZ,ZX	thin plate	free space	W=μδwad	1... 100 (8)	5°... 175(13)	0.05... 0.90(6)	range 5.28a				1.2... 3.2 (3)	curves created by computer /13/	/14/

coil config.	type of scatterer	surround-ings	response parameter	value of r.p.	α	h/a	x/a	p/a	e/a	h_1/a	b/a	remarks	ref.
GSF-system II /12/	thin plate	free space	W=μδwad	1.75... 398 (5)	0°... 180°(13)	0.35, 0.47	-2... +2.5					15° tilted ZZ-geometry	/8/
GSF-system III /12/	thin plate	free space	W=μδwad	0.87... 398 (9), ∞	0°... 90°(4)	dipping plate h/a=1...2 (3), x/a=-3...+3, vertical plate h/a=0.5...10 (10), x/a=-3...+3, coplanar coils							/2/
GSF-system IV /12/	thin plate	free space	W=μδwad	0.87... 398 (9), ∞	0°... 90°(4)	dipping plate h/a=1...2 (3), x/a=-3...+3, vertical plate h/a=0.5...10 (10), x/a=-3...+3, coaxial coils							/2/
XZ	thin plate	free space	W=μδwad	199... 398 (3)	0°... 90°(4)	dipping plate h/a=1...2 (3), x/a=-3...+3, perpendicular coils at wingtips							/2/
GSF-systems I,II,III, IV /12/	thin or thick plate	free space or horizontal plate	13 different scale modelling series, characteristic curves										/11/
GSF-system IV (coaxial coils, fa=80500 m/s)	Half-space δ=.0003...5000 (21), h/a=0.60...9.20 (12). Susceptive half-space δ= $3\cdot10^{-5}$...50 (18), μr=1...2 (6), h/a=1.2 and 1.6. Susceptive half-space δ=10^{-4}...0.005 (5), μr=1.1, h/a=1.2...4.0 (6). 2-layer-model $\delta_1 d_1$=0.002...100 (15), μ2r=1...2 (6), h/a=1.2 and 1.6. Horizontal thin plate δd=0.05...2500 (14), h/a=0.60...9.20 (10). Horizontal layer δ=0.005...50 (12), d=2...∞ (5), h/a=1.6. Sphere δ=0.2...1000 (12), r/a=0.3...7.2 (19), h/a to centre 1.6...8 (5), amplitudes. Thin plate in free space δd=0.37...56 (13), α=30° and 90° h/a=1.0...2.0 (3), amplitudes. Thin plate in free space δd=5.6, α=30°...90° (3), h/a=1.0, x/a=-5...+5. Thin plate under a horizontal plate δd=0.37...∞ (3), $\delta_1 d_1$=0.19 and 1.2, α=90°, h_1/a=1.0...2.0 (3), amplitudes. Thick plate δf=1000 and 5000, α=90°, h/a=1.0, x/a=-5...+5, p/a=0.5 and 1.0.												/12/

List of symbols

- a coil separation
- b depth extent along the plate
- d thickness of an inductively thin plate or horizontal layer
- e separation between the upper edges of conductors
- h depth to the upper edge of conductor
- h_1 depth to the layer simulating overburden
- p thickness of an inductively thick plate
- r radius of sphere, radius of syncline or anticline
- x coordinate of the measurement profile with the origin above the body
- α dip angle clockwise from the horizontal
- f measurement frequency
- τ delay time after transmitter current shut-down
- ω angular frequency
- w electrical response parameter
- χ magnetic susceptibility
- μ magnetic permeability
- μ_r relative magnetic permeability
- μ_1 magnetic permeability of overburden
- σ electrical conductivity
- σ_1 electrical conductivity of overburden
- ZX transmitter dipole points upwards, receiver dipole in the direction of movement

The model curves are given in the order of three parameters. For a thin plate these are response parameter, depth and dip, and for a thick plate thickness, depth and dip. The three-dimensional linear interpolation always needs the eight nearest model curves.

The accuracy of the method depends on the number of model curves it involves and the number of points each model curve has. A large data bank improves the accuracy of the result, but the calculation takes longer.

A computer program with this kind of interpolation acts like an algorithm that calculates the real and out-of-phase anomalies as a continuous function of the model parameters. The range of this algorithm is limited by the original model curves. Thus, for a thin plate the response parameter varies between 0.9 and 44, the dip between 5 and 175 degrees and the ratio of depth to coil separation between 0.1 and 0.6. (Ketola and Puranen, 1967; Kurimo-Salminen, 1979; Ovaskainen, 1976).

The program is intended for Slingram interpretation, which is dealt with in the next chapter. It can also be used for calculating model curves for transient methods. Theoretically, the time domain and the frequency domain results contain the same information. In 1979, Silvennoinen applied the Fourier transformation to calculate model curves for a transient method from slingram results.

Slingram interpretation with the computer

Outokumpu Exploration stores all systematic geophysical measurements in an IBM 4341 computer with a disk as a medium. This IBM mainframe is also used for drawing contour maps and measurement profiles.

The interpretation is performed with an HP 984 desktop computer. This small computer features a central processor, keyboard, graphic display, thermal printer and two tape drives. The interpretation system described in the following is similar in use for magnetic, gravimetric

and Slingram methods.

The IBM magnetic disk currently contains 3.6 million Slingram data points. The desktop computer is used as a time-sharing terminal of the mainframe in order to retrieve the required slingram data. The connection is through a telephone line modem, and hence it can be used anywhere in Finland.

The search for the measured data is based on coordinates, frequency and coil separation. The search program stores the data on the tape through the telephone line. As an example, the transmission speed is such that it takes five minutes to handle 2,000 data points at a speed of 1,200 baud.

The interpretation program of the desktop computer, which is written in Basic, has about 1,300 lines, and the data bank has 940 model curves and almost 32,000 points. A measured line may have 151 points, and up to 10 plate models can be used. All these fill the computer memory of 186 K. The interpretation program has the following characteristics:

- it is conversational and interactive
- operation is similar to that of the magnetic and gravimetric interpretation program; hence, one has to learn to use only one of them
- measured data are read from the tape file or given manually
- the interpretation models are thin and thick plates
- the theoretical result is calculated by interpolation
- the measured and calculated curves with models are shown graphically on the display
- interpretation is effected with 32 special function keys
- model parameters are varied graphically, numerically or by an optimization algorithm
- as an example, the calculation speed permits in-phase and out-of-phase anomalies with 100 survey points to be calculated in nine seconds per model
- the interpretation result is drawn with a thermal printer or plotter.

This system has been applied to interpret the field measurements shown in Fig. 2.

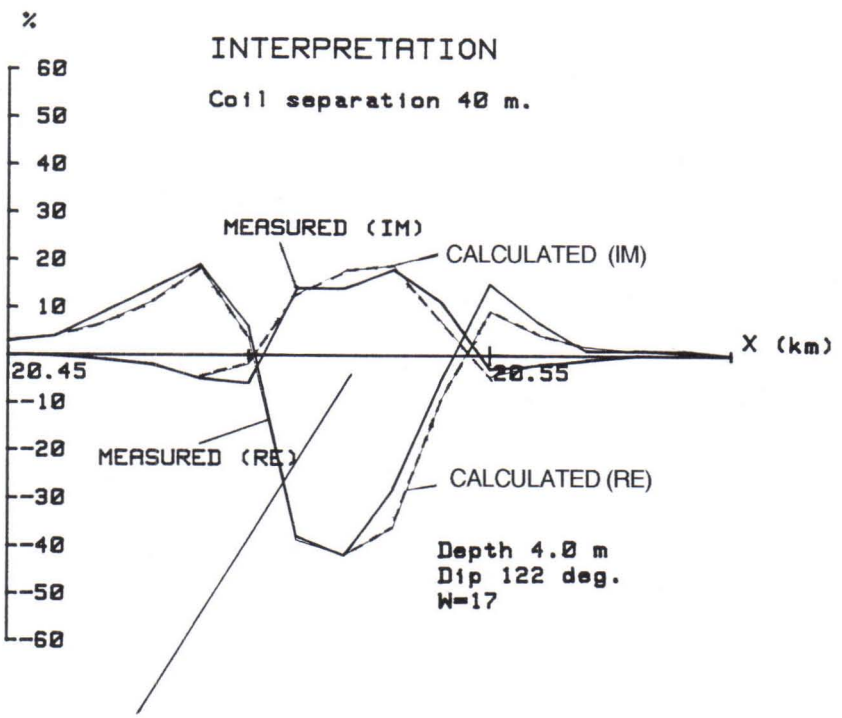

Fig. 2. Interpretation example.

The shape of the anomalies allows the thin plate to be used as a model. For the geometrical parameters, the interpretation agrees well with the drilling results.

Determination of the depth extent of plates and utilization of a horizontal component be means of numerically calculated type curves

A more recent, numerically calculated, data bank contains 132,480 anomaly values in per mille of the primary field arranged in six tables. To limit the size of the bank, a procedure was applied that did not require storage of the coordinates of the stations.

For calculation of the anomaly corresponding to a chosen parameter combination (α, W, h/a, b/a), the program, GEFINT (Rossi, 1985), performs a hyperparabolic interpolation in three or four dimensions. Third degree polynomial surfaces are used in a two-dimensional interpolation. Finally, the anomalies at the stations measured are obtained by Lagrangian interpolation.

It takes between 4 and 10 seconds to calculate and display a HLEM profile containing 60 anomaly values. The same interactive main program that controls the interpretation based on the scale modelling data bank (half-infinite plates and without a horizontal component) is used as the link between the interpolation procedures and the user.

It has been established that the in-line horizontal component is sensitive to small changes in the dip angle of a plate close to 90 degrees (Fig. 3).

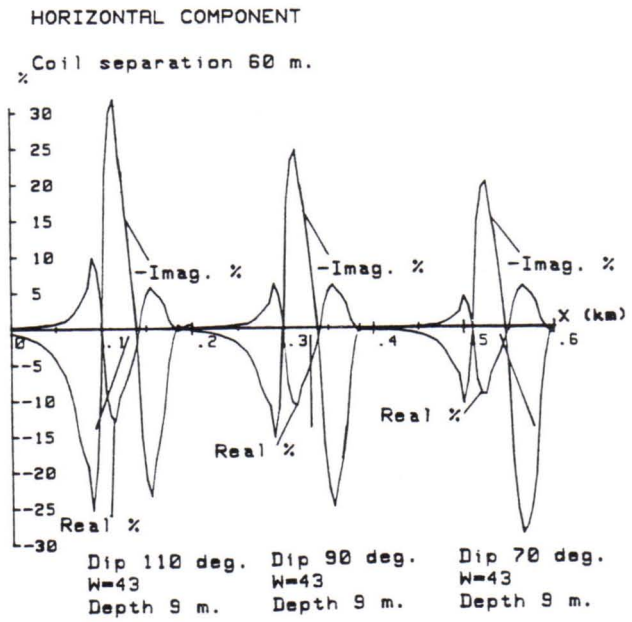

Fig. 3. Effect of the dip angle on the horizontal component anomaly. The depth to the lower edge is 111 m and the coordinate of the transmitter is greater than that of the receiver.

Combined use of vertical and horizontal components enhances the reliability of interpretation. The setting of the lower edge of the plate to a finite depth may considerably improve the compatibility between the measured and calculated anomalies. An experimental

interpretation was performed for a case in which a resistive horizontal fracture zone is likely to exist in the prospecting area. The optimization algorithm sets the lower edge to a finite depth. A horizontal mylonite zone 2 m thick was detected at a depth of 1.2 a in the target rock volume in two boreholes spaced 100 m apart. Fig. 4 illustrates the effect of the size of a finite plate on a vertical anomaly.

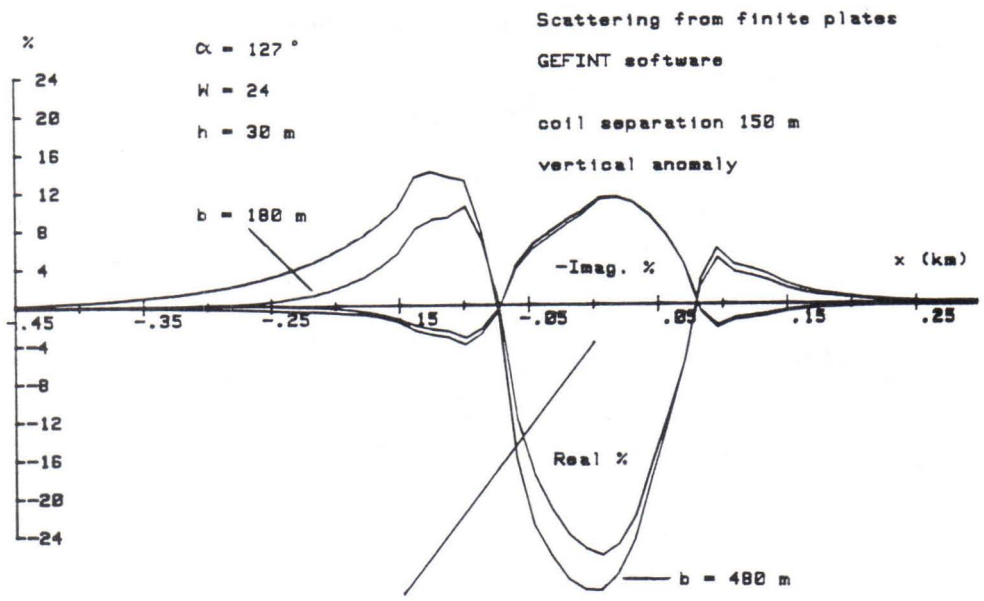

Fig. 4. Effect of depth extent on the anomaly when $\alpha = 127°$, w = 24, h/a = 0.20.

The computer program GEFINT is being used with the Finnish GEFINEX EM 303 HLEM system, which automatically measures the three orthogonal field components at five frequencies and stores the results in a 256 Kb CMOS RAM.

Usability and extension potential of the interpretation system

The interpretation system based on the data bank is useful only within the limits of the original model curves. However, an individual thick plate seldom meets the requirements for an interpretation model. In the case of a thick plate there is usually an imaginary component anomaly, and hence the conductivity is no longer infinite. Even more difficult to handle are the cases that involve a conductive medium, conductive overburden or several plates close to each other. This interpretation system cannot be applied under these conditions.

There are several ways of extending the interpolation solution for new parameters. The simplest is to generate correction coefficients and functions. Then there is no need to increase the data bank. However, this could lead to difficulty with the accuracy of the space of extension.

Another procedure would be to calculate or measure model curves for a new interpretation parameter, for instance, thickness. This, however, would make the data bank larger and reduce the speed of the interpretation program. Furthermore, the desired parameter cannot necessarily be dealt with using the present scale model equipment or numerical

solution program.

The case of plates situated close to each other involves, in principle, consideration of all possible combinations. This would, however, lead to far too many model curves for an application of this kind.

Despite these limitations, we conclude that the solution based on the interpolation of model curves is useful. Its use should be considered whenever calculating a geophysical anomaly would be slow or difficult. Because scale model measurements and numerical solutions can be utilized effectively in this system, it is worthwhile developing them both in the future to meet the demands of practical interpretation problems.

References

Hjelt, S.E., 1968. On the half-plane model in double-dipole electromagnetic prospecting. Acta Polytechnica Scandinavica Ph 60.

Hämäläinen, T., 1975. Aerosähköisiin matalalentomittauksiin liittyviä pienoismallimittauksia. Unpublished M. Eng. thesis (in Finnish), Helsinki Univ. of Tech.

Jain, S.C., 1973. Inline and broadside EM dipole dipole profiling over a thin vertical infinitely conducting vein. Geophysical Prospecting 21: 648 - 659.

Ketola, M. & Puranen, M., 1967. Type curves for the interpretation of slingram (horizontal loop) anomalies over tabular bodies. Geol. Surv. Finland, Rep. Invest. 1.

Ketola, M., 1968. The interpretation of slingram (horizontal loop) anomalies by small-scale model measurements. Geol. Surv. Finland, Rep. Invest. 2.

Kurimo-Salminen, M., 1979. Loivakaateisen puolitason ja homogeenisen irtomaakerroksen slingram-anomalioista. Unpublished M. Eng. thesis (in Finnish), Helsinki Univ. of Tech.

Leino, K., 1972. Sähköisista pienoismallimittauksista ja johtavan irtomaapeitteen vaikutuksesta Slingram-anomaliaan. Unpublished M. Eng. thesis (in Finnish), Helsinki Univ. of Tech.

Liljestrand, B., 1972. Pienoismallimittauksia aerosähköisten anomalioiden tulkintaa varten. Unpublished M. Eng. thesis (in Finnish), Helsinki Univ. of Tech.

Linnakylä, T., 1983. Sähkömagneettisia pienoismallikokeita pallomaisilla naytteillä Unpublished M. Eng. thesis (in Fin nish), Helsinki Univ. of Tech.

Ovaskainen, E., 1976. Pienoismallimittauksia Slingram-menetelmällä. Unpublished M. Eng. thesis (in Finnish), Helsinki Univ. of Tech.

Ovaskainen, E. & Peltoniemi, M., 1979. Geologisen tutkimuslaitoksen käyttämille aerosähköisille mittauslaitteistoille suoritettuja pienoismallimittauksia. Geol. Surv. Finland, Dept. of Geoph., rep. Q 16.2/24.8/79/2 .

Peltoniemi, M., 1982 . Characteristics and results of an airborne electromagnetic method of geophysical surveying. Geol. Surv. Finland, Bul letin 321 .

Rajala. J. & Sarvas, J., 1985. Electromagnetic scattering from a plate-like, non-uniform conductor. Acta Polytechnica Scandinavica Ma 43.

Rossi, M., 1985. Monikomponenttimittaus ja tulosten levymallitulkinta pystyn magneettisen dipolilähteen jarjestelmässä. Unpublished M. Eng. thesis (in Finnish) with an English abstract, Helsinki Univ. of Tech.

Rouhiainen, P., 1983. Sähkömagneettisen malminetsintälaitteen pienoismalli. Unpublished Lic. Eng. thesis, Helsinki Univ. of Tech.

Silvennoinen, H., 1979. Transienttitulosten tulkinnan kehittämisestä ohutta levymallia käyttäen. Unpublished M. Eng. thesis (in Finnish), Helsinki Univ. of Tech.

Valkeila, T., 1978. Slingram-menetelmän tietokonetulkinnan kehittäminen. Unpublished M. Eng. thesis (in Finnish), Helsinki Univ. of Tech.

MULTIFREQUENCY EM MEASUREMENTS NEAR CONDUCTIVE OREBODIES

by

K. Aittoniemi, M.T. Hirvonen, J. Rajala, J. Sarvas and J. Soikkeli

Aittoniemi, K., Hirvonen, M.T., Rajala, J., Sarvas, J. & Soikkeli J., 1990. Multifrequency EM measurements near conductive orebodies. *Geologian tutkimuskeskus, Tutkimusraportti 95.* 38-45, 5 figs.

Some aspects of frequency-domain EM measurements with controlled sources are briefly described together with a plate model for their interpretation. Studies of two conductive dikes, one containing metal sulphides, the other graphite schists, are reported in detail. In each case, the results of the multifrequency measurements are interpreted in terms of an electrically heterogeneous plate model. Good agreement is reached between the experimental and theoretical results. The principal conclusions emerging from the interpretations concern the depth extents and conductivity-thickness distributions of the dikes. In both cases, the minimum depth extent consistent with the experimental results exceeds that verified by drilling. The conductivity-thickness product increases with depth in both dikes. In the graphite dike, a minimum is observed in the strike direction, agreeing with earlier investigations.

Key words: electromagnetic methods, electromagnetic induction, frequency sounding, numerical models, electrical conductivity, anomalies, dikes, Kiuruvesi, Kiihtelysvaara, Finland

Айттониэми, К., Хирвонен, М.Т., Раяла, Й., Сарвас, Й., Сойккели, Й., 1990. Спектральные электромагнитные измерения вблизи проводящих рудных тел. Геологический центр финляндии, Рапорт исследования, 95. 38-45. Идд. 5.

Кратко описываются некоторые аспекты широкочастотных электромагнитных измерений с управляемым источником и пластинная модель для их интерпретации. Детально описаны исследования на двух проводящих дайках - одной, содержащей сульфидные минералы, и другой с графитовыми сланцами. В обоих случаях результаты спектральных измерений интерпретированы с помощью модели электрически неоднородной пластины. Получена хорошая корреляция между опытными и теоретическими данными. Основные выводы, возникающие при интерпретации, касаются протяжения на глубину и распределения проводимости и мощности даек. В обоих случаях минимальное значение глубины, соответствующее опытным данным, превышает значение, установленное бурением. Произведение проводимости и мощности возрастает с глубиной в обеих дайках. В графитовой дайке отмечается минимум в направлении простирания, что подтверждает полученные ранее данные.

Introduction

Electromagnetic fields have long been utilized in prospecting for metallic orebodies, as such bodies often differ from their surroundings in electrical conductivity, magnetic permeability or electric polarizability. The incident or primary fields used in practice are almost always time-dependent, whether they are natural or artificial. The time dependence of an artificial source can be chosen by the user, and it is usually pulse-like ("time-domain" measurements) or sinusoidal ("frequency domain") (Ward et al., 1974; Lodha ,1977; Pridmore et al., 1979). In this article we restrict ourselves to continuous sinusoidal primary fields generated by artificial sources. The primary purpose of the work reported here was to learn to what extent measurements taken on the various spatial and time components of the B-vector near conductive bodies with controlled sources can be made to agree with detailed model calculations in a broad frequency range. We make two simplifying assumptions throughout this report. First, there is no magnetic contrast between the target body and its surroundings. Second, there is a substantial conductivity contrast in the sense that the inductive response of the target appears in a frequency range clearly separated from the range where the environment responds. The latter condition ensures the possibility of an interpretation of the observed results in terms of scattering models.

Conductive dikes were chosen as targets, because they are common in Finland and because a computer program is available which calculates the EM field of an oscillating source in the presence of a plate-like conductor under reasonably general conditions (Rajala and Sarvas, 1985). The targets are not known to have interfering conductors in their vicinity. We will show that a remarkably good agreement in a broad frequency range can be achieved between measurements and model calculations. In addition, we obtain new information on the targets, which was our secondary purpose in this study.

The conductive deposits are modelled by a thin plate of finite extent, situated in a homogeneous space of conductivity σ_0, of permeability $\mu_0 = 4\pi \cdot 10^{-7}$ Vs/Am, and of permittivity $\varepsilon_0 = 8.8542\text{-}10^{-12}$ As/Vm. The system is excited by a point dipole of arbitrary location and orientation, or by a larger inductive or galvanic transmitter, and the position of the point of observation is also arbitrary. The plate can differ to an arbitrary degree from the environment in its conductivity. The discretized integral equation method is used to calculate the scattered B-vector. The plate is divided into rectangular cells, and a constant conductivity-thickness product is assigned to each cell. Thus the plate can be electrically heterogeneous. The secondary current density js is assumed to be constant within any given cell, and the resulting matrix equation is solved for the values of js. The scattered field is then calculated by using js as the source. Because of the discretization, the results become inaccurate especially when the source is very near the plate. An approximate rule is that a distance of two cell dimensions is enough to ensure sufficient accuracy in practice. Before the computed results were compared with experimental ones, it was made sure that they stabilized within reasonable limits as the cell size was decreased.

Study of a sulphide deposit

A deposit of pyrite and pyrrhotite at Hallaperä, Kiuruvesi, central Finland, was chosen for detailed studies. The deposit is a thin dike whose upper edge is covered by an overburden only a few meters thick. The thickness of the dike is of the order of ten meters or less, the total length is about 1800 m, and the dip angle about 60°. This information had been derived earlier from magnetometric (maximum anomaly 4μT) and slingram measurements, and a few drillholes. The drillholes being rather shallow (penetrations at vertical depths between 40 m and 150 m), the position of the lower edge is unknown. The deposit seems to be continuous along its strike, but in the transverse direction it is known to consist in somr places of separate branches. Measurements on core samples indicate that the small-scale conductivity is not uniform.

The measurements were conducted on a section 200 m long at about the middle of the deposit using a square loop of measuring10 m x 10 m as the transmitter (Fig. 1). The loop was mounted on a wooden frame in order to have it lie entirely in a horizontal plane. There are three drillholes on the central profile K = O, and the dike seems to be unbranched there, while the holes on the side profiles K = -80 and K =120 indicate branching.

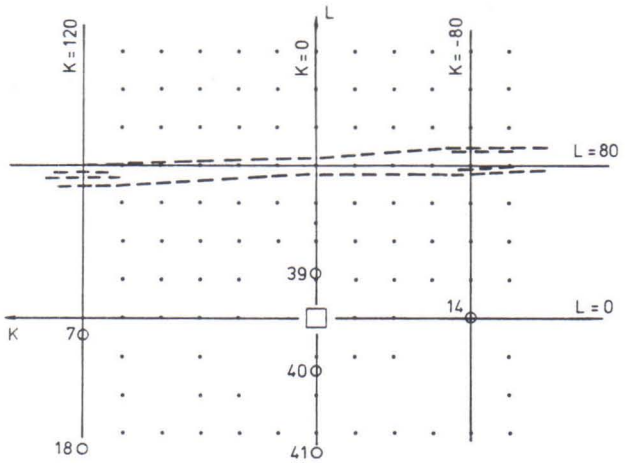

Fig. 1. Schematic drawing of the measurement situation from above. □ Transmitter , ... Observation points, --- Outcrop of the deposit, O Drill hole.

The points of observation were arranged in a square network of 20 m x 20 m cells with additional points on the central profile. The altitude of each point relative to the center of the transmitter was carefully determined. The Z-, L- and K-components of the total flux density B at 16 logarithmically spaced frequencies in the range 10 Hz - 10 kHz were measured at each point of observation. In addition, the component parallel to the hole axis was measured in drillholes 39 and 40 at the points where the holes penetrate the deposit. A description of the sensing equipment, the measurement system and the data processing is given elsewhere (Aittoniemi et al., 1985).

For the interpretation of the results, it is assumed that the actual geological situation is well enough represented by the plate model, the rectangular model is soaght that best explains the observations. In the absence of evidence for significant lateral variation (K-dependence) in the conductivity-thickness product, we chose to use only the data obtained on the central profile K = O. Since the observed K-components of B were very small on this profile, the upper edge of the plate was constrained to be parallel to the K-axis. These restrictions make it easier to evaluate the most interesting parameters, namely, the downward extent and the conductivity-thickness variation in the plate. The horizontal length of the plate was fixed at 400 m, which was practically equivalent to infinity.

Fig. 2 shows the experimental results obtained at selected points on the central profile, together with the corresponding responses of the best model, to be described later. The overall frequency dependences are typical in that the real parts rise from zero at low frequencies to saturation at high frequencies, while the imaginary parts exhibit a maximum at an intermediate frequency. The more subtle features, especially the saturation levels at high frequencies and the positions of the maxima on the frequency axis, can be used for detailed interpretation. Since the influence of the conductivity distribution eventually disappears as the frequency is raised, we may use the levels at 10 kHz to determine the geometrical parameters independently of the conductivity. The real part of B_Z exhibits a sharp transition, and that of B_L a peak above the upper edge. The observed values are best explained by setting the upper

edge at L = 80 ± 3 m, in good agreement with the available geological information.

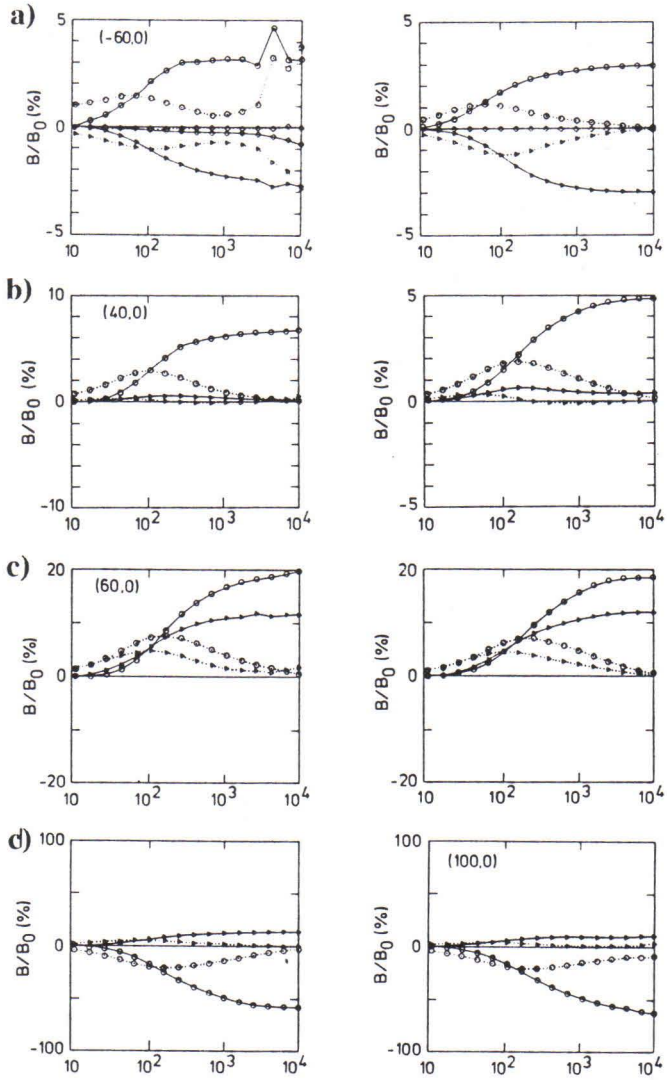

Fig. 2. Results of measurements at points on the central profile K = 0 (left) and the corresponding model results (right) computed from the model of Fig. 3. The vertical scale is normalized by B , the real part of B_Z at 10 Hz, and the real parts at 10 Hz have been subtracted from all three components at all frequencies. O B_Z; Δ B_L; ◊ B_K; — Re; ···· Im. a) Observation point (-60,0), b) (40,0), c) (60,0), d) (100,0).

Similarly, the best value of the depth of the upper edge is between 2 m and 5 m, also in agreement with other data. For the determination of the dip angle, values of B_Z and B_L were computed for various angles. Comparison with the observed values showed that the best value of the dip angle is very near 60°. Finally, to determine the downward extent of the plate, values of the B_Z and B_L were computed for various extents and compared with the observed values. Apparently, the plate must extend more than 150 m downward to explain the observed values. However, below about 200 m the sensitivity is lost, and it can only be concluded that the plate must extend at least 200 m downward.

The geometrical parameters having been determined one looks for that distribution of the conductivity-thickness product which best explains the observed frequency dependences of B_Z and B_L. Attempts to reproduce the observed dependences by a homogeneous model resulted in qualitative agreement, with 65 S as the best value of the average conductivity-thickness product. However, the observed positions and shapes of the maxima of the imaginary parts of B_Z and B_L at the various points could be reproduced in detail only by an inhomogeneous plate. The smoothly varying distribution shown in Fig. 3 gave the closest agreement with the observations, and it was used to compute the responses in Fig. 2. The observations can be explained only with a downward increasing distribution down to about 100 m, below which the distribution no longer influences the computed response.

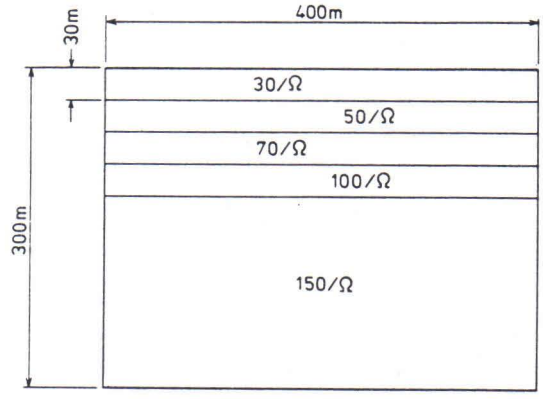

Fig. 3. The model that best explains the observed results on the central profile K = O.

The above interpretation was carried out using only data obtained on the ground. The results of measurements in drillholes 39 and 40 are in qualitative agreement with the corresponding results from the model, but the maximum in the imaginary part from drillhole 40 lies at a lower frequency than in the computed results. This indicates that the conductivity-thickness product may actually increase faster with increasing depth than in the model.

Study of a graphite deposit

A deposit containing up to 40 % of amorphous graphite at Kiihtelysvaara in eastern Finland was chosen as another target. This schist dike exhibits only a slight magnetic anomaly. The thickness of the dike varies from 2 m to about 30 m, and the horizontal length is at least 2000 m. The upper overburden covering the edge is only a few meters thick. The dip angle varies between 60° and 75° according to slingram measurements The deposit is possibly discontinuous at some points along the strike, and it is known to split into parallel branches in some places. The few existing drillholes are less than 80 m deep, and the depth of the lower edge of the dike is unknown.

The measurements were conducted on a section 200 m long located some 400 m north of the estimated midpoint of the deposit. The outcrop is less than 15 m thick throughout this section, with a very thin point in the middle, and the dip seems to be close to 70°. Preliminary measurements showed that very low frequencies were needed to observe the details of the inductive response, which indicated a very high conductivity in the dike. A frequency band of 0.2 Hz to 130 Hz was chosen accordingly, and in order to reach adequate signal levels a

two-turn unshielded loop measuring100 m x 100 m and of low-frequency moment 200 kAm^2, laid freely on the ground, was used as the transmitter. The final measurement situation is shown schematically in Fig. 4.

The Z-, L- and K-components of the total flux density produced by the loop transmitter were measured at each observation point. The K-components were very small on the central profile K = O, and the results at (50,-100) and (50,100) also indicated approximate symmetry with respect to K = O. However, the maxima of the imaginary parts indicated some lateral variation in the conducti vity-thickness product. Some measurements of the flux density produced by the electric transmitter were also made, but their results were not used in the interpretation.

An interpretational procedure similar to the one just described was carried out with the important difference that the results on three profiles (Fig. 4) were considered simultaneously. Several properties of the plate were fixed at the beginning. The upper edge was horizontal and directed as the vector (-1,20) in the LK-plane. Its horizontal distance from the center of the loop along the central profile was 100 m, and its length was fixed at 500 m.

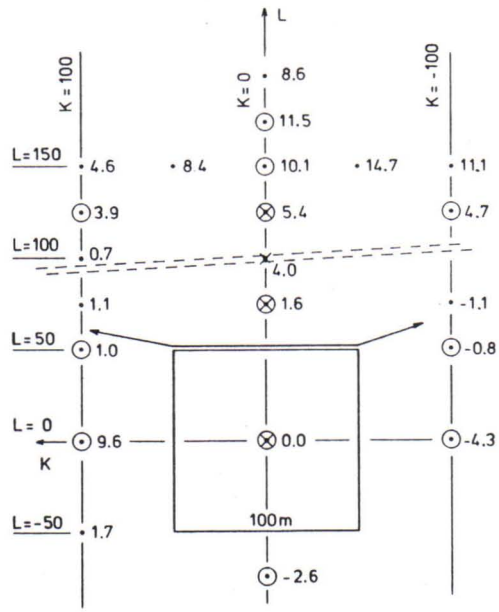

Fig. 4. Diagram of the foregoing measurement situation. --- Outcrop of the deposit, · · · Observation points, O Point used in the interpretation.
The square loop was not planar owing to the topography. The grounding points of an electric transmitter are marked with arrows and the corresponding observation points with X. The numbers give the relative altitudes in meters.

The other geometrical parameters were determined on the basis of the saturation levels at 130 Hz. The best values of the depth of the upper edge and the dip angle turned out to be 2 m (6 m below ground level at (100,0)) and 65°. The computed results were sensitive to the downward extent of the plate up to about 200 m, and it can be concluded that the plate extends at least 200 m down.

The distribution of the conductivity-thickness product was finally determined. About 60 trials were made altogether using seven frequencies selected from the experimental band. The goodness criterion was the sum of the squares of the differences of the experimental and theoretical results, over the frequencies, the components and the points of observation. The

distribution was sought in the form

$$\sigma d = (\sigma d)_0 \ (1 + a_1 x + a_2 x^2) \cdot \ (1 + b_1 y + b_2 y^2),$$

where the y-axis is parallel to the upper edge and the x-axis points downward in the plate. Such a distribution gave clearly better fits than constant ad. To avoid excessively high values for large values of y the values of ad were limited to a maximum of 7000/Ω which resulted in better fits than the unlimited parabolic dependence. The approximate x-dependence was first determined on the basis of B_Z and B_L on the central profile. The final distribution was L, then determined by considering all three components of at points on all three profiles. The distribution that best explains the observed response is shown in Fig. 5. As in Section 2, the computed results are not sensitive to variations below about 100 m. Two general conclusions can be drawn. The value of ad in the plate increases downward, and in the lateral direction it exhibits a minimum close to the central profile. The latter feature agrees with earlier information about the thickness of the dike.

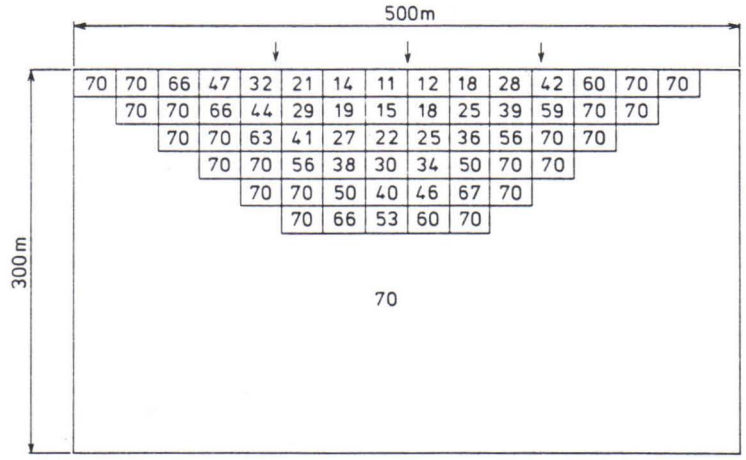

Fig. 5. The model that best explains the observed results at the points encircled in Fig. 4. The values of σd are given in units of 100 S. The approximate locations of the measurement profiles are marked by arrows.

Discussion

In principle, measurements at a single high enough frequency are sufficient for the determination of the geometrical features of the target. However, the use of a broad frequency band offers several advantages. It reveals the possible influence of the environment of the target and thus indicates roughly its conductivity. An initial frequency sweep is needed to choose the right band for the response of the target. A broad-band measurement offers a good experimental means of removing the primary field from the results and makes it easier to assess their reliability. Broad-band data are necessary for the determination of the distribution of the conductivity-thickness product in the target.

The measurement of at least two spatial components of the field is essential if a detailed mapping of the geometry of the target is intended. It is even more important for the determination of the conductivity distribution. If the conductivity varies in two directions, all three components are required. Multicomponent measurements may generally help to reduce the number of observation points needed for the interpretation.

Acknowledgment

The authors are grateful to the Outokumpu Oy Electronics Division for its support to this work.

References

Aittoniemi, K., Hirvonen, M.T., Rajala, J., Sarvas, J. & Soikkeli, J., 1985. Broadband electromagnetic measurements over conductive orebodies and their interpretation with heterogeneous plate models, Acta Polytech. Scand. Ph 151.

Lodha, G.S., 1977. Time domain and multifrequency electromagnetic responses in mineral prospecting Ph.D. Thesis, University of Toronto.

Pridmore, D.F., Ward, S.H. & Motter, J.W., 1979. Broadband electromagnetic measurements over a massive sulfide prospect, Geophysics 44, 1677.

Rajala, J. & Sarvas, J., 1985. Electromagnetic scattering from a plate-like non-uniform conductor. Acta Polytech. Scand. Ma 43.

Ward, S.H., Pridmore, D.F., Rijo, L. & Glenn, W.E., 1974. Multispectral electromagnetic exploration for sulfides, Geophysics 39, 666.

Electromagnetic methods and equipment

GROUND EM METHODS AND EQUIPMENT USED IN ORE PROSPECTING IN FINLAND

by

S.-E. Hjelt, A. Hattula, T. Jokinen and E. Lakanen

Hjelt, S.E., Hattula, A., Jokinen, T. & Lakanen, E., 1990. Ground EM methods and equipment used in ore prospecting in Finland. *Geologian tutkimuskeskus, Tutkimusraportti 95.* 47-52, 3 tables.

The paper brings together information about the EM methods and equipment used in Finland in connection with prospecting for mineral ore bodies (the situation at the beginning of 1986). The material is organized following the type of the source field into plane wave, long cable, large loop and magnetic dipole methods. The time domain equipment is described as a separate group. Only ground measurements are considered and the data is presented in table form. Examples of data presentation and special interpretation procedures are also given, but detailed case histories are confined to other papers in this issue.

The Slingram (horizontal loop) method has traditionally been the main method used in EM prospecting in Finland. It has been used to locate well conducting (out-cropping) bodies in the upper part of the bedrock. During the late '70s, greater emphasis was given to structural studies, whence methods allowing also for the determination of resistivities have been taken into use. Multifrequency methods have become popular very slowly in Finnish mineral prospecting.

Key words: geophysical methods, electromagnetic methods, electromagnetic induction, mineral exploration, geophysical surveys, frequency sounding, transient methods, instruments, Finland

Ельт, С.-З., Хаттула, А., Йокинен, Т.И., Лаканен, З., 1990. Наземная электромагнитная методика и аппаратура, преименяемая при поисках полезных ископаемых в финляндии. Геологический центр финляндии, Рапорт исследования, 95. 47-52.

В работе сведены данные по электромагнитной методике и аппаратыре, применяемой в финляндии при поисках месторождений полезных ичкопаемых. Материалы распределены по типам источника поля на следующие главы: методы плоской волны, длинного кабеля, большой петли и магнитного диполя. В особую группу выделена аппаратура временной области. Рассматриваются исключительно наземные измерения, и данные представлены в виде таблиц. В работе приведены также примеры изложения денных и специальные алгоритмы для их интерпретации, но детальное описание действительных случаев выходит за рамки данной статьи.

Традиционно, основным методом электромагнитьой разведки в финляндии всегда был метод горизонтальной петли (Slingram). Его целью была локализация хорошо проводящих (обнажающихся) рудных тел в верхней части кристаллического фундамента. В конце седьмидесятых годов внимание стало больше уделяться структурным исследованиям; при этом стали применяться методы, позволяющие также определение сопротивления. Потихоньку в геологоразведочной практике в финляндии получили распостранение и спектральные (многочастотные) методы.

This paper summarizes the information about the ground EM methods and equipment used in Finland in mineral prospecting. The data are presented in table form and describe approximately the situation at the beginning of 1986. (*Editor's note: During the late '80s, mineral prospecting in Finland was completely reorganized. The prospecting department of Rautaruukki Co. ceased to operate. Its geophysics field crew and equipment were overtaken by Outokumpu Oy , only to be soon transferred, together with the majority of the ground geophysics field crew at the Geological Survey of Finland, to Suomen Malmi. Originally, the manuscript also contained examples of data presentation and a table on interpretation and computer modelling programs. Because of the reorganization and rapid changes in advanced measuring, data processing and interpretation techniques, this material would have been less informative and has thus been omitted from the final version of the paper.*)

Detailed case histories are confined to other papers included in this issue, which also discuss the virtues and drawbacks of various methods in more detail. A separate paper (Valkeila and Rossi, this issue) summarizes the extensive scale modelling work for the EM dipole method, that has taken place over the years in Finland. The history of exploration geophysics in Finland has recently been presented by Ketola (1986), to whose paper the reader is referred for more detailed information on the development of EM methods in Finland.

The horizontal loop (Slingram) method has traditionally been used in EM prospecting in Finland. It has been suitable for locating well conducting (out-cropping) bodies the main method used in the upper part of the bedrock in resistive environments. During the late '70s, greater emphasis was given to structural studies also in prospecting. The methods allowing also for the description of the resistivities of the bedrock surrounding good conductors have therefore become more and more important and been taken into use. Multifrequency- and time-domain methods have become popular more slowly in Finnish mineral prospecting. Over the years, in Finland, more interest seems to have been drawn to instrumental than methodological developments in ground EM methods.

EM methods can be classified in a number of different ways. In this paper, the type of the source field has been used, since in addition to frequency of operation it is the basic factor controlling the depth of penetration of EM methods. The material is organized into plane wave, long cable, large loop and magnetic dipole methods. Time domain methods and equipment are described as a separate group. For the basic theory of the various EM methods the reader is advised to consult either any of the general textbooks on applied geophysics or the wealth of special monographs, that have been published during the past few years.

Definition of methods

Plane wave methods

A plane EM wave field has the greatest depth penetration at a given frequency. The primary fields may be either natural or artificial. In the VLF method, signals from distant radio transmitters are measured; and in the audiomagnetotelluric (AMT) method, the time variation of the Earth's geomagnetic field is registered. The VLF method is a single frequency method suitable typically for regional reconnaissance work, whereas AMT is a multifrequency method, thus providing sounding information (distribution of electrical conductivity versus depth).

Methods using long cable transmitters

The primary field of a long grounded cable is attenuated approximately as 1/r in a highly resistive environment. For shorter cable lengths, the primary field resembles that of an electrical

dipole. For measurements taken close to the side of a large, ungrounded rectangular loop, the long cable approximation is also valid (cf., next paragraph).

The TURAM long cable method was more extensivley used in Finland during the '50s. Of the recent long cable measurements in Finland, the CSAMT experiment described by Hjelt et al. deserves to be mentioned.

Methods using large loop transmitters

For measurements taken close to the side of a large, ungrounded rectangular loop the long cable approximation for the primary field is valid, whereas far from the loop the field is that of a magnetic dipole. Elsewhere around large loop systems the primary field has a complicated geometrical pattern and interpretation requires advanced computer modelling techniques.

Large loop transmitters have been employed in Finland in connection with time domain measurements, using, for examples, MPP and SIROTEM equipment and in connection with some recent multifrequency experiments. These measurements contain a wealth of information, of both geometrical and sounding types. The interpretation consequently again requires rather complicated techniques.

Methods using magnetic dipole transmitters

The source field is produced by small (diameter typically 0.5 - 2 meters), ungrounded loops. Similar loops (or their equivalent ferrite cored rods) are employed as receivers. The primary field is that of a magnetic dipole, which decreases in a resistive environment as $1/r^3$.

Magnetic dipole systems can be easily varied to produce a large variety of transmitter-receiver geometries. These variations have been exploited more in airborne EM systems. In the most popular ground EM method used in Finland, the Slingram method, both the transmitter (Tx) and the receiver (Rx) loops are horizontal. In certain one-man instruments (referred to in the tables as mini-Slingrams), the receiver rod is oriented so as to be perpendicular to the transmitter field.

The Slingram method has proven useful for locating well conducting (out-cropping) bodies in the upper part of the bedrock in resistive environments. Recent instrumental developments allow several transmitter-receiver separations and/or multifrequency operation, thereby giving additional information of a sounding type.

Time-domain versus frequency-domain measurements

Theoretically, there is no difference between the time- and frequency-domain methods when the same transmitter-receiver geometry is used, since any time-domain response is the integral over all the frequencies of corresponding frequency-domain responses and vice versa. The exact two-directional correspondence holds only for an inifinite frequency band. Therefore there is no one-to-one correspondence between the response of a certain target at one frequency and the response at a given decay time. In general, however, high frequency information is contained in the early parts of a transient field signal and the low frequency information in the late parts of a transient field signal.

The main advantage of time domain systems is, that the secondary field response can be measured when the primary field introduces no signal in the receiver. Thus the geometrical properties of time domain systems can be much more easily varied than those of frequency-domain systems. Borehole variants of ground EM methods typically employ time-domain techniques.

Time-domain measurements contain sounding information. Changes in the transmitter pulse forms change the frequency content of the transient responses. This has to be taken into account when the performance and depth penetration properties of the various instruments are compared.

Methods used in ground EM prospecting in Finland

Table 1. Gound EM methods used for ore prospecting in Finland until the end of Grouping according to the type of source field.

METHOD	SOURCE	FIELD COMPONENT MEASURED	DOMAIN F = FREQ. T = TIME	USE R = ROUTINE S = SPECIAL T = TEST	SITE G= GROUND B = BORE-HOLE
AMT	PLANE WAVE	HX, HY, EX, EY	F	S	G
VLF-Resistivity	PLANE WAVE	HX, EY	F (1)	R-S	G
VLF tilt angle	PLANE WAVE	HX, HZ	F (1)	S-R	G
CSAMT	LINE CURRENT	HX, HY (EX, EY)	F	T	G
TURAM	LINE CURRENT	HX1, HX2	F (1)	S	G
	LARGE LOOP	HZ (HX, HY)	T	S	G
SLINGRAM	EM DIPOLE	HZ	F (1)	R	G
mini-SLINGRAM	EM DIPOLE	$H_{sek} \perp H_{prim}$	F (1)	R	G
MULTIFQ.	EM DIPOLE	HX, HZ	F (n)	T and S	G
TD	EM DIPOLE	HZ (HX, HY)	T	S	G, B

EM prospecting equipment used in Finland

Table 2. List of ground EM equipment in active use in Finland until 1985.

METHOD	EQUIPMENT	MANUFACTURER	IN FINLAND SINCE	USER ORGANIZATION	NO. of UNITS (1985)
AMT	ECA 541-0	SOCIETÉ ECA, FRANCE	1976	UO, OK	2
-"-	ECA 542-0	SOCIETÉ ECA, FRANCE	1980	UO	1
VLF-resistivity	EM-16R	GEONICS, CANADA	197?	UO, OK, GSF	5
VLF tilt angle	VLF/GSF	GSF	1968	GSF	10
VLF tilt angle	EM-16	GEONICS, CANADA	1969	SM, GSF, OK, UO	14
TURAM	GSF/Puranen	GSF	1960	GSF	-
SLINGRAM	OK	OUTOKUMPU, FINLAND	1962	OK, (UO)	7
SLINGRAM	OK/HF	OUTOKUMPU, FINLAND	1969	OK	3
SLINGRAM	GSF/Puranen	Geol.Surv.F., FINLAND	1960	GSF	16
SLINGRAM	GSF/HF	Geol.Surv.F., FINLAND	1960	GSF	16
SLINGRAM	EM-69-2	BOLIDEN, SWEDEN	1977	RR	1
SLINGRAM	EM 31	GEONICS, CANADA	1977	OK	1
mini-SLINGRAM	PROXAN	OUTOKUMPU, FINLAND	1968	RR, OK	3
mini-SLINGRAM		SGU, SWEDEN	197?	GSF	-
mini-SLINGRAM		GSF, FINLAND	1953	GSF	12
mini-SLINGRAM	Double-dipole	APEX, CANADA	1975	RR	2
mini-SLINGRAM	GEFINEX 200	OUTOKUMPU, FINLAND	1981	OK	25
MULTIFQ.	MaxMin II	APEX, CANADA	1978	RR, OK, GSF, SM	10
MULTIFQ.	MaxMin II ++	APEX, CANADA	1985	RR, OK, GSF	4
MULTIFQ.	GEFINEX EM303	OUTOKUMPU ELECTR.	1985	OK (GSF)	5
MULTIFQ.	GEFINEX EM400S	OUTOKUMPU ELECTR.	1986	OK	1
TEM	PEM	CRONE, Canada	1975	SM	1

Table 3. Properties of ground EM frequency domain equipment used in Finland until 1985.

EQUIPMENT	FREQUENCY [Hz]	Tx - Rx [m]	OUTPUT	COMMENT
EM 16	15 000 - 20 000	∞	Re{Hz/Hx}	
EM 16R	15 000 - 20 000	∞	$\rho a, \phi$	
VLF/GSF		∞	H_{vert}, H_{hor}	
ECA 541-0	8 - 3 700 (9 fq's)	∞	$\lvert \rho a \rvert$	
ECA 542-0	4.7 - 2 700 (9 fq's)	∞	$\lvert \rho a \rvert$	
SLINGRAM, GSF	3 600	20; 40; 60	Re, Im{H_{sek}/H_{prim}}	manual comp.
SLINGRAM, GSF/HF	14 000	20; 40; 60	Re, Im{H_{sek}/H_{prim}}	manual comp
SLINGRAM, OK	1 775	20; 40; 60; 80	Re, Im{H_{sek}/H_{prim}}	1962 -
SLINGRAM, OK/HF	18 350	20; 40; 60; 80	Re, Im{H_{sek}/H_{prim}}	1969 -
EM-69-2	3 600	40; 60	Re, Im{H_{sek}/H_{prim}}	
EM 31	40 000	4	Re, Im{H_{sek}/H_{prim}}	
MaxMin II	222; 444; 888;1 777; 3 555	40 - 250	Re, Im{H_{sek}/H_{prim}}	
MaxMin II ++	222; 444; 888;1 777; 3 555	60 - 400	Re, Im{H_{sek}/H_{prim}}	1985 -
GEFINEX EM 303	223; 523; 1 623;3 663; 9 524	4 - 200	H_x, H_y, H_z	1985 -
GEFINEX EM 400S	80 frequencies: 2 - 20 000	500 - 1000	H_x, H_z	proto 1986
GEFINEX 200	50 000	1.0	H_x, H_y, H_z	
APEX	8 000	1.5	$H_{sek} \perp H_{prim}$	54.7° tilt
PROXAN	50 000	0.9	$H_{sek} \perp H_{prim}$	54.7° tilt
mini-SLINGRAM/GSF	8 000	1.22 / 2.5	$H_{sek} \perp H_{prim}$	
TURAM, GSF	820	var.	$H_{z1}/ H_{z1}; \Delta\phi_{12}$	manual comp

Reference

Ketola, M., 1986. The development of exploration geophysics in Finland. Geol. Survey of Finland, Bulletin 336, 205 - 231.

MAJOR MODIFICATIONS OF ELECTROMAGNETIC SOUNDING AND EXAMPLES OF PRACTICING THEM IN ORE PROSPECTING

by

A. Savin

Savin, A., 1990. Major modifications of electromagnetic sounding and examples of practicing them in ore prospecting. *Geologian Tutkimuskeskus, Tutkimusraportti 95.* 53-68, 8 figs.

Major modifications of EM sounding with artificial excitation of a field are described. Considered are the sounding problems of ore prospecting geophysics, viz., (a) distinguishing buried valleys as favourable for placer accumulation, (b) direct prospecting for ore bodies as good conductors and (c) finding geological structures controlling various ores. The comparative efficiency of applied sounding methods is demonstrated by modelling a two-layer medium and half-space containing a spherical inhomogeneity. Several examples are presented of the application of EM sounding methods in the USSR.

Key words: geophysical methods, electromagnetic methods, electromagnetic induction, frequency sounding, transient methods, numerical models, spherical models, mineral exploration, USSR

Савин, А.П., 1990. Основные варианты электромагнитного зондирования и примеры их применения при поисках рудных месторождений. Геологический центр финляндии, Рапорт исследования 95. 53-68, Идд. 8.

Приводится описание основных вариантов электромагнитного зондирования с искусственным возбуждением поля. Рассмотрены задачи зондирования в рудной геофизике: а) выделение погребенных долин, благоприятных к сосредоточению россыпей, б) непосредственные поиски хорошо проводящих рудных тел, в) выявление различного рода рудоконтролирующих факторов. Сравнительная эффективность используемых вариантов зондирования иллюстрируется на моделях двухслойной сроды и полупространства, содержащего неоднородность в форме шара. Приводятся примеры использования электромагнитного зондирования в СССР.

Modifications and problems of sounding

Electromagnetic sounding with artificial EM fields, which differs in its properties from magnetotelluric sounding (audio-magnetotellurics included), is commonly used in the USSR when examining a geological section both in the structural geophysics of gas and oil prospecting and in ore prospecting. There are numerous modifications of EM sounding differing from each other in:

a) the mode of the EM source field: either harmonic or transient (the terms frequency or time domain are also frequently used);
b) the type of current source: electrical or magnetic dipole, ungrounded loop, long cable;
c) the measured parameter (s): for instance one of the space components of the electrical or the magnetic field, field ellipse elements, relation between the intensity of space components or semiaxes of the field ellipse: in the case of space components measurement of the modulus, phase, real and imaginary components is possible;
d) the sounding parameter in question: the frequency of the harmonic field, transition time or distance between the field source and measurement point (array spacing).

Below are described the most common sounding array modifications operating in the harmonic mode:

1. Vertical magnetic dipole serves as the EM field source. The measured components comprise: the vertical component of magnetic field intensity (H_z); the azimuthal component of electric field (E_φ); the H_z/r, H_a/H_b and E_φ/H_r ratios, where H_r is the radial component of magnetic intensity (use is made of the spherical coordinate system with its centre in coincidence with the source and its Z axis oriented upwards). H_a and H_b are respectively the major and minor semiaxes of the ellipse of the magnetic field polarization in the plane zor. In each case, the modulus of intensity is measured, while the phases of either real or imaginary components have so far been less used.

2. The field source is nothing else than a horizontal electric dipole; measured here is a horizontal component of the electric field. In this case we use a so-called axial array, when both dipoles (i.e. source and measuring dipoles) are coaxial, and an equatorial array, when both dipoles are normal to a line running through their centres (the measured components of these arrays can be designated as E_r and E_φ, respectively).

3. A combined-loop array made of two ungrounded loops combined in plan and an adequate single-loop array. Judging by the sounding results, this array hardly differs from the modification for measuring E_φ in the field of a vertical magnetic dipole, at least in a near-field zone. [The near-field (induction), intermediate or farfield (wave) zone of an EM field can be derived from the numerical value of the reduced distance $p = \sqrt{\mu_0 \omega / \rho} \cdot r$, where μ_0 - magnetic permeability of vacuum, ω - cyclic frequency, ρ = resistivity, r - array spacing. The complete range of "p" values breaks down into 3 zones, viz., near-field ($p<<1$), far-field ($p>>1$) and intermediate zones. The field intensity values for the near-field and far-field zones are calculated in terms of simple analytic functions, while those for the intermediate zone are obtained by numerical integration].

In case of a transitional mode of operation, the same modifications work well (except for the arrays measuring the ratio of intensity components), yet the incorporated-loop array is most frequently used. All the modifications mentioned are to some extent applied in the USSR for solving various geological problems, ore prospecting included.

There are also various forms of presenting measurement data, each requiring an appropriate processing of field information. As a rule, measurements are presented in terms of apparent or effective resistivity as a function of argument (frequency, time). Now, one should see clearly the difference between the apparent and the effective resistivities.

Apparent resistivity ρ_ω (in harmonic mode) or ρ_τ (when measuring transitional processes) stands for a value of resistivity ρ derived from asymptotic formulae, which correspond to the source-receiver-distance and show the manner in which ρ of homogeneous isotropic half-space is related to the regular dimensions of the said distance, the numerical

values defining a field source and the measurements. The asymptotic formulae in use refer to the wave (far-field) or the induction (near-field) zone.

Veshev (1978, 1980) introduced a definition of effective resistivity ρ, which implies the ρ of a homogeneous half-space giving for the source-receiver-distance used the same field source-measured value relation as above a real heterogeneous medium. Unlike the apparent resistivity (ρ_ω, ρ_τ), the effective one ρ is derived from the tabularly or graphically presented characteristics, which cannot be expressed by simple analytic formulae. In the near-field and far-field zones, the ρ values in fact coincide with the ρ_ω, and ρ_τ values, respectively, while essentially differing from the said values in the intermediate zone.

In addition to the apparent resistivity in the EM sounding practice use is being also made of the apparent values of longitudinal conduction, penetration depth, etc. A so-called "visualization" of measurements is a special way of data processing, whereof an example is given in the following.

Whether the efficiency of this or that modification and data processing method is relatively high enough depends upon the problem to be solved and the type of geoelectrical section. In practice, however, a choice of an adequate modification is most often predetermined by the technological capabilities of geophysicists, while the data processing method is a matter of tradition.

Application of EM sounding in ore prospecting is associated with the solution of the following problems:

1. Sounding in horizontally layered medium in order to detect those depressions in the bedrock topography that are favourable for aggregation of ore mineral placers.
2. Direct finding of deep-seated highly conductive ore objects.
3. Determination of the geoelectrical structure of an ore district in order to solve various problems in ore prospecting.

Sounding above horizontally layered medium

In ore placer prospecting, a major goal of sounding is to determine the thickness of loose sediments. Knowing this parameter, we can outline the bedrock topography and discriminate the buried valleys that facilitate an aggregation of placer deposits. Such a problem is typical as far as the slopes of the Baltic Shield are concerned.

Placer deposit prospecting is effected both on the mainland and on the coastal solid ice in the shallow portion of the shelf. In each case a geoelectrical section over the relatively small areas can be regarded as horizontally layered (generally, 2 to 5 layers). This usually implies such sections where resistivity increases with depth; a so-called A-type three-layer section ($\rho_1 < \rho_2 < \rho_3$) is most often used.

Electromagnetic sounding, yielding the thickness parameter of loose sediments, is made in a harmonic mode since the transient one requires too short measuring time intervals to fall within the time range the existing types of equipment possess.

Most hard conditions of sounding are known to be in the shelf area since there a section in question is overlain by a highly conductive sea-water layer, which produces its screening effect upon the results. As far as the shallow-water shelf zone with a small amount of marine activity is concerned, this problem has been solved by vertical electrical sounding (VES) through coastal solid ice. Under such conditions, however, VES is, not commercially efficient enough, for it requires drilling in ice in order to obtain an electrical contact with the water surface. With ice, it is therefore more practical to run EM sounding, where the field excitation is effected by a vertical harmonic magnetic dipole simulated through an ac-loop.

To choose an appropriate sounding technique, we had to decide on such a modification, which could yield easily and explicitly decoded data. It turned out to be a distance-parameter (geometric) sounding in the near-field zone, with its fairly low frequencies and results that do not depend upon the latter. Specific conditions of sounding in a near-field

zone can well be illustrated on theoretical charts of two-layer sections with a poorly conducting basement (Fig. 1); very roughly speaking, similarity can be recognized between this type of a section and the marine sections. Resistivity and thickness of a top layer are marked as ρ_1 and d_1 respectively. The common presentation of theoretical charts as a function of r/d_1 (Fig. 1a) fails to yield a clear differentiation of curves when r/d_1 is not sufficiently high. More useful for interpretation is, therefore, the presentation of curves as a function of S_ω/S_1 (Fig. 1b), where $S_1 = d_1/\rho_1$ is the longitudinal conductance of the top layer and $S_\omega = r/2\rho_\omega$ as apparent longitudinal conductance (Molochnov and Radionov, 1982).

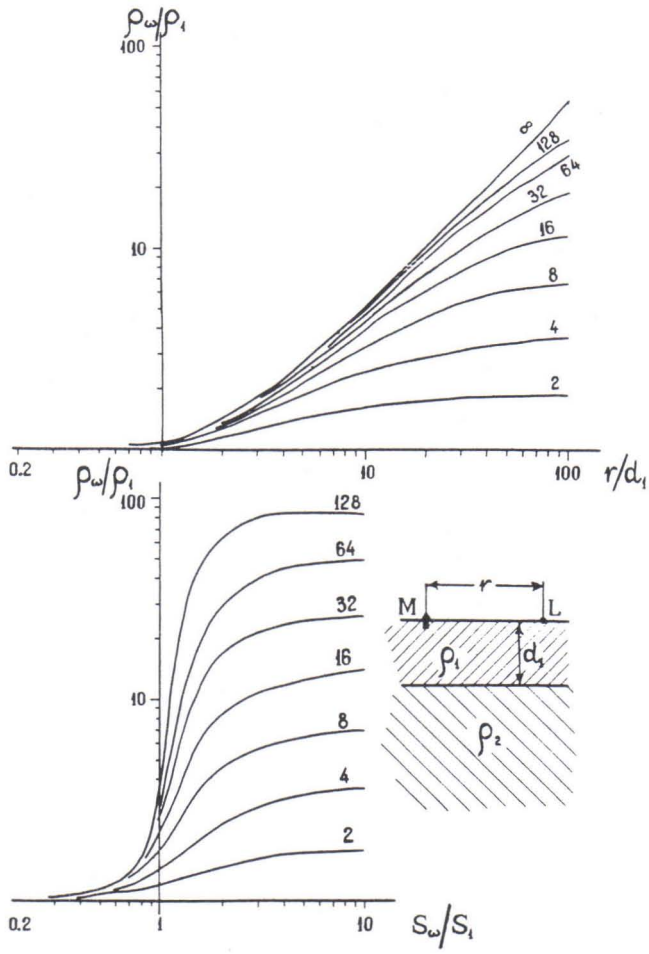

Fig. 1. Theoretical chart showing the curves of distance-parameter (geometric) sounding in a near-field zone of a vertical magnetic dipole above a two-layer section with a poorly conducting basement (Molochnov and Radionov, 1982). The curve parameter values of ρ_2/ρ_1; M - magnetic dipole; L - measurement point.

The foregoing simple relation holds true, however, only as long as the measurement conditions correspond to a near-field zone ($p << 1$). To maintain these conditions we need a certain set of parameters, viz., some frequency of EM field, array spread (spacing) and properties of a medium (in particular ρ_1); again, a frequency limit of the near-field zone may vary with the data processing method used. To study a whole set of the said conditions an example

is given of the measured parameters' behaviour with different processing methods as determined by the ratio λ_1/d_1 with $\rho_2/\rho_1 = 64$, $r/d_1 = 4$, where $\lambda_1 = 2\pi\sqrt{2}\rho_1/(\mu_0\omega)$ is a wave length, $\mu_0 = 4\pi \cdot 10^{-7}$ H/m - magnetic permeability of vacuum, ω = cyclic frequency (Fig. 2).

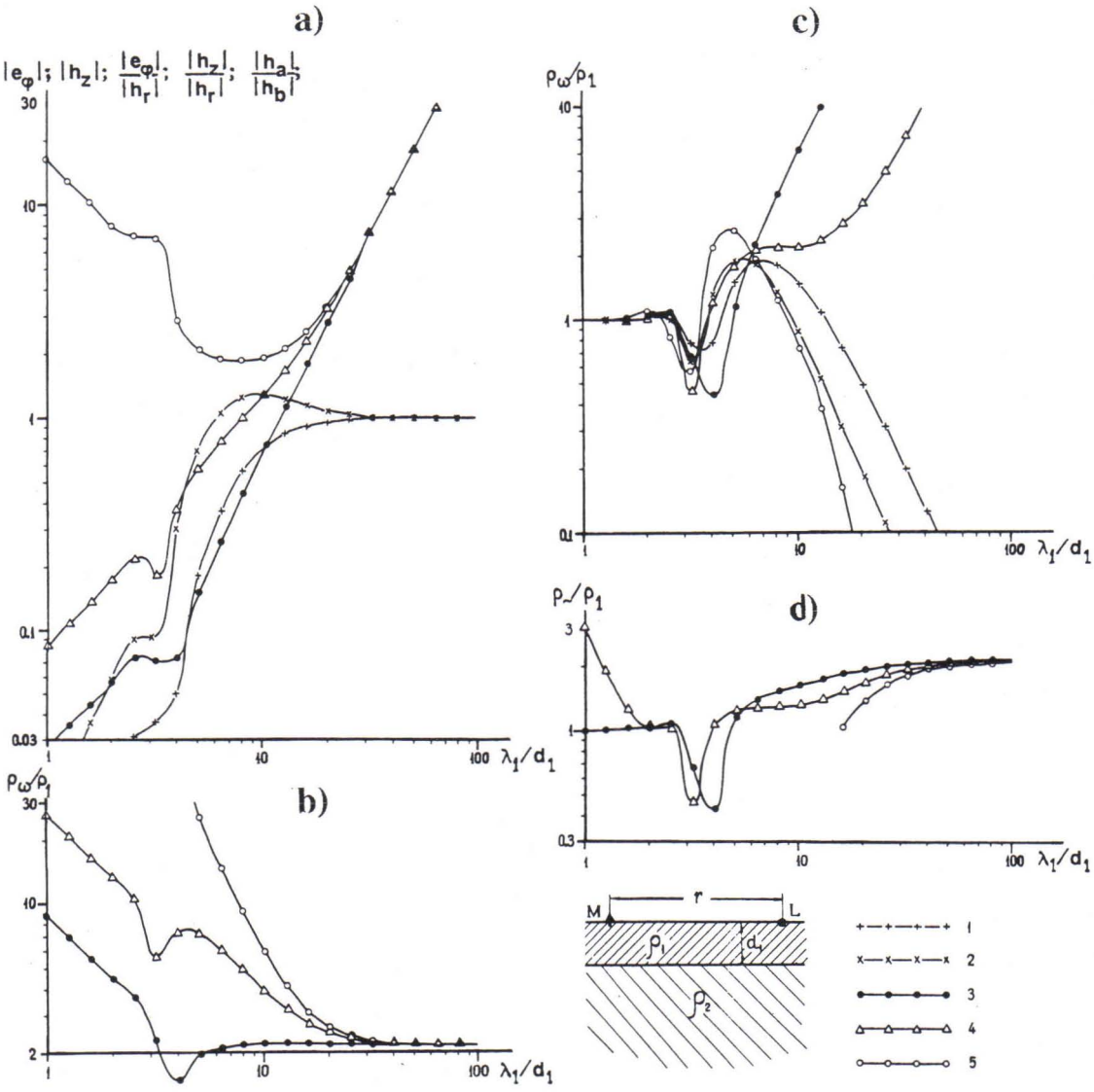

Fig. 2. Behaviour of parameters the vertical magnetic dipole field over a two-layer section with a poorly conducting basement with $\rho_2/\rho_1 = 64$, $r/d_1 = 4$; a) normalized electric field e_φ, normalized field h_z, ratio between electric and magnetic fields, b) ρ_ω/ρ_1 as in the near-field zone, c) ρ_ω/ρ_1 as in the far-field zone, d) ρ/ρ_1.

1 - $|e_\varphi|$, 2 - $|h_z|$, 3 - $|e_\varphi|/|h_r|$, 4 - $|h_z|/|h_r|$, 5 - $h_a/|h_b|$.

The characteristics of normalized electric and magnetic fields corresponding to the intensity of electric and magnetic fields, respectively, are shoen in Fig. 2a. Now, electric (e)

and magnetic (h) fields are expressed through the appropriate values of E and H intensity components in terms of the ratios $e = (E/j\omega\mu_o m) \cdot 4\pi r^2$ and $h = (H/m) \cdot 4\pi r^3$, where m denotes the magnetic moment of a source, the letter symbols z, r, φ characterize a spatial orientation of the components, and a, b are respectively the major and minor semiaxes of the magnetic field ellipse.

Practically most convenient for measurement, and also yielding the highest accuracy, are the relative parameters $|e_\varphi| / |h_r|$, $|h_z| / |h_r|$, $h_a / |h_b|$, the values of which coincide for sufficiently high values of λ_1 / d_1 (i.e. in the near-field zone). The ρ_ω / ρ_1 values have been derived from the following relations:

In the near-field zone:

$$\frac{\rho_\omega}{\rho_1} = 2\pi^2 \cdot Q \cdot R_{nf}$$

$$\text{with } Q = \frac{r/d_1)^2}{(\lambda_1/d_1)^2} \quad \text{and } R_{rf} \text{ either}$$

$$\frac{|e_\varphi|}{|h_r|}, \quad \frac{|h_z|}{|h_r|} \text{ or } \frac{|h_a|}{|h_r|},$$

In the far-field zone:

$$\frac{\rho_\omega}{\rho_1} = \frac{4\pi^2}{3} \cdot Q \cdot R_{ff}$$

$$\text{with } R_{ff} = |e_\varphi|, |h_z| /3, 6 (|e_\varphi| / |h_r|)^2,$$

$$\frac{2}{3} \cdot \frac{|h_z|^2}{|h_r|^2} \text{ or } \frac{4}{3} \cdot \left(\frac{|h_b|}{|h_a|}\right)^2,$$

With the increase of λ_1/d_1, the near-field ρ_ω / ρ_1 characteristics (see Fig. 2b) tend to an asymptotic value at which no frequency distortion effect is observed. The asymptotic area, corresponding to the near-field zone, turns out to be optimum for a distance-parameter sounding in complex sections of marine type, since the frequency distortions might make the results hardly recognizable. As seen from Fig. 2b, the curve derived from the ratio $|e_\varphi| / |h_r|$ is the first one to approach the asymptote. In fact at $\lambda_1/d_1 = 5.2$, the accuracy is 10 %, while in every other case the ρ_ω/ρ_1 curves approach the asymptote at $\lambda_1/d_1 = 22$ and 25. These values determine the maximum possible EM-field frequency (f) which at prescribed values of d_1 and ρ_1 are calculated from the formula $f = \omega/2\pi = 10^7 \rho_1 / \{ (\lambda_1/d_1)^2_{min} \cdot d_1^2 \}$.

In particular, if we take $\rho_1 = 2\Omega m$ and $d_1 = 30$ (conditions typical of the shallow shelfs), the maximum possible frequency, when measuring $|e_\varphi| / |h_r|$, amounts to 685 Hz, but with $|h_z| / |h_r|$ and $|H_a| / |H_b|$ measurements it should not exceed 46 and 35 Hz respectively. It is obvious that in this particular case variations of $|E\varphi| / |H_r|$ are preferable, inasmuch as reduction of the frequency to some tens of cycles per second entails a necessity of increasing

the power of a generator and the total weight of the equipment.

Plotting the characteristics of effective resistivities ρ (see Fig. 1d) does not produce the expected result, especially in the far-field zone (Fig. 1c).

Based on the analysis of the characteristics, the appropriate measurement procedure was elaborated, its fundamentals being given in a monograph (Titlinov, 1979). Contactless measurement of $|E_\varphi|$ has been performed by using a dipole made of two pieces of insulated wire, each 5 m long (and 1 m long with a small array spacing). The frequency of the EM field being 312 Hz, the ρ_ω value was derived from the formula $\rho_\omega = r/4 \cdot \{ |e_\varphi| / |h_r| \}$.

Shown in Fig. 3a is an example of sounding curves. Interpreted as a four-layer curve of the HA-type ($\rho_1 < \rho_2 < \rho_3 < \rho_4$) it shows the following section: 1st layer - ice (relatively low values specify the state of ice in the springtime); 2nd layer - sea water, sea-floor sediments and water-impregnated portion of loose sediments; 3rd layer - loose sediments and bedrock disintegration zone; 4th layer - bedrocks (siltstone). The geoelectrical section of Fig. 3b was constructed right on the asis of the data interpretation. Again, the EM sounding data agree well with the drilling and VES data, thus indicating a depression at the top of the bedrocks.

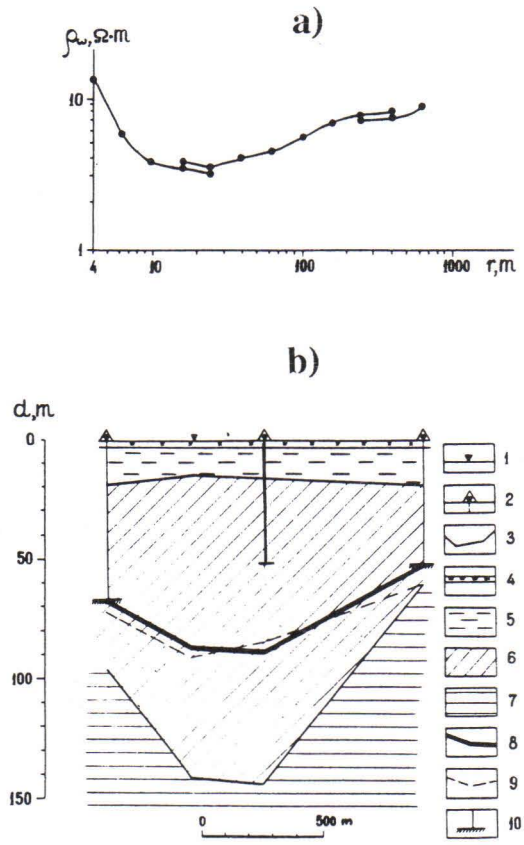

Fig. 3. Results of distance sounding through the coastal solid ice in a vertical magnetic dipole field; a) ρ_ω curves, b) geoelectrical section.

1, 2 - location of distance sounding which (1) does not or (2) does coincide with a borehole mouth, 3 - boundary of geoelectrical layers, 4 - ice layer, 5, 6, 7 - geoelectrical layers with resistivity of (5) 2-4, (6) 8-12 and (7) 15-40 Ωm respectively, 8, 9,10 - bedrock top according to (8) sounding data , (9) VES and (10) drilling.

When working on the coastal solid ice and the coast, wide use was made of EM sounding with the modified $|H_b|/ H_a$ ratio in the intermediate zone (Molochnov and Radionov, 1982). Most of the soundings in the said zone were effected by a frequency-distance parameter method, where extreme values of the ρ_ω-frequency characteristics derived in the far-field zone (see Fig. 2c) are used. The method is based upon the relation between ρ_ω max and adequate values of $p_\omega = 2\sqrt{2} \cdot r / \lambda_1$, on the one hand, and r/d_1, on the other. Fig. 4 just shows one sample of how well this modification works in the area surrounding the shallow shelf coast. The sounding data enabled us to construct the schematic view of the bedrock topography in the sea and coastal areas, and to outline a buried river valley as a promising object of ore-placers. In the loose sediments, resistivity measurements made it possible to recognize 5 zones, differing in their state of being water-impregnated and frozen. The sounding data agree with the results of the drilling and acoustoseismic profiling.

As for the ground measurements, most of the soundings to determine the thickness of loose sediments and to reveal the buried valleys have been performed in permafrost areas. In such situations geoelectrical sections of the K-type ($\rho_1 > \rho_2 > \rho_3$) are common, comprising: 1 - a molten surface layer, 2 - frost and 3 - bedrock. This kind of a problem is solved through a remote EM sounding with measuring $| H_z| / | H_r|$ of a vertical magnetic dipole (Veshev et al., 1978; Veshev, 1980). The processing involved ρ calculations, whereas the interpretation was done by using a large set of theoretical charts taking account of frequency distortions caused by inappropriate conditions of the near-field zone.

Under normal ground conditions most common is a two-layer section with a poorly conducting basement ($\rho_1 < \rho_2$). To determine here a thickness of loose sediments, various frequency sounding methods are applicable. The Geological Amalgamation "Sevzapgeologia", in particular, performs such frequency soundings on the slope of the Baltic Shield using a one-loop array. In other regions, frequency sounding with dipole-source excitation is commonly practiced.

Sounding in ore prospecting

Electromagnetic sounding is widely applied in prospecting for deep and highly conductive ore objects. Deep prospecting calls for taking the measurements solely in the near-field zone with an adequate processing of the results obtained. The most common features in the behaviour of ρ_ω-curves plotted by sounding in the near-field zone can well be illustrated on a model of a conductive sphere placed in a conductive half-space (Fig. 5). Concerning the geometric sounding with a vertical magnetic dipole and using relative measurement ($| e_\varphi | / | h_r |$, $| H_z | / | H_r |$, $H_a / | H_b |$), an isometric object is detected by a reduced value of ρ_ω; the maximum corresponds to $r/d \approx 1$, where d - depth to the centre of an object (Fig. 5a). Geometric sounding with electric dipole (equatorial array) produces a decrease, yet very insignificant, of ρ_ω, with an maximum at $r/d > 1$.

Analysis of the behaviour of the characteristics as a function of λ_1/d (Fig. 5b) proves the conditions of the near-field zone in this particular case to be valid for $\lambda_1/d > 50$, and, what is more, there is hardly any great difference between various groups of measured ratios. As it was shown above, however, the $| E_\varphi | / | H_r |$ ratio appears to be most suitable, provided there is a conductive layer of loose sediments, and that is precisely why this modification was used in deep ore prospecting.

Fig. 6 presents an example of applying this modification at a pyrite deposit locality in the Ural Mountains. The deposit is clearly traced on a vertical section of differential apparent resistivities $\rho_{\omega df}$ (Fig. 6b), which for two adjacent separations r_{n-1} and r_n are given by

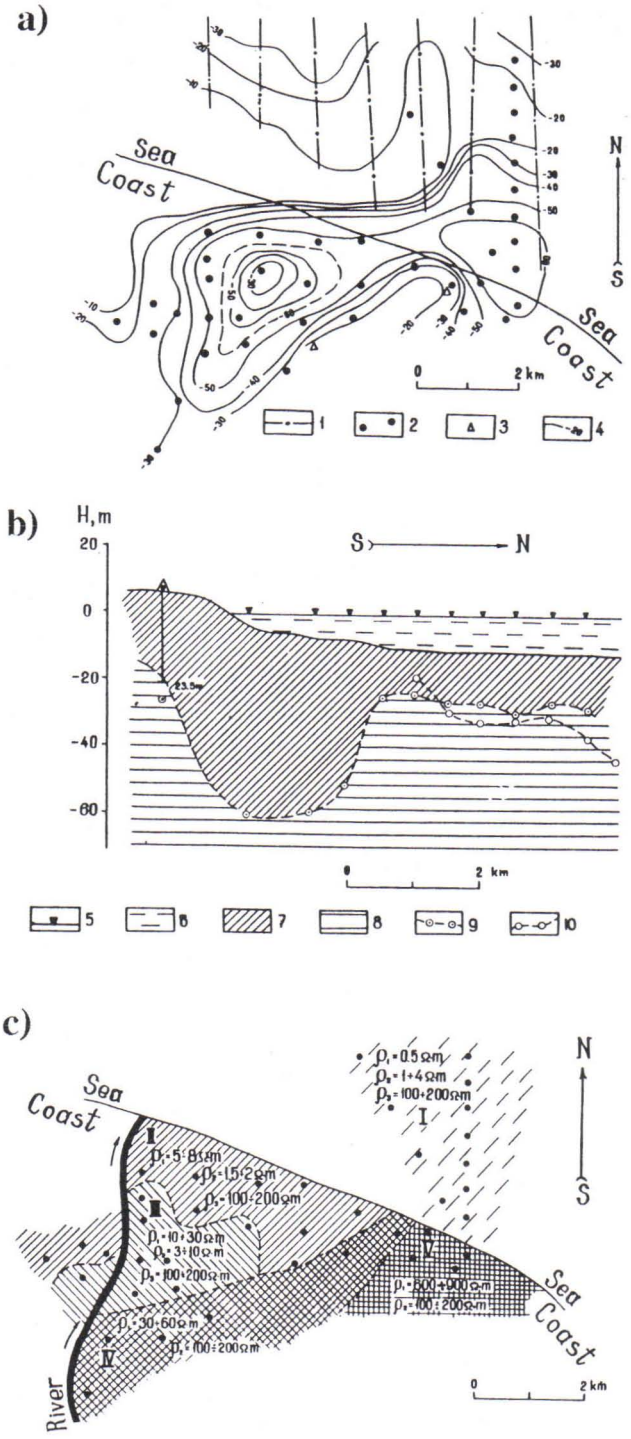

Fig. 4. Results of frequency-distance parameter sounding with a vertical magnetic dipole through coastal solid ice and on the coast (Molochnov and Radionov, 1981); a) schematic view of the bedrock top topography according to EM sounding and seismoacoustic profiling data, b) geoelectrical section, c) schematic presentation of resistivity values of the layers composing loose sediments.
1 - seismoacoustic profiles, 2 - EM sounding points (a, c), 3 - boreholes that reached the bedrock, 4 - isohypses of bedrock top, 5 - EM sounding points on profile (b), 6 - sea water, 7 - loose sediments, 8 - bedrock, 9, 10 - bedrock boundary according to EM sounding data, (9) and seismoacoustic profiling (10).

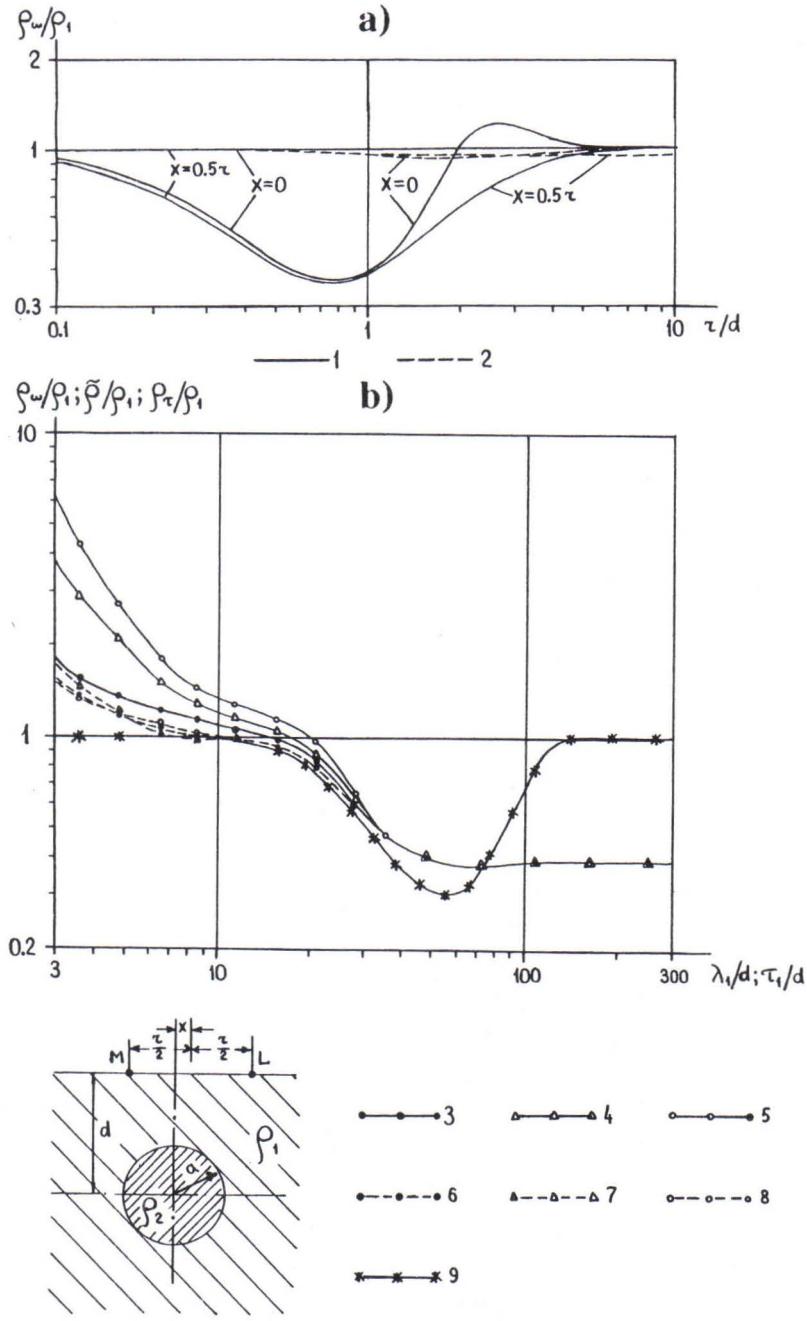

Fig. 5. Geometric sounding curves a) and wave characteristics ρ_ω/ρ_1 and ρ/ρ_1 at r/d = 1, b) above a half-space containing a spherical inhomogeneity with $\rho_2/\rho_1 = 1000$, a/d = 0.4.
1, 2 - curves of geometric sounding in the near-field zone of (1) a vertical magnetic dipole and (2) an horizontal electric dipole for the equatorial array; 3, 4, 5 - ρ_ω/ρ_1 characteristics for (3) $|e_\varphi| / |h_r|$, (4) $|h_z| / |h_r|$ and (5) $h_a/|h_b|$; 6, 7, 8 - ρ/ρ_1 characteristics for (6) $|e_\varphi| / |h_r|$, (7) $|h_z| / |h_r|$ and (8) $h_a/|h_b|$ (3-8 - in a field of vertical magnetic dipole); 9 - ρ_τ/ρ_1 characteristics for a combined loop array.

$$\rho_{\omega df} = \frac{r_n - r_{n-1}}{4} \cdot \frac{Z_n \cdot Z_{n-1}}{Z_{n-1} - Z_n}, \quad \text{where } Z = \frac{|E_\varphi|}{|H_r|}$$

The ore zone, which occurs near to the contact of metasomatites and slightly altered volcanogenic rocks, is registered as a deep conductor, its resistivity ranging from 30 to 300 Ωm. That the apparent differential resistivity at the centre of the profile becomes low at $r \leq 200$ is because of the increasing thickness of loose sediments, whereas the reduction of the said resistivity in point IX at r = 700 to 1200 m is seemingly due to the influence of another metasomatic zone that crops out at a distance of 5 km from this deposit.

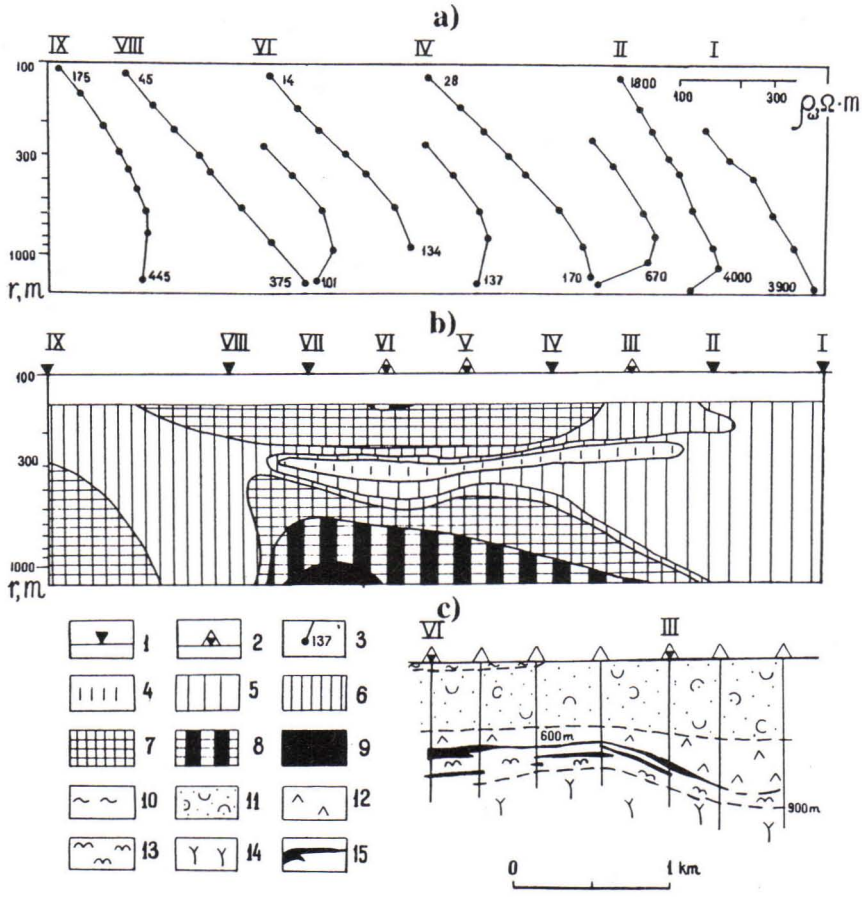

Fig. 6. Results of geometric sounding with a vertical magnetic dipole above a pyrite deposit (Titlinov, 1977); a) ρ_ω curves, b) vertical section $\rho_{\omega df}$, c) schematic geological section.

1, 2 - location of geometric sounding which does not (1) and does (2) coincide with a borehole mouth, 3 - value of ρ_ω in Ωm, 4-9 - values of $\rho_{\omega df}$: (4) $>10^4$Ωm, (5) 10^4- $3 \cdot 10^3$ Ωm, (6) $3 \cdot 10^3$ - 10^3 Ωm, (7) 10^3 - 300 Ωm, (8) 300 - 100 Ωm, (9) 100 - 30 Ωm, 10 - clays, 11 - tuffstones, 12 - diabases, porphyrites, 13 - quartz-chlorite-sericitic rocks, 14 - metasomatites, 15 - orebodies.

If ore prospecting includes operating in a transient mode (TEM sounding) then the measurement in the near-field zone is performed with a combined-loop array. The measured

time response ρ_T is reduced value in the presence of a conductive object. As seen from an example in Fig. 5b, the extreme value of ρ_T is registered when $\tau_1 / d = 54$, where $\tau_1 = 2\pi\sqrt{2t\rho_1/\mu_0}$ and t is the transient time.

Recently, apart from plotting the $\rho_T(t)$ and $S_T(t)$ (= apparent longitudinal conductance) characteristics, a new processing method has been put into practice: so-called visualization of measurement data (Isaev and Filatoc, 1981). The idea of visualization is based on approximate restoration (in a halfspace) of a function depending upon the density of anomalous currents induced in the medium owing to an inhomogeneity. Fig. 7 shows how this kind of processing works on theoretical models and in a field case. The visual processing helps to locate more accurately and outline the geometry of an orebody. The method is most efficient, however, when the object has a gentle dip, while vertically dipping portions of the orebody are not recorded at all (see Fig. 7c).

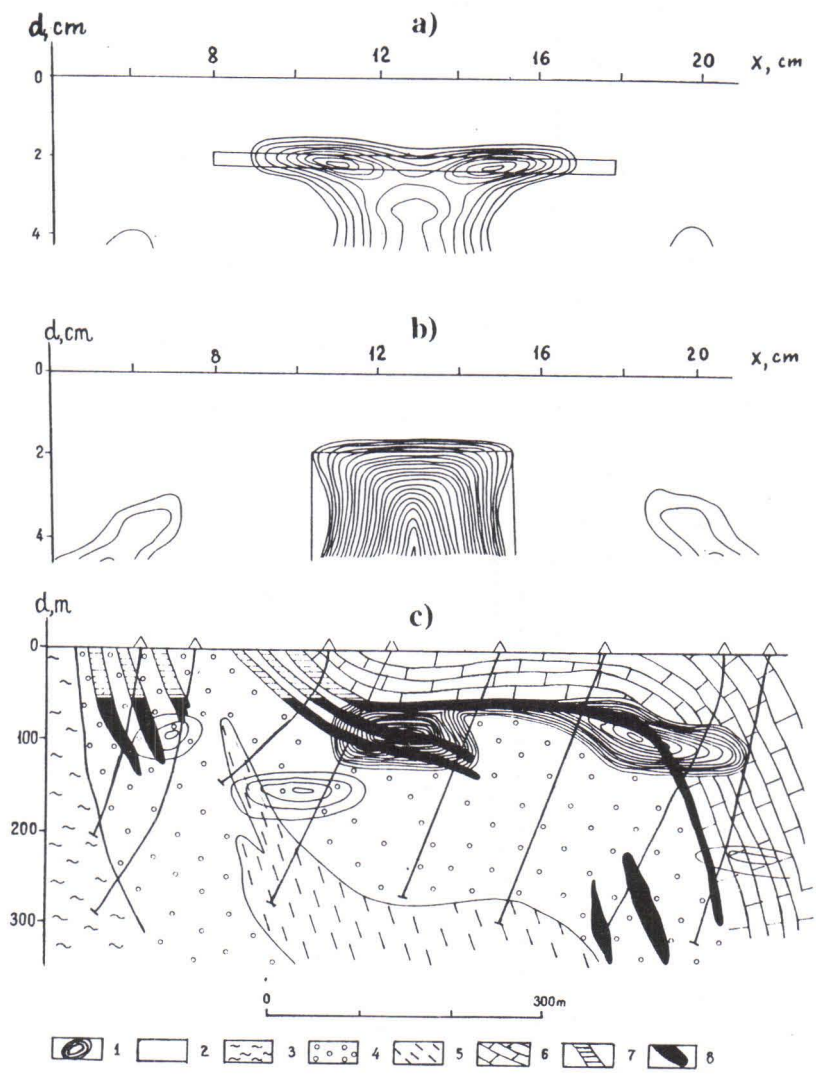

Fig. 7. Results of TEM sounding processed by the field visualization method (Isaev and Filatov, 1981). a) above a disk model, b) above a vertical cylinder model, c) above an iron deposit.
1 - isolines of S-function (x, y, z), 2 - outlines of disk and half-cylinder models, 3 - gneisses, 4 - skarns, 5 - quartz-feldspar metasomatites, 6 - limestones, 7 - martite, 8 - magnetite ores.

For the present, TEM sounding with the combined-loop array is a prevailing method for deep ore prospecting in the Kola-Karelian region (Vargin et al., 1985). Practical success in sounding in the harmonic mode using the combined-loop array has been experienced here, too. In order to obtain characteristics, that are qualitatively similar to the transient ones, when measuring the quadrature component of e.m.f. (Im U), one must use differential values of $\Delta(\text{Im } e) = \text{Im } e_1 - (f_1/f_2) \cdot \text{Im } e_2$, where e_1 and e_2 are the relative e.m.f. values measured at the frequencies f_1 and f_2, respectively (it is usually assumed that $f_2 = 4f_1$) (Svetov, 1973).

Study of geoelectrical structures of ore districts

As far as ore districts are concerned, EM sounding enables various problems to be solved, viz. (a) mapping of rocks differing in composition, (b) recognizing and detecting tectonic faults and conductive metallotectonic zones or (c) finding the depth, dip and strike of bedrocks and other structural and lithological components of ore fields and deposits.

A good illustration of how to study the geoelectrical structure of an ore field is offered by the results of frequency sounding in one of the volcanic provinces in the northeastern USSR. Work was aimed at researching the conditions under which the gold and silver were deposited (Pyatnitski et al., 1979). The sounding was done using an axial array (measuring the electric intensity of an electric dipole field) with a radius of 2 to 3 km and frequencies ranging from 1.6 to 1250 Hz.

The ore field district displays a two-level structure with a subhorizontal interface. The lower level, or stage, is composed of metamorphosed sandstones (quartzose and compacted) and siltstones, while the upper one comprises volcanites, basically of andesite and liparite-dacite composition, and their tuffs. The following structural control features have been established for the ore field: 1) uplifts of the volcanic belt basement, 2) development of subvolcanic liparite-dacite bodies, 3) development of ore controlling faults.

As seen from Fig. 8, the foregoing geological formations, when occurring at the depth interval of 0.5-1.5 km, can be detected by means of EM sounding:

1) uplifts of the volcanite basement are recognized as elongated plate-like bodies yielding high values of ρ_ω (700-2000 Ωm) and possessing subhorizontal interfaces (Fig. 8b, observation stations (OS) 25 through 50; Fig. 8c, OS 35 through 20);

2) subvolcanic liparite-dacite bodies are identified as bodies with steep, often tectonic, contacts and with fairly low values of ρ_ω = 100-600 Ωm (Fig. 8a): OS 4-7, 10-14, 21-26; Fig. 8c: OS 75-65); dacite formations show here the lowermost ρ_ω (100 to 300 Ωm), which enables to distinguish between the liparite and dacite bodies with ρ_ω, respectively, 400-600 (Fig. 8a) and 100-300 Ωm (Fig. 8b,c);

3) faults are usually plotted as narrow zones with a low ρ, and they also reveal a break-off in a regular run of a ρ_ω isoline.

The areas where the said three structural control features intermingle can, basically, be regarded as prospects in search of blind orebodies. In the area under consideration, sounding can not only contribute to efficient geological deep mapping, but also, with all the indicators put together, can help directly in outlining the prospects.

The same kind of activity is at present taking place in the Kola-Karelian region where prospecting for Cu-Ni deposits has been for a long time under way. Here, the regional geoelectrical structure of the Baltic Shield is being investigated, too; yet this work bears only an indirect relation to the objectives of ore prospecting. Application is made in this region of such methods as (a) deep sounding method with powerful sources using magnetohydrodynamic (MHD) generators, (b) electric frequency sounding with several kilometers of spacing and (c) magnetotelluric depth sounding (Isaev et al., 1980; Velikhov et al., 1982; Velikhov et al., 1983).

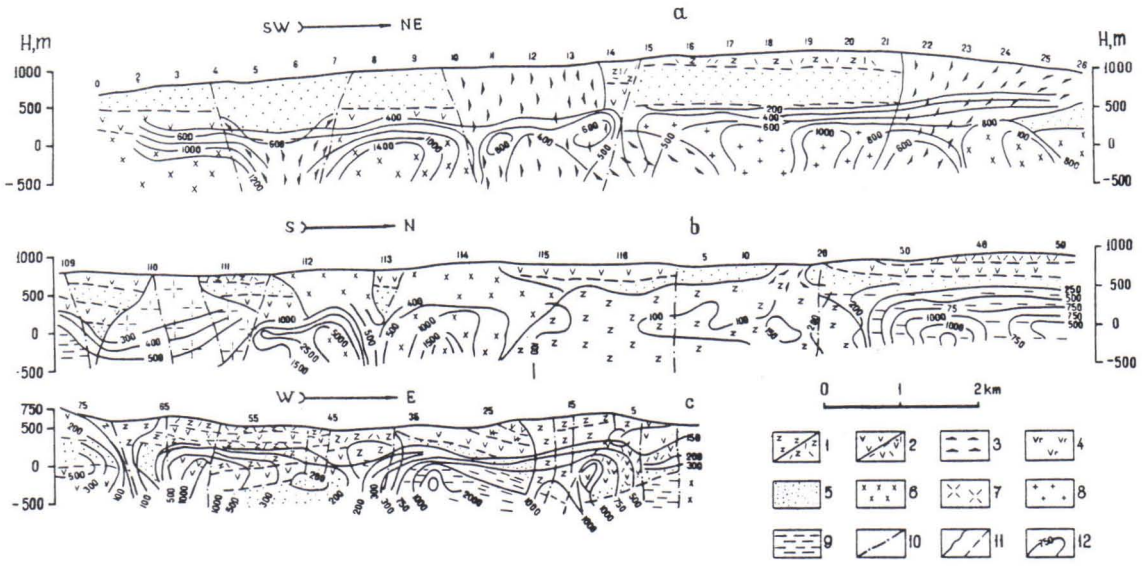

Fig. 8. Schematic geological and geophysical sections along electric frequency sounding profiles (Pyatnitski et al., 1979).
1 - dacites of subvolcanic and cover facies, 2 - covers of andesite porphyrites and their tuffs, 3 - subvolcanic bodies of liparites and trachyliparites, 4 - andesite-basalt cover, 5 - sandstones, 6 - subvolcanic bodies of diorite porphyrites and diorites, 7 - plagiogranite-porphyry intrusions, 8 - granite intrusions, 9 - rocks of volcanic belt basement (quartzite-like sandstones), 10 - tectonic faults, 11 - boundaries of rocks, a) transverse and b) conformable, 12 - ρ_ω isolines.

Conclusions

The present article deals solely with the most general notions on the application of EM sounding in ore geophysics; some case histories have also been presented. Nothing is said here about the data interpretation techniques connected with sounding since much comprehensive information on this matter is to be found in the publications dealing with both harmonic field sounding (Vanyan, 1965; Matveev, 1974: Ivanov andSkugarevskaya, 1978; Yeshev et al., 1978, Titlinov, 1979; Kuznetsov et al., 1980; Molochnov and Radionov, 1982) and on transient field sounding (Vanyan, 1965; Matveev, 1974; Rabinovich et al., 1976; Sidorov et al., 1977; Rabinovich and Finogeev, 1983; Isaev et al., 1983). These two modes of sounding differ in the recommendations made on the field technique and on the interpretation. As for harmonic field sounding, the most original interpretation technique for increasing the accuracy and resolution of sounding is suggested by Molochnov and Radionov (1982).

Electromagnetic sounding is being successfully applied in geophysical prospecting as one of the most effective ways to study geological structures. However, the full potential of this method has not yet been utilized.

References

Isaev, G. & Filatov, V., 1981. On physical and mathematical principles of visualizing the transient EM fields. (О физико-математических принципах визуализации неустановившихся электромагнитных полей). J. Geology and Geophysics, No. 6,

Novosibirsk, 89-95.

Isaev, G., Itskovich, G. & Poletaeva, N., 1983. Recommendations on technique of TEM method when prospecting for deep-seated iron deposits. (Методические рекомендации по применению метода переходных процессов при поисках глубокозалегающих железорудных месторождений). Novosibirsk, Siberian Sci. Research Inst. of geology, geophysics and mineral resources, 48 p.

Ivanov, A. & Skugarevskaya, O., 1978. Frequency EM sounding technique (Методика частотных электромагнитных зондирований) Moscow, Nauka, 140 p.

Kuznetsov, A., Morozov, G., Pyatnitski, V., Svetov, B., Sidelnikova, T., Skugarevskaya, O., Sokolov, V. & Tabarovski, L., 1980. Dipole frequency sounding of two-layer medium. (Дипольные частотные зондирования двухслойной среды). Novosibirsk, Siberian Dep. USSR Acad. Sci., Inst. of Geology and Geophysics, 123 p. with theoretical charts (pt. II).

Matveev, B., 1974. Interpretation of EM sounding data (Интерпретация электромагнитных зондирований). Moscow, Nedra, 232 p.

Molochnov, G. & Radionov, M., 1982. Frequency EM sounding with vertical magnetic dipole. (Частотные электромагнитные зондирования с вертикальным магнитным диполем). Leningrad, University Publ. House, 216 p.

Pavlovski, V., Sviyazheninov, F., Tyuremnov, V. & Zakharova, V. (eds.), 1980. Procedure and results of geophysical prospecting in the north-eastern part of the Baltic Shield. (Методика и результаты геофизических исследований северо-восточной части Балтийского щита). Apatity, Geol. Inst., Kola Branch of USSR Acad. Sci., 141 p.

Pyatnitski, V., Konstantinov, M., Yeleeva, I. & Malashev, G., 1979. On the efficiency of frequency electronic sounding when mapping a deep structure of gold and silver deposits in volcanic areas. (О возможностях метода частотных электрических зондирований при картировании глуоинного остроения золото-серебряных месторождений в вулканических областях). J. Kolyma, No. 7, 34-36.

Rabinovitch, B. & Finogeev, V., 1983. Recommendations on technique of analyzing the near-field zone transient field sounding in a horizontally inhomogeneous medium. (Методические рекомендации по анализу зондирований становлением поля в ближней зоне (ЗСБ) в горизонтально-неоднородных средах). Novosibirsk, Siberian Sci. Research Inst. of geology, geophysics and mineral resources, 48 p.

Rabinovitch, B., Zakharkin, A., Goldman, M., Morozova, G., Gerasimov, L., Rogatchevski, B., Iomdina, E., Shatokhin, V., Katruk, Yu., Kunin, D., Goldort, V., Satchenko, G., Popov, E., Ruban, S., Borovikov, V., 1976. Transient field sounding in a near-field zone. (Зондирование становлением поля в ближней зоне). Moscow, Nedra, Siberian Sci. Research Inst. of geology, geophysics and mineral resources, 102 p.

Sidorov, V., 1985. Electrical inductive pulse methods of prospecting. (Импульсивная индуктивная электроразведка). Moscov, Nedra, 192 p.

Svetov, B., 1973. Theory, technique and interpretation of LF induction electric prospecting (Теория, методика и интерпретация материалов низкочастотной индуктивной електроразведки). Moscow, Nedra, 256 p.

Titlinov, V., 1977. On the application of radial induction sounding method in the deep-seated pyrite deposit. (Применение метода падиального индукционного зондирования на глубокозалегающем колчеданном месторождении). Pp. 49-52 in: Electrometry involved in prospecting and exploration of mineral deposits. Sverdlovsk, Ural Sci. Centre of USSR Acad. Sci.

Titlinov, V., 1979. Inductive EM sounding in mineral deposit prospecting (recommendations in technique). (Индукционное электромагнитное зондирование при поисках месторождений (методические рекомендации)). Sverdlovsk, Ural Sci. Centre of USSR Acad. Sci., Proc. Inst. of Geophysics, 132 p. with theoretical charts.

Vanyan, L., 1965. The fundamentals of EM sounding. (Основы электромагнитных зондирований). Moscow, Nedra, 108 p. (English translation with additional material: L.L. Vanyan, 1967. Electromagnetic depth sounding. Consultants Bureau, New York, 312 p).

Vargin, H., Shorbatov, S., Kvashnin, V. & Savin, A., 1990. Influence of EM methods involved in geophysical prospecting for Cu-Ni deposits in the Kola-Karelian region. (Роль

электромагнитных методов разведки в комплексе геофизических работ, связанных с поисками медно-никелевых месторождений в Карело-Кольском регионе (В настоящем сборнике)). This issue.

Velikhov, E., Gorbunov, G., Volkov, Yu., Zhukov, B., Vanyan, L.L., Demidova, T.A., Zhamaletdinov, A.A., Hjelt, S.E. & Heikka, J., 1983. First Soviet-Finnish experiment in recording MHD-generator pulses. (Первый советско-финский эксперимент по регистрации сигналов МГД-генератора). Rep. of USSR Acad. Sci. 271, No. 2: 324-327.

Velikhov, E., Pavlovski, V., Volkov, Yu., Zhamaletdinov, A.A. & Zakharova, V. (eds.), 1982. Electromagnetic depth sounding utilizing MHD-generator pulses. (Глубинные электромагнитные зондирования с применением импульсов магнитогидродинамических генераторов). Apatity, Geol. Inst., Kola Branch USSR Acad. Sci., 158 p.

Veshev, A., 1980. Electric profiling with a-c and d-c. (Электропрофилирование на постоянном и переменном токе). Sec. ed., rev. and enl., Leningrad, Nedra, 391 p.

Veshev, A., Lyubtseva, E., Leontchikov, V. & Alekseev, E., 1978. Temporary manual to EM sounding with vertical magnetic dipole. (Временное руководство по методу электромагнитного зондирования с вертикальным магнитиым диполем). Moscow, Ministry of non-ferrous metallurgy, 43 p.

THE AUDIOMAGNETOTELLURIC (AMT) METHOD AND ITS USE IN ORE PROSPECTING AND STRUCTURAL RESEARCH

by

S.-E. Hjelt, J.V. Heikka, E. Lakanen, R. Pelkonen and R. Pietilä

Hjelt, S.-E., Heikka, J.V., Lakanen, E., Pelkonen, R. & Pietilä, R., 1990. The audiomagnetotelluric (AMT) method and its use in ore prospecting and structural research. *Geologian tutkimuskeskus, Tutkimusraportti 95*, 69- 86, 13 figs.

When the audiomagnetotelluric (AMT) method is used, several components of the Earth's natural electromagnetic field are registered simultaneously in the frequency band 1 to 10000 Hz. The primary field is produced mainly by lightning discharges and the secondary fields carry information about the distribution of the electrical conductivity within the subsurface.

In Finland, the scalar variant of the AMT method has been succesfully applied both in ore prospecting and structural research. The present paper reviews the main properties of scalar AMT measurements and the basic principles of data processing and interpretation. Three case histories are presented.

A general structural study was made at Talvivaara in the Kainuu schist belt. In the area of the Rautuvaara iron mine, the scalar AMT technique was successfully used to locate gently dipping, conducting and ore-critical horizons at depths ranging from a few tens of meters to about 500 meters. In a regional survey, covering about 15 km^2 in the Hannukainen area, the AMT results were a relevant complement to other geophysical studies.

Some results are presented from a study made at Polvijärvi, on the Outokumpu formation, where the scalar AMT data are compared with recordings using a electrical dipolar source (so-called controlled source AMT = CSAMT measurements). The CSAMT technique has superior signal-to-noise ratios, but the interpretation becomes increasingly complex.

Key words: electromagnetic induction, audiomagnetotelluric methods, sounding, inverse problem, mineral exploration, crust, case studies, Talvivaara, Hannukainen, Saramäki, Finland

Ельт, С.-З., Хейкка, Й.В., Лаканен, З., Пелконен, Р.И., Пиэтиля, Р., 1990. Магнетотеллурический метод на звуковых частотах (ЗМТ) и его применение при поисках рудных ископаемых и в структурной геологии. Геологический центр финляндии, Рапорт исследования 95. 69-86, Илл. 13.

При использовании магнетотеллурического метода на звуковых частотах (ЗМТ) одновременно регистрируется несколько составляющих естественного электромагнитного поля Земли в диапазоне частот от 1 до 10000 Гц. Первичное поле создается при этом обычно за счет молнийных разрядов, а вторичные поля несут информацию о распределении электропроводности в подповерхностном слое.

В финляндии метод ЗМТ в скалярной версии успешо применялся как при поисках рудых ископаемых, так и в структурных исследованиях. в статье приводятся главные характеристики скалярной съемки змт и основные принципы обработки данных и интерпретации полученных результатов. В качестве примера рассмотрэны три действительных случая.

В Талвиваара, в пределах сланцевого пояса кайнуу, данный метод употреблялся для общеструктурных исследований. В железорудном районе Раутуваара скалярная технология змт была с успехом применена для локализации пологопадающих провадящих рудокритических горизонтов в диапазоне глубин залегания от первых десятков метров до 500 м. При региональной съемке на территории около 15 км^2 в районе месторождения Ханнукайнен данные АМТ успешно дополнили остальные геофизические исследования.

На преимере района Полвиярви (пояс оутокумпу) представлены результаты исследований по сравнению результатов скалярного метода ЗМТ с данными, полученными с применением электрически диполярного источника (т.н. съемка ЗМТ с управляемым источником = CSAMT). Технология CSAMT является несравненной по отношению сигнала к помехе, однако интерпретация результатов оказывается крайне сложной.

Description of the method

The source field and its properties

Most of the energy in the audio frequency EM spectrum (1 to 10 000 Hz) is due to the energy released in lightning discharges. This energy is propagated all over the world and forms the source field for the AMT method. Because the thunderstorm activity around the world varies geographically and seasonally, the energy level changes, too. In principle the most suitable times for measurements in Finland are the summer season and the afternoon hours.

The lightning discharge is essentially a vertical electric dipole, but far away, on the measuring site, the primary field can be described by plane waves. Locally the data are distorted by noise fields, mainly of man-made origin. Power-lines are especially harmful, since the measuring frequency band includes the mains frequency, 50 Hz and its harmonics. In very resistive environments, even rather high harmonics have been identified up to several kilometers from the power line.

In recent years the use of frequency sounding (FS) has increased in prospecting. Systems, in which the horizontal field components of a grounded long wire are recorded have become known in the western literature as the CSAMT (Controlled Source AMT) method (Goldstein and Strangway, 1975; Zonge et al., 1980). The prize paid for higher signal-to-noise ratios and improved reliability of the data is increasing the complexity of interpretation.

The measurements

In complete MT measurements all four horizontal components are recorded and the most up-to-date systems make use of the additional information in the vertical magnetic field component. The components of the electric and magnetic fields **E** and **H** are linearly related

$$\mathbf{E} = \mathbf{Z} * \mathbf{H} \qquad (1)$$

The connecting factor is the impedance **Z**, which depends on the distribution of electrical conductivity within the Earth. It is a complex tensor, which can be mathematically rotated to obtain its extreme directions. These directions are related to those of the electrical conductivity of the subsurface, which again are controlled by geological structures, such as the strike and fractures of the bedrock.

Often AMT work is restricted to the scalar case, where only one electrical and one magnetic horizontal component are measured. Directional information on the impedance can then be obtained only by rotating the measuring layout at the field site and registering the field components in various directions. Scalar AMT corresponds to the classical Tikhonov-Cagniard theory (Cagniard, 1953, Tikhonov, 1950) and gives correct results for a horizontally layered medium. In Precambrian geology, scalar AMT data must normally be interpreted by 2D numerical modelling.

Equipment

In Finland, all measurements have been made with the French scalar instruments ECA 541-0 and 542-0. The systems have built-in filters for fixed frequencies. The high frequency part of AMT recordings is always checked by the VLF-R method. This gives a crucial control over the high frequency part of the AMT sounding curve, which otherwise often remains useless because of poor signal levels from around 1 to 3 kHz. The mains frequency and its first harmonics are suppressed by notch-filtering techniques.

Table 1. Frequencies (in Hz) of the French scalar AMT-systems 541-0 and 542-0.

541-0	8	17	37	80	170	370	800	1700	3700
542-0	4,7	7,1	23	47	71	230	470	710	2300

Data processing

The impedance tensor is usually obtained from the recorded electrical and magnetic field time series using spectral methods. Instead of the impedance **Z**, magnetotelluric data are usually presented as (scalar) apparent resitivities ρ_a and phases.

$$\rho_a = | Z_{ij} |^2 / (\omega\mu \qquad (2)$$
$$\phi = \arg (Z_{ij})$$

When the tensor component ij of **Z**, corresponding to the electric field measured (or rotated) along the geological strike, is used, one speaks of parallel apparent resistivity $\rho_a||$ or E-polarization. In H-polarization results, the magnetic field component along the geological strike is used and consequently one speaks of perpendicular apparent resistivity, $\rho_{a\perp}$. For a horizontally stratified Earth, $\rho_a|| = \rho_{a\perp} = \rho_a$. For a homogeneous half-space, ρ_a equals the true resistivity of the half-space. There exist several other ways of defining the phase shift.

When AMTequipment records only two components of the EM field, only scalar apparent resistivities can be calculated. In the instruments ECA 541-0 and 542-0, this is performed electronically. At the same time, the phase information is lost.

Presentation of sounding curves

The MT results are usually presented as sounding curves, ie., ρ_a as a function of decreasing frequency on a log-log scale. It has become standard practice to draw AMT results directly on the H-S-nomograms already in the field. The H- and S-lines give the possibility of rapidly estimating these interpretation parameters immediately after and/or during field work. Normally, a suitable number of readings (3-5) are taken at each frequency, and their average value is drawn (together with their extremes) on the nomogram at the measuring site. When an appropriately short distance between the sounding points has been used, the presentation of all the sounding curves along a profile simultaneously gives a qualitative quick-look on the behaviour of the electrical cross-section. The 2D distortion effects (Berdichevsky and Dmitriev, 1976) are easily recognized, provided sounding profiles in two perpendicular directions are used.

Electric cross sections

At the lower frequencies, the electromagnetic field penetrates deeper into the subsurface. The apparent resistivities are sometimes plotted along the profile so that the frequency decreases downwards and the ρ_a-values are contoured. The result is called a pseudosection, which is a rough estimate of the conductivity versus depth. If true vertical resistivity cross-sections are wanted, 2D numerical modelling is necessary for the complete

measuring profile. A suitable formal 1D model is used as a starting model. For the most reliable fit, measurents in two independent directions should be used simultaneously.

1D interpretation

Nomograms

As explained, nomograms with H- and S-lines can be used for the first quantitative interpreration even in field conditions. Since the resistivity contrasts are often large, formal 1D models give reasonable estimates for the most reliable parameters: the depth to a well-conducting layer and the layer conductance. Layer model curve fitting is also possible and may be useful when the sounding points are situated far from each other.

Resistivity-depth transformations

Several methods have been proposed in the literature. The Niblett-Bostick transformation (Niblett and Sayn-Wittgenstein, 1960, Bostick, 1977) and its variants (Jones 1983, Goldstein and Strangway, 1975) have at present gained the greatest popularity. The transformation is very efficient as a first 1D approximation of MT data. It can be written as (Goldberg and Rotstein, 1982)

$$\rho_{NB}(z) = \rho_a(T)\,(\pi / \{2\phi(T)\} - 1)\,, \tag{3}$$

where $\phi(T)$ is the phase of the apparent resistivity. Alternatively the transformation can be written (Weidelt, 1972, Jones 1983) in a form suitable for calculation also from scalar data

$$\rho_{NB}(z) = \rho_a(T)\,\{1 + m(T)\} / \{1 - m(T)\}, \tag{4}$$

where

$$m(T) = \partial\,\{\log[\rho_a(T)] / \partial \log(T)\} = \{T / \rho_a(T)\}\,\partial[\rho_a(T)] / \partial T$$

is the slope of the apparent resistivity sounding curve in log-log presentation. Two points at both ends of the sounding curve have to be sacrificed to the determination of the slope m(T).

Fig. 1 shows a theoretical example of using the Niblett-Bostick transformation. The forward problem has been calculated with the recursive algorithm of Kunetz (1972). The layers are shown by dashed lines. The transformation gives realistic depths and conductivities for conducting layers. The transformation works less well for resistive layers.

Curve fitting

For selected soundings, where a closer model is required, a layer model can be fitted to the data by standard least-squares inversion (optimization) techniques. The method consists of fitting the logarithm of apparent resistivity by the so called hyberparabolic method (Lakanen, 1975), where 2-4 model parameters (layer resistivities and thicknesses) are optimized simultanously. A layer model fit (Pelkonen et al., 1979) seldom significantly improves the model obtained from, H-S-line estimation, provided proper distortion corrections have been applied.

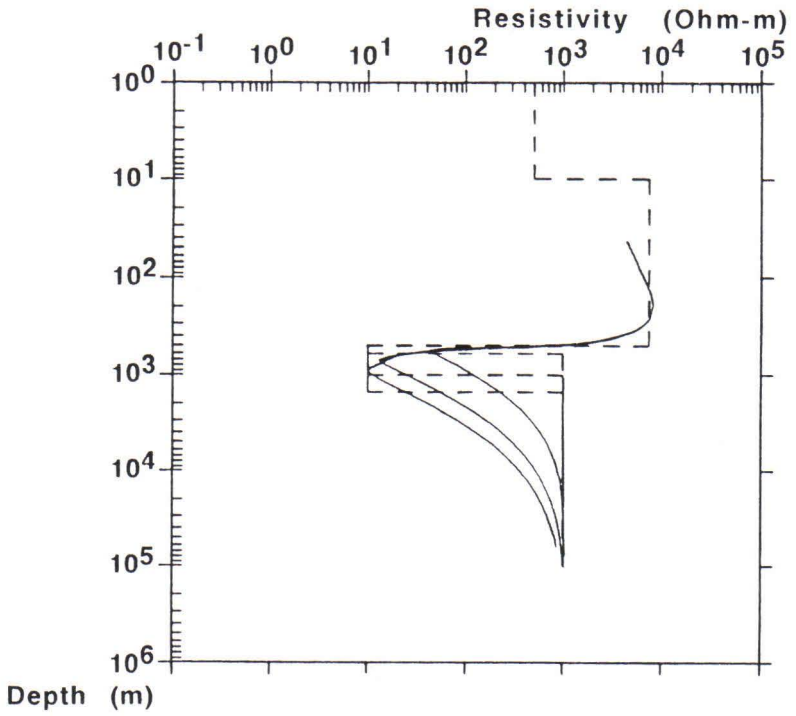

Fig. 1. Niblett-Bostick inversion of theoretical 4-layer AMT data with varying thickness of the 3rd (conductive) layer. The well-conducting layer is resolved and located with good accuracy. The frequency band 0.01 - 100 000 Hz is used (Heikka, unpublished material).

2D interpretation

Modelling principles

In most cases relevant in prospecting, the conductive structures are not 1D, and in these cases more complicated models have to be used. Because of the complexities of the EM equations, numerical methods like finite differences (FD), finite elements (FE) or integral equations (IE) have to be used (e.g., Kaikkonen, 1980). Although several program variants are in use in Finland, the most efficient programs are using the Finite Element method and are capable of handling simultaneously up to 10 units with different conductivity, dielectric and/or magnetic parameters (Kaikkonen, 1979). An illustrative collection of examples has recently been presented by Pelkonen (1985).

Case histories

Structural mapping

In 1981, test measurements were performed jointly in the Talvivaara area by the Geological Survey of Finland and the University of Oulu. The aim was to study the applicability of the AMT method in obtaining geoelectrical structural information about the area. The VLF-R results along the same profiles are described in paper of Hjelt et al. of this collection .

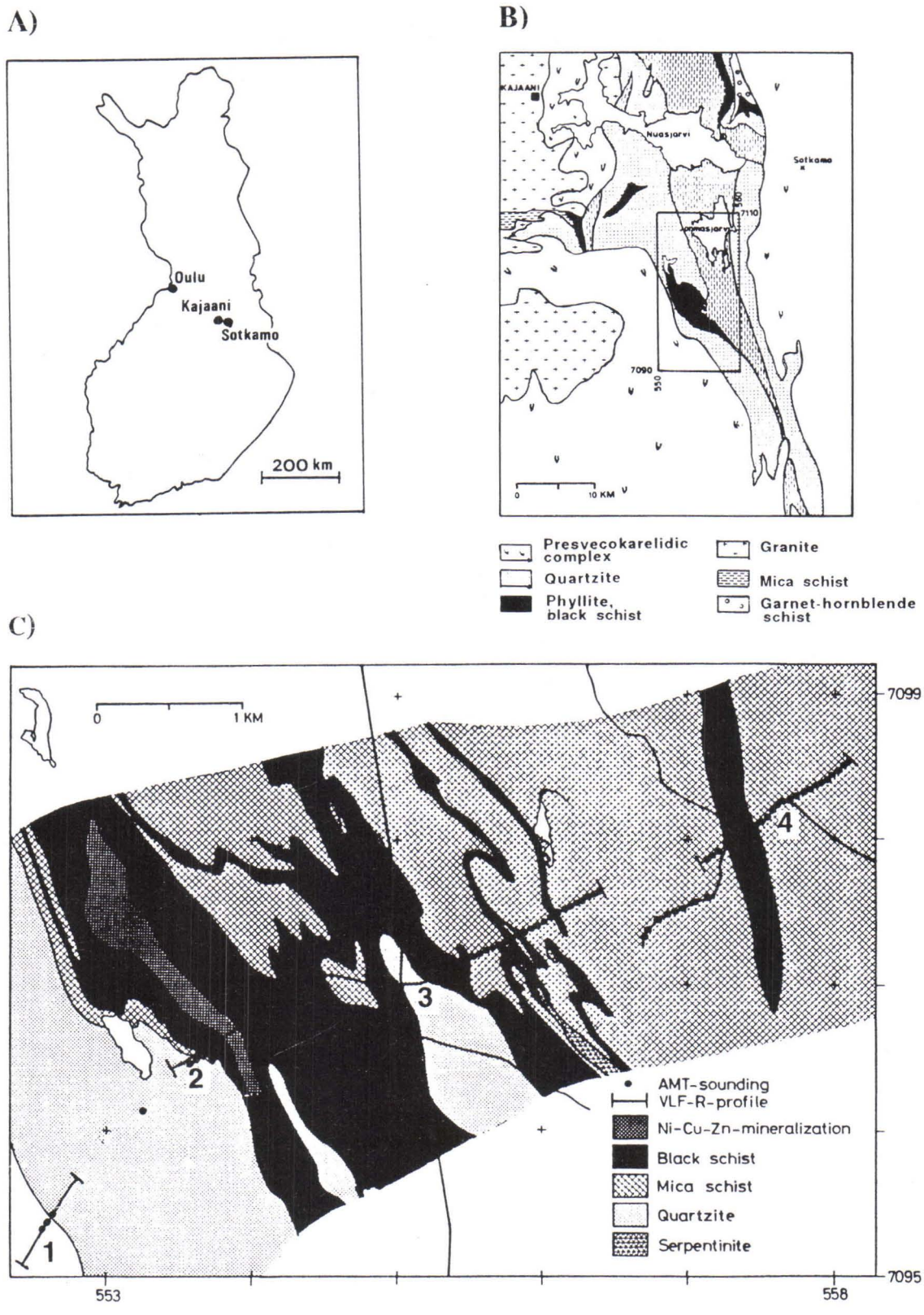

Fig. 2. Location (A) and geology (B) & (C) (Heino and Havola, 1980) of the survey area of Talvivaara in the southern part of the Kainuu schist belt.

The survey area is situated in Sotkamo, in the southern part of the Kainuu schist belt (Fig. 2). The measuring profiles are located perpendicular to the structural trend (227^{0}) of the area. The sounding curves are given in Fig. 3 for two perpendicular directions of the electric field.(Please observe that the sounding points are not equispaced along the profile).

A)

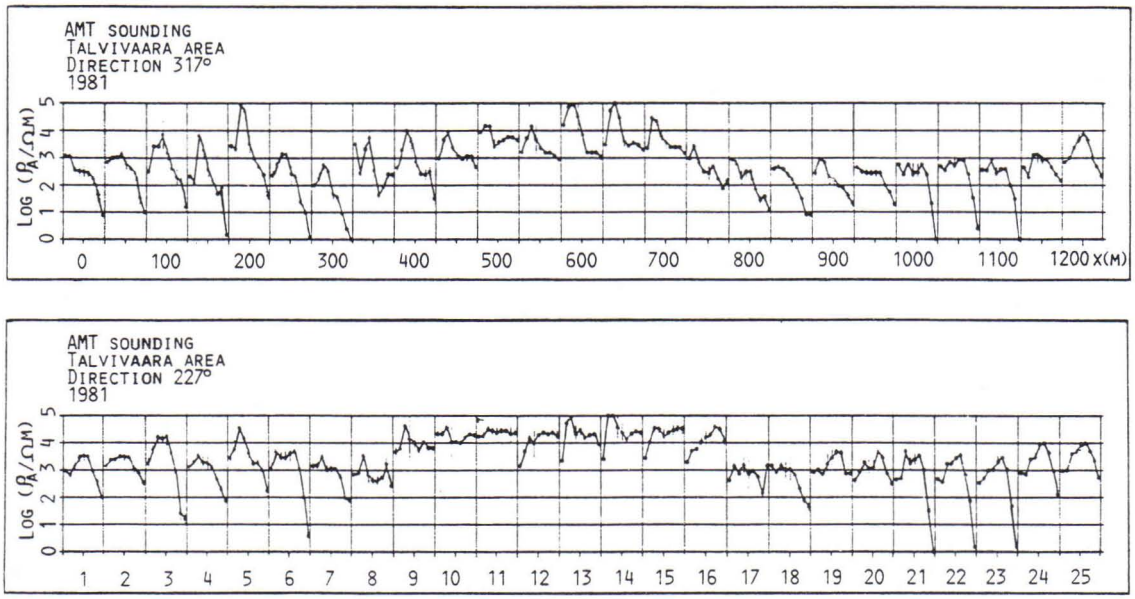

B)

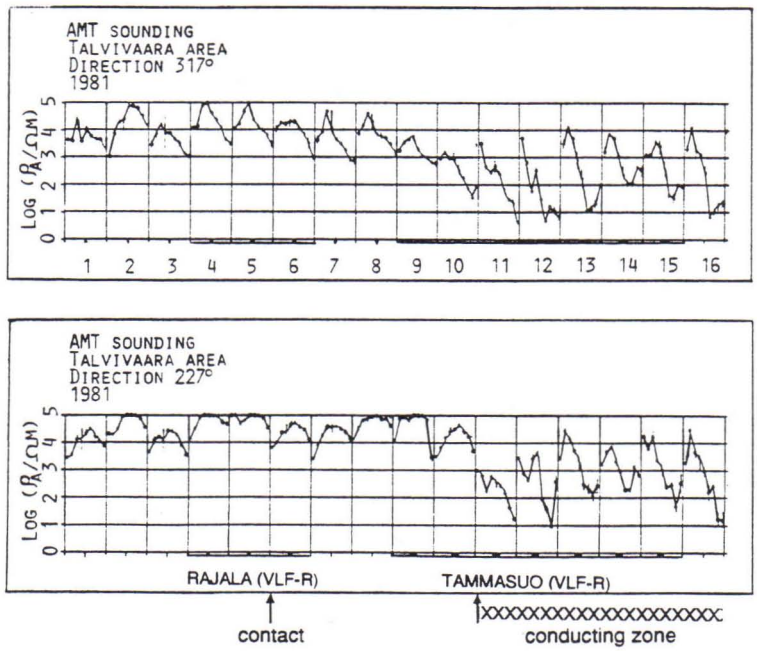

Fig. 3. AMTS profiles in the Talvivaara area. The direction 317^{0} is perpendicular to and 227^{0} along the regional strike respectively. A. The Rajala profile (no 1, Fig. 2c) across the contact between the granitic surrounding and the Kainuu schist formation and the Tammasuo profile (no 2, Fig. 2c) across the western boundary of the black schist block (note that the sounding points are not equispaced). B. The Kohisevanpuro profile.

The contact between the resistive (mica schists) and conductive (black schists) blocks of the area is sharp when the electric field is measured in the 227° direction. Because of the approximate two-dimensionality of the structure, this can be considered as the E-polarization direction. Above the conductive schist belt formation, the low frequency parts of all the sounding curves have a decreasing slope. Also the general level of apparent resistivity is lower than above the resistive areas.

A)

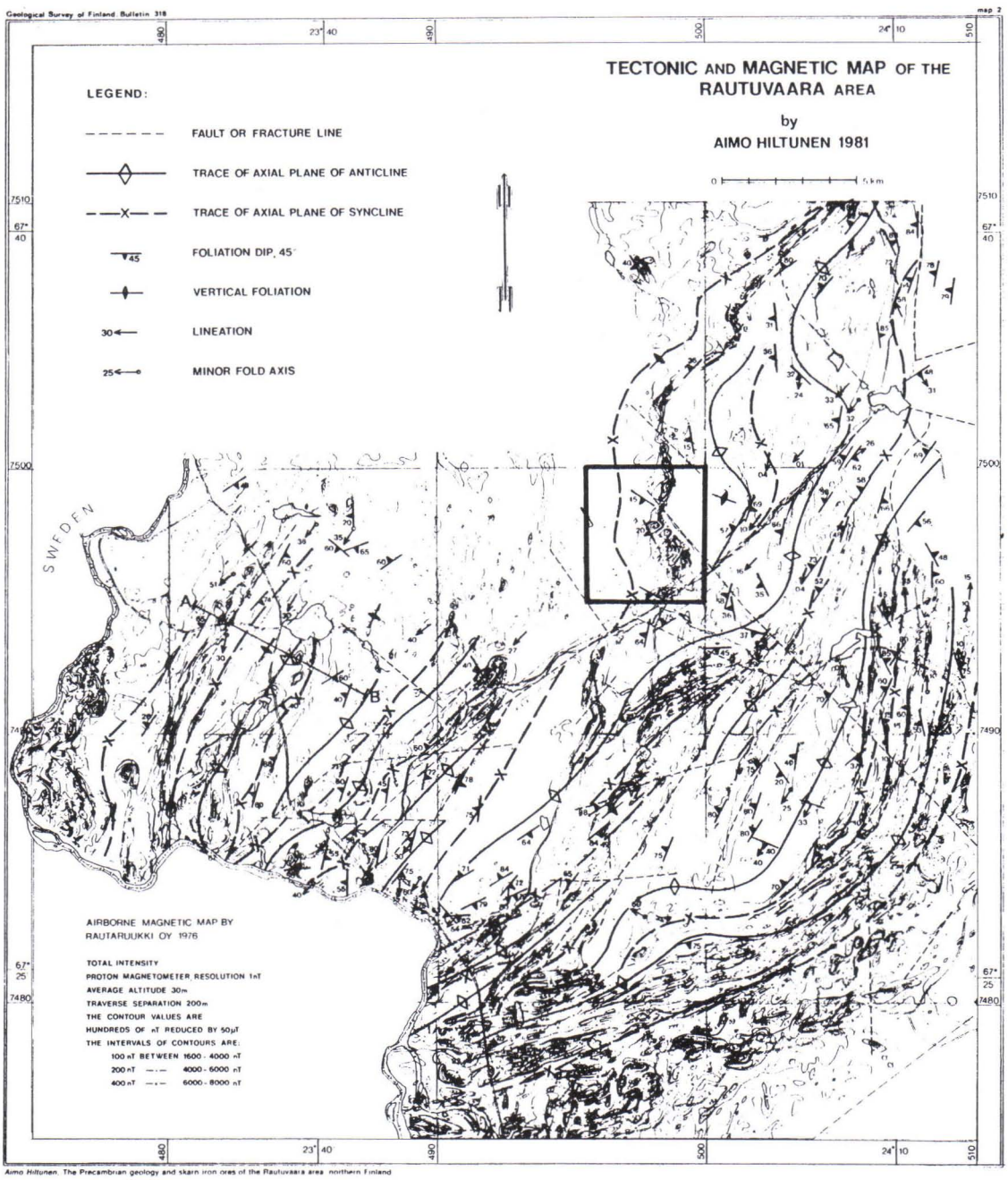

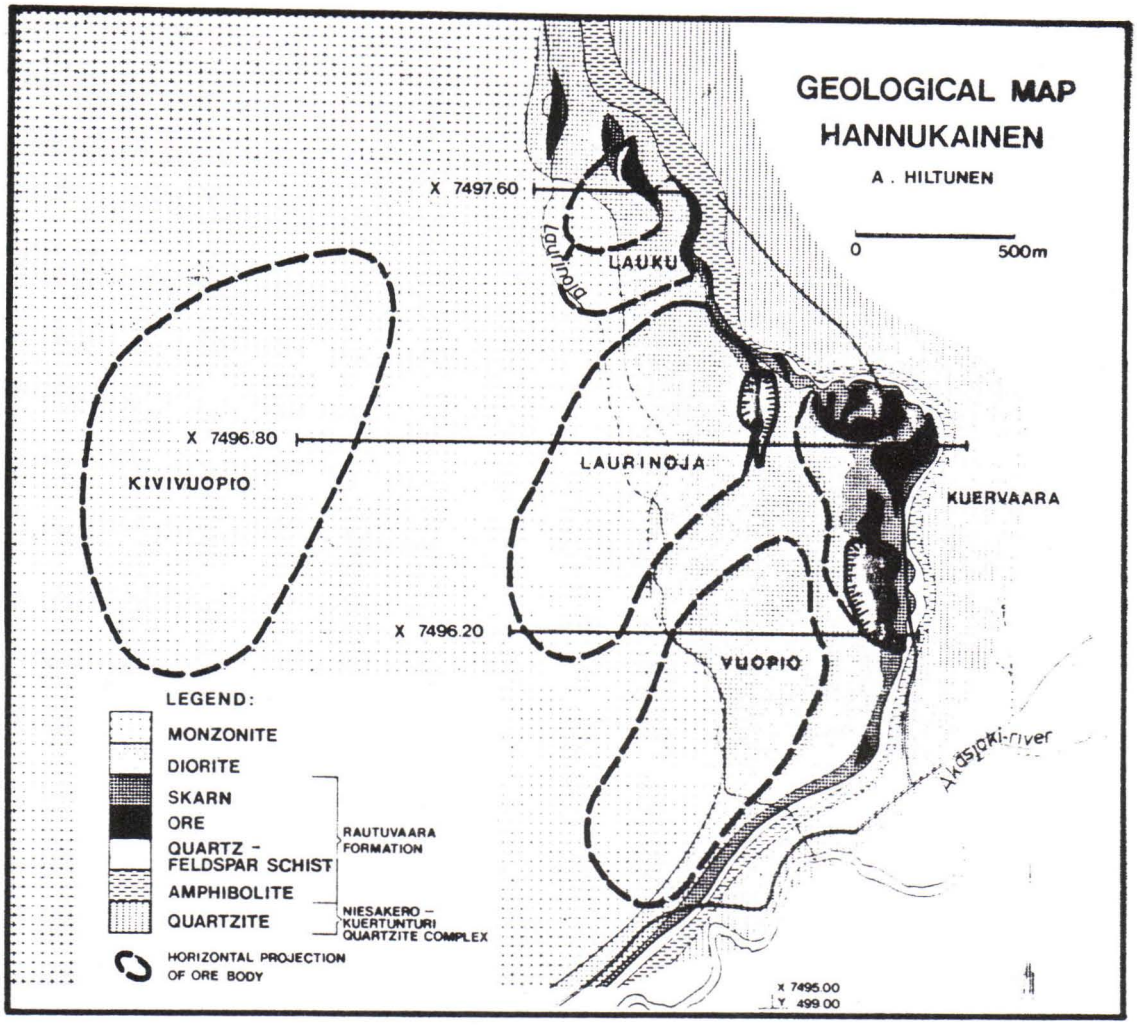

Fig. 4. The tectonic and magnetic map of the Rautuvaara area (A) and the Hannukainen deposits (B). (Hiltunen, 1981).

Mapping of conducting horizons

The first application of the AMT method to mineral prospecting in Finland was made in 1976 near the Rautuvaara iron mine of Rautaruukki Oy (Pelkonen et al., 1979). The sounding points were located mainly along the profile x= 96.80, which traverses the gently dipping, conductive (1 to 10 Ωm) skarn iron ore lenses of the Hannukainen area. This survey, carried out as a co-operative study by Rautaruukki Oy and the Department of Geophysics, University of Oulu, with the French ECA 541-0 system, revealed deeper continuations to the known ore lenses along the dip. Hole R-162 was drilled in response to the AMT results. A conductive magnetic layer was found at a depth of 417 m, in fairly good agreement with the AMT interpretation.

Encouraged by the first experimental AMT survey and the favourable geological structure of the area, more extensive AMT surveys have been conducted later in several stages. In 1981 an extensive, systematic AMT survey was carried out in order to map the deep ore reserves of the Hannukainen area. Within the area (Fig. 4),15 km^2 of scalar AMT data were

obtained using the new ECA 542-0 system. Altogether 950 sites were sounded in a grid of 200 m by 100 m (sometimes 50 m).

In a region where the depth of the conducting layer was known, the azimuthal dependence of the apparent resistivity was studied. Within reasonably small e margins of error, the depth of the conductive layer was obtained from the sounding curves for most measuring directions. The S-values (conductivity x thickness) are different only if determined from EW directed scalar soundings. The direction of the E-polarization of the AMT field was assumed to be in major parts of the area parallel to the geological strike. Thus the systematic AMT survey was performed measuring the E-field along this strike.

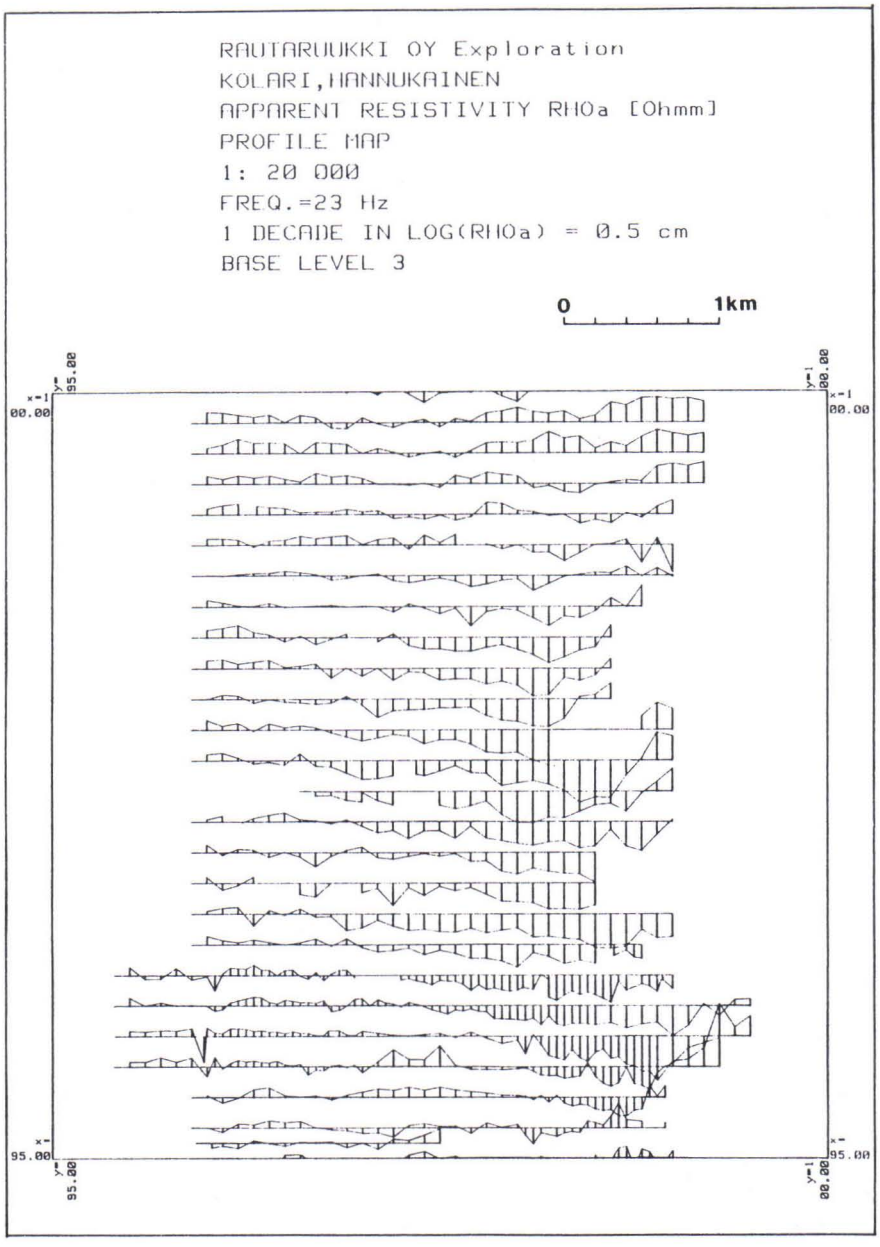

Fig. 5. Apparent resistivity profile map of the Hannukainen AMTS area for the frequency of 23 Hz.

The well known energy minimum of the source field around 1 to 3 kHz was clearly noted during the whole survey. Thus the resistivities for this frequency band had to be omitted from the interpretation in most cases. These data were replaced by the apparent resistivity value from VLF-R-measurements at 16.4 kHz. The interpretation included the three main steps, data processing (presentation of sounding curves and removal of unreliable data points), 1D inversion and qualitative estimation of 2D and 3D effects. The sounding curves were plotted on the HP 9845B desktop computer of Rautaruukki Oy Exploration. From the data base created, a great variety of graphical representations could be easily obtained, individal sounding curves, profile and contour maps, pseudosections or residual profiles. A 1D interactive curve fitting system was included in the data processing.

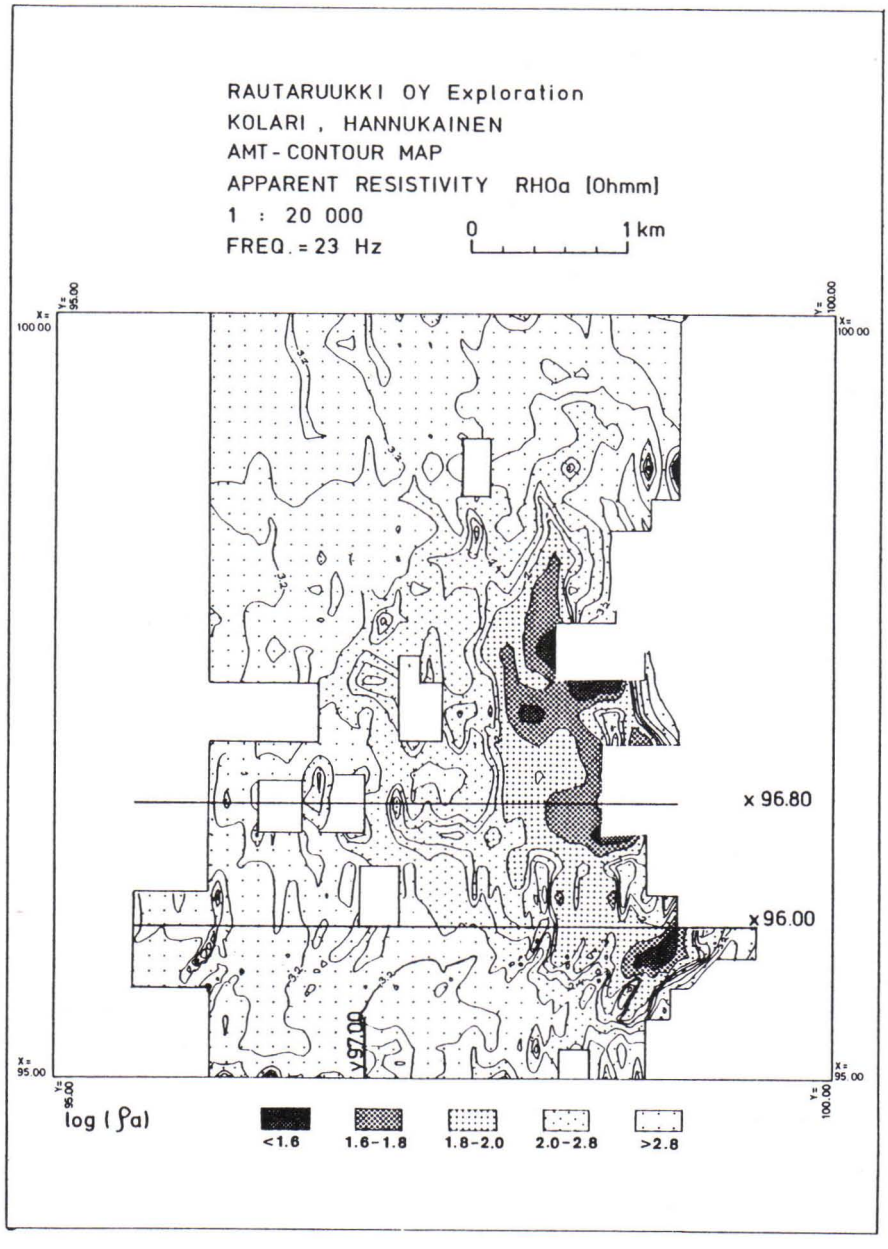

Fig. 6. Apparent resistivity contour map of the Hannukainen AMTS area for the frequency of 23 Hz.

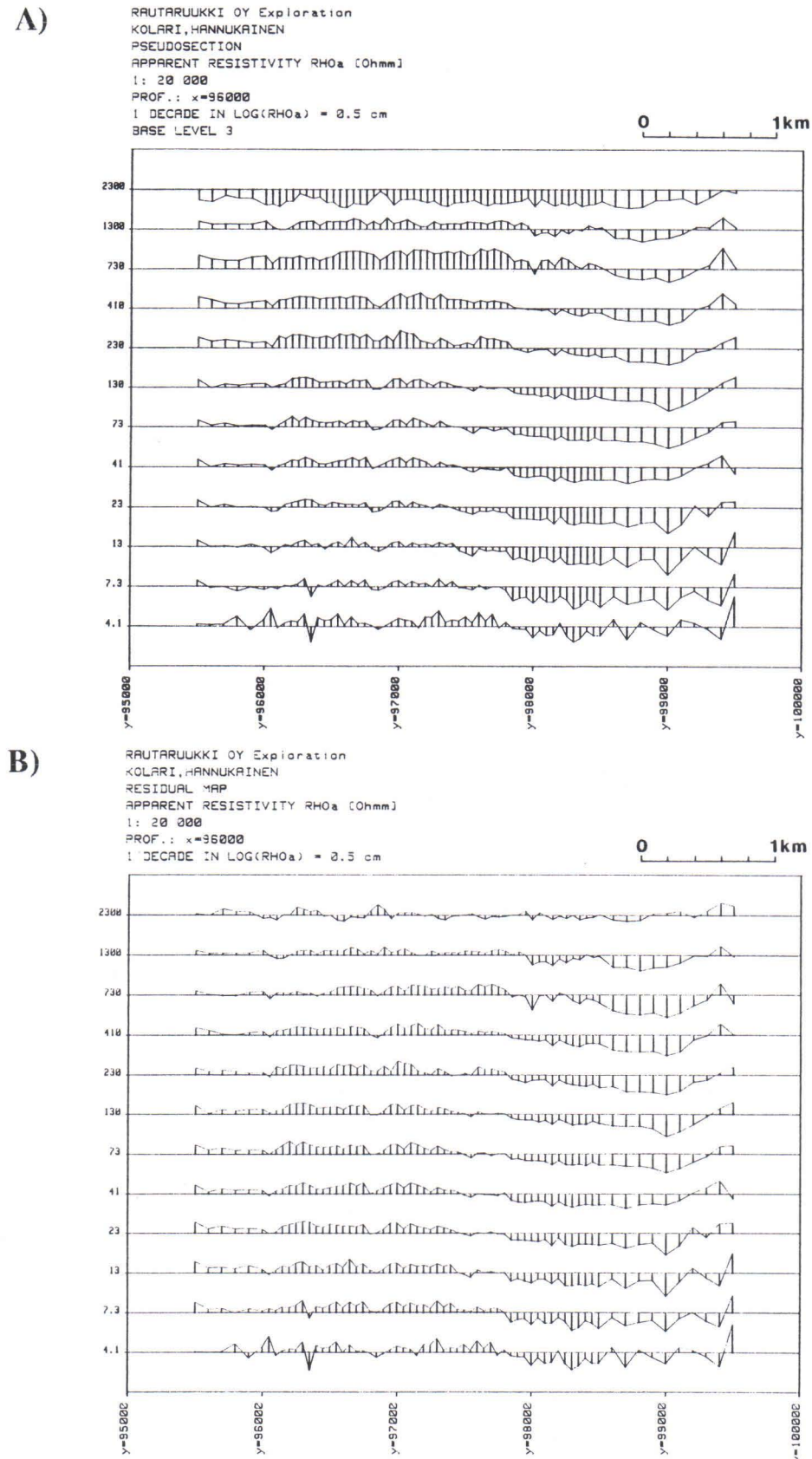

Fig. 7. Apparent resistivity pseudosections (A) and residual profiles (B) of the Hannukainen AMTS area.

A reasonable accuracy was obtained with1D interpretations using the simple H-S-line technique (Berdichevsky, 1968), since the geology of the area was clearly layered and the resistivity contrast between the conductor and the surrounding rock was great (>300). Some problems of equivalence were studied more in detail using the 1D curve fitting method (Pelkonen et al., 1979). Figures 5 and 6 give a curve presentation for the qualitative interpretation stage. From profile (Fig. 5) and contoured (Fig. 6) ρ_a maps, the initial estimate of the geoelectrical cross-section can be obtained approximately at the skin depth of the frequency in question. The pseudosection (Fig. 7A) gives simultaneously lateral and frequency dependent variations of apparent resistivity. In the residual technique (Koziar, 1976), apparent resistivity profiles are constructed by normalizing the resistivity values with the regional average at each frequency. The most resistive and most conductive parts of the survey are easily separated (Fig. 7B).

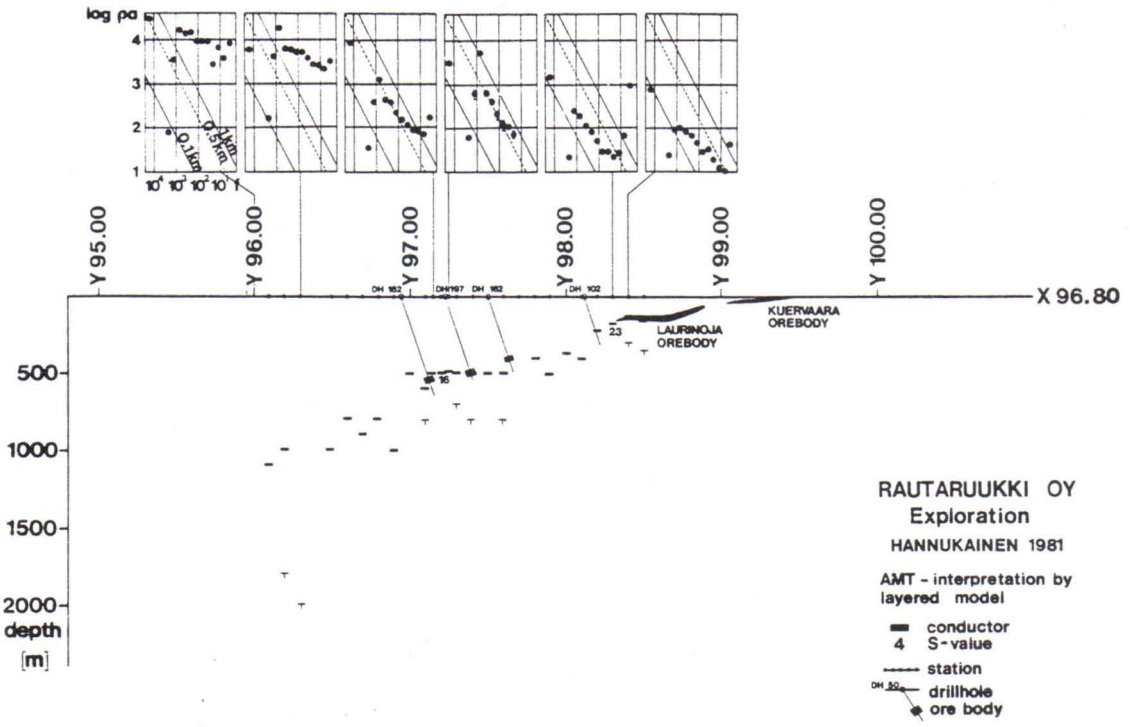

Fig. 8. 1D interpretation of the Hannukainen AMTS data along profile X = 96.80. Drill holes DH 182, DH 197, and DH 162 intersected conducting and magnetic material at depths corresponding to the conducting layers of the 1D model.

In the 1D interpretation result (Fig. 8), the eastern part of the conductor is associated with the known ore body. The plotted 1D conductor depths give the impression of a continuous, gently dipping structure. At the extreme sounding sites in the western part of the profile, the depth of the conductor increases rapidly. This is a typical behaviour of 1D inversion close to the edge of a 2D (or 3D) structure. By measuring at such locations, the azimuthal properties of the apparent resistivity, 2D effects are easily recognized also from scalar AMT data (for tensor MT data, such parameters as the skew and tipper give corresponding information).

The AMT method played a very important role when the ore bodies of the Hannukainen area were mapped with geophysical methods (Hattula, 1978). The AMT data gave valuable information about both the horizontal and the vertical location of conducting structures related to the ore formations in the area.

Use of controlled sources

In 1980, the Outokumpu Co did CSAMT field work using a rented Geotronics Co. EMT-5000 (transmitter) and EMR-1 (receiver) system. The apparent resistivities are calculated separately at 16 frequencies from 1 to 9600 Hz. The test aimed at a comparison of the CSAMT results with earlier natural field scalar AMT results.

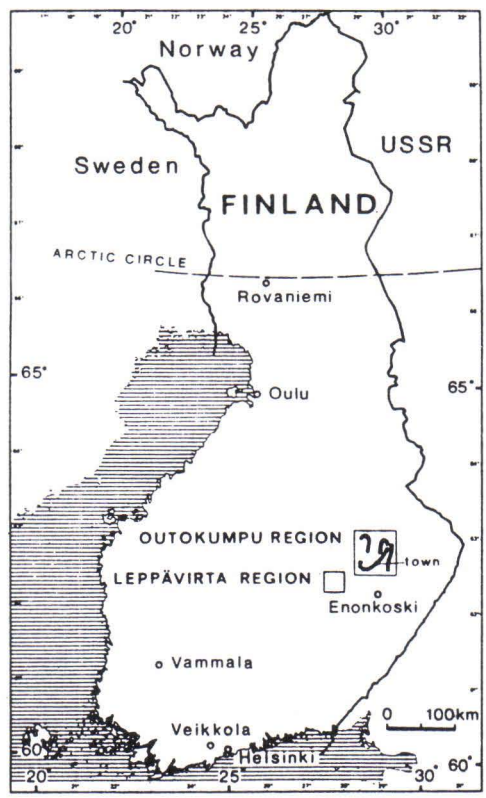

Fig. 9. Map marking the location of the Outokumpu formation.

Tests were made during a two month period in the Polvijärvi area , northeast of the town Outokumpu (Fig. 9). The Outokumpu formation includes a horizon with copper-ore potentiality. The horizon extends to the north and includes a small mineralization at Saramäki. The geology of the Outokumpu formation has been described in detail by Koistinen (1981), and the geophysical work done in the area has been summarized by Ketola (1979). The AMT measurements in the area have been described by Lakanen (1986).

In the first CSAMT test, the signal levels and the distortions of the Tikhonov-Cagniard conditions were established. The transmitted power was about 3 kW, the source dipole length (the length of the current cable)100 m and the resistivity of the environment on the average 5000 Ωm. A comparison between the CSAMT and AMT soundings is shown in Fig. 10. A fracture zone, located about 1.6 km from the transmitter, caused an anomaly, which made a comparison difficult. The increasing distortion of apparent resistivity from the Tikhonov-Cagniard-condition, when approaching the transmitter site, is evident. The resistivities at low frequencies differ by a factor of 4 and higher frequencies by a factor of less than 2, approximately as expected from theoretical considerations (e.g., Kaufmann and Keller, 1983). The low level of resistivity is attributed to a conductive horizon at depth.

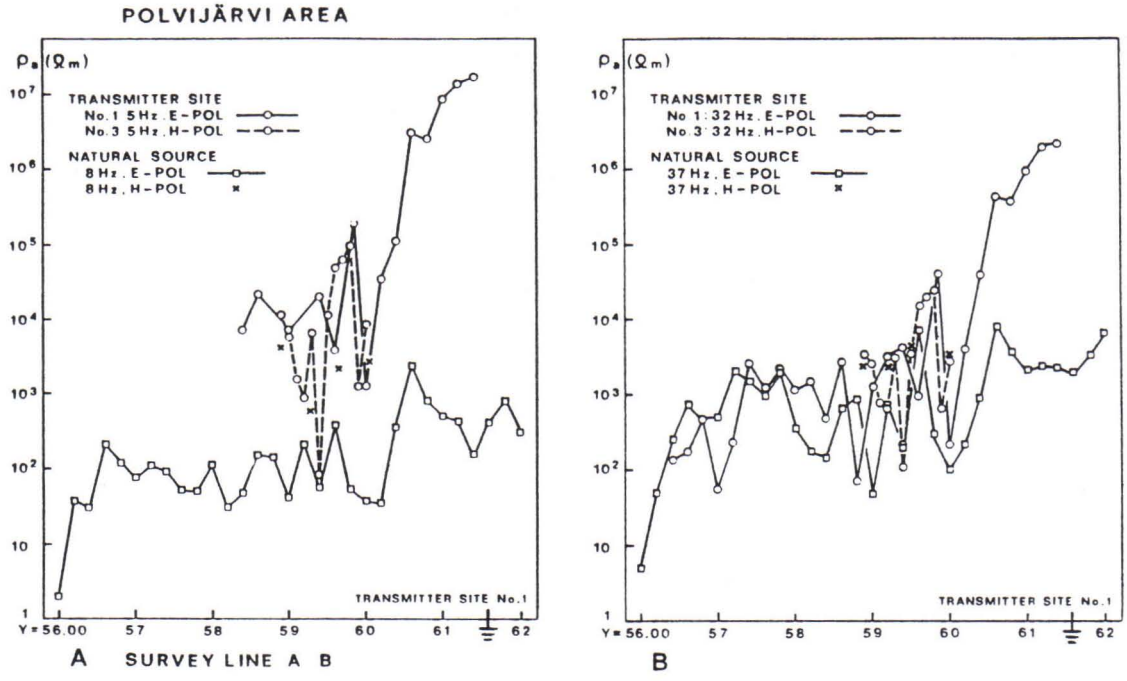

Fig. 10. Comparison of CSAMT and AMT apparent resistivity profiles in the Polvijärvi area of the Outokumpu formation. A. Lowest AMT frequencies (5-8 Hz), B. medium AMT frequencies (32-37 Hz).

At the lowest frequencies (5 Hz) the magnetic field component became too weak to be measured when the distance from the transmitter approached 3 km. The apparent resistivity of the CSAMT was still two orders of magnitude higher than for the natural source AMT (8 Hz). At 32 Hz a useful signal was still obtained 4 km away from the source. The measured mode was in principle equivalent to E-polarization.

When a long transmitter cable (3000 m) was used in the H-polarization mode, the level of the magnetic field signal was accordingly strongly enhanced. At 5 Hz (compared with 8 Hz fo AMT) the apparent resistivity values differed by a factor of 5 to 10, whereas the same values were obtained at 32 Hz. The result supports the 3 times skin-depth condition given by, among others, Goldstein and Strangway (1975).

With its complex but well-studied geology, the Saramäki area is interesting target for geoelectrical studies. There is an abundance of long, good conductors, which crop out and dip gently (20° to 30°) towards the east. One of the profiles of Fig. 11 was surveyed using four different transmitter sites (Nos. 4-7 in the Figure). All the transmitters are located at a distance of 3 km from the measuring site. The results on the lowest frequencies (5 and 8 Hz, respectively, Fig. 12) along profile X = 82.4 differ markedly depending on the location of the transmitter.

Transmitter location 4 is closest to the H-polarization mode situation, whereas the others can be more or less approximated as E-polarization modes. The lowest resistivities are naturally obtained for transmitter position 6, which is located on the footwall side of the bed with several conducting layers. When the results are interpreted by 1D modelling, the most consistent results are obtained for the AMT data. The depth to the conducting horizon connected to the drilled ore formation is well resolved. The orebody is very highly conductive, with a conductivity of more than 1000 S/m. (The black schists are accounting for only 10 to 100 S/m and the rest of the formation from 1 to 0.01 S/m.). The best CSAMT interpretation using this technique is obtained for transmitter position 6. A 2D modelling test yielded a much broader anomaly than the measured one when a single conductor was located at the depth of the drilled ore body (Fig. 13).

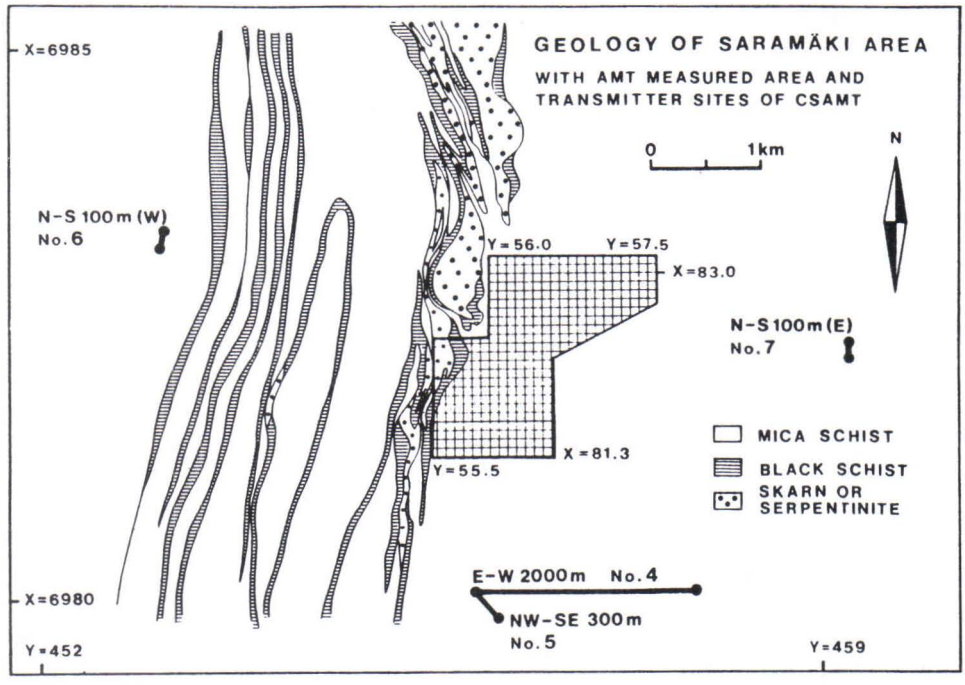

Fig. 11. Geology of the Saramäki area of the Outokumpu formation showing the survey area (hatched) and the transmitter sites of the CSAMT experiment.

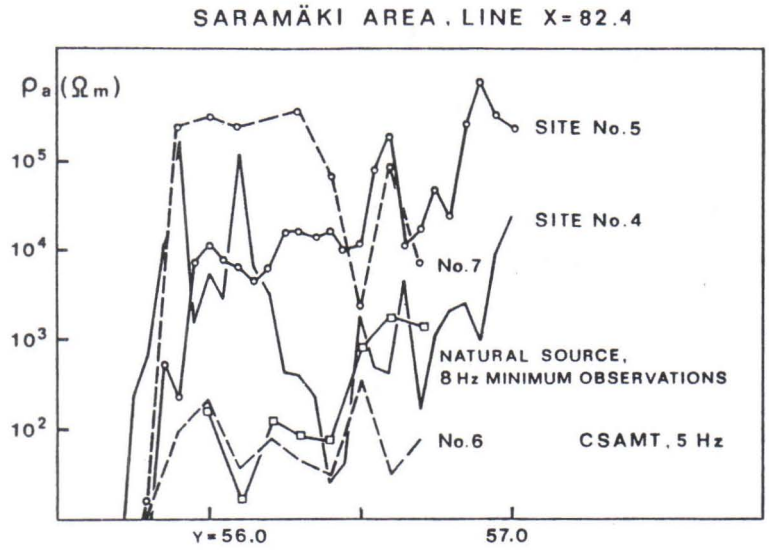

Fig.12. Comparison of CSAMT and AMT apparent resistivity profiles in the Saramäki area of the Outokumpu formation for the lowest AMT frequencies. Variation of apparent resistivity with the transmitter location in the CSAMT indicates variations in the geoelectrical structure of the area.

Some experiments were also performed with the directional properties of the apparent resistivity measurements. Although some results indicate minimum resistivities in directions that sometimes correspond to the strike of the primary fold axes in the area and sometimes to the strike of layers outcropping against an uplifted granitic dome, no definite conclusions can

be made based on these limited tests.

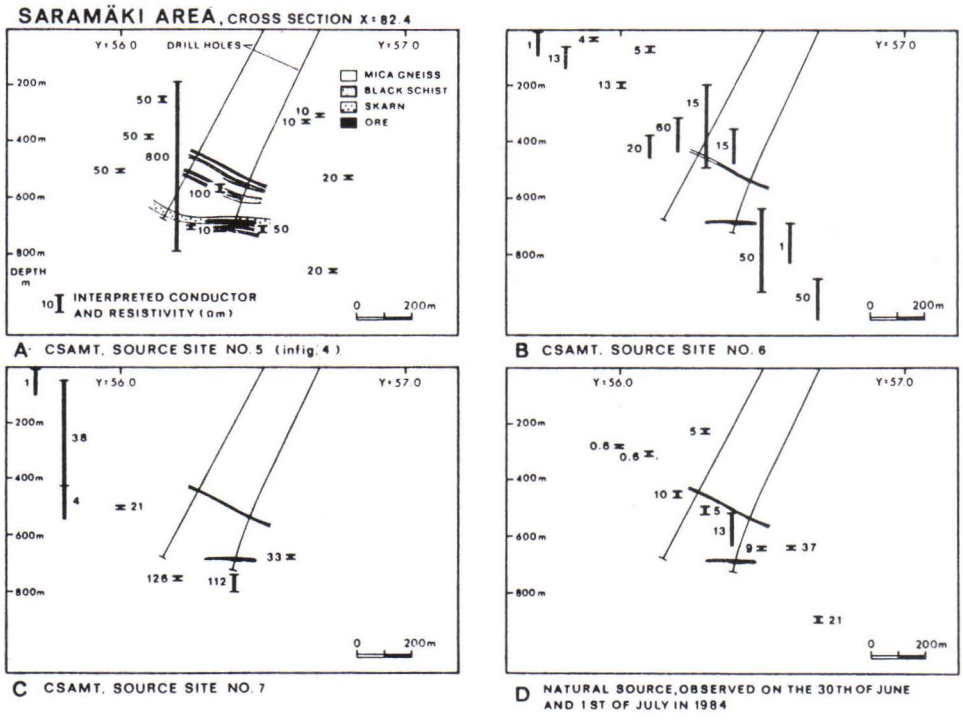

Fig. 13. 1D inversion results of three CSAMT soundings with different transmitter sites (A.- C.) and the inversion of AMTS data (D.). The geological cross section is indicated in A and the existing boreholes in all the sections interpreted.

It is evident that more elaborate interpretation procedures are needed for CSAMT data, although performance of the measurements in the field are easier and quicker to perform. Higher power could in principle be used to increase the signal-to-noise ratio at greater distances, but then safety problems and disturbances from, e.g., general telephone communication will arise. The use of loop transmitters seems to require, according to theoretical estimations, still higher power.

References

Berdichevsky, M.N., 1968. Электрисечкая разведка методом магнитотеллурисечкого профилирования. Nedra, Moscow, 255 pp.

Berdichevsky, M.N. & Dmitriev, V.I., 1976. Basic principles of interpretation of magnetotelluric sounding curves. In A. Àdám (ed.): Geoelectric and geothermal studies. Akademiai Kiadó, Budapest, 165-221.

Bostick, F.X., 1977. A simple and almost exact method of MT analysis. Workshop on Electrical Methods in Geothermal Exploration, U.S. Geol. Survey, Contract No 14080001 - 8 - 359.

Cagniard, L., 1953. Basic theory of the magnetotelluric method of geophysical prospecting. Geophysics18, 605-635.

Goldberg, S. & Rotstein, Y., 1982. A simple form of magnetotelluric data using the Bostick

transform. Geoph. Prospecting 30, 211-216.

Goldstein, M.A. & Strangway, D.W., 1975. Audiofrequency magnetotellurics with grounded electric dipole source. Geophysics 40, 669-683.

Hattula, A., 1978. Charged potential method (mise-a-la- masse) in Hannukainen and Sokli area of northern Finland. Geoexploration 16, 311 (abstract only).

Heino, T., & Havola, M., 1980. Geology of the Jormasjärvi-Talvivaara area (in Finnish). Report M 19/3344/-80/ 3/10, Koskee 3433, Sotkamo, Talvivaara. Geological Survey of Finland.

Hiltunen, A., 1981. The precambrian geology and skarn iron ores of the Rautuvaara area, northern Finland. Bull. Geol. Survey of Finland 318,133 pp.

Jones, A.G., 1983. On the equivalence of the "Niblett" and "Bostick" transformations in the magneto-telluric method. J. Geophys. 53, 72-73.

Kaikkonen, P., 1979. Numerical VLF modeling. Geophys. Prospecting 27, 815-834.

Kaikkonen, P., 1980a. Numerical VLF, VLF-R and AMT profiles over some complicated models. Acta Univ. Oul. A 91, Phys. 16, 34 pp.

Kaufmann, A..A.. & Keller, G.V., 1983. Frequency and transient soundings. Elsevier, Amsterdam-Oxford- New York, 685 pp.

Ketola, M., 1979. On the application of geophysics in the indirect exploration for copper suplhide ores in Finland. *In* P.J. Hood (ed): Geophysics and geochemistry in the search for metallic ores. Econ. geology report 31, Geol. Survey of Canada, 665-684.

Koistinen, T.J., 1981. Structural evolution of an early Proterozoic strata-bound Cu-Co-Zn deposit, Outokumpu, Finland. Trans. Royal Soc. Edinburgh, Earth Sciences 72, 115-158.

Koziar, A., 1976. Applications of audiofrequency magnetotellurics to permafrost, crustal sounding and mineral exploration. Ph.D. Thesis, Univ. Toronto, Toronto, Ont. Canada.

Kunetz, G., 1972. Processing and interpretation of magnetotelluric soundings. Geophysics 37, 1005-1021.

Lakanen, E., 1975. An overall computer graphics software for geophysical profile interpretation. Geop. Prosp. 23, 606 (abstract only).

Lakanen, E., 1986. Scalar-AMT applied to base metal exploration in Finland. Geophysics 51, 1628-1646.

Niblett, E.R. & Sayn-Wittgenstein, C., 1960. Variation of the electrical conductivity with depth by the magnetotelluric method. Geophysics 25, 998-1008.

Pelkonen, R., 1985. On numerical AMT profiles and sounding curves over some two-dimensional structures. Department of Geophysics, University of Oulu, Report No. 11., 57 pp.

Pelkonen, R., Hjelt, S.-E., Kaikkonen, P., Pernu, T. & Ruotsalainen, A., 1979. On the applicability of the audiomagnetotelluric (AMT) method for ore prospecting in Finland. Contribution, Dept. of Geophysics, Univ. of Oulu, No 94, 25 pp.

Tikhonov, A.N., 1950. Определение электрисечких характеристик глыбоких члоев земнож корй. Докл. Акад. Наык СССР:73, 295-297.

Weidelt, P., 1972. The inverse problem of geomagnetic induction. Zs. f. Geophysik, 38, 257-289.

Zonge, K.L., Emer, D.F. & Ostrander, A.G., 1980. Controlled source audio-frequency magnetotelluric measurements. Geophysics 46: 460 (abstract only).

EXAMPLES OF THE APPLICATION OF THE VLF-R METHOD TO PROSPECTING BEDROCK STRUCTURES

by

S.-E. Hjelt, J.V. Heikka, T.K. Pernu and E.I.O. Sandgren

Hjelt, S.-E., Heikka, J.V., Pernu, T.K. & Sandgren, E.I.O., 1990. Examples of the application of the VLF-R method to prospecting bedrock structures. *Geologian tutkimuskeskus, Tutkimusraportti 95.* 87-99, 8 figs, 1 table.

The present paper describes the use of the VLF resistivity (VLF-R) method. The source field is essentially a plane wave originating from distant radio transmitters. The method is a quick and versatile means of determining various structures of the bedrock, of importance also in connection with mineral prospecting. The depth extent of the method is also good (in favourable situations up to 300 m). All Finnish VLF-R measurements have been made with the Canadian GEONICS EM 16-R system.

A two-layer model is routinely employed in interpreting the data, either with the help of nomograms or using an equivalent computer program. Also 2D computer modelling has been used.

The application examples describe the main features of VLF-R measurements, the importance of the phase information and the use of sufficient point density. Typical applications include the location of contacts between different rock types and vertical or nearly vertical zones of conductive and resistive veins, the determination of the relief of a resistive bedrock or of the thickness of a ground-water layer. Also the quality (resistivity and its anisotropy) of the bedrock can be obtained.

Key words: electromagnetic induction, VLF, electrical conductivity, mineral exploration, crust, two-dimensional models, case studies, Talvivaara, Suhanko, Finland

Ельт, С.-З., Хейкка, Й.В., Перну, Т.К., Сандгрен, З.И.О, 1990. Примеры применения метода сверхнизких частот (VLF-R) для структурного картирования коренных пород. Геологический центр финляндии, Рапорт исследования 95. 87-99, Идд. 8.

В работе описывается использование резистометрибеского метода сверхнизких частот (VLF-R). Излучающее поле при этом представляет практически плоскую волну от далеких радиопередатчиков. Метод является быстрым и гибким инструментом для определения различных структур в горных породах, имеющих важное значение в частности в геологоразведочной практике. глубинность метода также неплоха. В финляндии все измерения по названному методу выполнены с помощью канадской аппаратуры марки GEONICS EM 16-R.

При интерпретации данных в производственном масштабе используется двуслойная модель, либо при помощи номограм либо с помощью соответствующей вычислительной программы. Есть опыт применения двумерного моделирования на ЭВМ.

Приведенные примеры показывают главные особенности измерений по методу VLF-R, как-то важность наличия данных о фазовом режиме и съемки с достаточной частотой точек измерения. Типичными видами применения метода являются прослеживание контактов разнотипных пород и вертикальных или субвертикальных жил, различающихся своей проводимостью; определение рельефа коренных пород с омическим сопротивлением или мощности слоя грунтовых вод. Далее, с помощью данного метода возможно определение параметров качества (сопротивления и его анизотропии) копенных пород.

Description of the method

The source field

The VLF method was first taken into use in the late 1960`s (Fraser, 1969, Paterson and Rönkä, 1971). The source field consists of a plane EM wave which is generated in the frequency range of 15-30 kHz by powerful radio stations used for long distance telecommunication purposes and for the transmission of standard time signals. Also semitransportable stations for prospecting purposes have been used.

Table 1. VLF-stations with useful field strengths in Espoo, S. Finland (GSF annual report 1986).

Freq. [kHz]	Code	Location	Bearing [degrees]	Distance [km]	Field strength dB[μV/m]	Comments
15.1	FUO	France	236	2409	67	
16.0	GBR	U.K.	253	1808	60	
16.4	JXZ	Norway	325	908	63	irregular
16.8	FTA2		238	1918	52	weak
17.1	UMS	USSR	118	877	63	irregular
18.1	UPD8	USSR	18	1052	66	irregular
18.5	DHO35	FRG	241	1308	68	irregular
19.0	GQD	U.K.	256	1884	60	
19.6	GBZ	U.K.	253	1808	57	

In order to make efficient measurements, the direction of the transmitter should be along the strike of a conducting structure. Then the magnetic field component of the source field is perpendicular to the largest plane of the conductor and the induction effect is at its maximum. Although the number of possible stations is limited at many places in Finland, measurable signals of properly directed VLF can be found at most loactions in Finland.

The measurements

Above a homogeneous, conducting ground, both the magnetic and electrical componenets of the radiowave field are essentially horizontal. Lateral conductivity changes distort the current distribution induced in the ground. The resulting anomalous magnetic field depends on the current distribution. Inside good conductors, the flow of current is enhanced, and the direction of the total magnetic field tilts in the vicinity of the conductors. Since the anomalous part of the field has a phase shift in relation to the homogeneous primary field, the total field is elliptically polarized.

The first applications of the VLF method were intended to measure these distorted polarizations of the magnetic field. These so called tilt angle measurements are suitable for the detection of vertical conductivity boundaries or conductors. The measured data are transformed using filtering techniques (Fraser, 1979) in order to facilitate interpretation or to produce apparent current cross-sections (Karous and Hjelt, 1978, 1983).

Tilt angle measurements have lately been to a large extent replaced in regional reconnaissance and structural studies by the VLF-R resistivity,VLF-R method. In the variant, the quotient between the electric and the magnetic field is measured. Since the primary field is a plane wave, the quotient is proportional to the apparent resistivity and the phase between the

fields (Tikhonov, 1950; Cagniard, 1953).

$$\rho_a = (1/\omega\mu)\,[E/H]^2$$
$$\phi = \arg\,(E/H) \qquad (1)$$

The phase is a very sensitive and useful parameter for determining the conductivities of the bedrock structures.

Equipment

Practically all measurements in Finland are performed with the Canadian Geonics EM16R instrument, one of the main designers (V. Rönkä) of which is Finnish by birth. The magnetic field components are recorded using standard ferrite coils and the electric field using two electrodes positioned 10 m apart. Amplification of the signal is provided by circuitry inside the electrode handles. Lately, instrumental development has been going on at the Geological Survey of Finland to produce an airborne variant of the VLF-R system. (GSF Annual Report 1986).

Interpretation principles

2-layer models, nomogram interpretation

The common procedure in VLF-R interpretation has been to use the 2-layer nomograms provided by the manufacturer of the instrument (Geonics, 1975). As Hjelt et al. (1985) have pointed out, the nomograms are only a graphical counterpart of the classical two-layer apparent resistivity of magnetotellurics:

$$|\rho_a| = \rho_1\,[\coth^2 x + \tan^2 y] \,/\, [1 + \coth^2 x * \tan^2 y] \qquad (2)$$
$$\phi = 2\,\mathrm{atan}\,\{[(\coth^2 x - 1) + \tan y] \,/\, [\coth x\,(1 + \tan^2 y)]\}$$

with

$$x = -y + \coth^{-1}[\sqrt{(\rho_2/\rho_1)}]$$
$$y = -h_1\,\sqrt{(\pi\mu_0 f / \lambda_1)}$$

The nomograms provide a rapid means of establishing the main electric parameters of the bedrock. Provided the surface layer conductivity can be estimated (normally from the properties of the soil at the measuring sites), the thickness of the overburden and the conductivity (resistivity) of the bedrock can be found. Since only two parameters are measured at each site (ρ_a and ϕ), only two model parameters can be found per site. If two perpendicular (or nearly perpendicular) signals are available, additional layer parameters can be determined (Hjelt et al., 1985).

2-layer models, computer methods

Since the two-layer curves are mathematically quite simple, the nomogram two-layer

intrepretation can also be performed quickly on a modest calculator or microcomputer. The most efficient interpretative procedure is to combine the VLF tilt angle and VLF-R measurements as has been pointed out by Kaikkonen (1980b). 2D modelling requires a numerical calculation program, e.g. of the finite element type (Kaikkonen, 1979, 1980a, 1980b).

Computer 2D modelling

An alternative to 2D interpretation is to calculate apparent current distributions, by e.g., using the filtering technique proposed by Karous and Hjelt (1978, 1983). In this technique, the current density induced in the ground is assumed to be confined to a layer of preselected thickness Dz. The distribution of the current density in this layer is obtained by the linear filter (Karous and Hjelt, 1983)

$$\Delta z * \underline{I}(0)/(2\pi) = -0.102\, H_{-3} + 0.059\, H_{-2} - 0.561\, H_{-1} + 0.561\, H_1 - 0.059\, H_2 + 0.102\, H_3 \quad (3)$$

$$\underline{I}(0) = 0.5\, [I(\Delta x/2) + I(-\Delta x/2)]$$

Repeating the filtering for data sets with various Δx, the current density is factually approximated at various depths. The result can be considered as an apparent current distribution (pseudosection) and it is highly illustrative for picturing the qualitative behaviour of the subsurface electrical structure. It is straightforward to produce a similar nonlinear filter and thus to approximate the true current distribution more realistically.

Field examples

VLF-R measurements are often used as a complementary and high-frequency check ("calibration") on AMT soundings, but their greatest value is as such in reconnaissance profiling. The productivity of VLF-R measurements is very good and in highly resistive environments well conducting zones may be detected from depths of about 200-300 meters. Resistivity work should, whenever feasible, be completed by tilt angle measurements, since these are the most sensitive ones for detecting vertical conductivity contrasts. The use of both versions of the VLF-method is described in the subsequent examples.

The location of contacts between different rock types (Sotkamo, Talvivaara)

This VLF study was carried out jointly in 1981 by the Department of Geophysics, University of Oulu, and the Geological Survey of Finland. The survey area is situated in Sotkamo, in the southern part of the Kainuu schist belt (Fig 1.) Three main profiles were measured in order to study the detectional capabilities of the AMTS and VLF-R methods. One of the measured profiles crossed the contact between two bedrock blocks. The block of mica schists is resistive (typical in situ resistivities being 2000-3000 Ωm) whereas the block consisting of black schists is a good conductor (typical in situ resistivities being 0.01-10 Ωm).

The thickness of the overburden is only a few meters. The contact can be located quite accurately, within a few meters, when the H-polarization is measured and when the density of the measuring points along the profile is sufficient (Fig. 2A). The change in E-polarization curves is more gradual (Fig. 2B). For reliable interpretation tests, measurements in different

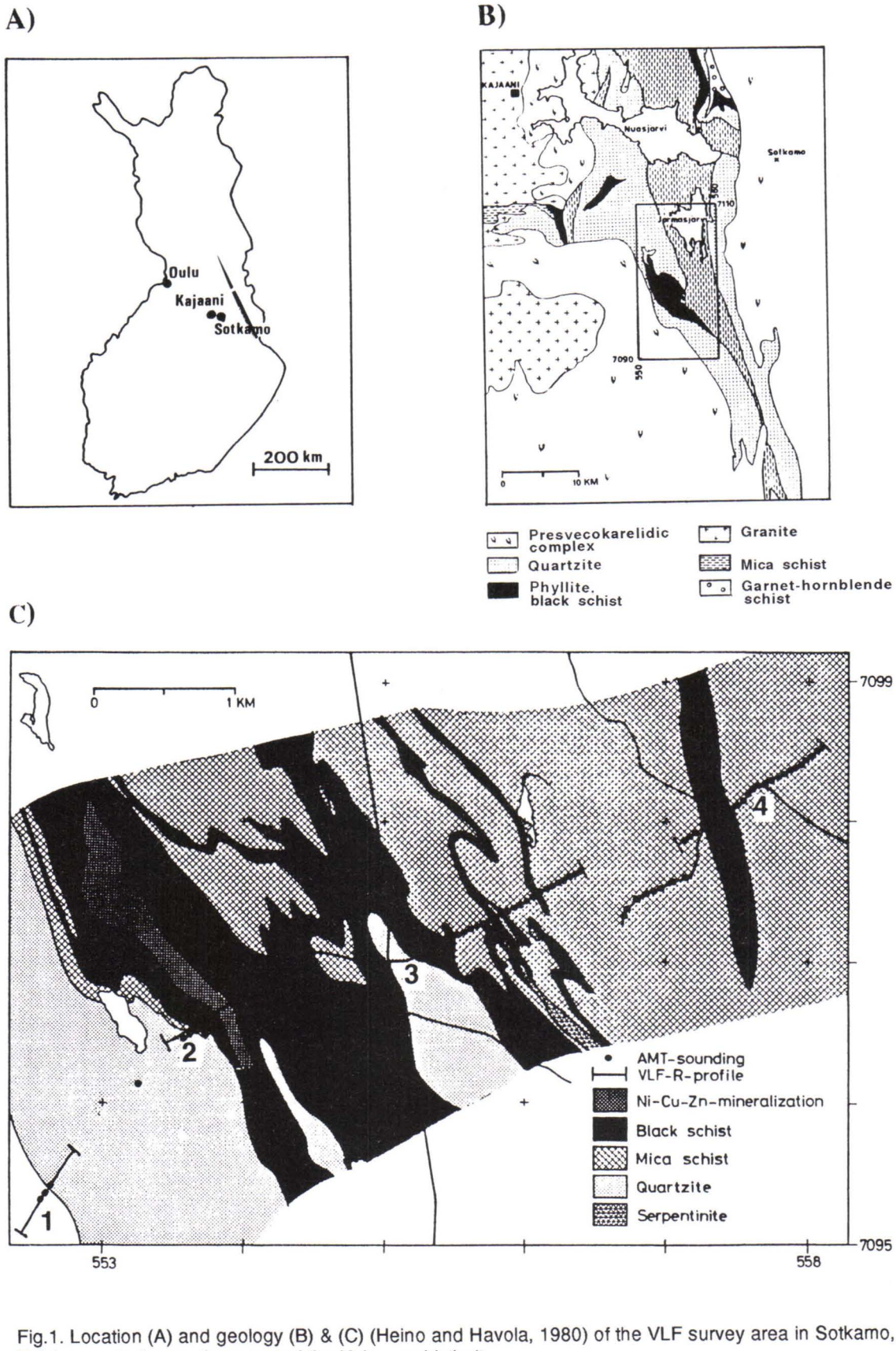

Fig.1. Location (A) and geology (B) & (C) (Heino and Havola, 1980) of the VLF survey area in Sotkamo, Talvivaara, in the southern part of the Kainuu schistbelt.

directions in the survey region are essential to make sure that true H-polarization data are obtained.

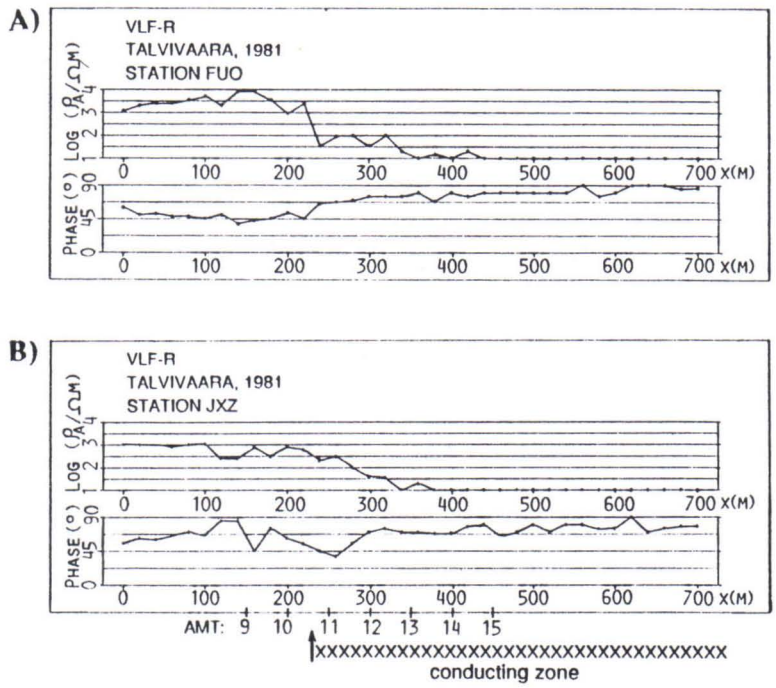

Fig. 2. VLF-R profiles above the contact between blocks of resistive mica schists and conductive black schists in the Talvivaara area: (A) H-polarization, (B) E-polarization.

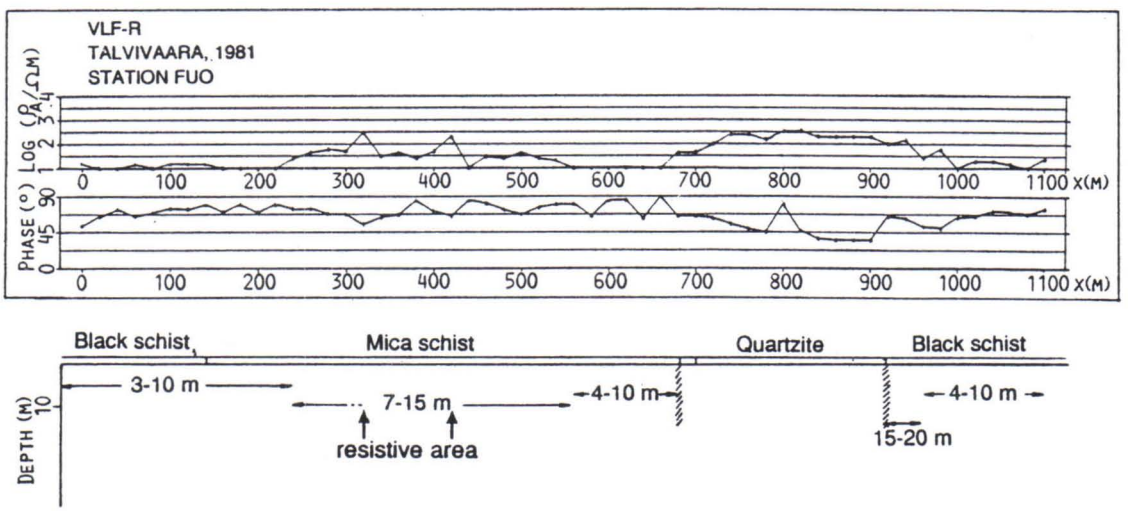

Fig. 3. VLF-R H-polarization profile across the bedrock contact of Fig. 2 and its 2-layer interpretation. At each part ofthe profile the typical range of depths to the conductive bedrock is given in meters. The rocks marked mica schists based on geological mapping are good conductors, suggesting that the black schist block continuees up to the quartzite area (cf., the text).

The interpretational value of the phase angle is demonstrated in Fig. 3 (profile 3 of Fig. 1). The contact between the mica and black schist blocks (at about x = 150 m) is based on geological mapping of the surface rocks with uncertainties resulting from the overburden. The apparent resistivity is higher above the area mapped as schists. But since the phase is still on a high level, it may be concluded that the mica schist area in fact contains more highly conductive material, i.e., the black schists extend up to the quartzite area. The depth of the surface of the conductors can be determined by the 2-layer nomogram technique. Increasing apparent resistivity values together with a simultaneous low level of the phase angle above the quartzite area shows that no conductors can be detected in this area.

Fig. 4 shows a comparison between the VLF-R data and the interpreted AMT 1D conductive models for profile 4 in Fig. 1. (For further discussion of the AMTS profiles, see Hjelt et al., this issue). In the resistive area (AMT points 8-16) the apparent VLF-resistivity is high and the phase well below 45¤. Indications of conductors can be seen between 260-320 m and 780-860 m on the profile (the apparent VLF-resistivity descreases and the phase is above or close to 45¤). Here the AMT-soundings support the conclusions drawn from the VLF-R data. According to the AMTS interpretation, conductors are located at a depth of 200-300 m. The VLF field does not penetrate deep enough at these sites to give indications about the deeper conductors of the 2D AMT model. Thus the VLF-R can be useful as a reconnaissance tool for locating conductors in resistive regions down to a few hundred meters. It is preferable that the VLF-R results are complemented by either AMTS or DCS results.

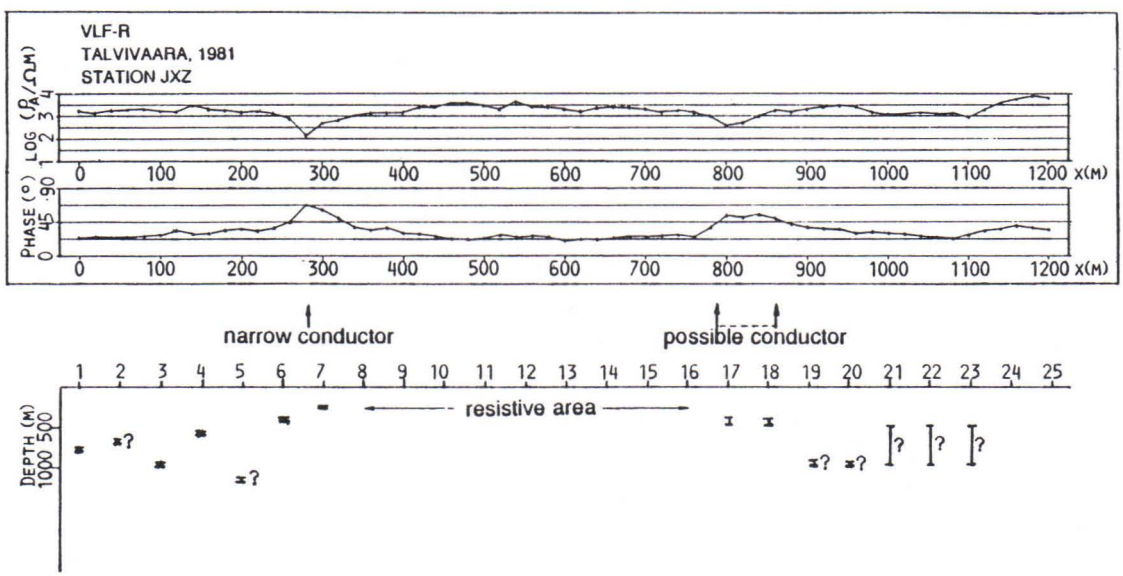

Fig. 4. Correlation between VLF-R, H-polarization data and interpreted AMT conducting layers.

The location of vertical or nearly vertical zones of conductive and resistive veins (Haukipudas, Northern East Bothnian schist area)

The northern East Bothnian schist area represents a typical Finnish bedrock complex. Greywackes and volcanics with layers of graphitic schists containing some (pyrite and pyrrhotite) mineralizations alternate with resistive granitic rocks. The topography is rather flat and the Quaternary overburden is typically 1 to 8 meters thick, and seldom exceeding twenty meters. The bedrock at the sample profile of the northern East Bothnian schist area is layered and consists of mainly steeply dipping, parallel and thin conducting layers of graphitic schist.

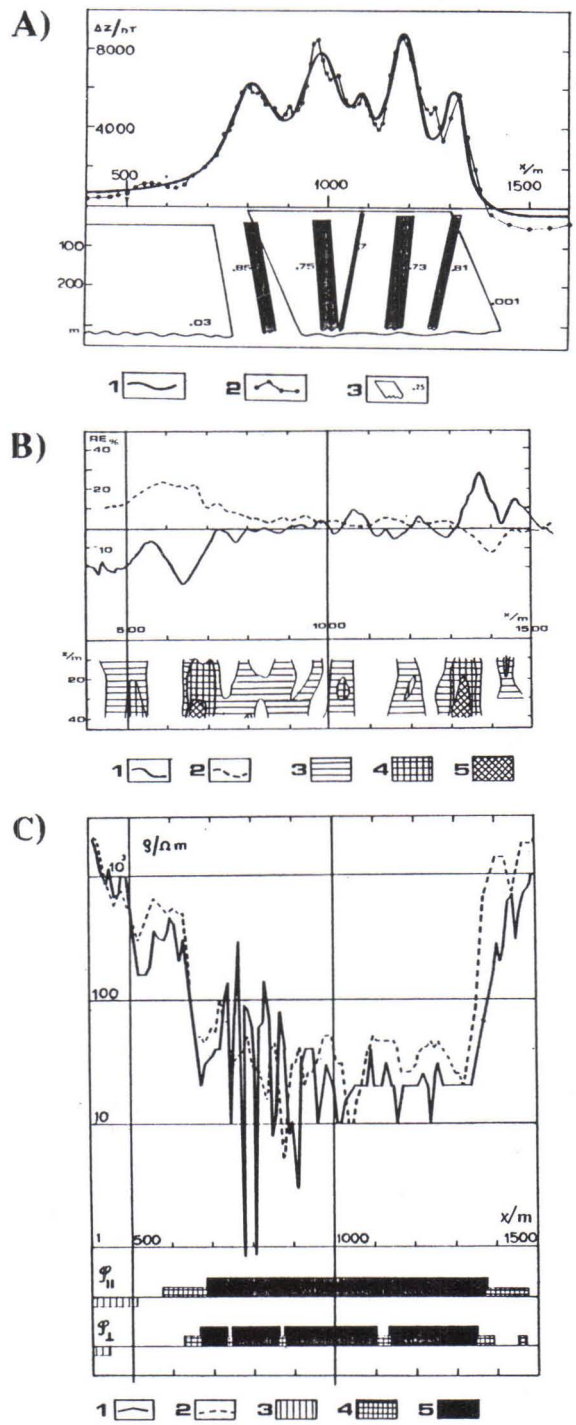

Fig. 5. Part of a test profile across the northern East Bothnian schist area. A. Ground magnetic vertical anomaly and its 2D interpretation: 1 = calculated anomaly; 2 = measured anomaly; 3 = 2D model with susceptibility in SI units. B. VLF tilt angle and corresponding apparent current density pseudosection: 1 = Re{H_Z}; 2 = Im{H_Z}; 3 = j_{rel}; 4 = 2*j_{rel}; 5 = 3*j_{rel}. [VLF-station JXZ, 16.4 kHz]. C. VLF-R data: 1 = parallel apparent resistivity [E-pol, JXZ, 16.4 kHz]; 2 = perpendicular apparent resistivity [H-pol, FUO, 15.1 kHz]; 3 = phase (E, H) from 25 to 40°; 4 = phase (E, H) from 50 to 70°; 3 = phase (E, H) above 70° (from Hjelt, 1979).

The sample profile, only a part of which is shown in Fig. 5, runs across a distinct aeromagnetic anomaly. The corresponding magnetic vertical component ground profile confirms the verticality of the conducting and magnetized structure. Many VLF tilt angle anomalies correlate with the magnetic anomalies. The magnetic anomalous part extends from about x = 700 m to 1.400 m with a clear internal structure of strongly magnetized veins (Fig. 5A). The VLF tilt angle profile has anomalies on the order of 15-25 % at both ends of the magnetized region (Fig. 5B). The tilt angle profile can qualitatively be interpreted either as two distinct vertical conductors at about x = 700 and 1400 m or as a broader conductive block of about the same width as the main magnetized region, but with a possible internal structure. The equivalent current density interpretation (bottom part of Fig. 5B), obtained by the Karous-Hjelt filter (Karous and Hjelt,1977, 1983), confirms the verticality of the structure and bears vague evidence in favour of the latter interpretation.

The VLF-R results (Fig. 5C) indicate that the whole structure from x = 700 to 1400 m conducts well, since both the apparent resistivity is low and the phase angle clearly exceeds 45¤. This profile shows definitely that also the conductivity has an internal structure and consists apparently of vertical conductive bands (veins). As in magnetotellurics, the perpendicular apparent resistivity (H-polarization) delineates the conductors more properly than the parallel (E-polarization) data.

Around x = 800 m, an exceptionally small point separation (5, even 2.5, meters) was used. The result demonstrates the horizontal resolution capacity of the VLF-R method in such vertically layered conductive regions. (One should recognize that the GEONICS EM16R instrument used is actually insensitive to apparent resistivities below 10 Ωm, so all the lower values in Fig. 5C should be considered only qualitatively . Therefore all the phase values are given in three broad categories only.)

Regional structural research (Suhanko intrusion)

A discontinuous belt of layered mafic intrusions extends 270 km across northern Finland from Tornio, on the Swedish border, to Näränkävaara, at the Soviet border (cf. , Fig. 2 in Rekola, 1985). The intrusions of Suhanko and Konttijärvi, belonging to this belt, intruded between the Archean basement complex and the Peräpohjola Schist Belt of Svecokarelian metasediments and volcanics about 2.25 Ga ago (Vuorelainen et al., 1982). The Suhanko intrusion is composed mainly of monotonous gabbro. Discontinuous belts of ultramafic rocks, predominantly peridotite, occur at the marginal zone near the base of the intrusion, in contact with the gneissose granite of the basement. The lower part of the marginal zone has discontinuous layers of pyrrhotite with some Cu-Ni-mineralizations. Some minerals of the platinum group have been found in the Konttijärvi intrusion (Isohanni, 1971, Vuorelainen et al., 1982). Geophysical studies of the Niittylampi- Vaaralampi mineralization of the Suhanko intrusion have been described by Rekola (1985).

A project was carried out in 1984-86 by the Department of Geophysics, University of Oulu, in co-operation with the Lapin Malmi Company (Outokumpu Oy) and financed by the Finnish Ministry of Trade and Industry to study and determine the main structure of the Suhanko intrusion. A considerable number of VLF (94 line-km) and AMT measurements (about 500 soundings) were carried out and interpreted during the project (Pernu et al. ,1986; Keränen, 1987; Lerssi,1988). A wealth of other data gathered since 1964 by the Lapin Malmi company (previously Outokumpu Oy) and by the project itself was combined to obtain an integrated structural model for the intrusion.

The western and southeastern wings of the intrusion are wedgelike basins with thicknesses varying from 100 to 500 m. The conducting layers in the contact between the gabbros of the intrusion and the surrounding granites are clearly to be seen in the VLF-R data. Thus the method can be used to locate the boundary along most parts of these wings. The depth of the intrusion requires lower than VLF frequencies to follow the conducting layers at the contact. The northern wing is thicker and the exact geometry of its boundary cannot be

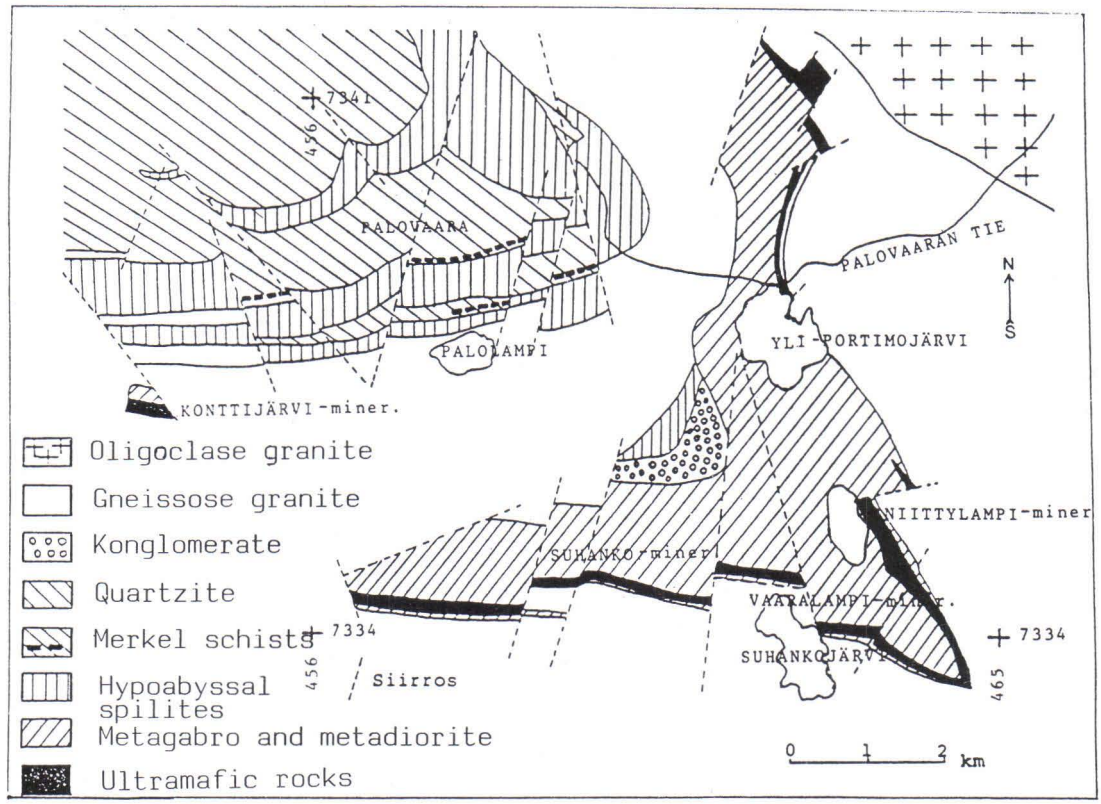

Fig. 6. Simplified geological map of the area studied, Suhanko (Isohanni, 1971).

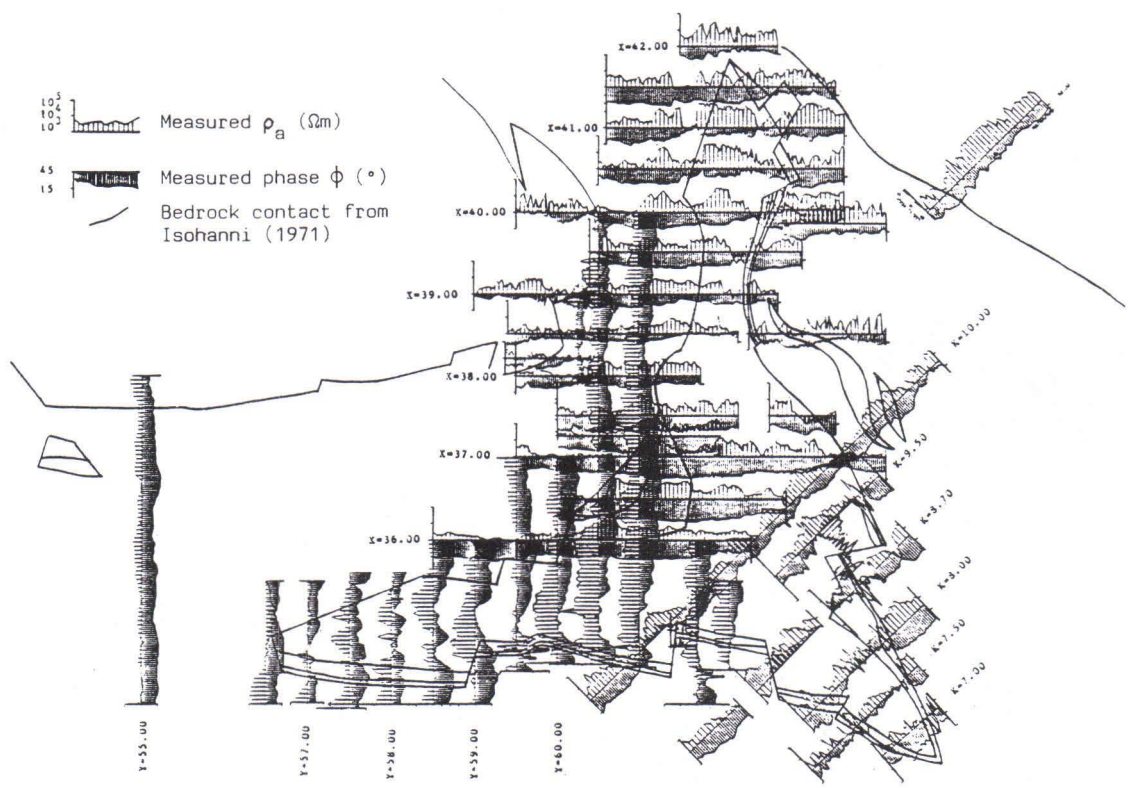

Fig. 7. Map of VLF-R profiles across the boundaries of the Suhanko intrusion.

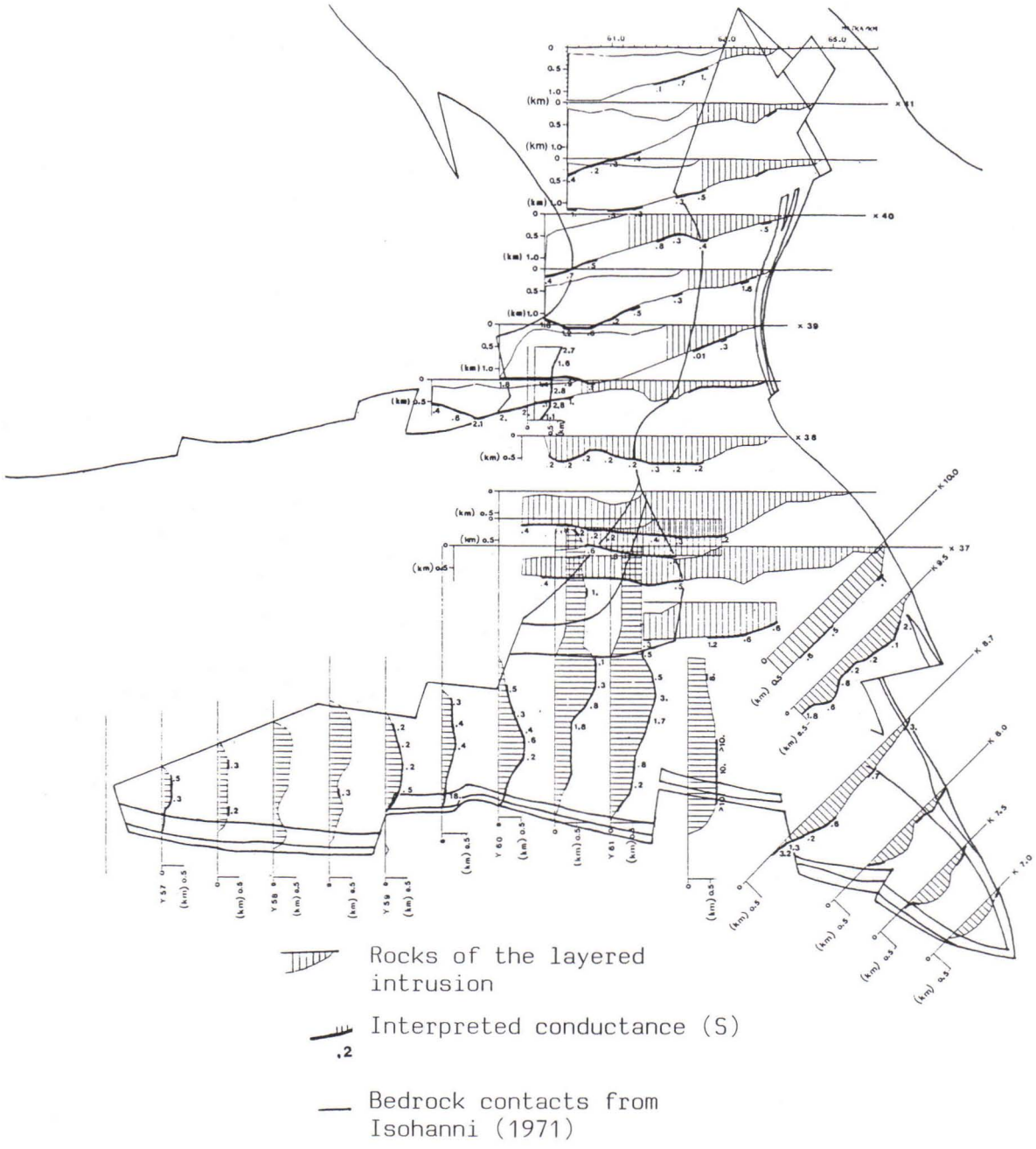

Fig. 8. Electrical structural interpretation of the Suhanko intrusion, based on AMTS and VLF data.

determined unambiguously. The central part of the intrusion is about 700-1000 m thick and the western boundary is steep or dips subvertically westwards.

The map of Fig. 7 brings together all the VLF profiles on and around the Suhanko intrusion. The profiles have been classified and summarized into the interpretation map of Fig. 8. The surface conductors can be located and the whole intrusion can be divided into parts based on conductivity. Three categories were used: surface conductors, deep conducting horizons and resistive areas. The surface conductors were situated between the surface and depths from 200 to 300 m. They occur mainly at the southeastern and southern

contacts of the intrusion. The deep conductors are located 300 m or more below the surface. Areas are classified as resistive whenever the apparent resitivity is higher than1000 Ωm and the phase angle below 20¤ simultaneously. When the resistivity at the surface is high (about 10000 Ωm), the VLF-R method can be used to locate conducting horizons down to about 300 m.

When one combines the VLF-R data with the AMTS results, a final electrical interpretation map (Fig. 8) is obtained, clearly indicating the basinlike structure of the intrusion. The gravity and magnetic structural interpretations, which mainly support the electrical models, will not be discussed here further, although they have been essential to arriving at with the final result of Fig. 8.

Other applications

In addition to the foregoing examples,VLF and VLF-R profiling can and has been applied to a variety of geological problems. The relief of a resistive bedrock can be reliably determined in cases where the thickness of the overburden is a significant part of the skin-depth at VLF frequencies. The conductance of a ground-water layer is the dominating part of the overburden conductance. Since the resistivity of a typical ground-water layer does not vary significantly, the two-layer interpretation of VLF-R measurements can provide reasonable estimates of the thickness of the ground-water layer.

The quality of the bedrock can be assessed from directional information about the ground electrical conductivity/resistivity and its anisotropy. Since the VLF method is essentially a plane wave method, this would require recording of the complete impedance tensor as in magnetotelluric measurements. Whenever two VLF transmitting signals with a difference in bearings from the transmitters close to 90 degrees are available, such directional surveys can be made. Several factors, such as fracturization, less the resistive minerals and overburden depressions, affect bulk bedrock resistivity in a similar manner. This makes interpretation of VLF data a demanding task indeed, which cannot be solved without additional information obtained by other methods. The best result requires - as in any application of geophysics - an intelligent, problem-integrated and professional combination of geophysical and geological data.

References

Cagniard, L., 1953. Basic theory of the magnetotelluric method of geophysical prospecting. Geophysics18, 605-635.

Fraser, D.C., 1969. Contouring of VLF-EM data. Geophysics 34, 958-967.

Geonics Ltd., 1975. EM16-R(RADIOHM). Two-layer interpretation curves.Techn. Note TN-1., 8 + 14 pp.

GSF Annual Report 1986. VLF-stations. (in Finnish).

Heino, T. & Havola, M., 1980. Geology in the Jormasjärvi-Talvivaara area. Report M 19/3344/-80/3/10, Geol. Survey of Finland (in Finnish)

Hjelt, S.-E., 1979. Electromagnetic plane wave methods in prospecting. Proc. 24th International Geophysical Symposium, 4.-7. Sept., Krakow, 11 pp.

Hjelt, S.-E., Kaikkonen, P. & Pietilä, R., 1985. On the interpretation of VLF resistivity measurements. Geoexploration: 23, 17-181.

Isohanni, M., 1971. The bedrock of the Palovaara-Suhanko area in the southeastern part of the Peräpohja schist zone (in Finnish). M. Sc. thesis, Dept. of Geology, Univ. of Oulu, 127 pp.

Karous, M. & Hjelt, S.-E., 1978. Determination of apparent current density from VLF measurements. Dept. of Geophysics, Univ. of Oulu, Contrib. 89, 18 pp.

Karous, M. & Hjelt, S.-E., 1983. Linear filtering of VLF dip-angle measurements. Geophys. Prospecting 31, 782-794.

Kaikkonen, P., 1979. Numerical VLF modeling. Geophys. Prospecting 27, 815-834.

Kaikkonen, P., 1980a. Numerical VLF, VLF-R and AMT profiles over some complicated models. Acta Univ. Oul.: A 91, 1980, Phys.16, 34 pp.

Kaikkonen, P., 1980b. Interpretation nomograms for VLF measurements. Acta Univ. Oul.: A 92, 1980, Phys.17, 48 pp.

Keränen, T., 1986. A study of the structure of the Suhanko layered intrusion by using the AMT and the VLF-R methods. (in Finnish) M. Sc. thesis, Dept. of Geophysics, Univ. of Oulu, 71 + I pp.

Lerssi, J., 1986. A study of the structure of the Suhanko layered intrusion by using the gravity and magnetic methods (in Finnish). M. Sc. thesis, Dept. of Geophysics, Univ. of Oulu, 77 + VIII pp.

Paterson, N.R. & Rönkä, V., 1971. Five years of surveying with the Very Low Frequency-Electromagnetic method. Geoexploration: 9, 7-26.

Pernu, T., Keränen, T., Lerssi, J., & Hjelt, S.-E., 1986. The geophysical structural study of the Suhanko layered intrusion. (in Finnish). Final project report, Dept. of Geophysics, Univ. of Oulu, 44 pp.

Rekola, T., 1985. Results of electrical and electromagnetic measurements in Vaaralampi-Niittylampi, Ranua. In L. Eskola, A. Phokin (eds): Electrical prospecting for deposits in the Baltic Shield, part 1: Galvanic methods. Geol. Survey of Finland, Report of Investigations 73, 73-84.

Tikhonov, A.N., 1950. Определение электрисечких характеристик глыбоких члоев земнож корй. Докл. Акад. Наык СССР: 73, 295-297.

Vuorelainen, Y., Häkli, A., Hänninen, E., Papunen, H., Reini, J. & Törnroos, R., 1982. Isomerteite and other platinum-group minerals from the Konttijärvi mafic intrusion, Northern Finland. Economic Geology 77, 1511-1518.

THE CAPABILITIES OF ELECTRICAL PULSE METHODS WHEN PROSPECTING FOR ORE DEPOSITS IN GRAPHITIZED AND SULPHIDIZED FORMATIONS

by

H.N. Mikhailov and S.N. Sherechevsky

Mikhailov, H.N. & Sherechevsky, S.N., 1990. The capabilities of electrical pulse methods when prospecting for ore deposits in graphitized and sulphidized formations. *Geologian tutkimuskeskus, Tutkimusraportti 95.* 100-104, 3 figs.

Good results may be obtained with TEM involving the study of the later stages of the transient process in complex geological situations, when both sulphide mineralization, and the conductive formations of a non-ore nature (for instance, graphitized rocks) are present. In practice, however, such measurements are strongly disturbed by an unfavourable signal-to-noise ratio.

In prospecting for ore deposits in the presence of graphitized and sulphidized formations the most efficient of electrical pulse methods proved to be that of induced polarization when various time responses and nonlinear effects were studied over a wide time range.

Key words: electromagnetic methods, electromagnetic induction, transient methods, induced polarization, mineral exploration, metal ores, graphite, sulphides, USSR

Михайлов, Г.Н., шерешевский, С.Н., 1990. Возможности импульсной электроразведки при поисках рудных месторождений в условиях развития графитизированных и сульфидизированных образований. Геологический центр финляндии, Рапорт исследования 95. 100-104. Идд. 3.

В сложных геологических условнях, когда наряду с искомой сульфидной минерализацией присутствуют проводящие образования нерудной природы, например, графитизированные породы, положительный результат можно ожндать от метода переходных процессов, изучая поздние стадии установления поля. Однако на практике осуществить такие измерения сложно вследствие неблагоприятного соотношения сигнал/помеха.

При понсках рудных месторождений в условиях развития графитизированных и сульфидизированных образований наиболее эффективным из методов импульсной электроразведки является метод вызванной поляризации с изучением различных временных характеристик и нелинейных эффектов в широком временном диапазоне.

The ever-increasing bulk of prospecting activities involving the transient electromagnetic methods (TEM) and induced polarization methods (IP) under various geological conditions has resulted in anomalies, the relation to the target metallization of which has not been confirmed by subsequent chock drilling. Of great importance is therefore, is the study of the EM-field transient processes in real media in order to devise criteria for relating such anomalies to economic metallizations.

In a complex geological situation where, in addition to sulphide mineralization, the conducting formations of a non-ore nature (for instance graphitized rocks) are present, good results may be obtained with TEM involving study of the later stages of the transient process. In practice, however, this procedure is strongly disturbed by an unfavourably low signal-to-noise ratio. Such being the case, the IP method is needed.

The size of inclusions greatly affects the chargeability and its time responses to rock material. The experimental investigations carried out on different rock samples (1) show that the chargeability increases linearly along with the size of the sulphide grains, their cubic content remaining constant; in graphite, the chargeability decreases monotonically, its magnitude being correlated with the graphite porosity. As the latter increases, the true surface of the graphite becomes larger, while the current density diminishes, resulting in a decrease of chargeability.

The rate of the IP-field decay (ν) turns out to be a reliable interpretation parameter, which is characterized by the increment of the nduced potential iin a fixed time interval. Fig. 1 shows the difference in ν for pyrite-chalcopyrite ore and graphite. The measurement of abundant samples showed (1) that the rate of induced potential decay during a relatively short charge ($T = 0.3$ s) is on the average higher in the sulphides examined than that in the graphites. The difference in chargeability and decay rate values is associated with differences in the mineral composition of the samples assayed.

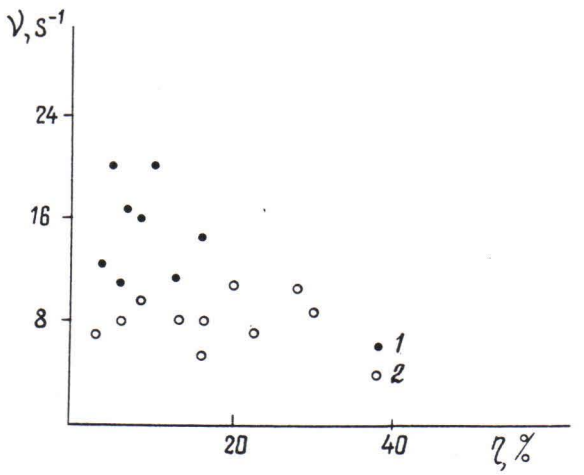

Fig. 1. The IP decay rate in pyrite-chalcopyrite ore (1) and graphite with varying porosity (2) (after V.V. Kormiltsev).

To devise a technique for interpreting field data from complex geological environment, modelling was applied. Wet quartz sand with a resistivity of $\rho_1 = 100$ Ωm and a chargeability of $\eta_1 = 0.2$ % was taken as a host medium. Metallic plates with a separation of 60 cm were used as current electrodes. The measurements were performed in the central part of the array where the primary field was nearly uniform. The polarizing current density (j) was taken rather low to establish the independence of the surface polarization factor (κ). In such conditions the similarity parameter must be consistent with the equation (1).

$$\frac{a^2\kappa}{h^3\rho} = \text{const}, \qquad (1)$$

where: h - depth to the center of the polarizable body;
a - its characteristic size;
κ - surface polarization factor;
ρ - host medium resistivity.

In the primary uniform field, κ is the factor of proportionality between the IP-emf and the polarizing current density. Note that, for ore minerals, κ varies in the range of 1 to 10, which corresponds to the IP-emf of tens mV when the current density is 1 μA/cm^2.

A graphite sphere and a sulphide ore sample were taken as the models of polarizable objects, both showing good resistance to oxidation. The current in the line was 15 μA.

The modelling results with the gradient array prove that both objects are characterized by intense anomalies of differential chargeability ($\tilde{\eta}$) in the specified measuring range (t = 64 ms). Considerable discrepancies are seen in the $\Delta\tilde{\eta}$ plot reflecting the rate of change in $\tilde{\eta}$, which has a negative value above the model of impregnated sulphide ore and a positive one above the graphite sphere.

The possibility of sorting the anomalies according to the IP time responses is based on principal variations, which, for each geoelectric section, exist as numerical values of maximum abscissae (T_0) of derivatives of the IP-intensity taken by the logarithm of time. Experience proves the possibility of discriminating the anomalies associated with carbonaceous graphitized rocks and those caused by objects with a streaky-impregnated and massive sulphide mineralization. Fig. 2 comprises the $\tilde{\eta}$ differential chargeability plots for different geological situations in the Karelia-Kola region. The increase of $\tilde{\eta}$ in time above good conductors represented by streaky-impregnated copper-nickel mineralizations is very slow; therefore T_0 may attain some tens of hours. Above the graphitized rocks $\tilde{\eta}$ does not vary over a wide time range, while above the nonmineralized host rocks the value of $\tilde{\eta}$ grows less in time and T_0 varies in the millisecond range.

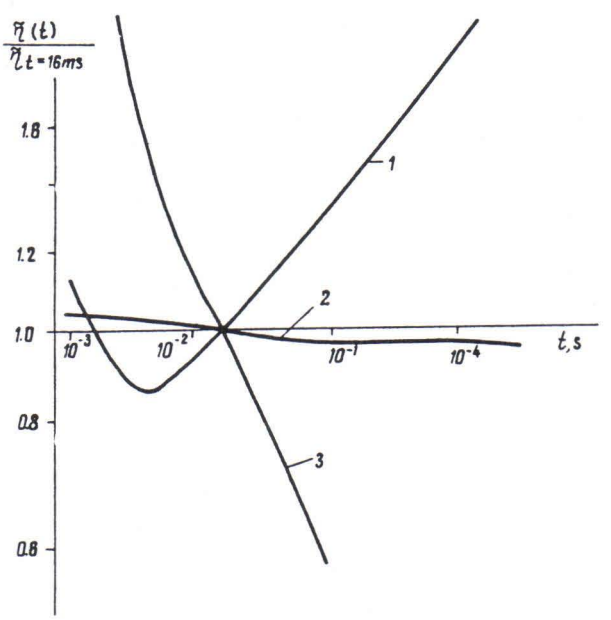

Fig. 2. The plots of differential chargeability of sulphide copper-nickel ore (1), graphitized rocks (2) and gneisses (3).

The practical application of electrical pulse prospecting methods in media with a low contrast in polarization and electrical conduction indicates that the most reliable parameter for distinguishing between anomalies associated with graphitized rocks or with sulphide mineralization is the second derivative of the IP-field by the logarithm of time ($\tilde{\tilde{\eta}}$). It is measured with modern equipment as the finite increment of differential chargeability in a fixed time interval. The measured responses of $\tilde{\tilde{\eta}}$ (t) are approximated by a sum of exponents with different time constants (τ_i) and amplitude values (K_i) . They are presented as spectra wherein K_i characterizes the contribution of each exponential signal to the measured total effect.

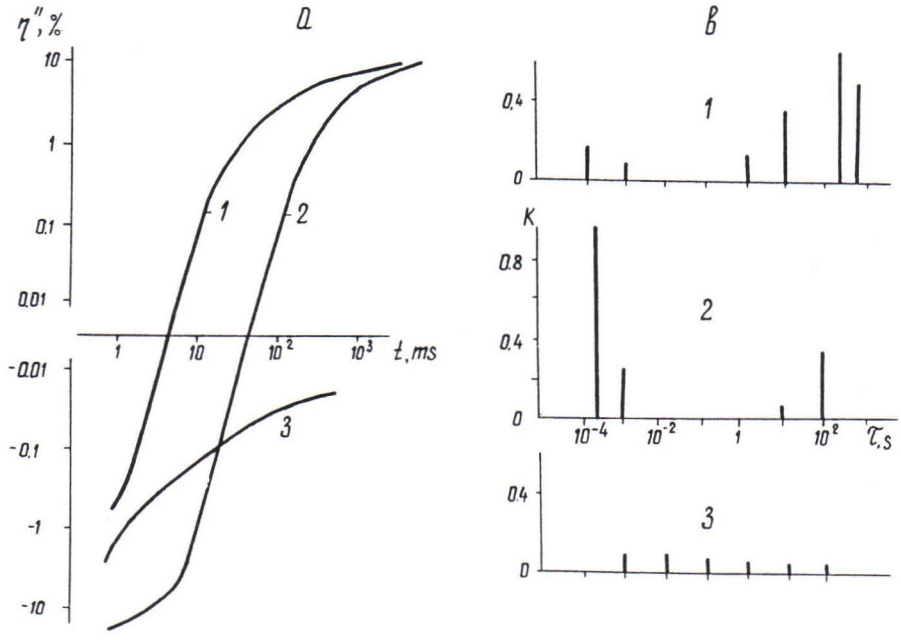

Fig. 3. The plots of time responses (a) and their spectral representation (b) above sulphide ore (1), graphitized rocks (2) and gneisses (3).

Fig. 3 illustrates the time functions $\tilde{\tilde{\eta}}$ (t), which, being typical of the Kola-Karelian region, were measured over impregnated sulphide ores, graphitized rocks and nonmineralized gabbro-diabases. The considerable differences in time responses $\tilde{\tilde{\eta}}$ (t) observed and their spectra confirm the practical effectiveness of the method developed in determining geological IP-anomalies. It was also established that the mineral composition of the electron-conducting inclusions determines the nonlinear IP effect, which is manifested in the differences between the charging and decay curves, when the inversion of the direction of the polarizing current takes place. Laboratory and field experiments show that time responses of nonlinear induced polarization over graphitized rocks have an extreme with a positive sign when the current is switched in and a negative one with the current switched off. Precisely the opposite situation is usually observed over the copper-nickel ores.

Conclusion

In prospecting for ore deposits in graphitized and sulphidized formations, induced polarization proved to be the most efficient of the electrical pulse methods. IP involves the

study of various time responses and nonlinear effects over a wide time range.

References

Kormiltsev, V.V., 1980. Transient processes in induced polarization. (Переходные процессы при вызванной поляризации). Moscow, Nauka, 110 p.

Komarov, V.A., 1980. Electrical prospecting by the induced polarization method. (Электроразведка методом вызванной поляризации). Leningrad, Nedra, 391 p.

Shereshevsky, S.N. & Litmanovich, J.L., 1983. Interpretation of the IP data with the spectral expansion of time responses. Pp. 3-11 in: A set of articles "Methods of exploration geophysics. Ground variants of electrical prospecting by pulse fields when searching for ore deposits". (Интерпретация результатов работ методом ВП с использованием слектрального разложения временных характеристик. - В кн.: Методы разведочной геофизики. Наземиые варианты электроразведки импульсными полями при поисках рудных месторождений). Leningrad, NPO "Rudgeofizika".

Results of EM methods

A SUCCESSFUL APPLICATION OF THE TRANSIENT METHOD

by

E. Lakanen

Lakanen, E., 1990. A succesful application of the transient method. *Geologian tutkimuskeskus, Tutkimusraportti 95.* 106-119, 6 figs, one appendix.

The Kalliokylä sulfide orebody, which was found in 1959, has been studied several times geophysically. Since 1979, electric deep sounding, AMT, TDEM and mise-a-la-masse measurements have been undertaken to establish the depth extensions of the highly conductive sulfide plate. Because of the high contrast and quite gentle dip, the results are satisfactory even when the data are interpreted with simple models. A new way of inverting the TDEM results is described.

Key words: electromagnetic methods, electromagnetic induction, transient methods, audiomagnetotelluric methods, mise-a-la-masse, inverse problem, metal ores, sulphides, Kalliokylä, Kiuruvesi, Finland

Лаканен, З., 1990. Пример успешного применения метода переходных процессов. Геологический центр финляндии, Рапорт исследования 95. 106-119, Идд. 6.

Сульфидное рудное тело Каллиокюля найдено в 1959 г. На этом рудном теле геофизические исследования производились геоднократно. Начиная с 1979 г. предпринимались измерения методами глубинного злектрического зондирования, змт, мпп и методом заряда для установления глубины протяжения высокопроводящего пластового сульфидного тела. Ълагодапя высокой контрастности и сравнительно пологому падению тела, результаты интерпретации получаются удоволетворительными даже при использовании простейших моделей. - В работе описывается в частности новый способ обратного анализа результатов съемки мпп.

Introduction

The discovery of the Kalliokylä orebody in Kiuruvesi in 1959 is one of the few made with an airborne EM method in Finland (Rotary field, Ketola et al., 1972), although a couple of years earlier some sulfides had been found in a nearby outcrop. After the airborne survey studies proceeded rapidly. In the same year, ground surveys and the subsequent drilling localized a pyrrhotite and pyrite mineralization with some zinc and copper. The known body increased in volume as studies progressed and it was soon found to be marginal for economic exploitation. In the late 1970s, interest was focused on tracing the extensions of the orebody. More drilling, deep EM soundings and a special structural study were undertaken (Koistinen, 1984). One aim was to discover a portion more enriched in zinc and copper.

Geology

The orebody is located at the contact between altered rocks (cordierite-anthophyllite) and gneisses (Fig. 1a). The Ruostesuo orebody has been estimated to contain 1.7 Mt of ore grading 35 % S, 2.5 % Zn and 0.36 % Cu down to about the150 m level. The total length of the orebody exceeds two kilometres, but little is known about the extensions in depth; there is room for ore reserves of even 10 Mt.

Outcrops are poor but 134 drill holes provide information on the shallow parts of the formation. There is only one deeper hole (350 m), drilled in 1983. According to Koistinen (1984), the structure is as shown in Fig. 1b. F2 is the fold axes of the predominant deformation phase, and F1 consists of small, isoclinal folds with amplitudes no longer than a few tens of metres. The NW component of F3 may be significant locally, whereas the NE component is an incidental occurrence. F4 is rare, weak and local; other phases have not been observed. The intensity of F1 obviously controls the thickness of the ore, and it is mostly weak.

Petrophysics

The rocks in the area are not complicated in their physical properties. The ore contains abundant pyrrhotite, rendering it moderately magnetic. However, the altered rocks contain magnetite showings in which the susceptibility may be up to one SI unit. In places the mafic volcanite is magnetized to some extent. The mica gneisses are neutral and no black schists have been encountered. The ore exceeds 4000 kg/m^3 and the altered rocks are c. 3000 kg/m^3 in density, a local increase being due to garnet. The density of the mafic volcanite is also c. 3000 kg/m and that of the acid volcanite and gneisses 2700-2800 kg/m^3. The ore is many orders of magnitude more conductive (up to 1000 S/m) than the other rocks of the area.

Magnetic survey enables the altered rocks to be located, but mostly the orebody can be detected, too. The gravity correlates with the magnetized area, indicating an increase in the abundance of garnet or the thickness of the altered rocks. The ore can be located unambiguously only by electric and EM methods, but the grade of Zn and Cu cannot be estimated.

Measurements

Various geophysical surveys have been carried out in the area, the older ones being reported by Laurila (1963). In the early 1980s, 73 stations with AMT, 200 stations with TDEM coincident loop 100 x 100 m (Sirotem), and 100 stations with a fixed transmitter loop 400 x 600 m (EM 37) were surveyed. Three holes totalling c. 600 m were measured with a Sirotem borehole probe. The sparsely spaced profiles covering the whole area and nine holes were

measured with the mise-a-la-masse (= CP = charged potential) method.

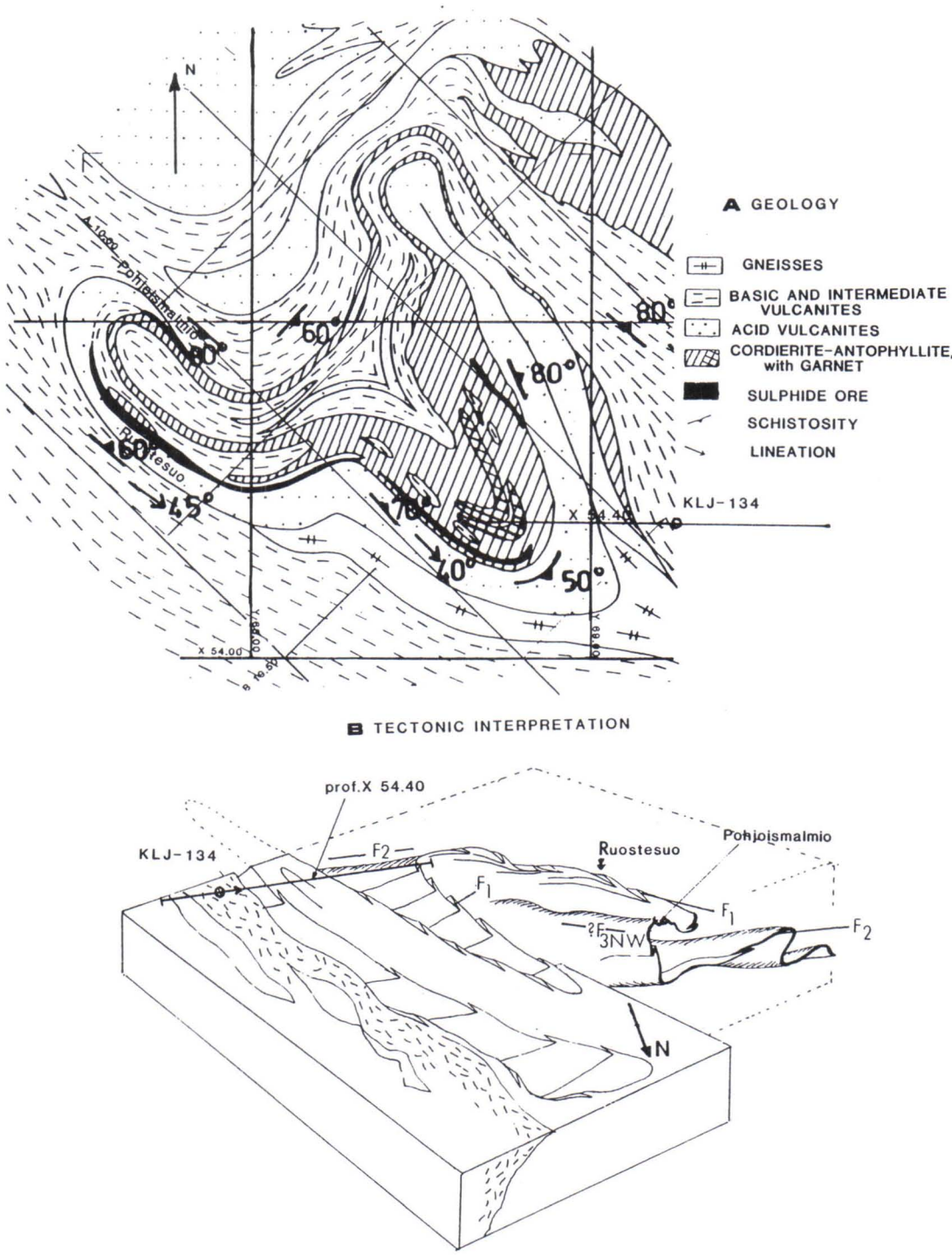

Fig. 1. The geology of the area. a) ground projection, b) structural model by Koistinen with the assumed deformation phases.

Results

The magnetic map (Fig. 2a) is complicated because of so many sources, but anomalous continuations marked A, B and C towards the SE are interesting, possibly indicating extensions of ore. HLEM (Slingram) outlines the ore outcrops (Fig. 2B). At the eastern end there is a separate smaller anomaly. The CP result is not very informative (Fig. 2b). The whole area of altered rocks is at the same potential. There are but few details. The boundary is sharp in the south and in the west but gradual towards the north and east. Extensions A and B are noticeable. The borehole data demonstrated that the ore intersections are at the same potential, which changes smoothly towards the country rock, indicating large extensions (see Fig. 3a).

TDEM with a coincident loop (Fig. 2c) produced more details than CP. The ore outcrops are well defined. There is an anomaly-free part in the middle of the area, and extensions A and B are clearly visible. Profile X = 54.4 passes over the extension A. Three shallow holes intersect the 2-10 m thick sulfide plate, the deepest one suggesting a more gentle dip. The TDEM results also suggest that the plate continues quite deep (Fig. 3b). The reliability of the interpretation, however, is reduced by the separate eastern conductor (cf., HLEM result) masking the anomaly of deeper parts of the known orebody. Both seem to dip gently to the east. Two other parallel profiles measured at intervals of 200 m are similar (not shown); the orebody continues for at least 300-400 m eastwards. The wo-layer modeling esult looks attractive, and the depth inversion technique (DIT), the principle of which is described in the appendix, shows the same behaviour except that the conductivity is abruptly reduced at Y = 69.2.

a)

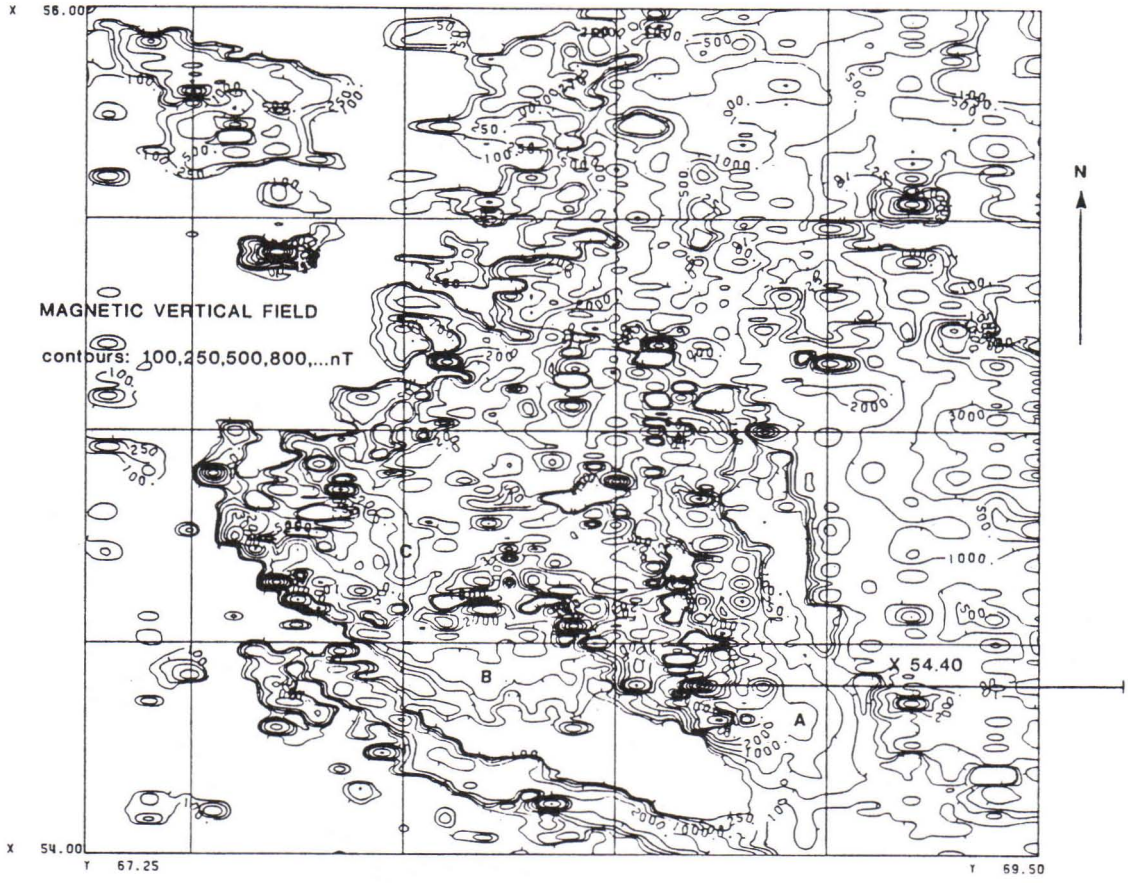

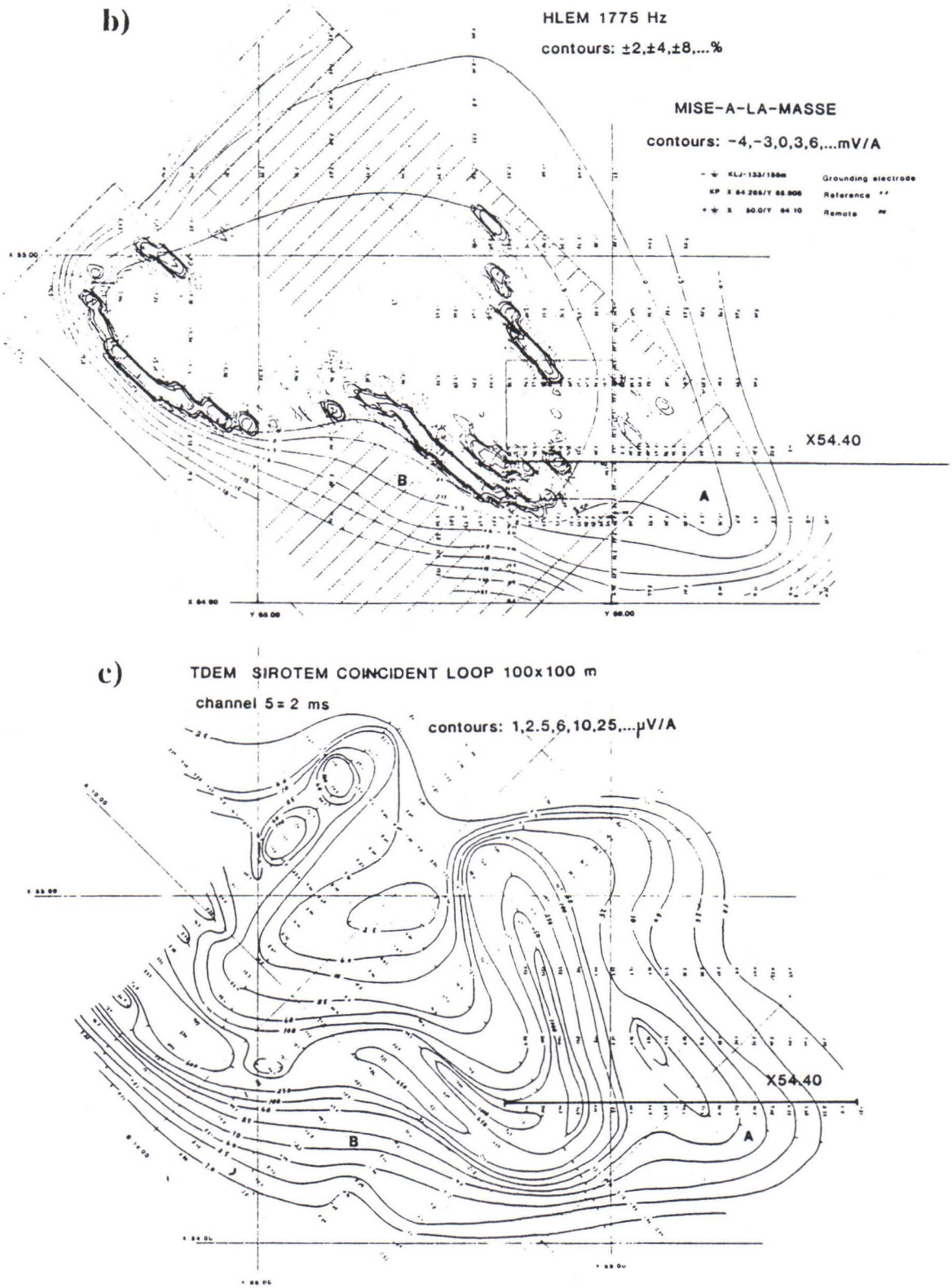

Fig. 2. Geophysical countour maps of the area. a) magnetic, b) HLEM and CP and c) Sirotem channel 5 = 2 ms. The extensions are marked with letters A, B and C. Also marked is profile X = 54.4.

The same profiles were surveyed with AMT in the late autumn, which was not very favourable timing in view of the intensity of the natural source fields. The results are poorly compatible with the assumed structure, and there is no suggestion of a gently dipping target (Fig. 3c). The easternmost conductor can be seen at higher frequencies and possibly as elevated depth values at Y = 69.1 and 69.2. The result is obviously distorted also by the 3D

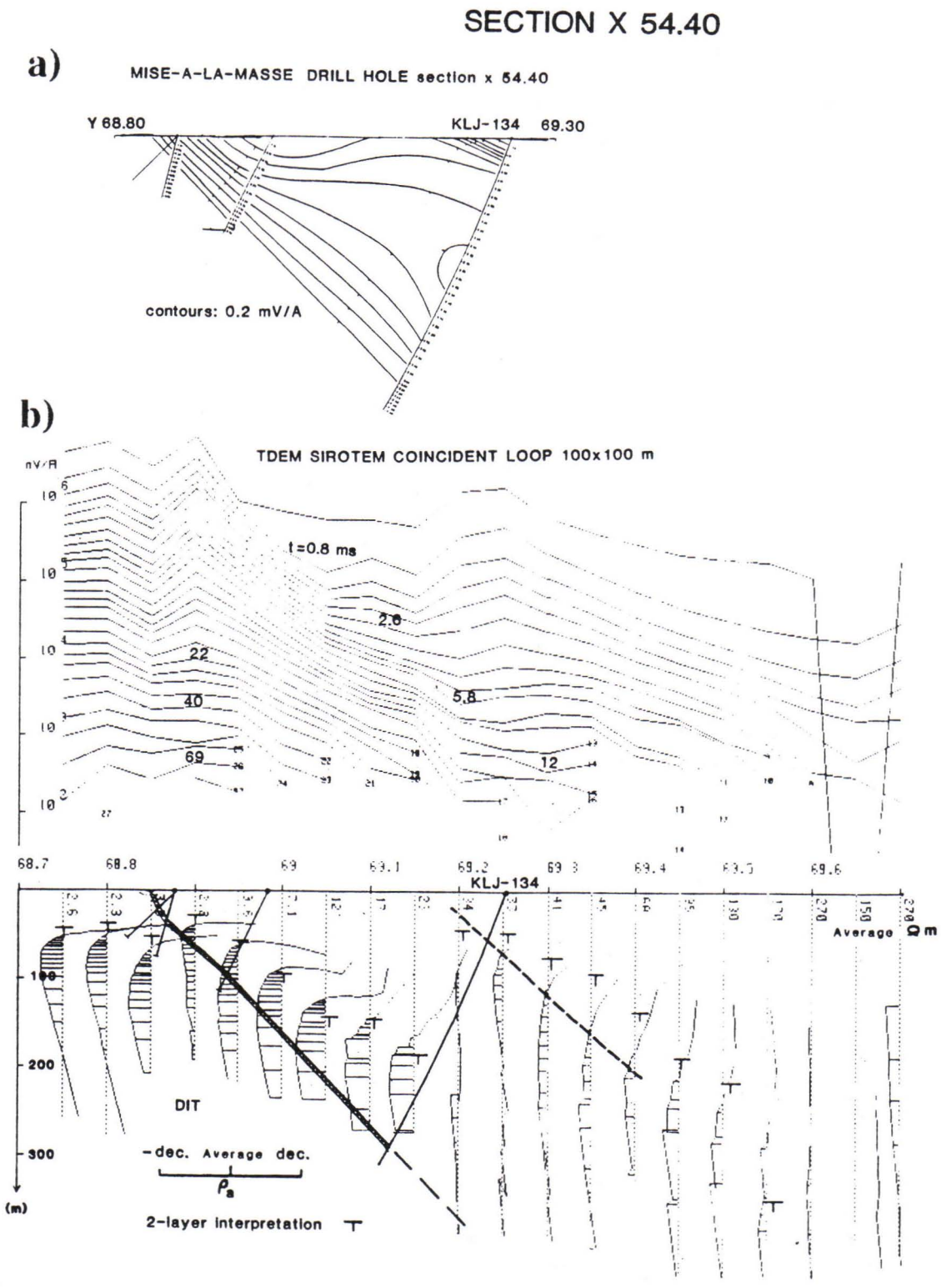

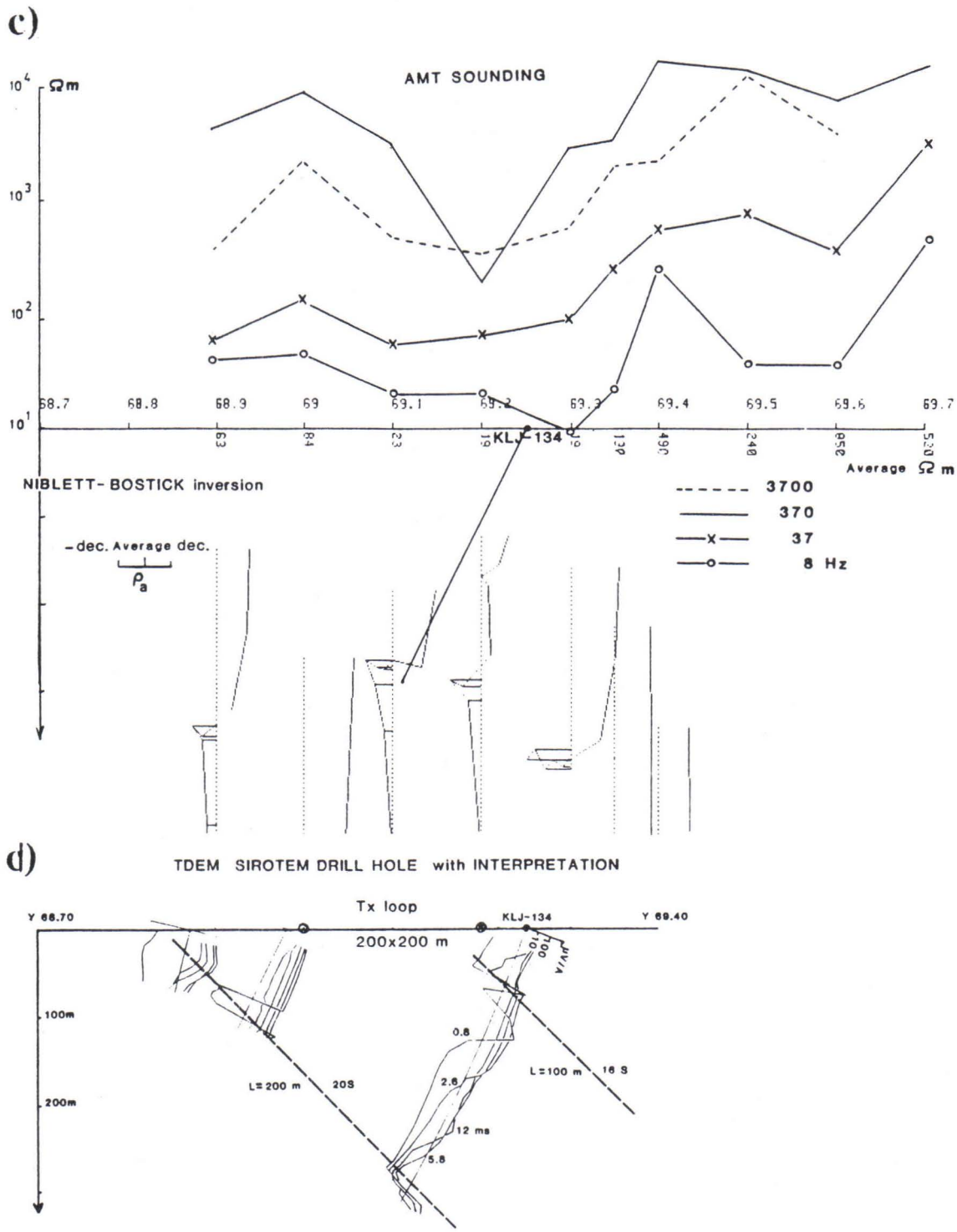

Fig. 3. Sections of profile X = 54.4: a) CP result, b) TDEM coincident loop result, 2-layer interpretation and DIT (dec. means one order of magnitude), c) AMT result and Niblett-Bostick inversion and d) TDEM borehole result with plate model interpretation.

effects. The structural model does suggest an anticlinal fold whose axis plunge ESE diagonally to the profiles.

a)

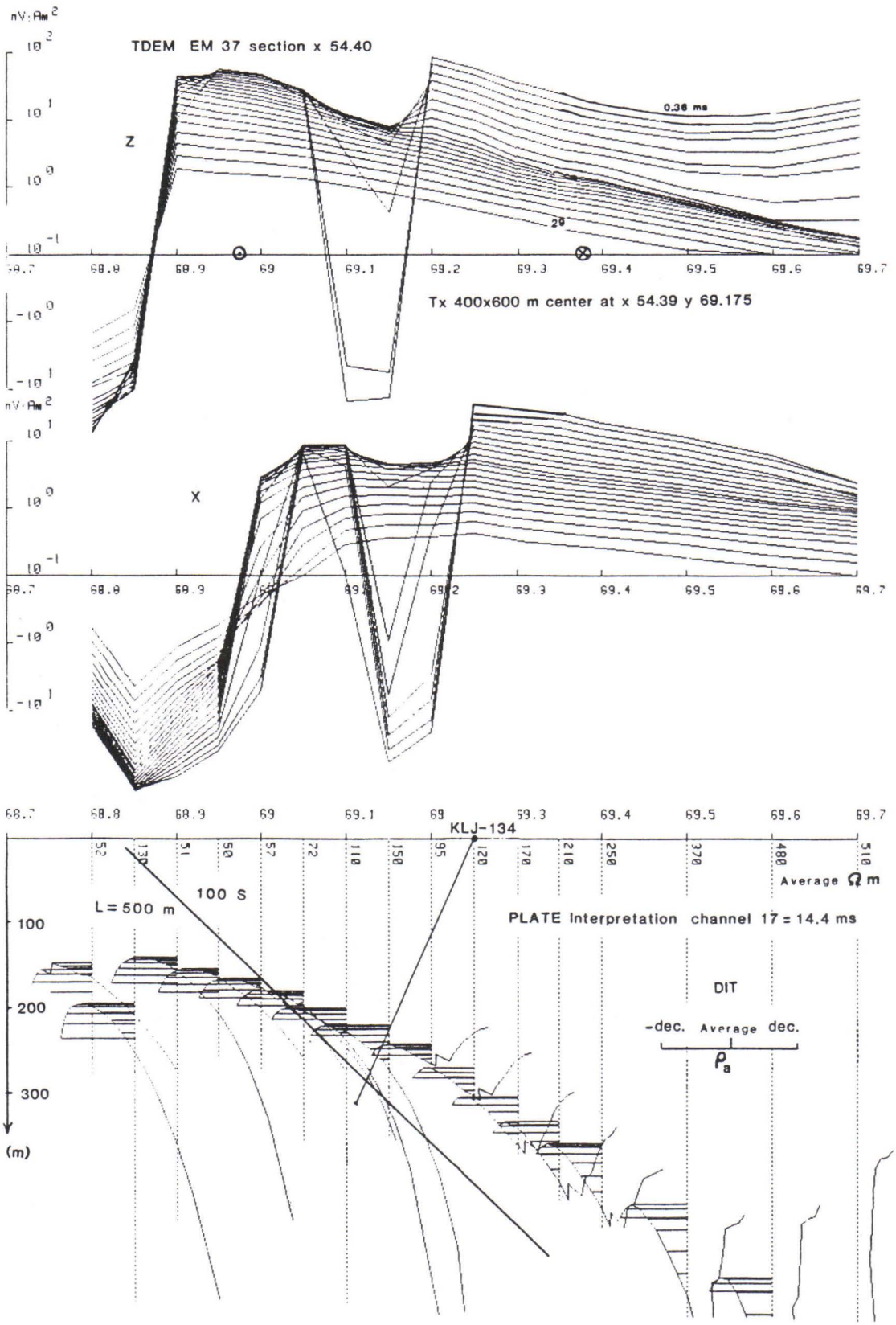
TDEM EM 37 section x 54.40
Z
0.36 ms
29
Tx 400x600 m center at x 54.39 y 69.175
X
KLJ-134
Average Ω m
L = 500 m
100 S
PLATE Interpretation channel 17 = 14.4 ms
DIT
-dec. Average dec.
ρ_a
(m)

b)

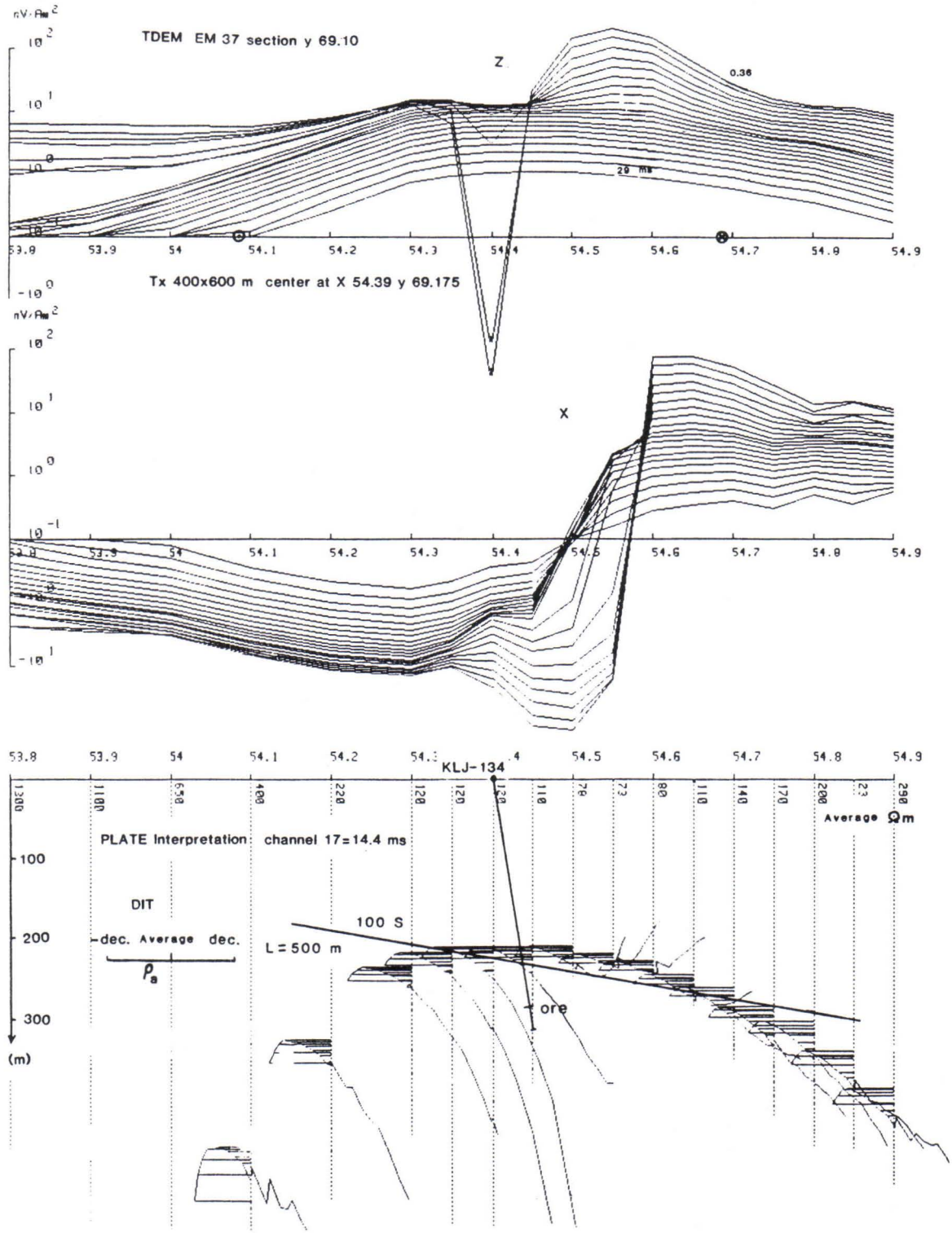

Fig. 4. TDEM fixed loop system results: A) profile X = 54.4 and B) profile Y = 69.1. Also included are the DIT and plate interpretations of channel 17 = 14.4 ms.

A deep hole (No. 134) collared at Y = 69.25 was drilled in section X = 54.4 to test the interpretation. It intersected the easternmost conductor at a depth of about 60 m, a thin sulfide body. The next intersection was anticipated at a depth of less than 200 m but was encountered at a depth of almost 300 m. Petrophysical checking, however, pinpointed a narrow conductive zone (1 S/m) at a depth of slightly less than 200 m, but it was not the right sort of rock.

CP and TDEM measurements in the drill hole (Figs. 3a and 3d) showed that the deepest intersection belongs to the extension of the known orebody, and hence the ground TDEM result must have been biased subtly by the response of the eastern conductor, which also dominates the TDEM borehole data. According to the interpretation of the borehole data the extension of the lower plate might continue less than 100 m, but the used plate algorithm (current filament approximation, Barnett, 1984) is not accurate and quite suitable for intersecting bodies.

After drilling, an EM 37 survey was carried out with a large transmitter loop, 400 x 600 m in size, and with the centre at X = 54.4, Y = 69.175, i.e., above the eastern conductor. The result from profile X = 54.4 can be interpreted with a single conductive plate, which corresponds fairly accurately to the intersections (Fig. 4a). The DIT, which is distorted close to the surface, because that site is outside the transmitter loop (cf., appendix), gives a value about 50 m too shallow over the deepest intersection. There is no sudden decrease in the conductivity and it suggests that the plate continues eastwards for at least 200 m from the intersection drilled deepest. The influence of the overlying conductor is perceived as a sign of reversal on the early channels, and an increase in the amplitude. This case shows the need for a model that takes the mutual inductance into consideration. The DIT of the transversal profile Y = 69.1 (Fig. 4b) is surprisingly uniform, demonstrating that the upper edge of the plate is fairly wide (200 m) and even, but the depth estimate is again 50 m too shallow. A sharp boundary is situated in the south, having a gentle dip northwards for another 200 m. The plate model interpretation gives a total width of up to 700 m, but again too shallow a location. Drill hole No. 134 intersects the plate close to its centre in X direction, since the hole is known to deviate northwards by 50 m. The time constant of the conductor was calculated to be about 10 ms.

There are no deep drill holes in the western part of the area and hence the results obtained there are beyond the scope of the present paper.

Summary

The extensions of the orebody, which differs clearly from the environment in conductivity, can be traced to depths of 200-400 m by TDEM. It suggests a marked augmentation of the potential ore reserves in the area. On account of the complex structures, the estimates are not reliable everywhere. Even so, new information has been obtained on the behaviour of the methods. TDEM with a coincident loop reveals details in the central parts of the area. The deep hole drilled in the eastern part of the area demonstrates that the depth estimates based on the layered earth model are too shallow. The borehole data and their interpretation, however, agree well with the assumed structure. The fixed loop system gave better depth estimates when the large transmitter loop had been placed over the eastern interfering conductor to eliminate its influence.

References

Barnett, C.T., 1984. Simple inversion of time-domain electromagnetic data. Geophysics 49, 925-933.

Bostick, F.X., Jr.,1977. A simple and almost exact method of MT analysis. Abstract: Workshop on electrical methods in geothermal exploration, Utah.

Gamble, I.D.,1983. Simple one-dimensional magnetotelluric inversions. Expanded abstract: Presented at the 53rd Annual International SEG Meeting, Las Vegas, September 11-15, 1983.

Jones, A.G. & Foster, J.H.,1983. An objective real-time data adaptive technique for efficient in-field model resolution improvement in magnetotelluric studies. Expanded abstract: Presented at the 53rd Annual International SEG Meeting, Las Vegas, September 11-15, 1983.

Kaufman, A.A. & Keller, G.V., 1981. The magnetotelluric sounding method. Amsterdam, Elsevier.

Ketola, M., Laurila, M. & Suokonautio, V.,1972. On a digital two-plane rotary field airborne system and its use in conjunction with the magnetic method in Finland. Geoexploration 10: 203-220.

Koistinen, T., 1984. Kiuruveden Kalliokylän geologiset tutkimukset. Malmin ja ympäristön rakennegeologiaa. Unpublished report, Outokumpu Oy, 10 p. (in Finnish).

Appendix
1(3)

AN APPROXIMATE DEPTH INVERSION TECHNIQUE, DIT, FOR TDEM

Electromagnetic sounding results are often transformed by asymptotic methods into resistivity-versus-depth profiles. These depth-inversion techniques are approximate, but rapid. Absolute resistivities are seldom obtained; the thickness should be exceptionally large. DIT results of adjacent soundings are plotted as profiles on a suitable distance scale. Certain manipulations, as, for instance, the static correction and automatic gain presented by Warner et al. (1983) can be used to improve readability.

For plane wave inversion, the Niblett-Bostick transformation (Bostick, 1977 and Hjelt et al., this issue; some modifications reported by Jones and Foster (1983) and by Gamble (1983)) has recently been used extensively. DIT has been applied to dipole-dipole multifrequency (Maxiprobe system) sounding by Sinha (1979). Apparent resistivity is obtained from the ratio of the vertical to radial component of the magnetic field. Other possibilities, described by Kaufman and Keller (1981, p.145), have been used by Valla and Gasnier (1984). DIT has recently gained popularity in the processing of airborne electromagnetic data (to eliminate the geometry of the system, e.g., Peltoniemi, 1982 and Mundry, 1984), but the number of frequencies available is too small to locate the layer boundaries. Similar processing could be derived for the HLEM and other EM methods as well.

It is well known that the TDEM apparent resistivity can be calculated for the coincident loop geometry channel by channel (Lee and Lewis, 1974, and more accurately Raiche and Spies, 1981). In order to derive DIT for TDEM, the late time approximation for conductance (in Siemens) is used:

$$S = 474\sqrt{t/\rho_a(t)} \quad \text{(Kvashnin, 1984, pers. comm.)} \qquad \text{(A1)}$$

where t is the time since the cut-off of the transmitted pulse (in seconds) and $\rho_a(t)$ is the respective apparent resistivity (in ohmmeters). DIT is completed simply by calculating the thickness

$$h(t) = S \cdot \rho_a(t) \qquad \text{(A2)}$$

A more accurate DIT nomogram was constructed (Fig. 5) using the two-layer model curves made by Spies (1980). Contrary to the frequency domain methods, the resistivity contrast affects considerably the depth estimate of the time domain data, since the response is a sum of many frequencies at every moment of time, and there is an overshoot which increases as the conductivity of the lower layer increases.

The nomogram was used on 1D calculations by Lee and Lewis (1974). For a three-layer case, where the second layer is much more conductive than the others, $\sigma_2/\sigma_1 = 400$, the thickness of the first one, $h_1 = 100$ m, h_2 not given, e.g., (A2) gave a depth of 70 m to the conductive layer; only 60 m was obtained from the nomogram with a large contrast. However, in the early channels, time 0.5 ms, the depth was 25 m more, which must be due to overshooting. If the contrast were about 50, the depth estimate would be correct (the conductance ratio is 50 if $h_2 = 12.5$ m). For a four-layer case, $\sigma_1 = 0.1$ S/m, $h_1 = 20$ m, $\sigma_2 = 0.01$, $h_2 = 155$, $\sigma_3 = 1$, $h_3 = 5$ m and $\sigma_4 = 0.01$, the third most conductive layer is weakly observable from the bending of the DIT curve, starting at the correct depth when formula (A2) or the nomogram is used. These and other tests have shown that the use of DIT is not straightforward.

Real massifs can seldom be regarded as 1D models. DIT was also used on some 2D examples of small-scale model results by Ogilvy (1983) (Fig. 6). For a vertical plate, the upper edge of the inversed curves on both sides of the plate descends rapidly (>45°). The thicker the plate, the better is the depth estimate at the middle of the plate. The DIT curves incline at a much slower rate on the hanging wall and the depth estimates correspond approximately to the perpendicular distance from the centre of the loop to the plate. The more gentle the dip, the better are the estimates, and even the depth extension might be noticed. With a horizontal plate wider than the loop size, the estimates are surprisingly accurate and the boundaries are

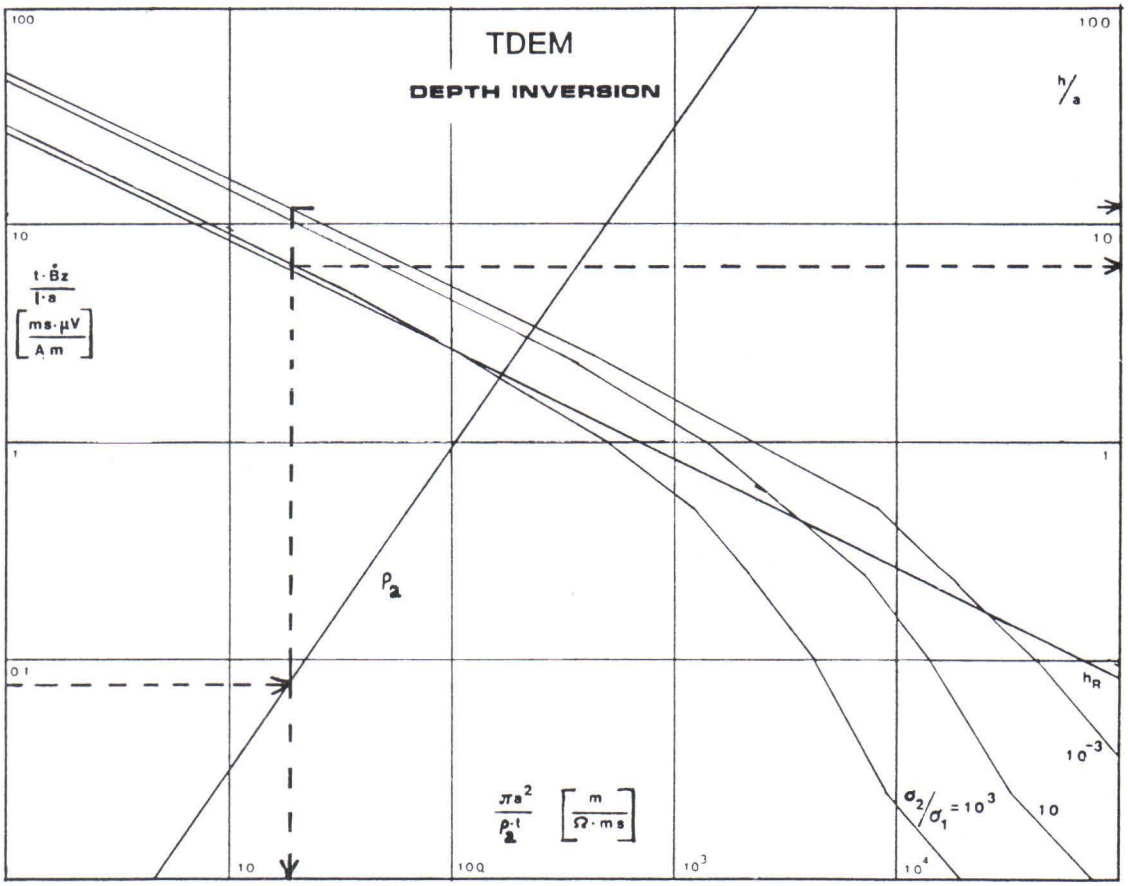

Fig. 5. DIT nomogram for TDEM coincident loop with derivation of apparent resistivity. The observed reading, Bz, normalized by current in μV/A, is multiplied by time t in ms and divided by the loop radius a in m. This value is plotted on the left-hand vertical axis and lined horizontally to intersect the ρ_a-curve (this is a late-time approximation). The apparent resistivity can now be read from the horizontal axis with the normalizing factors. At the same time, the intersection of the desired curve, h_R, for the formula (A2) or different conductivity contrasts, gives the depth in m from the right-hand vertical axis with the loop radius as a normalizing factor.

clearly visible (Fig. 6d). The conductive overburden does not jeopardize the DIT result, but it is almost impossible to estimate the thickness of the plate with this technique. Finally, the DIT result for the cylinder is shown (Fig. 6f) with a conductive overburden. These examples show that DIT can be used for 2D and even 3D situations to obtain the first estimate for the upper surface of a conductive body. Together with the plate approximation derived by Nabighian (published by Barnett, 1984 and McNeill et al., 1984), it is possible to make serious and yet rapid interpretations.

For the fixed loop TDEM, a rapid universal method for calculating the apparent resistivity does not exist, but again the late time approximation can be extended to the stations outside the transmitter loop.

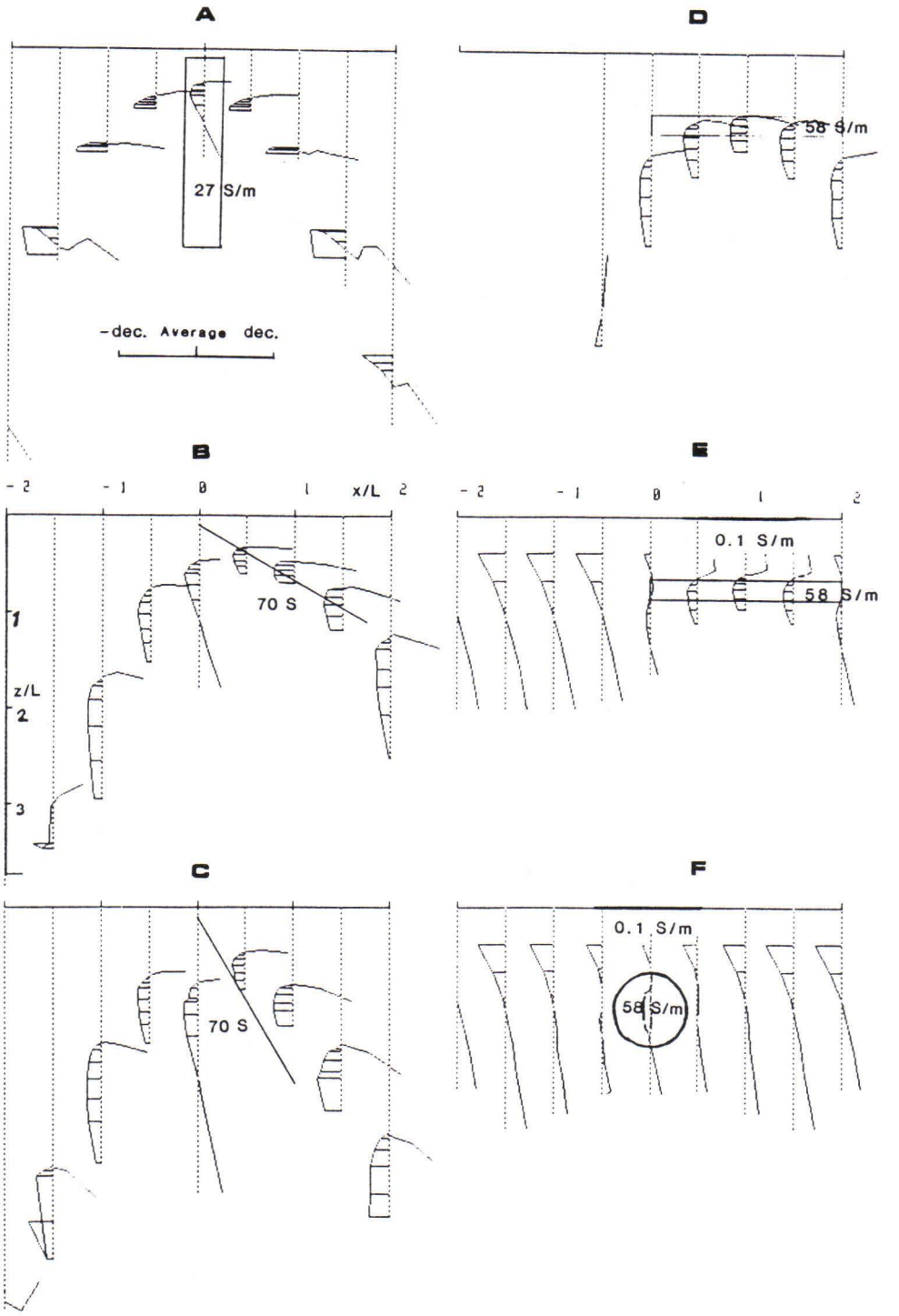

Fig. 6. 3D models of the small-scale measurements taken from Ogilvy (1983), and DIT results, h_R-curve applied: a) corresponds to Fig. 15, b) to Fig. 5, c) to Fig. 6, d) to Fig. 24, e) to Fig. 23 and f) to Fig. 22 of Ogilvy (1983). The strike length is 2L (L is a loop diameter).

DOWNHOLE VARIANTS OF DIPOLE ELECTROMAGNETIC PROFILING

by

L.V. Lebedkin

Lebedkin, L.V., 1990. Downhole variants of dipole electromagnetic profiling. *Geologian tutkimuskeskus, Tutkimusraportti 95.* 120-131, 7 figs, one table.

The article presents the principles of the single downhole and interborehole modifications of dipole EM profiling (DEMPS and MDEMP respectively). The physical fundamentals of the method are specified and the technical data of the ASMI-4OM equipment, now in serial production, are listed. Examples are given of the results obtained in physical modelling of the fields produced by layer-like conductors. The properties and distribution of the anomalous fields are explained from the standpoint of the zones with a prevalent eddy current concentration.

In the presentation of the practical aspects of DEMPS, emphasis is laid on the one hand, on the necessity of making 3-component measurements of anomalous fields, and, on the other, on the detailled information the DEMPS method yields concerning the size, geometry and spatial position of orebodies. The ASMI-4OM proves to be most efficient in cases where the targets possess an intricate morphology of orebodies, or when the orebodies occur in a low-resistance host medium. Examples are given of using the 3-component MDEMP method for ascertaining the continuity of orebodies in the interborehole space. Finally, the efficiency of MDEMP measurements below the bottom of the hole, is demonstrated.

Key words: electromagnetic methods, electromagnetic induction, boreholes, numerical models, mineral exploration, metal ores, USSR

Леъедкин, Л.В., 1990. Скважинные варианты дипольного электромагнитного профилирования. Геологический центр финляндии, Рапорт исследования 95.,120-131. Идд. 7.

В статье описаны принципы осуществления односкважинного (ДЗМПС) и межскважинного (МДЗМП) вариантов дипольного электромагнитного профилирования. Рассмотрены физические основы метода. Приведены примеры результатов физического моделирования полей от проводинков пластообразной формы. Особенности распределения аномальных полей объясняются на основе представлений о зонах преимущественной концентрации вихревых токов. Перечислены технические характеристики серийной аппаратуры АСМИ-40М и приведены примеры применения ДЗМПС. Подчеркивается необходимость трехкомпонентных измерений аномальных полей, детальность получаемой при ДЗМПС информации о размерах, форме пространственном положении рудных тел.

Наиболее существенные результаты с АСМИ-40М получены при разведке объектов, отличающихся сложной морфологией рудных тел, а также в случаях, когда рудные тела залегают в низкоомной вмещающей среде.

Приведены примеры применения трехкомпонентного МДЗМП для подтверждения сплошности рудных тел в про странстве между исследуемыми скважинами. Укзывается на возможность опоискования с помощью МДЗМП подзабойного про странства.

Introduction

Single borehole dipole electromagnetic profiling with three-component measurements of the anomalous magnetic field (DEMPS) was suggested and developed in the USSR in the 1960s (Lebedkin, 1971; Lebedkin et al., 1971).

In later years, this method of investigating the space surrounding to a borehole was extensively used in the USSR, initially while prospecting and exploring for sulphide ore deposits.

When the DEMPS is performed, the transmitter coil, coaxial with the borehole, is moved downhole. At a certain preassigned distance (from several tens of meters to a hundred meters) in the borehole, three orthogonal magnetic field components, oriented relative to the borehole dip plane, are received. It should be noted that the coordinate system is coupled with the receiving device, which occupies a certain position in the borehole. One of the transverse components measured is in the vertical plane tangent at the given point to the borehole dip plane (vertical component). Another transverse component is in the horizontal plane and is called the horizontal component. To convert the coordinate system, which is interconnected with the receiving device, into the geographical coordinate system, use is made of downhole directional survey data.

The necessity of three-component measurements is determined first of all by the peculiarities of borehole investigations, wherein, unlike in surface observations, one cannot randomly choose either the number of profiles or their position; again, the position of the objects being thus investigated is not limited by the lower half-space.

The key feature of the DEMPS, as one of the methods of low-frequency induction electrical prospecting, is its capability of distinguishing with clear resolution objects of good electric conductivity. Thus, a rather thick layer of sulphide massive ores may be discriminated against the background of a string-impregnated metallization.

Another, not less important, feature of the DEMPS is its capability of obtaining detailed information concerning the morphology and spatial location of orebodies. It is provided by the possibility of radial sounding of the space around the borehole as well as by multicomponent measurements of the anomalous field, and by the nature of the magnetic dipole field. At the same time, the effect of the host rock conductivity is to reduce the radius of the survey area around the borehole. Thus we have to measure the anomalous effects in relatively weak magnetic fields.

The main tasks resolved with the DEMPS are revealing the orebodies in the space around the borehole, evaluating their size and geometry, determining the spatial position of orebodies in relation to the borehole (distance to the nearest edges, azimuth to the ore body) and their attitude (dip and strike), deciding whether the conductive object is homogeneous in terms of conductivity, and ascertaining the way it crops out and the directions of the greatest variation in electrical conductivity or thickness.

Description of instruments

Most DEMPS measurements in the Soviet Union are performed with the ASMI-4OM apparatus. Besides the DEMPS, the equipment is designed to carry out downhole observations using a surface field loop source. The ASMI-4OM provides point measurements of the real (ReH_2) (in-phase with the current of the field source) and imaginary (ImH_2) components of the alternating magnetic field.

The main advantages of the ASMI-4OM, compared with the Canadian downhole induction equipment manufactured by McPHAR (D661) and SCINTREX (DHEM-%), are primarily the versatility and secondly the possibility to measure the magnetic field components orthogonal to the borehole axis. The latter advantage provides not only the possibility of

taking an azimuth bearing of the object causing the anomaly, but it also gives more information

Table 1. Technical specification, ASMI-40M.

Frequencies	125, 375, 1125, 3375 Hz
Spacings	25, 50, 75, 100 m
Measurement threshold sensitivity at 50 m spacing	better than 0.05 % (of the primary field amplitude)
Depth of the borehole being investigated (m)	1500 m
Diameter of boreholes devices	40 mm
Borehole deviation essential for oriented reception of magnetic field transverse component	3° - 5°
Operating temperature range	+10° - (-45)°C

Note: Besides DEMPS, the ASMI-4OM instruments make possible borehole induction measurement with a ground loop field source.

concerning the orebodies as well as extending the operating range of the equipment. The range of the ASMI-4OM operation in the DEMPS version, however, still does not exceed 50-80 m off the borehole under investigation.

The ASMI-4OM (ASMI-4O) is commonly applied in prospecting and exploration of sulphide deposits in the Urals, in Kazakhstan, in the Altai and other regions of the Soviet Union. The most significant results were obtained:

- above the deposits occurring in low-resistance geoelectrical sections;
- in cases where exploration is hindered by complex tectonic features of the orebodies;
- above deposits, where commercial ores with massive metallization occur among noncommercial string-impregnated ores or where the correlation between electrical resistivity and ore grades is observed.

In all the foregoing cases, the DEMPS has been the prevalent method of downhole geophysics.

The ASMI-4OM is employed at different stages of geological prospecting. During preliminary prospecting, the equipment furnishes the data as to the strike, dip and size of the ore zone, and also enables the geometry, structure and dimensions of ore deposits to be figured out. During the exploration stage we use the DEMPS to discern the structural details of the orebodies, to outline these bodies and to bring to light the ones overlooked. Again, here we can prove the continuity of individual metallization areas or alternatively reveal the pinches of orebodies, barren areas and fault zones. In this particular way, the reliability of evaluating commercial mineral resources can be significantly increased.

Estimation of parameters

The determination of the spatial position of the conductive object in relation to the borehole is based on the quasi-stationary assumption. Provided the conditions are such that the conductivity of the rock can be ignored, the pattern of the alternating magnetic field may at

any instant be replaced with satisfactory accuracy by the pattern of the direct current field. The downhole study of the spatial structure of the secondary field gives us an idea of the spatial position of areas with eddy current concentration, which in the first approximation coincide with the contours of the conductors sought. The azimuth from the borehole investigated to the conductive object (or, if the object is intersected by the borehole, to its main part) is defined by two mutually orthogonal transverse components. It is necessary to know the direction of the receiving coil moment (i.e., the sign of the measured signal in relation to the direction of the magnetic field strength vector). A right-handed system is used and the current in the source loop is assumed to flow in the clockwise direction as viewed by the observer.

The interpretation of the downhole inductive measurements is performed by comparing the field curves with the modelling or calculated fields produced by conductors of different geometry. Detailed catalogues of such plots have been prepared. Evaluation of the size, shape and attitude of bodies is done using the relations connecting the amplitude or the frequency response of the anomalous field, or the width of characteristic intervals on the field curves (normalized in units of spacing, L) with the proper parameters of the object causing this anomaly. It is a common practice to make all the determinations on the basis of several cross-checking indications, which increases the accuracy of the conclusions.

The arithmetic mean errors in the ASMI-4OM measurements of the main parameters of massive orebodies, based on copious check drilling data, are:

1. For objects intersected by the borehole:
   - when determining the distances to the edges downdip (updip) and along the strike: 10 %; across the thickness: 2 %;
   - when determining the borehole-conductor intersection angle: 3°;
   - when determining the strike azimuth: 7-20° (depending on the borehole dip angle);
2. For objects, not intersected by the borehole:
   - when determining the azimuth to the orebody: 10-20°; dip angle: 5-30° (depending on the dip of the orebody and the distance to the body);
   - when determining the distance to the edge: 10 %; and body size downdip (updip) and across its thickness: 10-20 %.

Examples of modelling

Shown as an example in Fig. 1 are the results of modelling the field of a thin conductive plate, its plane being orthogonal to the axis of the measuring array at various positions of the "borehole" relative to the model edge. The curves indicate that the characteristic feature of the anomaly is the positive sign of the axial component when the borehole does not intersect the object, and the negative sign of the anomaly caused by the intersected object which corresponds to the primary field screening.

The inductive coupling of the transmitting and receiving dipoles with the model is greater in the case of the intersected plate than with the same object located off the profile. Correspondingly, the frequency responses of the intersected plate field are shifted to the low-frequency region compared with the non-intersected plate, and the frequency parameter is approximately 2.5 times higher for the intersected plate than that of the non-intersected one.

The effect produced by the boundary of the half-infinite plate intersected by the borehole is indicated in the anomalous axial field component as a decrease of the negative anomaly in the middle part of the plots. This phenomenon is explained by the fact that, when the array in symmetrical to the conductor plane,one part of the magnetic field flux, envelopes it. The nearer the edge of the conductor is to the point of its intersection with the borehole, the deeper is the "trough" in the negative anomaly, which corresponds to the primary field screening effect.

The anomalous transverse field component is caused in this case by the eddy currents concentrating near the edge of the half-infinite plate. The nearer the conductor's boundary is

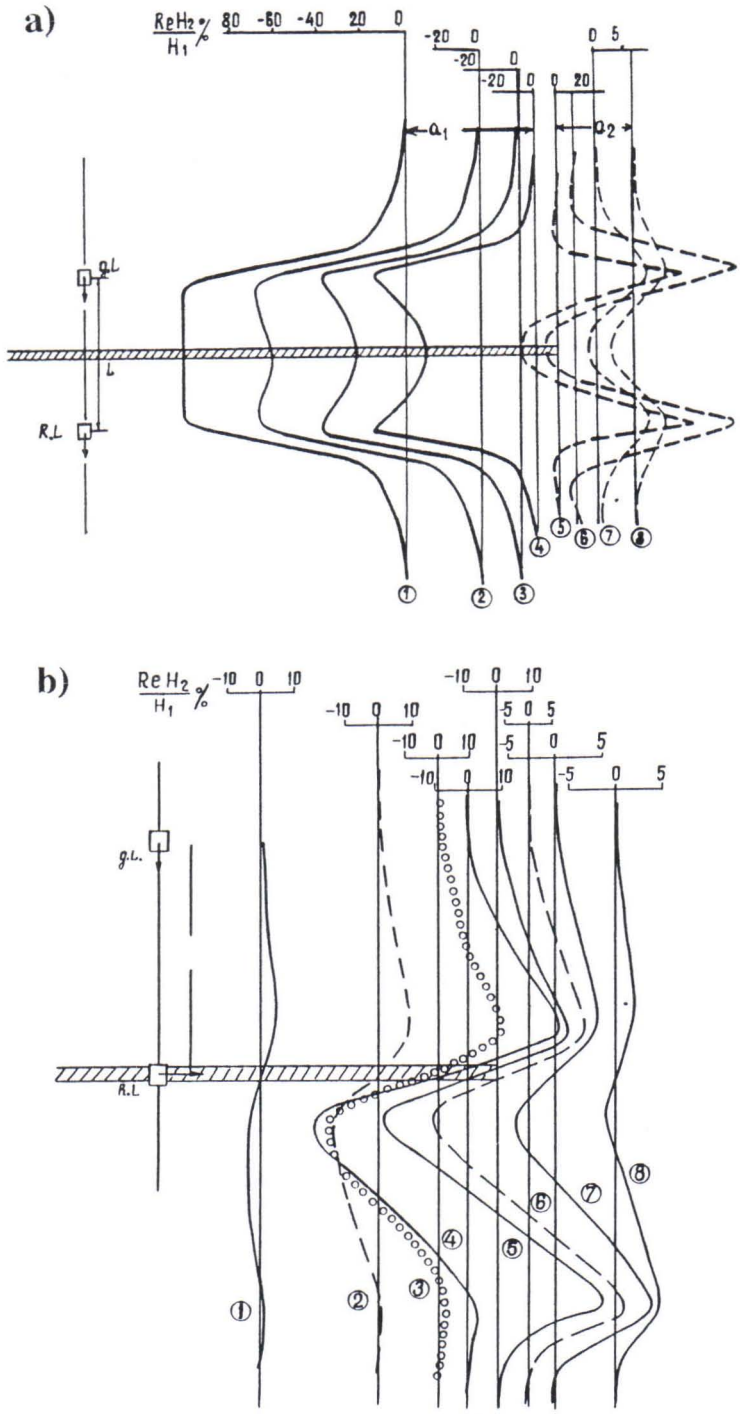

Fig. 1. The axial (a) and transverse (b) components of the anomalous field of the plate orthogonal to the "borehole" axis at various spacings between "the borehole" and the model edge. Model: 4 mm duraluminium plate, frequency: 1125 Hz. 1 - $a_1 = L$; 2 - $a_1 = L/2$; 3 - $a_1 = L/4$; 4 - $a_1 = L/8$; 5 - $a_1 = 0$; 6 - $a_2 = L/8$; 7 - $a_2 = L/4$; 8 - $a_2 = L/2$.

to the borehole, the greater is the amplitude.

The fields resulting from a thin plate intersected by the borehole at different angles ψ are shown in Fig.2. The most universal procedure followed in defining the borehole-conductor intersection angle is based on using the relation of ψ to the relative width l/L of the initial part of the anomalous transverse field component curve. With an accuracy high enough for practical purposes, the intersection angle can also be expressed in terms of l and L spacing by the formula ψ = arcot (l/100 L), where the linear dimensions are given in meters. To make a check, we use the recalculated transverse component amplitude, as usual, in terms of frequency response asymptotic values. With intersection angles of less than 50°, good results are also likely to be obtained from axial component measurements. The more acute the angle ψ is, the more "withdrawn" into the region of positive values are the curve segments corresponding to the measuring array's approach to the conductor and moving away from it.

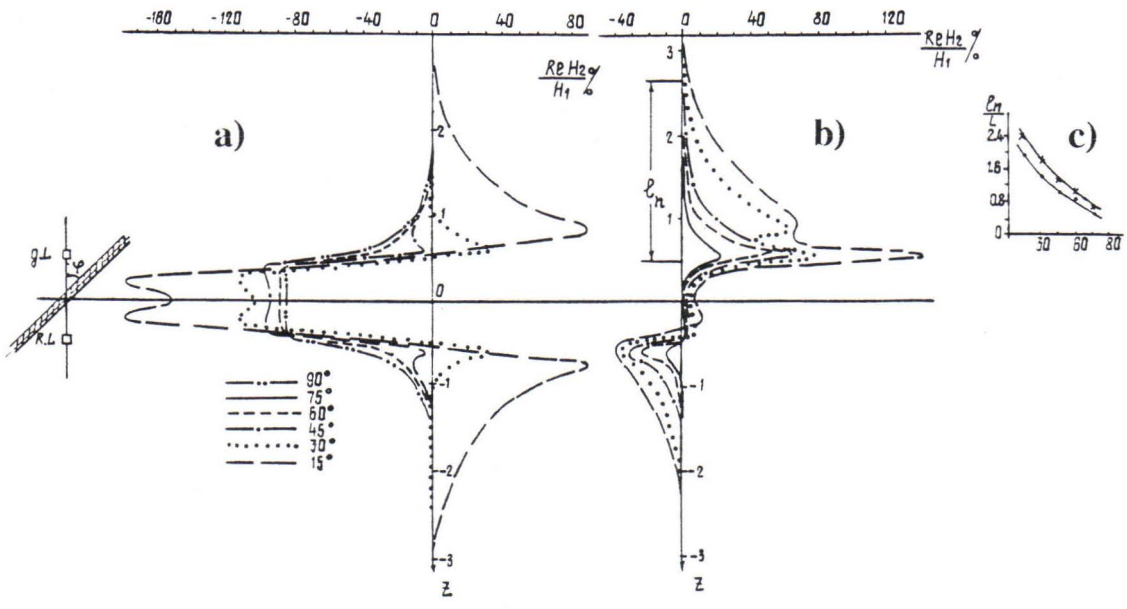

Fig. 2. The axial (a) and transverse (b) components of the anomalous field of the infinite plate intersected by a measuring array at the angle of ψ and master curve (c) for defining the borehole - conductive body intersection angle according to the width of the transverse component profile: L = 50 m (crosses), L = 100 m (dots).

A missing asymmetry in the axial component in such cases indicates the wedging-out of the conductor down or up the dip, depending upon from which side the anomaly is reduced.

Examples of applying the DEMPS method

Let us analyze some examples of the application of the DEMPS. Fig. 3 shows a rather simple example of the DEMPS application for revealing the orebodies missed by the borehole on one of the copper-zinc deposits in the Urals. The orebodies here are confined to the effusive rocks and the lens-like deposits are cut by porphyrite dykes into blocks of slight dimensions complicated by swells, pinches and numerous thin apophyses. The resistivity of massive ores is 0.5-10 Ohm · m according to the electrical log data. The resistivity of the host

rock is 200-600 Ohm · m.

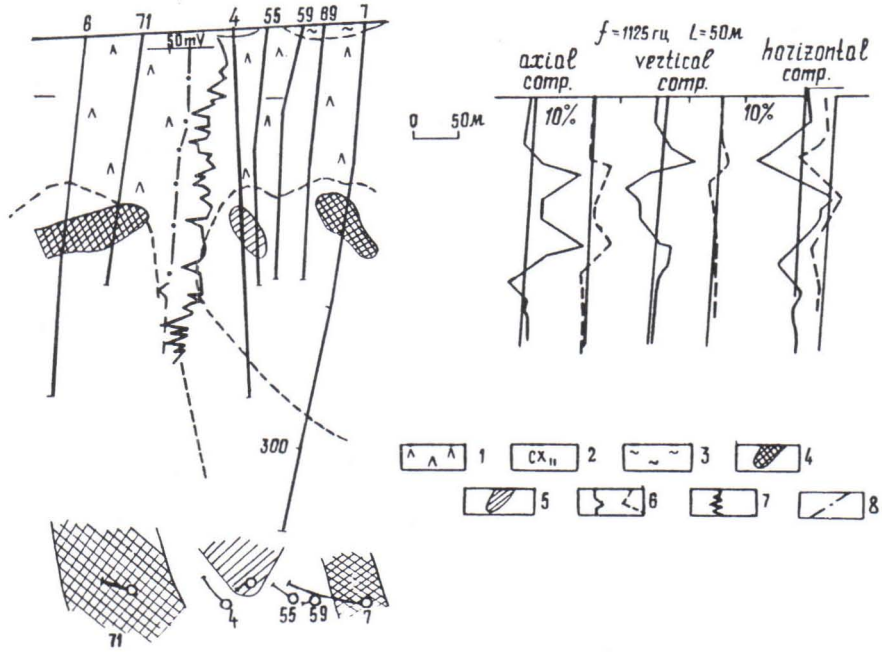

Fig. 3. Example of revealing a blind orebody with the DEMPS method. 1 - dacitic porphyrites, 2 - sericitic-chloritic-quartz rocks, 3 - loose sediments, copper-zinc orebodies, 4 - revealed previously, 5 - revealed with the DEMPS data, 6 - anomalous field profiles (frequency 1125 Hz, spacing 50 m), 7 , 8 - apparent resistivity and SP logging curves.

During the dipole electromagnetic profiling in borehole 4, which did not interesect the metallization, a typical positive anomaly of the axial component was obtained with two maxima displaced relative to each other at a distance roughly equal to the array spacing. Usually such an anomaly is due to the effect of an orebody outside the hole. The distance to the object causing the anomaly, judging by its size, does not exceed 8-10 m, and the longitudinal conductance of the object is about 50 S, which fairly corresponds to the conductivity of a massive pyrite orebody10-20 m thick. The direction of this orebody relative to the borehole under investigation is determined from the signs and relations of the transverse anomalous field component. Borehole 55, used for checking intersected the massive copper pyrite within the interval of 128-148 m.

Prior to the DEMPS application, the boreholes of this section had been examined by the electrical correlation and mise-á-la-masse methods, as well as by the radio shadowing method (boreholes 6, 4, 7). The anomalies were interpreted as the result of orebodies intersected by boreholes 6 and 7, adjacent to borehole 4. In fact, these anomalies were merely caused by the said orebody intersected later by borehole 55. Furthermore, from the DEMPS data it was inferred that the orebody intersected by borehole 7 is wedging out near the point of its intersection. Later on, boreholes 59 and 69 confirmed that fact.

It should be noted that the foregoing example implies the initial stage of applying the DEMPS. Drilling with due account of the capabilities of the DEMPS enables under similar conditions considerably increasing the spacing between boreholes.

In the same deposit, according to the DEMPS data obtained while examining borehole 30 (Fig. 4), the intersected orebody proved to wedge out 5-10 meters east of this borehole.

This can be deduced from the sudden reduction of the negative anomaly when the transmitting and receiving coils are symmetrical to the orebody and also from the considerable amplitude of the anomalous field transverse component. Boreholes 39 and 39a, drilled later, were located 50 and 15 meters, respectively, from borehole 30 without intersecting the metallization. On the other hand, borehole 30a, did as expected, intersect the orebody.

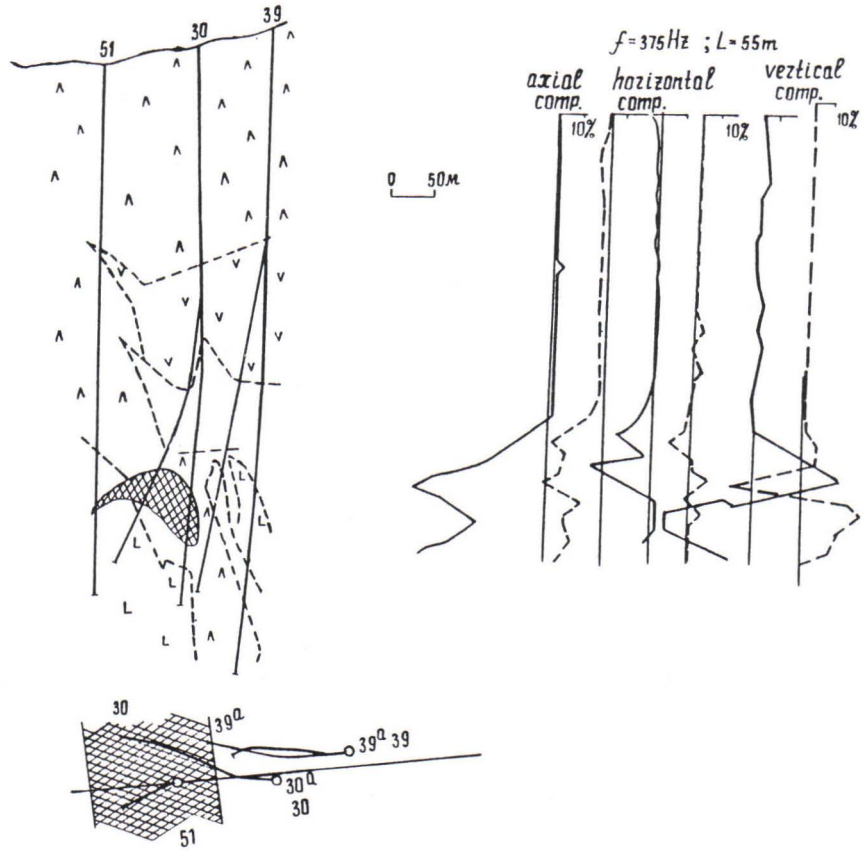

Fig.4. Example of verifying the orebody dimensions with the use of the DEMPS (frequency 375 Hz, spacing - 50 m). For symbols see Fig. 3.

Fig. 5 shows, as an example, the application of ASMI-40 (DEMPS) in exploring one of the polymetallic deposits in the Altai. The ore mineralization is represented by galenite, sphalerite, and pyrite. The richest massive orebodies, with which the basic reserves are associated, have the shape of steeply dipping veins and stocks of great length along the dip. In accordance with the DEMPS data, the borehole being examined intersected the 15-m-thick layer at 25-30°. This fact is indicated by a broad positive area in the upper part of the axial anomalous field component curve and also by the large width (about 2, 2L) and large amplitude of the transverse anomalous field components. From the asymmetry of the axial component curve, it may be concluded that the orebody is wedging out down the dip near the location of its intersection. The nearest lateral boundary of the orebody is 10-15 meters to the south. With the array spacing increasing up to100 m, the effect of the orebody's opposite, northern, boundary also becomes noticeable. The borehole seems to have run at an acute angle (30-40°) to the strike of the orebody. This can be judged from the large amplitude of the anomalous field component orthogonal to the dip plane of the borehole (horizontal component). Generally speaking, the orebody may be represented as an extended, nearly vertical band, stretching NE-SW for 40-50 m, elongated upwards and sharply wedging out

down the dip. These conclusions were fully confirmed by subsequent drilling.

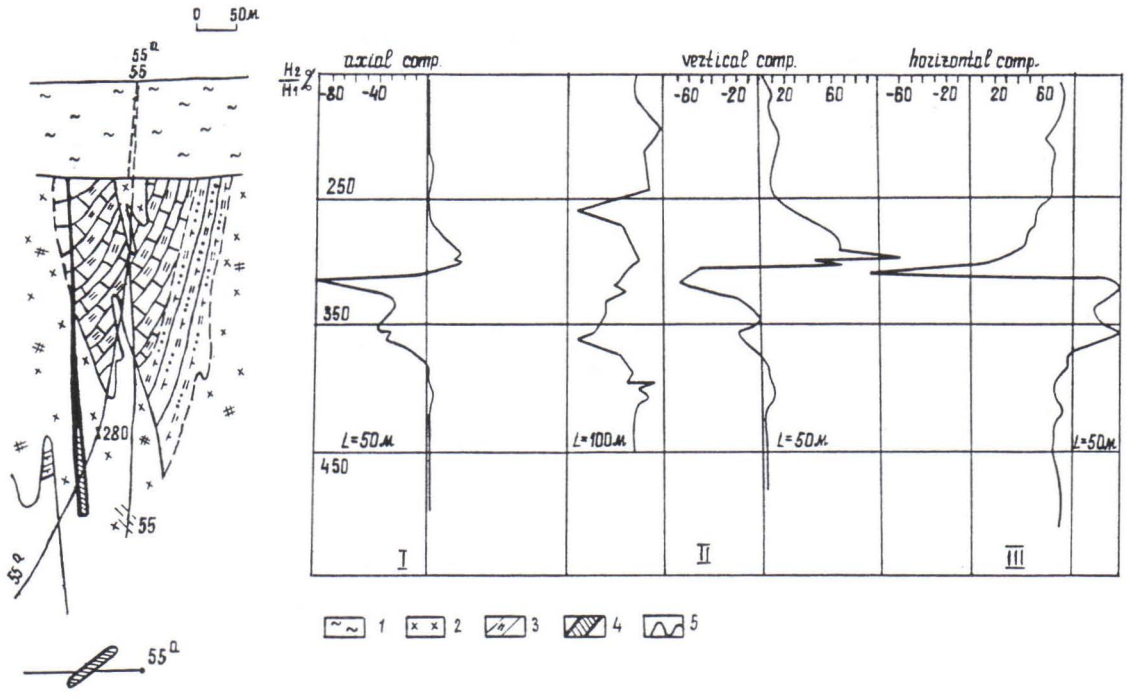

Fig. 5. Example of finding the shape and spatial position of the orebody on the basis of the DEMPS data. 1 - younger deposits, 2 - quartz porphyres, 3 - tuffaceous-sedimentary rocks, 4 - copper-pyrite ores, 5 - anomalous field, real-component curves (frequency 1125 Hz, L shown beside each curve).

The examples given, taken from routine DEMPS work, show good matching between the model and field results and the rather small effect of the host rocks.

Interborehole studies (the MDEMP method)

A new interborehole modification of dipole electromagnetic profiling (MDEMP) has been developed in the recent years in the Soviet Union (Lebedkin et al., 1978). The procedure is as follows: the transmitting coil, coaxial with the borehole being investigated, is moved downhole. In the adjacent borehole the downhole device with a receiving coil providing three-component point measurement of the total magnetic field is moved in synchronism with the transmitting coil. The field components being measured are oriented relative to the dip plane of the borehole examined, but as far as the MDEMP is concerned, it is normally i more practical to recalculate them with respect to the array axis (the array axis is a straight line interconnecting the field source and the receiver).

Considering the problem to be solved, the receiving and transmitting coils are located either at the same level, or vertically displaced relative to each other (the array with the offset). That one can vary the coils' offset and substitute one coil for another in many cases increases the capabilities of the MDEMP method.

The characteristic feature of the MDEMP as one of the low-frequency induction electrical prospecting methods is the high conductivity resolution of the objects. The

interborehole induction measurements can therefore be carried out in low-resistance geoelectrical sections where the radio shadowing method does not provide the required range and resolution. The MDEMP enables one to descriminate orebodies as zones differing in conductivity and to distinguish between the ruptures of the orebodies and their partial pinching. Unlike the galvanic excitation methods, the MDEMP yields results, which are not affected by the electrically conductive channels. The MDEMP results are estimated solely by the absolute resistivity value of the ore objects occurring right between the boreholes examined or beneath their bottoms.

What certainly restricts the efficancy of the MDEMP is that its results may become inaccurate owing to the borehole spacing variations, which are likely to occur with depth. As a matter of fact, such is the case when measurements are taken in the abrupt converging of diverging boreholes. The negative influence this has on the results can be essentially reduced by corrections based on directional survey data. Under such circumstances, the measured imaginary field component, which hardly depends on the variations of the borehole spacing, should preferably be used for the interpretation.

During several years of MDEMP applications, the most interesting practical results were obtained when the continuity of the orebodies were determined in the interborehole space. Let us briefly analyze the principles that constitute the basis for determining the continuity or discontinuity of the conducting body. The main portion of the currents induced by the magnetic dipole in the infinite conductive plate, with its plane orthogonal to the dipole axis, is concentrated in concentric zones with the centre located on the continuation of the transmitting dipole axis. Owing to the properties of the magnetic dipole field and eddy current interaction, the maximum effect of these currents is recorded in the ring-shaped zones located in such a way that the higher the field source is over the conductor, the farther are the rings away from the centre.

When the array is above an infinite continuous conductor at a height greater than 0.35 R (R - in the spacing between the transmitting and receiving coils), the radius of such a ring-shaped zone is greater than the borehole spacing. In the plots of the H_Z-magnetic field axial component (Fig. 6), one can see positive values amounting to 20-25 % of the primary field. The anomalous field component orthogonal to the borehole axis, H_X, and coinciding with the array axis direction when coils are moving over the conductor, does not reverse the sign and increases to 80 %. If the objects are not continuous but have a break between the boreholes, a significant redistribution of the eddy currents in the conductor results. The main portion of the induced currents is confined by the break and is concentrated near it. When the thickness of the conductor is small, the positive part of the axial component anomaly actually disappears and the H_X-component is reduced to half.

In fact, locating the break in the conductor is possible with the H_X (transverse component) measurements only. Therefore the measurements should be done with the mutual replacement of the transmitting and receiving coils in the boreholes investigated. Additional reversal of the anomaly sign on the curve section corresponding to the array approaching the conductor indicates that the break is somewhere near the borehole wherein the transmitting coil is moved. This additional sign reversal of the anomalous field results from the concentration of eddy currents near the continuity break; and it will be the sharper, the shorter the distance is between the borehole and the break.

Examples of applying the MDEMP method

As an example of detecting a break in the continuity, let us consider some results of the MDEMP at one of the copper-pyrite deposite in the Urals. The metallization is represented mainly by continuous, gently dipping bodies of a rather large thickness (up to 50-100 m) with

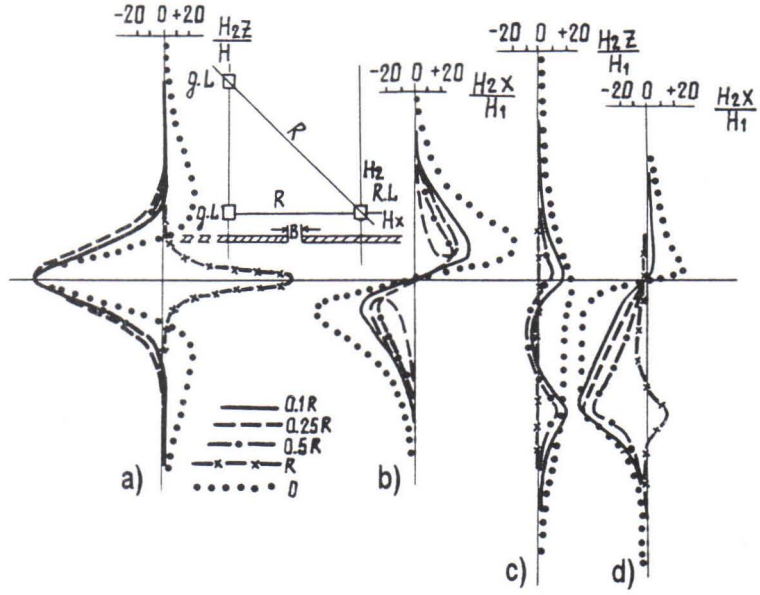

Fig. 6. Results of modelling the horizontal plate field with the break of its continuity at mid-distance between the boreholes. H_Z-axial (a) and H_X-transversal (b) components of an array with zero offset; axial (c) and H_X-transversal (d) components when the array is displaced. B - the width of the break (the gap). 1 - B = 0.1 R; 2 - B = 0.25 R; 3 - B = 0.5 R; 4 - B = R, 5 - B = 0.

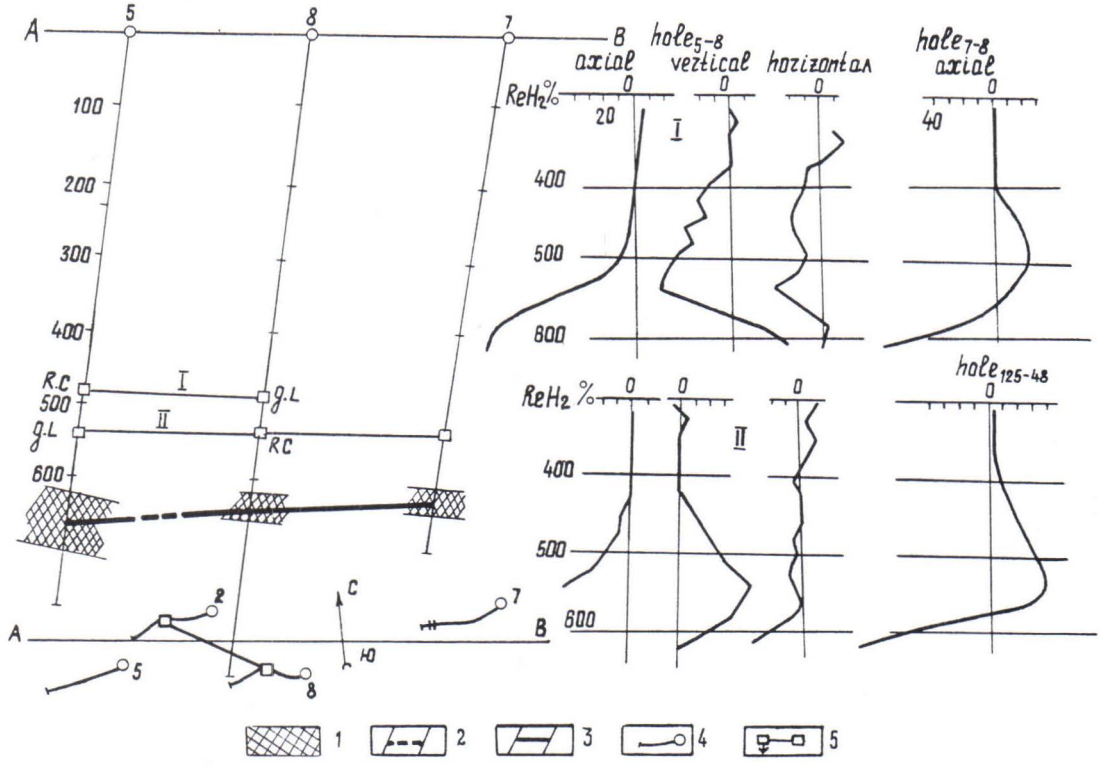

Fig. 7. Some examples of detecting a break in the continuity of the orebody. While a downhole survey was done in boreholes 5-9, the continuity was proved by boreholes 2-8 and 7-9.
1 - copper-pyrite ores, 2 - break in orebody 3 - continuous orebody, 4 - borehole projection onto the plan, 5 - location of the measuring array.

the resistivity ranging from some tenths to a few Ohm · m. Because of the low resistivity of the host rocks, the radio shadowing and electrical correlation methods were practically of no use here.

With the use of the MDEMP, whenever the values of axial component positive anomalies reached 20-25 % and the value of the transverse H_X-component was 80-90 %, the checking boreholes confirmed the continuity of the orebodies (for this, see the results of the measurements in boreholes 7-8 and 2-8 (Fig.7)). The presence of a positive area in the axial component plot and a decrease in the transverse component value obviously suggest the remarkable break in the continuity of the object. Rather typical in this respect are the results of measurements done in boreholes 5-8. Replacing one coil with another in these boreholes produced practically no effect upon the amplitude of the anomalous field and its distribution, which means that the barren area is somewhere halfway between the investigation boreholes.

The breaks revealed in the continuity of the deposit correlated well with each other and enabled tracing the fault zones, which had cut this deposit into individual bodies.

With the use of the MDEMP at this deposit, other problems have been solved as well. In particular, the flanks of the deposit have been outlined. The considerable width of the anomalous axial and transverse field components confirm the MDEMP capabilities for revealing large orebodies in the space below the level of the hole bottom at the depth of 0.7-1.0 R. When affecting the MDEMP method was applied over this deposit, the spacing between the boreholes investigated amounted to 220 m.

References

Lebedkin, L.V., Vostretsov, R.N. & Maksimova, T.M., 1971. Downhole induction electrical prospecting using ASMI-40 equipment. (Скважинная индукционная электроразведка с аппаратурой АСМИ-40). Leningrad, VITR, ONTI, 75 p.

Lebedkin, L.V., 1971. Downhole induction electrical prospecting. In: Volosjuk, G.K., & Safronov, N.I. (eds.): Borehole geophysics. ("Скважинная рудная геофизика"). Leningrad, Nedra, p. 81-161.

Lebedkin, L.V., Popov, N.I. & Maksimova, T.M., 1978. Interborehole dipole EM profiling. (Межскважинное дипольное электромагнитное профилирование). Leningrad, VITR, ONTI, 62 p.

THE ROLE OF ELECTROMAGNETIC METHODS INVOLVED IN GEOPHYSICAL PROSPECTING FOR COPPER-NICKEL DEPOSITS IN THE KOLA AND KARELIA REGIONS

by

G. Vargin, S. Shkorbatov, V. Kvashnin and A. Savin

Vargin, G., Shkorbatov, S., Kvashnin, V. & Savin, A., 1990. The role of electromagnetic methods involved in geophysical prospecting for copper-nickel deposits in the Kola and Karelia regions. *Geologian tutkimuskeskus, Tutkimusraportti 95.* 132-142, 6 figs.

EM methods play a dominant role in geophysical prospecting for Cu-Ni deposits in the Kola-Karelian region. The efficiency of EM methods is shown through their application in the Kamennoozero zone, Soviet East Karelia.

The EM methods, combined with other geophysical methods to locate Cu-Ni ores directly, are used at three different stages:

a) Airborne electrical prospecting for geological mapping and for locating Ni prospects

b) TEM surveys to detect good conductors in mafite-ultramafite massifs

c) Various TEM modifications, dipole inductive profiling, and IP-field characteristics along with drilling data and borehole geophysics for estimating the location, geometry and dimensions of objects and for preliminary assessment of their geological nature.

Depth penetration can be increased by using the TEM sounding method.

Key words: electromagnetic methods, airborne methods, ground methods, boreholes, transient methods, induced polarization, sounding, mineral exploration, geophysical surveys, metal ores, Baltic Shield, Kamennozero, Karelia, Kola Peninsula, USSR

Варгин, Г.П., шкорбатов, С.С., Квашнин, В.К., Савин, А.П., 1990. Роль электромагнитных методов разведки в комплексе геофизических раъот, связанных с поисками медноникелевых месторождений в карело-кальском регионе. Геологический центр финляндии, Рапорт исследования 95. 132-142. Идд. 6.

Отмечается ведущая роль электромагнтных методов в комплексе геофизических исследований, проводимых при поисках медно-никелевых месторождений в Карело-Кольском регионе. Рассмотрены задачи, решаемые этими методами на разных этапах поисковых работ. Эффективность электромагнитных методов иллюстрируется примерами их применения на площади Каменноозерской зоны в восточной Карелии. Намечаются пути повышения эффективности применения электромагнитных методов в регионе.

Introduction

Electromagnetic methods prevail in combined geological, geophysical and geochemical prospecting for Cu-Ni deposits in the Kola-Karelian region. Generally speaking, all the methods of research used are based on utilizing the evidence and criteria established (Belyaev et al., 1980; Kratz et al., 1983). Here are the most important of them:

- genetic and spatial relation of Cu-Ni ore deposits with intrusive massifs of mafite-ultramafite of various ages and sizes;
- single or swarms of mafite-ultramafite intrusions concentrated at the nodes or centres of plicate and fault-tectonics activity;
- typical of certain areas is flexure bending of ore-producing horizons, often accompanied by plastic shear zones, and variations in the grade of metamorphism of rocks forming the massif;
- epigenetic ores that are concentrated in large massifs of mafite-ultramafite are usually situated in the footwall, occasionally in the country rocks.

The wide variety of prospecting evidence, indicators and criteria is indicative of various peculiarities in the Ni-ore forming process in the region and requires a whole combination of prospecting methods to be used. Again, the effectiveness of the geophysical methods decreases because of the complicated petrophysical properties of the bedrock, which again result from its inhomogeneity composition, faults and tectonically affected zones, which are not considered to be metallotect, and many other factors. Furthermore, much of the territory in Karelia is covered by an inhomogeneous Quaternary overburden attaining in thickness several tens of meters, which also impedes prospecting operations.

Electromagnetic methods prevail among the geophysical procedures incorporated, because rocks and ores differ in their resistivity: for most types of Cu-Ni deposits in the region, the ore objects, or bodies, are better conductors than the country rocks (Vargin et al., 1985). The main problem which decreases the effectiveness the EM methods, is the presence of electrical conductors of a non-ore character, viz., black schists (phyllites), zones of graphitization and serpentinization, etc.

Based on the experience of Cu-Ni prospecting in the Kola-Karelian region, a geophysical research procedure, including the EM methods, was worked out (Vargin et al., 1977; 1983). At the first stage of preliminary prospecting, use is made of airborne geophysical methods (airborne electrical and magnetic prospecting) and a gravity survey in order to carry out the mapping of various rock complexes and to outline the nickel prospects in the complexes. At the second stage of operations, a loop version of TEM is employed together with a magnetic and gravity survey, as well as mise-a-la-masse (CP) and IP methods. As a result, mapping of producing formations is accomplished, mafite-ultramafite massifs are outlined and preliminary prospecting is done to select the areas for further exploration. There are some localities where, at the second stage of work, the EM VLF method is used. Finally, at the third stage of preliminary prospecting, detailled investigation of previously found combined anomalies is made by various versions of the TEM method, as well as by dipole induction profiling and estimating the properties of the IP field; also, along with drilling, the third stage involves borehole geophysics, viz., vector study by TEM, dipole induction profiling, RF-sounding and the mise-a-la-masse (CP) method. The results thus arrived at enable us to ascertain the morphology of conductors and their position in a geological section, and also to make a preliminary assessment of an anomaly from the geological point of view. Further detailled study of most Ni-promising targets drilling is then suggested.

Example from the Kamennoozero Zone

Stage1 (airborne survey)

The effectiveness of EM prospecting methods at various stages can well be illustrated by the results obtained in the Kamennoozero ultramafite zone, which is in Soviet East Karelia within the Windy Belt synclinorium zone (Bolgurtsev, 1974).

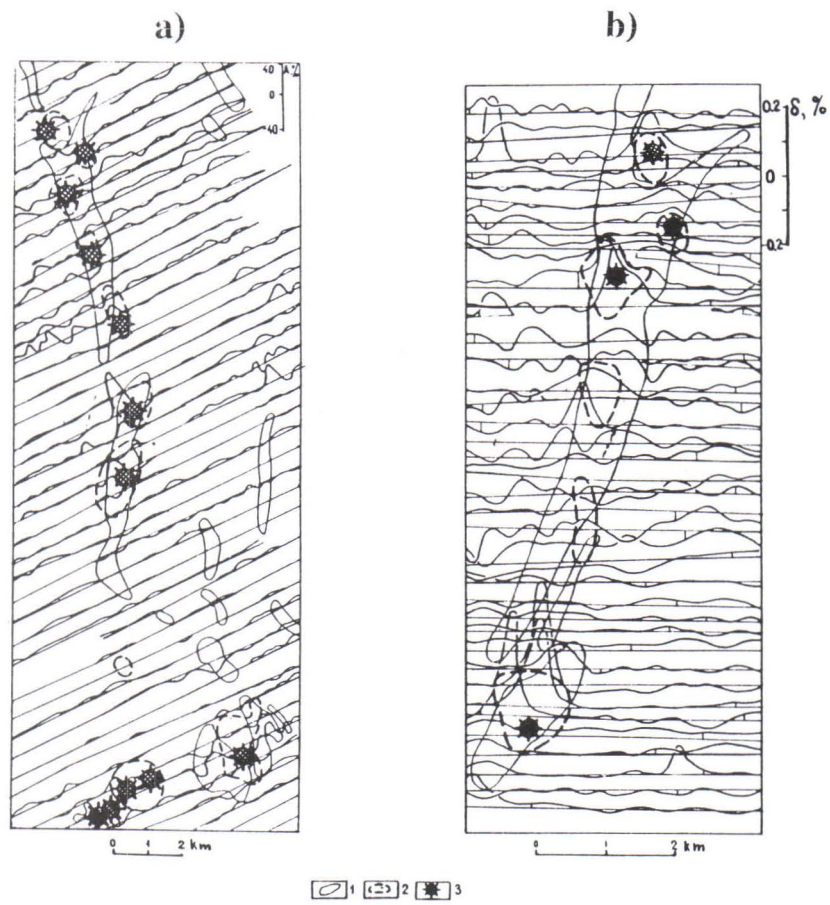

Fig. 1. Results of airborne electrical prospecting in two areas of the Kamennoozero zone: (a) map of amplitude parameter A based on the rotary-field method at a frequency of 1225 Hz (b) map of difference parameter δ based on the results of inductive dipole profiling at frequencies of 312 and 2500 Hz.
1 - boundaries of ultramafic massifs according to magnetic survey data; 2 - outlines of anomalously conductive zones according to ground TEM data; 3 - sulphide ore deposit.

Airborne electrical surveys to map various rock complexes of the Kamennoozero zone were carried out in different years by the rotary magnetic field method and inductive dipole profiling. In the first case, the amplitude parameter, A, was calculated:

$$A = \frac{2\,(|U_y| - |U_z|)}{|U_y| + |U_z|} \cdot 100\,\%,$$

where U_y and U_z = voltage values of signals induced in two receiving coils. In the second case use was made of the ratio of the minor semiaxis, H_b, to the major semiaxis, H_a, of the magnetic field polarization ellipse. The results were then reduced to the difference parameter:

$$\delta = -(|H_b|/H_a)_1 + f_1/f_2 (|H_b|/H_a)_2,$$

where $(|H_b|/H_a)_1$ and $(|H_b|/H_a)_2$ represent the field ellipse semiaxis ratio measured at two different frequencies f_1 and f_2 (usually $f_2 = 4f_1$). Some fragments of the results obtained by these two methods in two localities are shown in Fig.1.

According to the airborne electrical data, the ultramafite intrusions produce positive linearly stretched anomalies coinciding with magnetic anomalies, which is especially typical of the situation shown in Fig. 1a. Variations in the intensity and the sign of the anomalies (Fig. 1b) indicate a remarkable geoelectrical subsurface inhomogeneity. This was in due time proved by subsequent ground geophysical surveys. The most intense anomalies generally coincide with highly conductive zones (proved by subsequent TEM investigations), where sulphide ore deposits have been found.

Thus, airborne electrical prospecting at the first stage of work in this particular case enabled us to locate the areas of utmost geoelectrical inhomogeneity and the highly conductive zones, both of them being of considerable importance in the geological mapping and preparation of a so-called local prognosis for nickel.

The very-low-frequency (VLF) method can also be regarded as a constituent part of geophysical investigations of the first stage; notwithstanding its limited depth penetration, the VLF method is affectively applied in some areas for making a prompt reference to electrical anomalies.

Stage 2 (regional survey)

Dominating at the second stage of work was the TEM, loop version (single or combined loop array), covering the prospect area. Till recently, the MPP equipment was used for that purpose. Shown in Fig. 2a are the results of effective application of the single-loop TEM array with a loop size of 400 by 400 meters and MPP-3 apparatus producing a map of isolines U/1, where U - e.m.f. across the loop, 1 - current). The anomalous zone (the left one in Fig. 2a) revealed by the TEM underwent detailled study at the third stage, the loop sizes being 200 x 200 and 100 x 100 (Fig. 2c, d). As a result, a drilling site was chosen and drilling in the chosen direction was performed in a test borehole that struck a lensof rich Cu-Ni ores at a depth of more than 150 m. Subsequent study enabled this orebody to be traced as far as its outcrop at the erosion level (Fig. 2a). Another anomalous zone (the right one in Fig. 2a) is related to a graphitization zone.

The TEM survey is also made in the areas comprising the conductive zones detected by mise-a-la-masse method. The TEM serves in estimating electrical conductivity, the size of conductive zones and to distinguish good conductors regarded as promising for Cu-Ni ore. To increase the depth penetration of this method, a "CYCLE-2" apparatus is used; with it, the transient parameters can be studied within the time range from 0.2 ms to several seconds. Such a long time interval for the equipment, along with its remarkable noise resistance and powerful source (loop current about 50A), enable the sounding to be made by TEM, thus obtaining the data on the distribution of the resistivity with depth. The depth penetration of the equipment is estimated at several hundreds of meters.

In order to test the efficiency of sounding with the "CYCLE-2" equipment, measurements with a loop-size combination of 200 x 200, 100 x 100 and 50 x 50 m were made above the "Eastern" ore deposit. The ore object here is an almost vertical lenslike body of massive streaky-impregnated sulphide ores 7-18 m thick, traced along the strike for 400 m and down to the depth of 380 m (Fig. 3d).

On the basis of the data of TEM sounding, sections of apparent (Fig. 3a, b, c) resistivity,

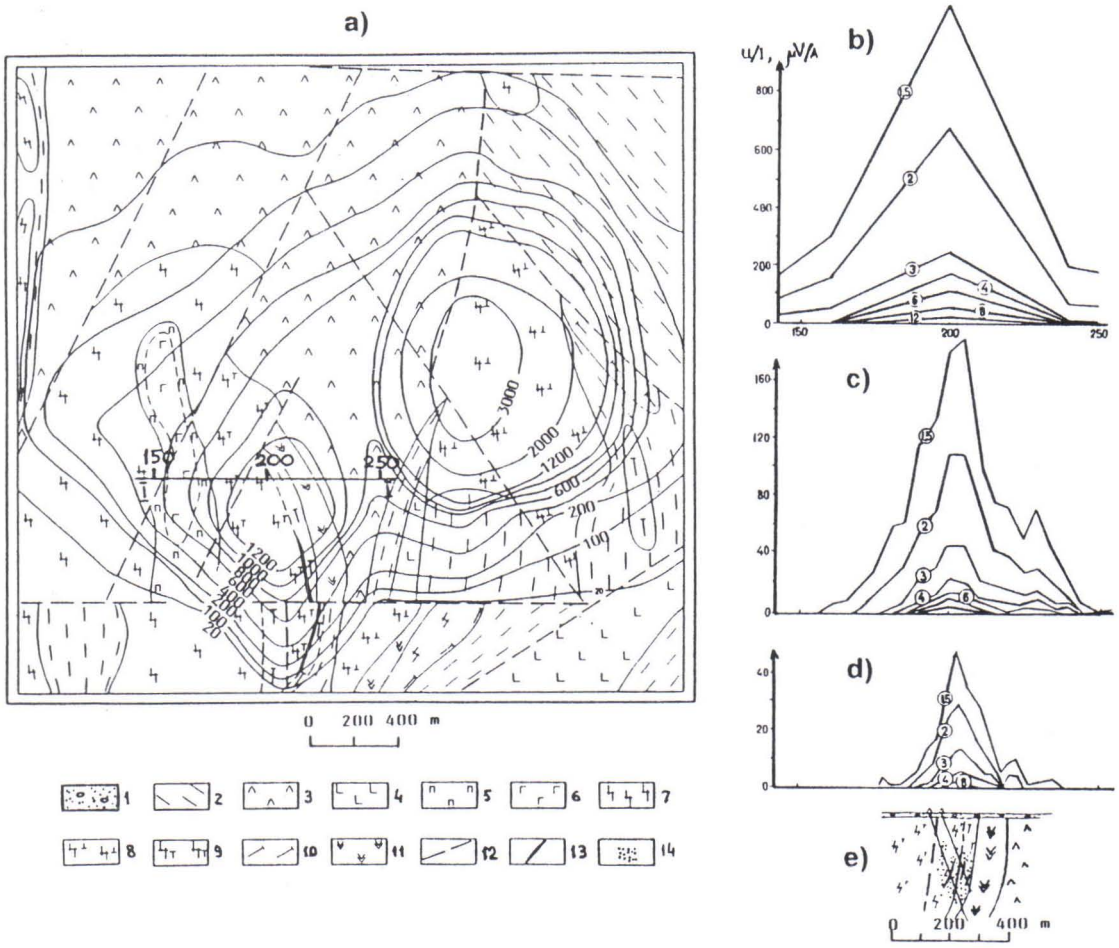

Fig. 2. Results of single-loop TEM prospecting in one of the areas of the Kamennoozero zone;
(a) map of U/1 isolines with a loop size of 400 x 400 m at measurement time 1 ms; (b, c, d) U/I plots along profile I-I- with loop size (b) 400 x 400 m, (c) 200 x 200 m and (d) 100 x 100 m; plot index - measurement time in ms; (e) - schematic geological section of profile I-I.
1 - Quaternary sediments; 2 - tuffites with intercalations of tuff and tuff-breccia of sedimentary rocks; 3 - andesite-diabases; diabases and their tuffs; 4 - diabases with green schists; 5 - rocks of metawehrlite-metapyroxenite-metagabbro composition; 6 - metagabbro; 7 - nondifferentiated ultramafites; 8 - apoolivinite serpentinites; 9 - apoperidotite serpentinites; 10 - talc-carbonate rocks; 11 - metagabbro-diabase dykes; 12 - tectonic faults; 13 - massive breccia-like Cu-Ni ores; 14 - ore impregnation.

ρ_τ were constructed; also, the depth to the top edge of the conductive object was interpreted (Fig. 3d). As shown by the graphs, the points obtained by means of interpretation and indicating the position of the object's top edge run actually along the projection that the hanging wall of the orebody forms on the vertical plane across the profile line. The direction and dip angle of the orebody can also be determined, but this is the subject of the third stage of preliminary prospecting.

The so-called "Southern" orebody turned out to be another area covered by TEM sounding; the ores there are streaky-impregnated, occurring at 150-200 m within the relict of volcanogenic-sedimentary rocks in the ultramafite massif (Fig. 5d). On the basis of the TEM sounding data, highly conductive zones were outlined (Fig. 5a, b). The best conductors among these are two zones coinciding with the orebody (observation stations 260-280) and one zone (observation station 320) at the contact of the ultramafite massif with country rocks.

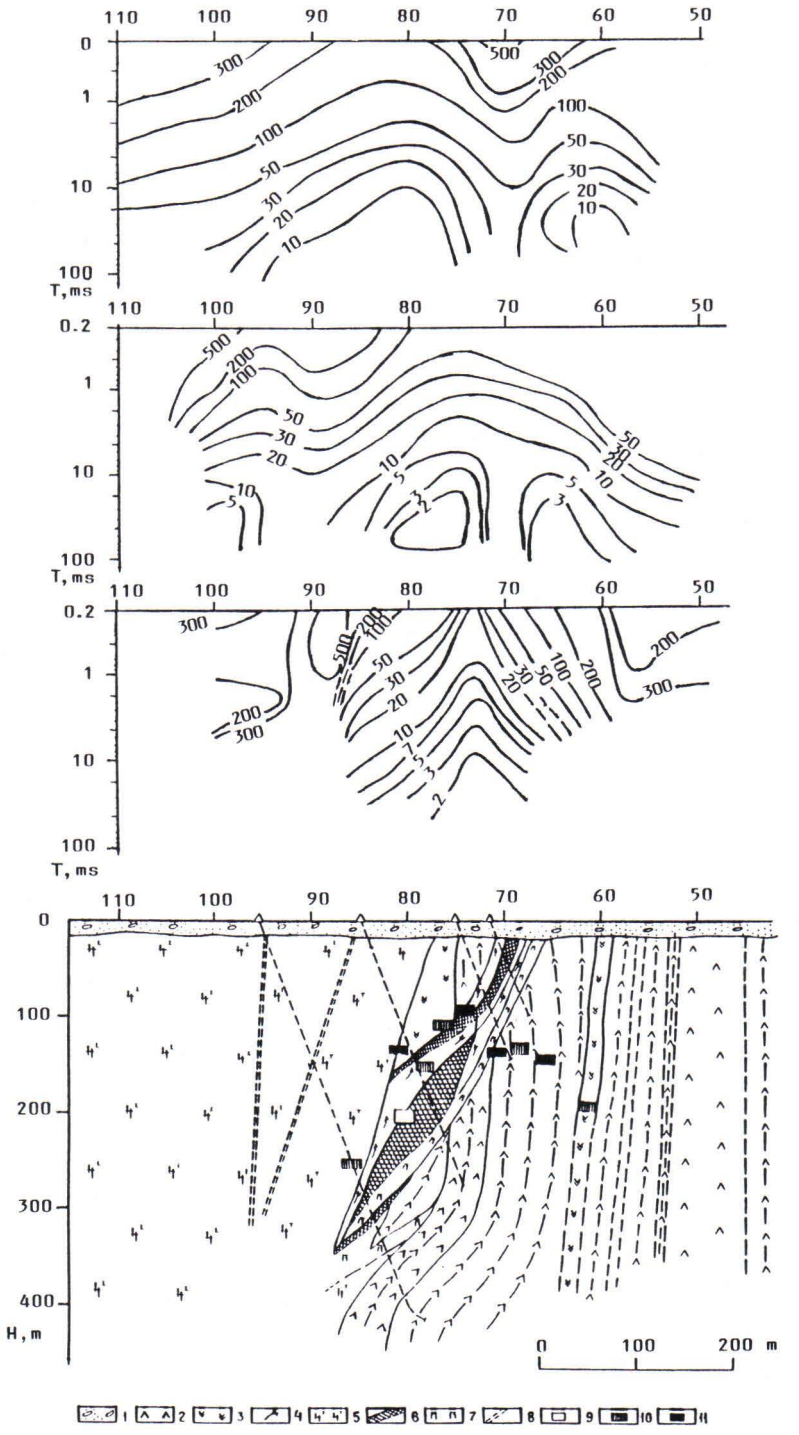

Fig. 3. Results of sounding by the TEM method above the Eastern ore body (Vargin et al., 1983). (a, b, c) sections showing ρ_τ (Ωm) with combined loop array (a) 200 x 200 m, (b) 100 x 100 m and (c) 50 x 50 m, (d) geological section.

1 - sand, loam sand, clay; 2 - dacites, dacite-andesites, plagioclase and quartz-porphyries; 3 - metagabbro-diabases; 4 - andesite-diabase and diabase porphyrites; 5 - amphibole and chlorite-amphibole rocks; 6 - streaky-impregnated and breccia-like Cu-Ni and pyrite Zn-Pb-Cu ores; 7 - pyroxenites; 8 - tectonic faults; 9, 10, 11 - position of the conductor's top edge according to TEM sounding with loop array 200 x 200 m (9), 100 x 100 m (10) and 50 x 50 m (11).

The presence of the sulphide ore deposit here was proved by drilling.

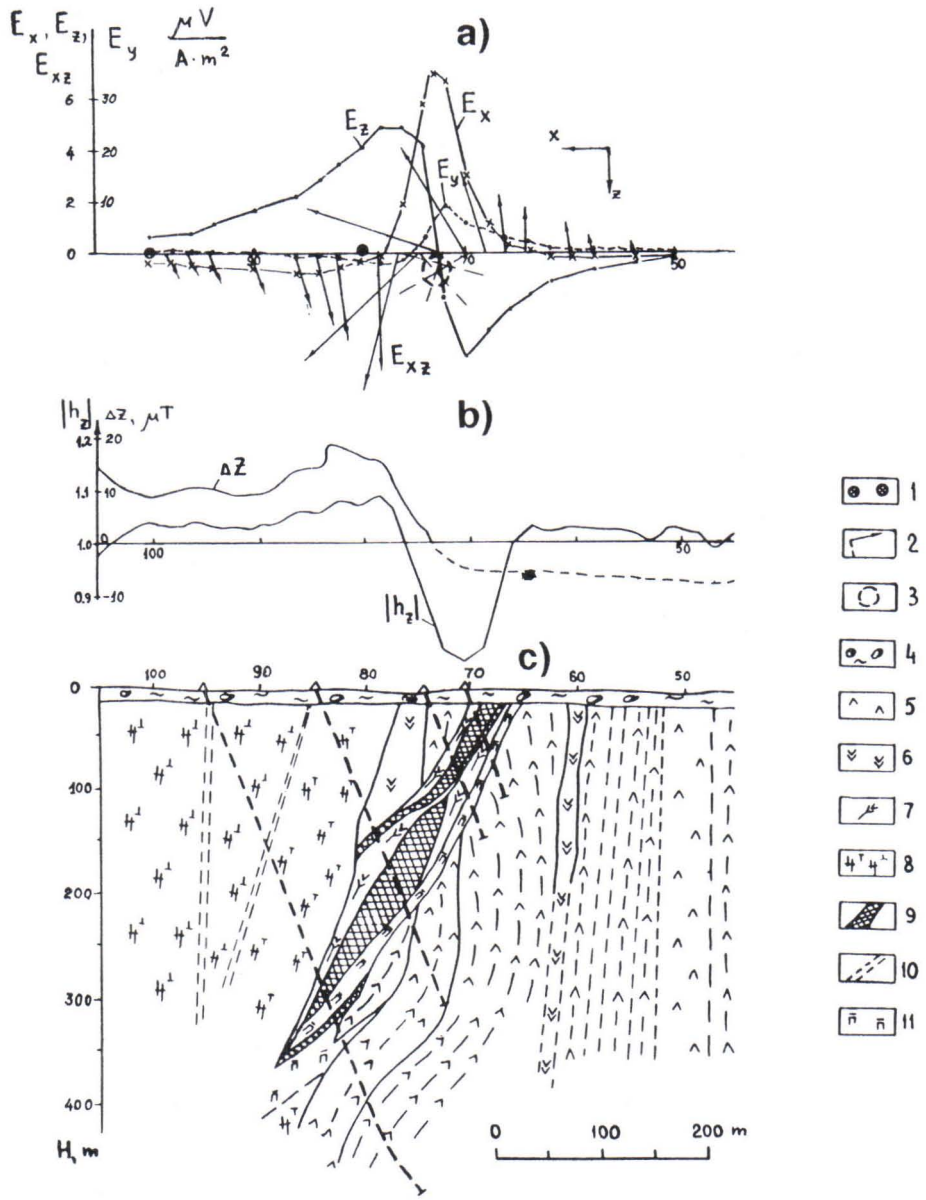

Fig. 4. Results of geophysical prospecting in the Eastern ore area. (a) Results of vector TEM measurement at t = 1 ms, (b) ΔZ plots according to magnetic prospecting data and $|h_Z|$ plots according to inductive dipole profiling data (r = 80 m, f = 2 kHz), (c) geological section.
1 - position of ungrounded loop; 2 - vector E_{XZ} and a normal to it; 3 - approximate position of current line on plane XZ (intersection of normals to vectors E_{XZ}); 4 - sand loam sand, clay; 5 - dacites, dacite-andesites, plagioclase and quartz porphyrites; 6 - metagabbro-diabases; 7 - andesite-diabase and diabase porphyrites; 8 - amphibole and chlorite-amphibole rocks; 9 - string-impregnated and breccia-like Cu-Ni and pyrite-Zn-Pb-Cu ores; 10 - tectonic faults; 11 - pyroxenites.

Stage 3 (detail studies)

The procedure followed at the third stage of work, as pointed out earlier (see Figs 2, 3), involves the TEM loop version (sounding included). Another TEM modification at this stage involves vector measurements, where an ungrounded loop serves as the EM field source. Measurements with the MPP-4 equipment are taken both inside and outside the loop.

The measured vector data, drawn in proportion to the magnetic field intensity, give us an idea of the position of secondary currents flowing through the conductive bodies. Thus we can determine rather precisely the spatial position of bodies which are discovered or require further research. Shown as examples in Figs 4a and 5c are vector plots with space components of $E = U/(IS)$, where U - e.m.f. across the receiving coil, S - area of ungrounded loop, I - loop current. Above the Eastern ore deposit (Fig. 4a) an anomaly above the orebody was defined rather easily using the components E_X and E_Z; also determined from the vector plots was the position of a point (area) of the secondary current line section, coinciding with the top portion of the orebody. We failed to locate the other (lower) current line point, for it is very deep below and has little influence,unlike the top one. As for the Southern ore deposit, the position of both current line intersection points was located making use of vector plots (Fig. 5c). The left current line lies fairly well within the known ore zone and the right point occurs in the hanging wall of the ultramafite massif and thus, apparently, corresponds to the conductive object that was revealed by the TEM sounding. Finding the position of current lines by several profiles enables the object to be spatially outlined.

When the preliminary prospecting of the third stage is done, as far as relatively shallow objects are concerned, inductive dipole profiling appears to be the quickest and commercially most efficient method. It is performed in the frequency range of 500-8000 Hz and with vertically oriented axes of source and receiving loops (ZZ array). Thus Fig. 4b shows the efficancy of this method in revealing and calculating the direction and dip angle of the object's top portion, while Fig. 6 is another example. An ore deposit was encountered in a borehole the site of which was selected on the basis of the results of dipole induction profiling that spotted a highly conductive ore object (using $r = 120$ m and $f = 8000$ Hz) and a conductor related with impregnated ore (using $r = 60$ m and $f = 500$ Hz).

The third stage of prospecting provides also for borehole measurements by dipole induction profiling and for vector measurements by TEM (in the second case, an ungrounded loop laid on the surface acts as an EM-field source). These measurements yield information about the near-hole space, which is then used to verify the geometry and location of conductive objects detected by the ground methods, as well as to discover new objects. Study of the space between the boreholes is managed through RF-sounding, which yields the most complete information about the object's shape and spatial position.

Electromagnetic methods fail to shed light on the geological nature of conductive objects; therefore, during the third stage of work, use is made of electrochemical prospecting methods. Most efficacious from the standpoint of conditions in the Kola-Karelian region, are those methods that involve study of the characteristics of the IP-field.

Some new developments

In order to increase the efficiency and depth penetration of prospecting, EM methods that previously had not been used here are now being tested and applied. previously have not been used here. To improve the geoelectrical section for making prognoses down to depths of several hundred meters, an experimental research program is being carried out using the EM frequency sounding method. It consists of measuring the strength of the electrical field created by an electric dipole at a constant distance (1-3 km) from the field source, with frequencies ranging from 1.2 Hz to 20 kHz (Pyatnitski & Malashev, 1975). Applying this method to selected profiles will help us to estimate on the spot the geoelectrical parameters of

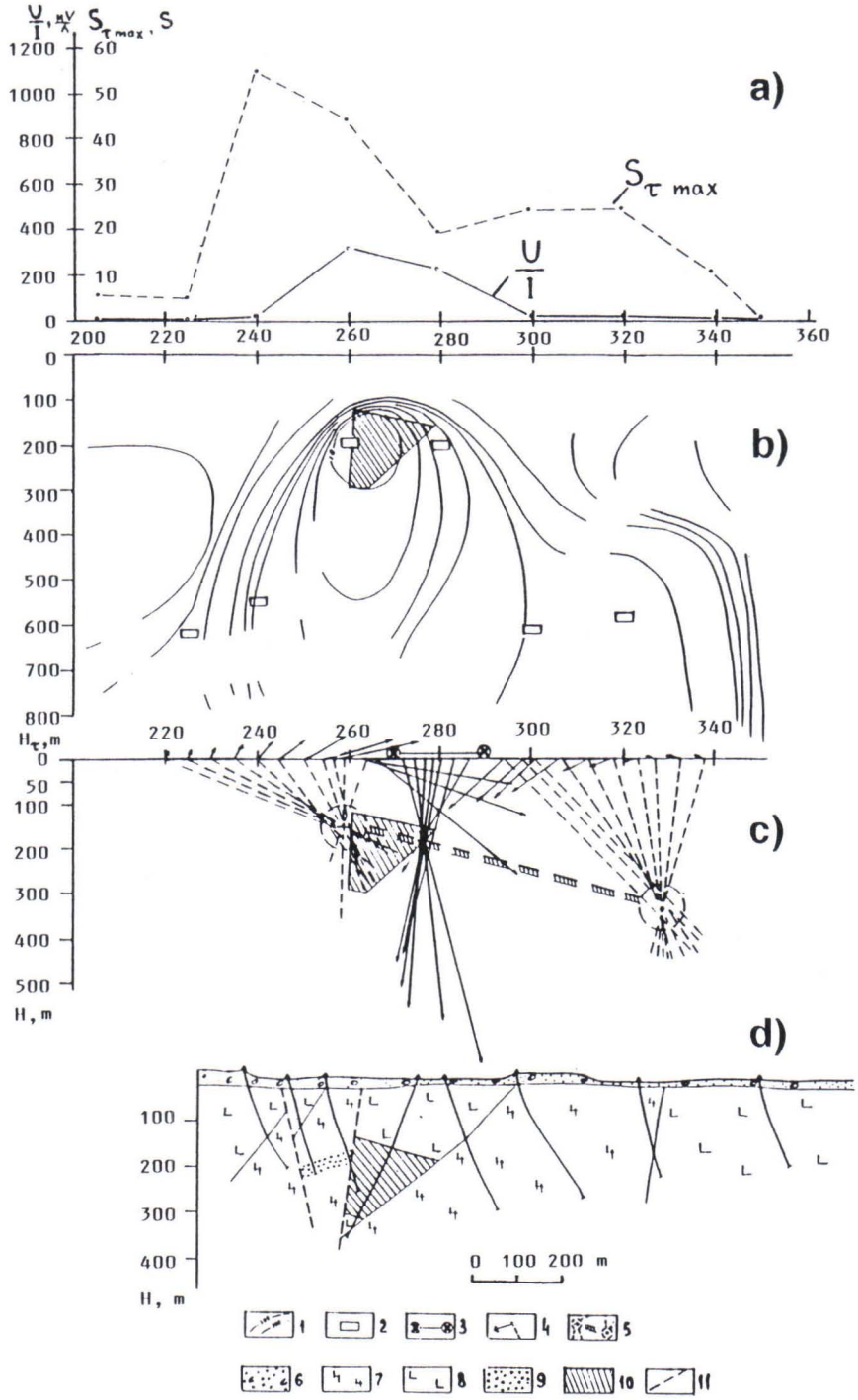

Fig. 5. Results of TEM prospecting in the southern ore area (Vargin et al., 1983). (a) U/I plot at t = 4 ms and $S_{\tau\ max}$ according to sounding data, (b) section showing ρ_τ according to sounding data, (c) results of vector measurements, (d) geological section.

1 - ρ_τ -isolines in Ωm; 2 - position of top edge of conductive object according to TEM sounding with 200 by 200 m loop array; 3 - position of ungrounded loop; 4 - vector E_{xz} and normal to it; 5 - position of the points where secondary current lines intersect with the section plane; 6 - sand, loam sand, clay; 7 - serpentinites; 8 - tuffaceous-sedimentary rock sequence; 9 - impregnated sulphide mineralization; 10 - impregnated and streaky sulphide ores; 11 - fault.

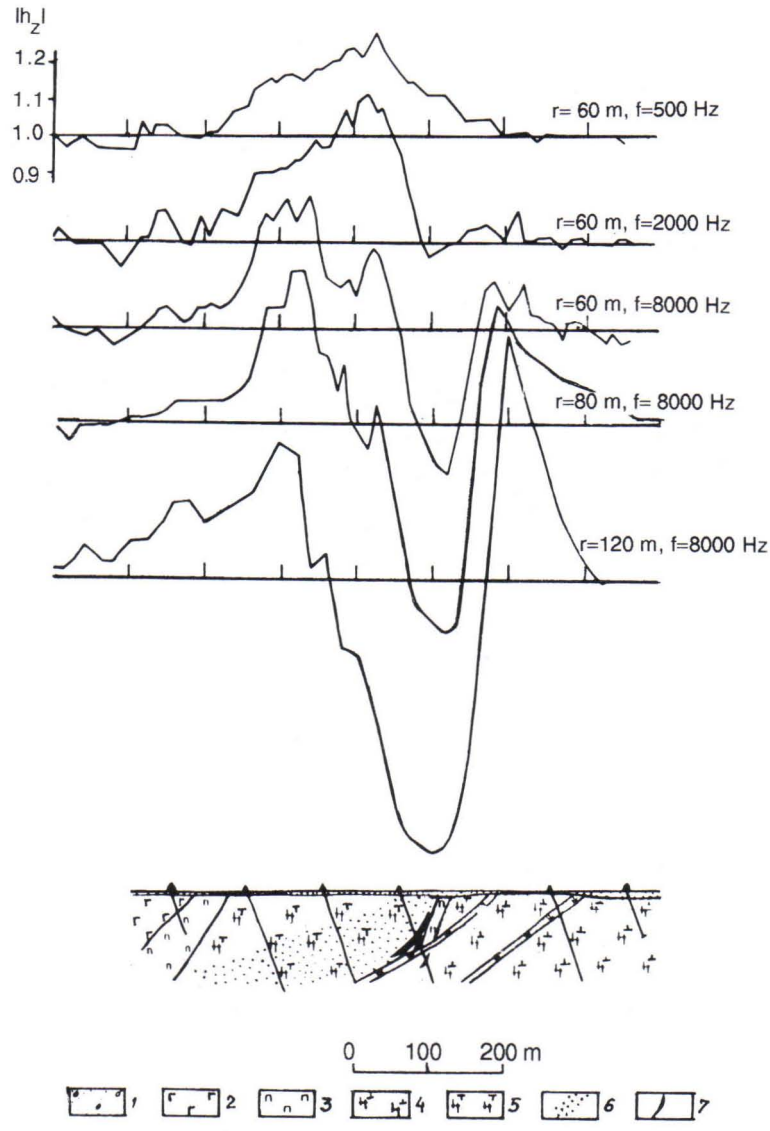

Fig. 6. Plots of $|h_z|$ drawn according to inductive dipole profiling data obtained over the Cu-Ni ore zone. 1 - quaternary sediments; 2 - gabbro, 3 - peridotites; 4 - apoolivinite serpentinites; 5 - apoperidotite serpentinites; 6 - ore zone; 7 - streaky-impregnated ores.

the prospecting area and to select anomalies of enhanced conductivity for subsequent study from the geological and structural standpoint.

Since the area being explored has an industrial noise level that impedes the implementation of the foregoing EM methods, we have commenced harmonic mode measurements with a combined loop array and a frequency range of from 17.5 Hz to 17.9 kHz (Laptev et al., 1972). The equipment used in this method affords some ten times better noise protection than that of TEM.

Conclusions

Summing up, it can be said that application of EM methods in prospecting for Cu-Ni ore deposits in the Kola-Karelian region makes the following possible:

1. Highly conductive sulphide ores and ore controls, or metallotects, are brought directly to light (a so-called "local" prognosis), in three successive stages:

(a) At the first stage, airborne electrical prospecting. together with airborne magnetic prospecting and ground gravity prospecting, is performed for solving the problems of geological mapping and locating nickel prospects.

(b) At the second stage, the TEM survey (sounding included), in combination with magnetic, gravity and mise-a-la-masse prospecting methods, enables1) good conductors to be detected in mafite-ultramafite massifs, and 2) providing the situation is favourable, the data to be obtained concerning the spatial position and size of objects (in some areas the survey is carried out by the VLF method to ensure reliable and prompt location of airborne electrical anomalies).

(c) Finally, at the third stage, as a result of detailled prospecting with the application of various TEM modifications and dipole induction profiling, in combination with research on IP-field characteristics, as well as with drilling and borehole geophysics, an estimation is made of the geometry and dimensions of conductive objects, their locaiton is verified and a preliminary assessment of their geological nature is made.

2. Maximum depth penetration of ground prospecting (several hundred meters) is achieved by geophysical methods, TEM sounding, in particular.

References

Belyaev, K., Grigorieva, L., Korsakova, M., Negrutza, V., Popov, V., Rabinovitch, Yu., Rundquist, D. & Snyslov, A. (eds.), 1980. Metallogeny of the Eastern Baltic Shield. (Металлогения восточной части Балтийского щита). Leningrad, Nedra Publ., 247 p.

Bolgurtsev, N., 1974. Peculiarities in geological structure of Windy Belt synclinorium zone. (Особенности геологического строения синклинорной зоны Ветреного пояса). Sovetskaya Geologia 12, 125-131.

Kratz, K., Bogaehev, A., Grib, V. & Proskuryakov, V., 1983. Earth crust and metallogeny of the South-Eastern Baltic Shield. (Земная кора и металлогения юго-восточной части Балтийского щита). Leningrad, Nauka Publ., 304 p.

Laptev, V., Lobacheva, E., Pris, G. & Svetov, B., 1972. Double-loop method of LF-induction electrical prospecting. (Двухпетлевой метод индуктивной низкочастотной электроразведки). Proc. of Central Res. Inst. Geol. Prosp., Moscow, iss. 104, 85-95.

Pyatnitski, V., Malashev, G., 1975. On possibility of applying EM-frequency sounding when mapping the ore fields. (О возможности применения частотных электромагнитных зондирований при картировании рудных полей). Proc.of Central Res. Inst. Geol. Prosp., Moscow, iss. 119, 54-61.

Vargin, G.P., Fischgeit, A. & Shkorbatov, S., 1977. Combined geophysical prospecting for nickel. (Комплексные геофизические работы на никель). J. Razvedka i okhrana nedr, 44-48.

Vargin, G.P., Fischgeit, A., Shkorbatov, S. & Kvashnin, V., 1983. On the increase of the efficiency in electrical prospecting when exploring and evaluating the Cu-Ni ore occurrences in Karelia. (Повышение эффективности электроразведки при поисково-оценочных работах на медно-никелевых рудопроявлениях Карелии), pp. 44-54 in Results of geophysical research through Precambrian formations of Karelia. Geol. Inst. of Karelian Branch of USSR Acad. Sci., Petrozavodsk.

Vargin. G.P., Borovko, N.N. & Savin, A.P., 1986. Construction of geoelectrical models for Copper-Nickel deposits of the Kola-Karelian region. Pp. 8-19 in Eskola, L., Fokin, A. (Eds.): Electrical prospecting for ore deposits in the Baltic Shield. Part 1: Galvanic methods. Geol. Survey of Finland, Rep. of Investigation 73.

ACKNOWLEDGEMENTS

The Editors are greatful to Ms. Paula Pöntiö, Department of Geophysics, University of Oulu for preparing the text and figures for the printers. Mr. Paul Sjöblom has kindly checked the English language of this issue.

Tätä julkaisua myy

GEOLOGIAN
TUTKIMUSKESKUS (GTK)
Julkaisumyynti
02150 Espoo

☎ 90-46931
Teleksi: 123 185 geolo SF
Telekopio: 90-462 205

GTK, Väli-Suomen
aluetoimisto
Kirjasto
PL 1237
70701 Kuopio

☎ 971-205 111
Telekopio: 971-205 215

GTK, Pohjois-Suomen
aluetoimisto
Kirjasto
PL 77
96101 Rovaniemi

☎ 960-297 219
Teleksi: 37 295 geolo SF
Telekopio: 960-297 289

Denna publikation säljes av

GEOLOGISKA
FORSKNINGSCENTRALEN (GFC)
Publikationsförsäljning
02150 Esbo

☎ 90-46931
Telex: 123 185 geolo Sf
Telefax: 90-462 205

GFC, Distriktsbyrån för
Mellersta Finland
Biblioteket
PB 1237
70701 Kuopio

☎ 971-205 111
Telefax: 971-205 215

GFC, Distriktsbyrån för
Norra Finland
Biblioteket
PB 77
96101 Rovaniemi

☎ 960-297 219
Telex: 37 295 geolo SF
Telefax: 960-297 289

This publication can be obtained from

GEOLOGICAL SURVEY
OF FINLAND (GSF)
Publication sales
SF-02150 Espoo, Finland

☎ 90-46931
Telex: 123 185 geolo SF
Telefax: 90-462 205

GSF, Regional office for
Mid-Finland
Library
P.O. Box 1237
SF-70701 Kuopio, Finland

☎ 971-205 111
Telefax: 971-205 215

GSF, Regional office for
Northern Finland
Library
P.O. Box 77
SF-96101 Rovaniemi, Finland

☎ 960-297 219
Telex: 37 295 geolo SF
Telefax: 960-297 289

ISBN 951-690-390-8
ISSN 0781-4240

Helsinki 1990. Valtion painatuskeskus